Alma Mater Studiorum – Università di Bologna

DOTTORATO DI RICERCA IN

CHIMICA

Ciclo XXXII

Settore Concorsuale: 03/A1 Chimica Analitica

Settore Scientifico disciplinare: CHIM/01 Chimica Analitica

Exploiting bioluminescence to enhance the analytical performance of whole-cell and cell-free biosensors for environmental and point-of-care applications

Presentata da: Antonia Lopreside

Coordinatore Dottorato:

Chiar.ma Prof.ssa Domenica Tonelli

Supervisore:

Chiar.ma Prof.ssa Elisa Michelini

Co-Supervisore:

Chiar.mo Prof. Aldo Roda

Esame finale anno 2020

Abstract

The routine health monitoring of living organisms and environment has become one of the major concerns of public interest. Therefore, there has been an increasing demand for fast and easy to perform monitoring technologies. The current available analytical techniques generally offer accurate and precise results; however, they often require clean samples and sophisticated equipment. Thus, they are not suitable for on site, real-time, cost-effective routine monitoring. To this end, biosensors represent suitable analytical alternative tools. Biosensors are analytical devices integrating a biological recognition element (i.e. antibody, receptor, cell) and a transducer able to convert the biological response into an easily measurable analytical signal. These tools can easily quantify an analyte or a class of analytes of interest even in a complex matrix, like clinical or environmental samples, thanks to the specificity of the biological components. Whole-cell biosensors among others offer unique features such as low cost of production and provide comprehensive functional information (i.e. detection of unclassified compounds and synergistic effects, information about the bioavailable concentration).

During this PhD, several bioengineered whole-cell biosensors have been developed and optimized for environmental and point-of-care applications. Analytical performance of biosensors have been improved (i.e. low limit of detection, faster response time and wider dynamic range) thanks to synthetic biology and genetic engineering tools.

Bacterial, yeast and 3D cell cultures of mammalian cell lines have been tailored at the molecular level to improve robustness and predictivity. Several reporter genes, i.e., colorimetric, fluorescent and bioluminescent proteins, have been also profiled for finding the best candidate for each point-of-need application. Furthermore, spectral resolution of different optical reporter proteins has been exploited and multiplex detection has been achieved. The inclusion of viability control strains provided a suitable tool for assessing non-specific effects on cell viability, correcting the analytical signal and increasing the analytical performance of ready-to-use cartridges with immobilized whole-cell biosensors.

In chapter 3, different reporter genes (fluorescent, bioluminescent and colorimetric) have been compared in both whole-cell and cell-free biosensors for mercury and quorum sensing molecule detection. Bioluminescent NanoLuc luciferase provideed the lowest limits of detection ≤ 50.0 fM $HgCl_2$ for the mercury biosensors and ≤ 0.38 pM for the signaling molecule 3-oxo-hexanoyl-homoserine lactone ($3OC_6HSL$) for quorum sensing, in fastest response time, 30 min.

In chapter 4 and 5, bioluminescent yeast biosensors for on-field application have been developed for the identification and quantification of (anti)estrogen-like compounds. A limit of detection of 1.08 ± 0.02 nM and 0.015 ± 0.001 nM have been obtained for hERα and hERβ, respectively, with an incubation time of 5 min. While, the best responses were obtained with 30 min of incubation time, showing a limit of detection of 0.016 ± 0.001 nM and 0.0011 ± 0.0002 nM for hERα and hERβ.

Biosensors robustness improvement was addressed in in chapter 5, with the implementation of a chimeric green-emitting luciferase (PLG2) as viability control. 3D printed devices based on Go-Pro Hero 5 camera (chapter 4) and OnePlus 5 smartphone (chapter 5) detection have been also implemented alongside a new straightforward whole-cell immobilization procedure.

In chapter 6, a whole-cell biosensor for (anti)inflammatory activity (NF-κB mediated) monitoring was developed based on genetically engineered 3D cell culture of human embryonic kidney cells. The reproducibility of mammalian cell biosensors was increased with a green-emitting luciferase as internal viability control; while NF-κB mediated activity was monitored with red-emitting luciferase. In optimized conditions, the biosensor gives a LOD of 0.15 ±0.05 ng/mL with TNFα as model analyte.

Index

1

Introduction

Adapted from: “Smartphone-Based Cell Detection”
Maria Maddalena Calabretta, Laura Montali, Antonia Lopreside, Aldo Roda, Elisa Michelini
Handbook of Cell Biosensors. 2019.

Adapted from: “Live Cell Immobilization”
Antonia Lopreside, Maria Maddalena Calabretta, Laura Montali, Aldo Roda, Elisa Michelini
Handbook of Cell Biosensors. 2019.

1.1 Biosensors

Biosensors are analytical devices that combine a biological recognition element with a transducer [1]. The combination of the transducer with the specificity and selectivity of the biological system offers a unique tool for the generation of a digital signal without any need of sample preparation. Thanks to this close connection, biosensors can be used for several analytical applications. During the last decades, multidisciplinary studies have been made, resulting in several different combination between biological recognition elements and transducers. Among others, antibodies, receptors, enzymes, aptamers and cells are the most commonly used biological recognition elements. While, electrochemical and optical signal are usually generated by the interaction between sample and biological recognition elements [2-6].

A schematic representation of a biosensor is shown in Fig.1:

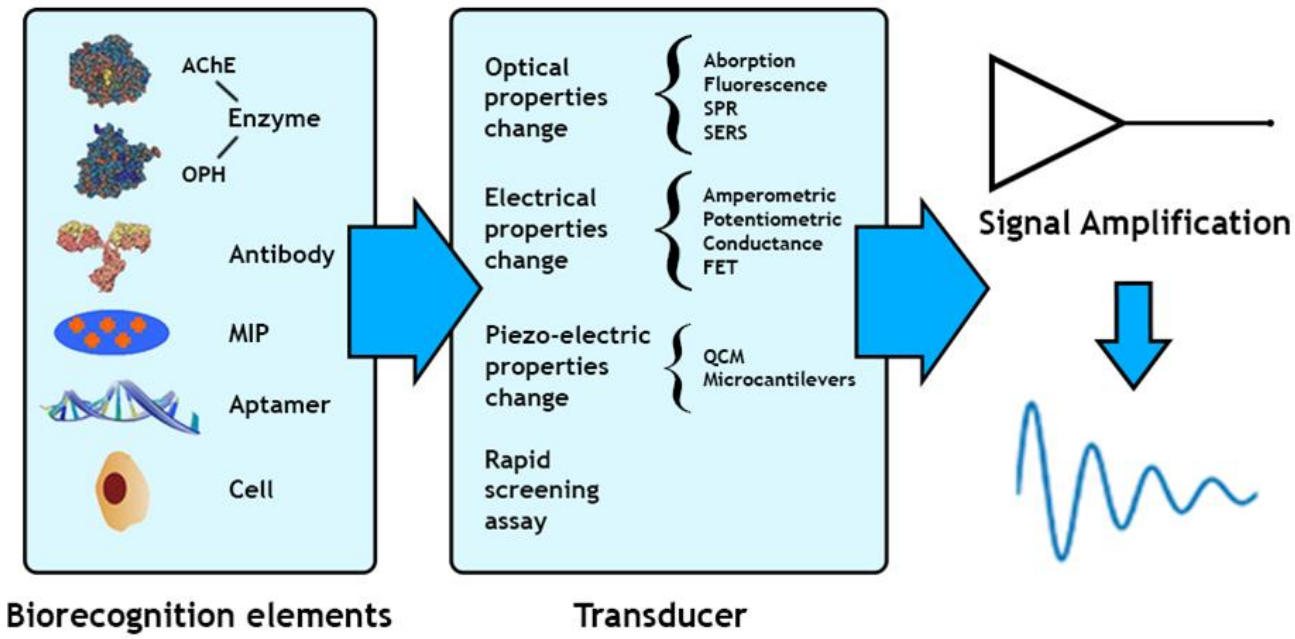

Fig. 1: Schematic representation of a biosensor with some examples of the most used biorecognition elements (i.e. enzyme, antibody, MIP, aptamer, cell) and transducers (i.e. optical, electrochemical). [3]

The ideal biosensor should fulfil the following characteristics:

- Robustness in different environmental applications;
- Miniaturization;
- Enable long-term storage;
- Short response time;
- Multiplexing detection;
- Low cost of production;
- Reusability.

All biological recognition elements allow high selectivity for the analyte among a matrix of other chemical and biological components as they are the results of naturally selective evolution processes. Despite this, some recognition elements are preferred over others depending on the application [7].

Enzyme-based biosensors are the most used and widely studied biosensors. They are usually easy to be produced, cheap and sensitive. These biosensors can be also coupled with different transducers, as they are able to produce a variety of different quantitative dose-dependent signals like light, heat, electrons or protons. In particular, enzyme-based biosensors for glucose and urease detection are largely used, due to the need for glucose/urea monitoring for medical and environmental applications [7-8].

Several glucose biosensors have been produced over the years and until now they cover the majority of the biosensors' world market. Nevertheless, a few modifications have been made from the first prototype with efforts for the development of implantable biosensors for non-invasive and continuous monitoring of glucose level in the blood of diabetic patients [9].

Nowadays, most glucose biosensors use as recognition element the glucose oxidase, which catalyses the oxidation of glucose to gluconolactone with the production of H_2O_2.

Prussian blue and inorganic redox couples are also the most commonly used electrochemical mediators for H_2O_2 detection, as shown in the figure below (Fig.2) [7,10].

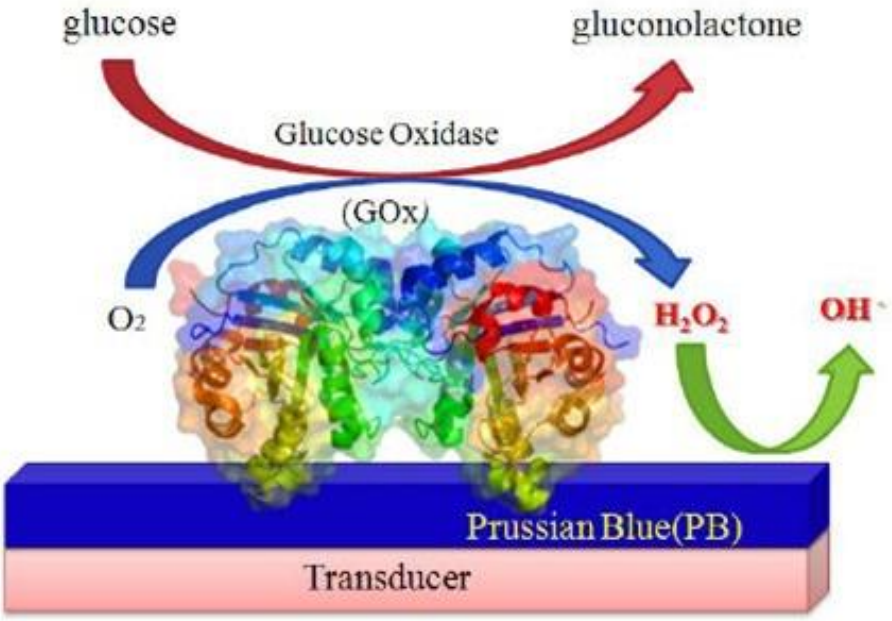

$$\text{glucose} + O_2 \xrightarrow{\text{Gox}} \text{gluconolactone} + H_2O_2$$

$$(PW)\ Fe_4K_4[Fe(CN)_6]_3 + 2H_2O_2 \longrightarrow (PB)\ Fe_4[Fe(CN)_6]_3 + 4OH^- + 4K^+$$

Fig. 2: Schematic representation of enzyme-base glucose biosensor [10].

Another important class of biosensors use antibody as biological recognition elements and are called immunosensors. These biosensors are highly valuable in those situations in which there is the need to detect ultra-low concentrations of analyte. Indeed, the high specificity and sensitivity of the interaction between antigen and antibody is the main advantage of this class of biosensors. They are ideal for point-of-need identification of HIV, hepatitis, cardiovascular diseases and cancers biomarkers because of their low concentration in clinical samples. Furthermore, they are widely used for detecting toxins, explosives, pesticides' residues and other micropollutants in environmental and food samples.

Thanks to recent advances in molecular biology, new and more stable antibodies and nanobodies can be easily produced, leading to more and more applications for immunosensors (as can be seen in Tab.1) [11-13].

Tab 1. Examples of immunosensors applications [12-34].

Analyte	Detection Techniques	Detection Limits (LOD)	Detection Time/ Reference
Avian influenza virus (AIV)	Impedimetric	10^3 EID_{50} mL^{-1}	2h [14]
Avian influenza virus (AIV)	Fluorescence	3 ng μL^{-1} H_5N_1	[15]
Avian influenza virus (AIV)	Bulk acoustic waves (BAW)	0.0128 HA unit	2h [16]
Avian metapneumovirus	Conductometric	10^2 $TCID_{50}$ mL^{-1}	2 h [17]
Bovine viral diarrhea virus (BVDV)	Conductometric	10^3 CCID mL^{-1}	8 min [18]
Phenyl urea herbicide-Diuron	Electrochemical SWV	4.0 pM	[19]
Atrazine	Conductometry	0.16 µM	[20]
Dengue virus	Voltammetric	0.33 ng mL^{-1}	[21]
Japanese encephalitis virus (JEV)	Impedimetric	0.75 µg mL^{-1}	20 min [22]
Rabies virus	Impedimetric	0.5 µg mL^{-1}	[23]
Rabies virus	SPR	~ 70 pg mL^{-1}	[24]
Picloram	Electrochemical CA	5.0 ng mL^{-1}	[25]
Aflatoxin B1	absorbance detection	5 µg kg^{-1}	[26]
Aflatoxin M1	electrochemiluminescence	0.3 pg mL^{-1}	[27]
Ochratoxin A	Amperometric	0.11 ng L^{-1}	[28]
Deoxynivalenol	Chemiluminescence	10–7 mg L^{-1}	[29]
Bovine viral diarrhea virus (BVDV)	Light scattering	10 $TCID_{50}$ mL^{-1}	5 min [30]
Feline calicivirus virus (FCV)	Surface plasmon resonance (SPR)	10^4 $TCID_{50}$ mL^{-1}	15 min [31]
Feline calicivirus virus (FCV)	Fluorescence	1.6×10^5 PFU mL^{-1}	[32]
Somatotropin	Surface plasmon resonance (SPR)	0.0034 µM	[33]
C-reactive protein (CRP)	Surface plasmon resonance (SPR)	3 ng mL^{-1}	[34]

A variety of signal transduction, both optical and electrochemical, have been coupled with immunosensors, but colorimetric and chemiluminescent based detection are until now the most used.

Indeed, the high catalytic capability of enzymes leads to a signal amplification and increased sensitivity of the assay.

In the last few years, a new class of biosensors is becoming more popular especially for the identification of small molecules, the aptamer-based biosensors. Aptamers are short, 3D-folded single strand nucleic acids (i.e. DNA, RNA and PNA) that are able to recognize an antigen by their conformation. Thanks to their self-annealing properties, they are more stable than antibodies. An aptamer specific towards an analyte is obtained by an in vitro artificial selection process called SELEX (Systematic Evolution of Ligands by Exponential enrichment) leading to a potentially unlimited range of applications (Fig. 3). Although, they cannot be used for the identification of low concentrated molecules as their specificity and selectivity for the analyte are still not competitive with those obtained with antigen-antibody interaction [35-37].

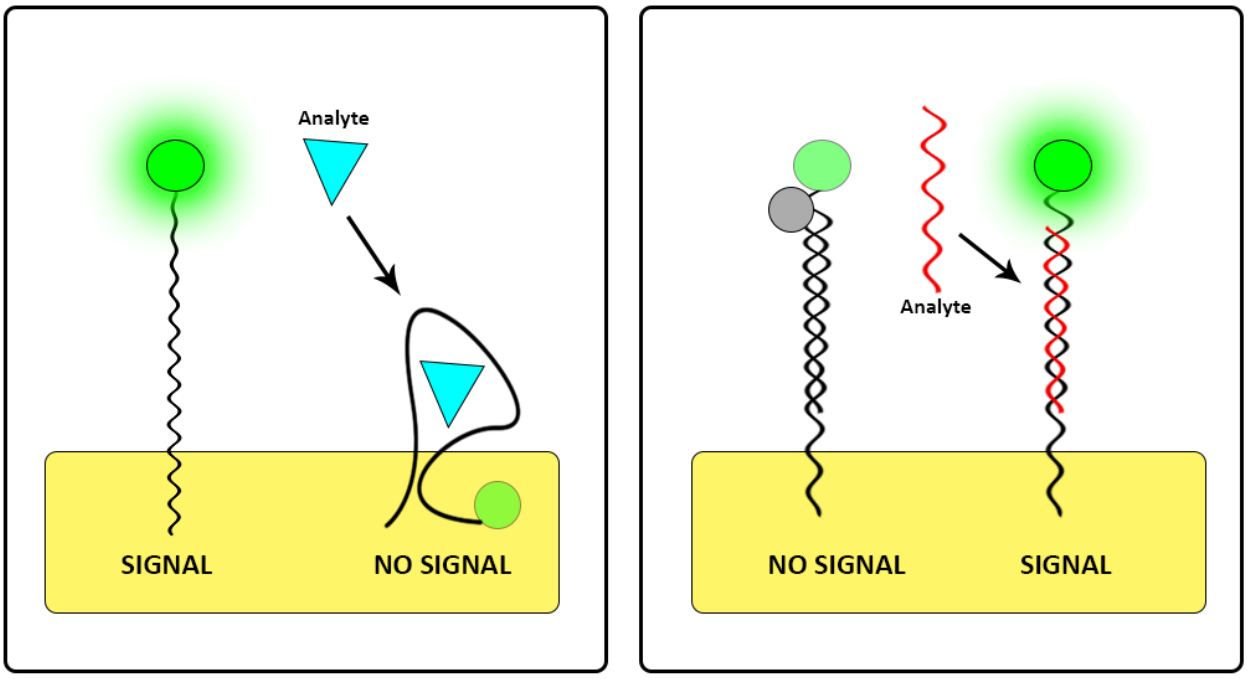

Fig. 3: Schematic representation of aptamer-based biosensors

Aptamers -based biosensors are appearing as highly promising biosensors for the identification of specific DNA/RNA sequences. These biosensors have great potential applications for sensitive early detection of several pathologies like cancer and genetic related diseases, for example those related with mutations in small non-coding miRNA and mRNA (Fig. 3) [37].

The emerging ability to control new materials at nanometric length scale is triggering the development of new biosensor classes, i.e., implantable nano-biosensors for continuous, in vivo, non-invasive detection [38]. However, the applicability of this type of biosensor has still some limitations due to the expensive cost of production and short useable lifetime.

1.1.1 Whole-Cell based Biosensors

Whole-cell biosensors, relying on living cells as sensing elements, possess unique advantages compared to other biosensors [39-40]. Some of the main advantages of the whole-cell-based biosensors are here summarized:

- Versatility (cells can be engineered to express biorecognition element for several classes of analytes, even more than one in the same cell);
- They measure the bioavailable fraction (the fraction of analyte able to enter into live cells and activate specific signalling pathways);
- They provide information about general toxicity;
- They provide information about synergic effects (nonlinear cumulative effects of two or more analytes able to interact with the same cell pathway, or converging pathways, leading to an increased biological outcome);
- They provide comprehensive functional information about pharmacology, toxicology, and physiology;
- High sensitivity due to intracellular transcriptional and translational cascade mechanism;
- Higher predictivity of human effects.

Over the years, several comparisons have been made between the performance of whole - cell biosensors and other standard analytical techniques. In many cases, some divergences have been found between the response of the different analytical methods, as it is shown in the figure below for phenanthrene identification using whole-cell biosensors and High-Performance Liquid Chromatography (HPLC) (Fig. 4) [40-41].

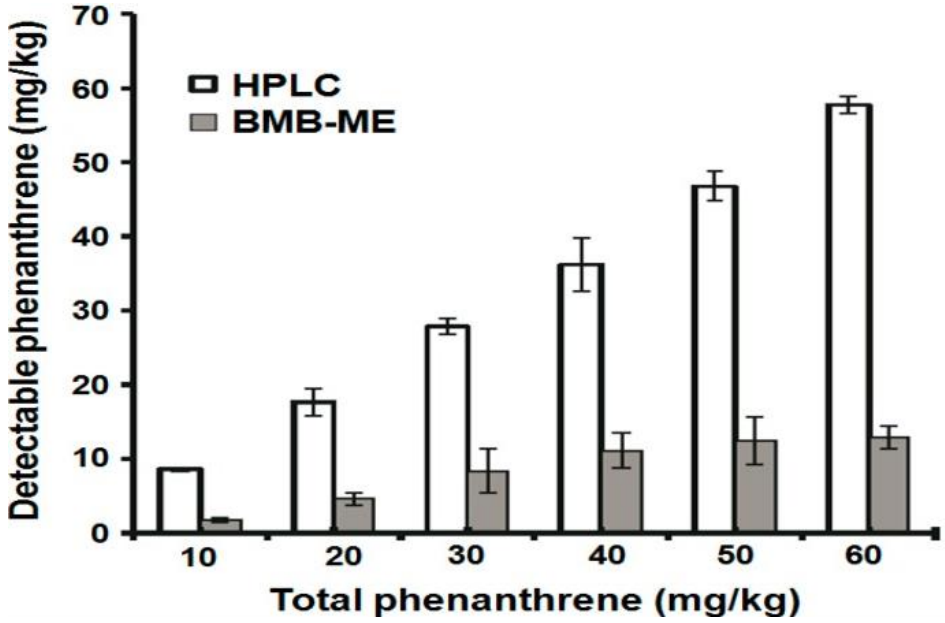

Fig. 4: Comparison of phenanthrene identification with whole-cell biosensor and HPLC [40-41]. Reproduced by permission of the MDPI (https://www.mdpi.com/1424-8220/17/7/1623)

Bacteria, yeast and mammalian cell lines have been widely used for whole-cell biosensors application. Each cell line shown its own advantages and disadvantages.

Naturally bioluminescent microorganisms (i.e. *V. fischeri)* have been the first whole-cell biosensors reporter to data as they can be easily cultivated and integrated with the transducers. Yeast based biosensors offer the same advantages of bacterial biosensors combined with an increased predictivity; due to the higher degree of conservation of cellular processes and molecular pathways with human cells. Mammalian cell lines are highly valuable when predictive information about bioactivity or toxicity to humans, is required.

However, their implementation in biosensors is less common as they have several disadvantages compared with yeast and bacterial cell. Mammalian cell lines are characterized by slow growth, requirement for cell culture facilities and their viability is highly affected by external factors. While microbial cells offer specificity and robustness, mammalian cells provide more predictive results [42].

Tab 2. Examples of whole-cell biosensors for different analytical applications [43-59].

Analyte	Host cell	Detection Techniques	Detection Limits (LOD)	Detection Time/ Reference
Cadmium	*Chlorella vulgaris*	Conductimetric	1ppb	30 min [43]
Bioavailable Arsenic	*E. coli*	Bioluminescence	0.012mg L^{-1}	30 min [44]
Methyl parathion	*Flavobacterium*	Spectrophotometry	0.3µM	3 min [45]
Acrylamide	*Pseudomonas aeruginosa*	Amidase activity	4.48x10^{-5}M	55 sec [46]
Naphthalene in air	*Pseudomonas fluorescens*	Bioluminescence	20nmol L^{-1}	[47]
Biochemical oxygen demand (BOD)	*Bacillus subtilis*	Bioluminescence	25 mg L^{-1}	[48]
Biochemical oxygen demand (BOD)	*Microbial consortium*	Clark oxygen electrode	1 mg L^{-1}	[49]
Biochemical oxygen demand (BOD)	*Pseudomonas putida*	Fluorescence	0.5 mg L^{-1}	[50]
Copper ions	*S. cerevisiae*	Colorimetric	0.0067mg L^{-1}	[51]
3,5-Dichlorophenol	*V. fischer*	Bioluminescent	30–100 mg L^{-1}	[52]
Arsenite	*Rhodovulum sulfidophilum*	Colorimetric	3 µg L^{-1}	[53]
Surfactants	*Achromobacter*	Amperometric	0.25 mg L^{-1}	[54]
LAS	*Trichosporon cutaneum*	Amperometric	0.2 mg L^{-1}	[55]
Mercury arsenite	*Pseudomonas fluorescens*	Bioluminescent	0.003 µg kg^{-1}	[56]
Cupric ions	*Circinella spp.*	Voltammetric	0.0034mg L^{-1}	[57]

Whole-cell-based biosensors thanks to genetic engineering and reporter gene technologies can be tuned to detect a wider range of analytes for medical and environmental applications. Using these approaches, several whole-cell-biosensors have been developed that can detect heavy metals, organic xenobiotic, toxins and other biomarkers (tab.2) [43-59].

The well-known unsolved problems of whole-cell biosensors are related to their limited portability and scarce shelf-life due to the difficulty of keeping cells alive and responsive for long periods of time. The goal is to obtain cells in a ready-to-use format, in which cells can be stored for a long period of time (at least months) under controlled conditions and, once activated (i.e. by a defined temperature change or addition of nutrients), a constant and reproducible number of viable cells can be revitalized [60].

1.2 Synthetic Biology for biosensing

Synthetic Biology is a new interdisciplinary field that enables to (re-)design and optimize biological components by completely artificial or nature inspired approaches. In particular, two different approaches, a top-down and a bottom-up, are usually considered [61-62]. The top-down synthetic biology approach is more spread and widely accepted, as it is based on the well-established technology of genetic engineering. In this approach a protein/ biological pathway responsible for a specific response is transferred into a different host providing it with new functions and capabilities. This approach has completely changed whole-cell biosensor development by providing new and powerful tools in several fields, spanning from biosensing, to diagnostics, bioremediation and therapeutics. Rewriting a genetics circuit is highly valuable on the biosensor field as it combines the advantages of both the components, i.e., the donor strain from which genetic circuits are used and the recipient host strain. Indeed, during the last years, more robust host cells like prokaryotes or unicellular eukaryotes have been selected as chasses for human or mammalian complex cell pathway expression [63-64].

These new developed biosensors are more robust and predictive leading to less false negative and false positive response.

They are also more resistant to sample toxicity and easier to manipulate for on-field applications [65]. Another important advantage, in particular for diagnostic applications, is the absence of crosstalk between the endogenous systems present in the chassis and the introduced synthetic systems [61,66-67].

Different biological components have been also integrated into the same cell allowing them not only to respond to different specific externa stimuli, but also to integrate more signals and perform logic operations. [68] Recently, a more specific signal amplification has also been performed through the design of artificial synthetic cascade inside a cell (Fig. 5) [68-69].

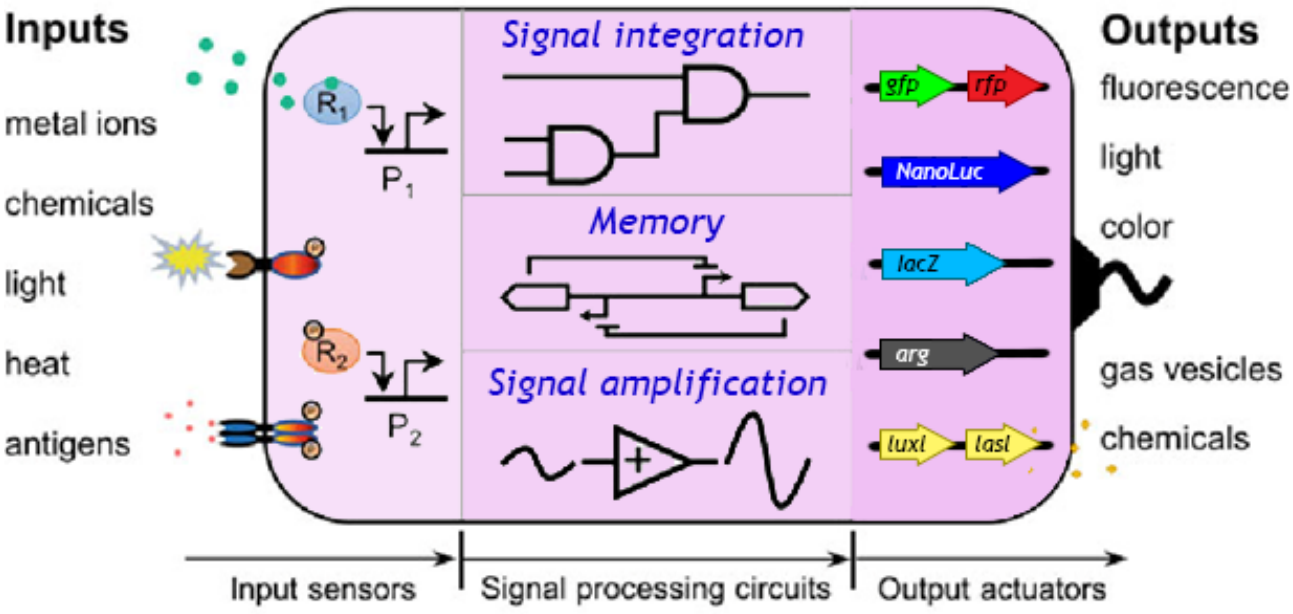

Fig. 5: Schematic representation of different synthetic biology top down-approaches for biosensors applications [68].

Several genes of the host organism can also be deleted in order to obtain a living organism with a minimum set of gene, reduce the host pathogenicity, or prevent the cell grow. In particular, the introduction of self-killing pathways could be an important feature in biosensor for point-of-need applications, in order to avoid spreading of genetically modified organisms into the environment.

The synthetic biology bottom-up approach is based on the possibility to generate a living cell from the basic components. In particular, one approach is trying to put together only the necessary genes for a new, completely synthetic, living -cell able to grow, perform fixed task and even duplicate.

Another approach relies on the possibility to introduce all the necessary proteins to perform *in vitro* transcription and translation, as response of a precise input. These systems are call transcription-translation systems (TX-TL systems) (Fig. 6) [70-71].

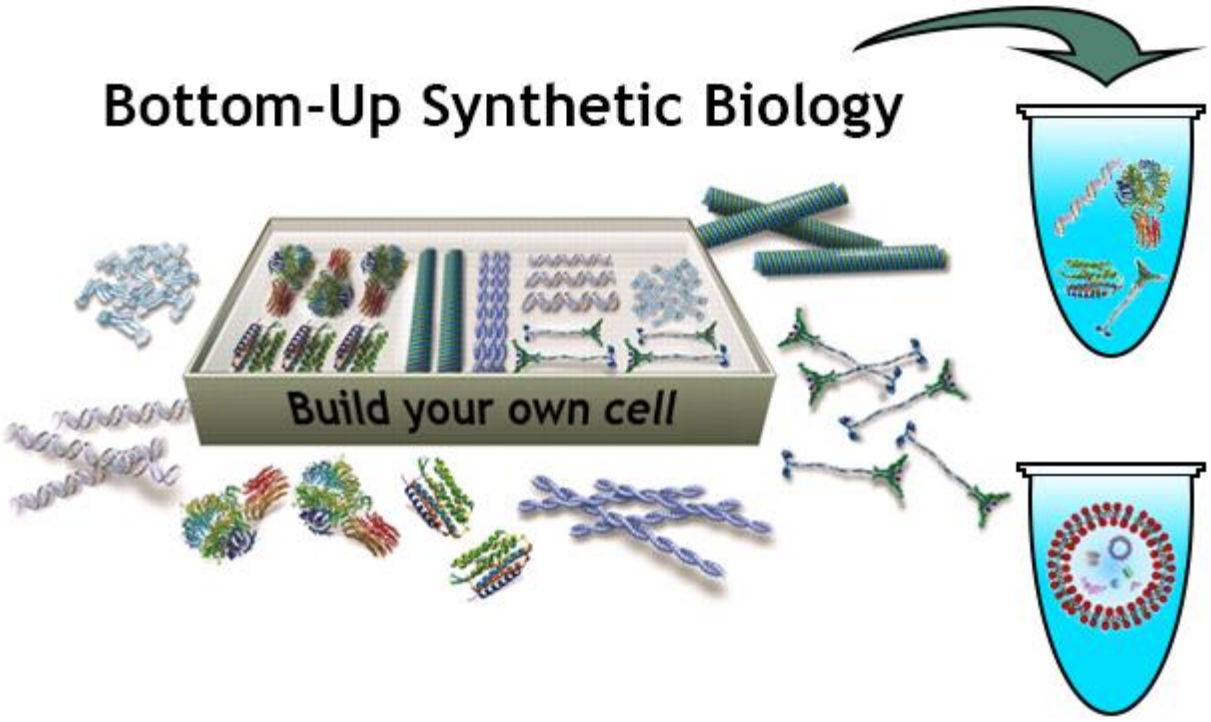

Fig. 6: Schematic representation of synthetic biology bottom-up approaches for biosensors applications [70]

For biosensing applications, the new developed TX-TL systems offers a unique opportunity for analyte detection, particularly for on-field application. It's high predictive like whole-cell biosensors, but it's abiotic, can be lyophilized and stored for long time even at room temperature.

They do not have cell walls, that could be a problem if we want to identify the bioavailable concentration, but it offers a direct access to the inner workings of the cell [72-73].

1.3 Optical reporter genes

A reporter gene is a gene whose activity is easily distinguished, measured and quantified over a background of endogenous proteins [74]. Reporter genes have been often used as markers for gene expression, for monitoring signal transduction pathways and regulation of translational efficiency in a cell or transgenic organism (Fig.7).

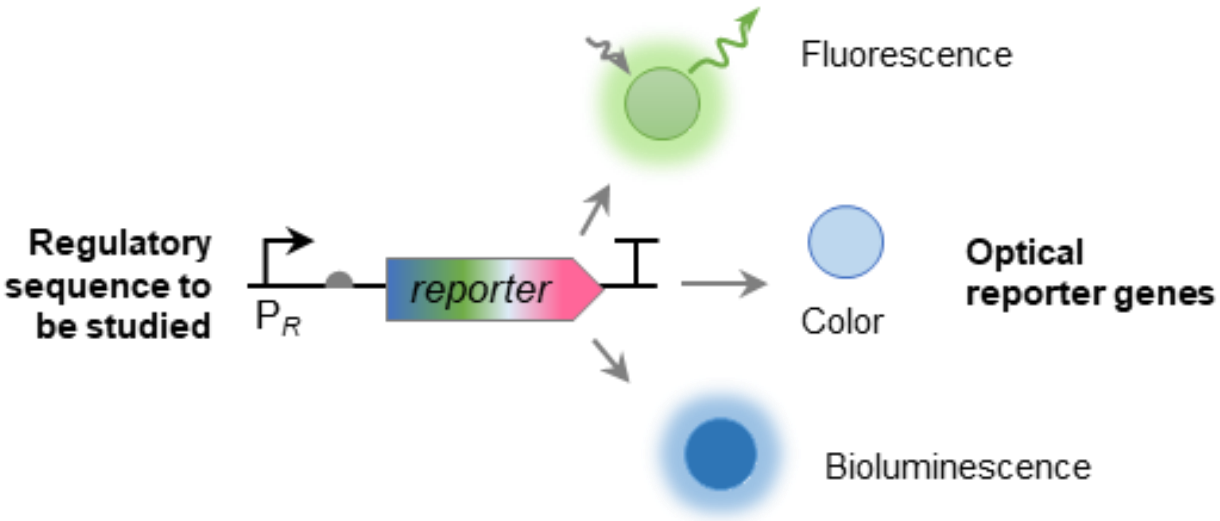

Fig. 7: Schematic representation of reporter gene technology uses for monitoring of cis-regulatory sequence.

Thanks to genetic engineering the sequence of a reporter gene can be easily fused to the protein of interest or its enhancer/cis-regulatory sequences providing an efficient tool for direct/indirect gene monitoring [75-76]. Several applications for this technology have been developed, such as continuous real-time monitoring of endogenous gene expression in specific cell or tissues, for monitoring of real-time response for diseases treatment, for in-vivo monitoring of cell migration and drug delivery [77-81].

During the last years, several inducible promoters have been easily tailored to respond to specific analytes with several reporter genes for whole-cell biosensing applications.

Thanks to their high sensitivity, optical reporter proteins are the most used reporter genes in whole-cell biosensors (i.e. colorimetric, fluorescent and bioluminescent). Each class of optical reporter genes has its own pros and cons [82]. In particular, fluorescent reporter genes need an external light source for signal detection, while colorimetric and bioluminescent reporters need the addition of a substrate. Furthermore, bioluminescent reporters show higher quantum yield emission and lower signal to noise ratio, due to almost zero background even in complex matrix and in living organisms.

However, the substrate required for the bioluminescent reaction is generally not stable at room temperature for long periods of time [83-85].

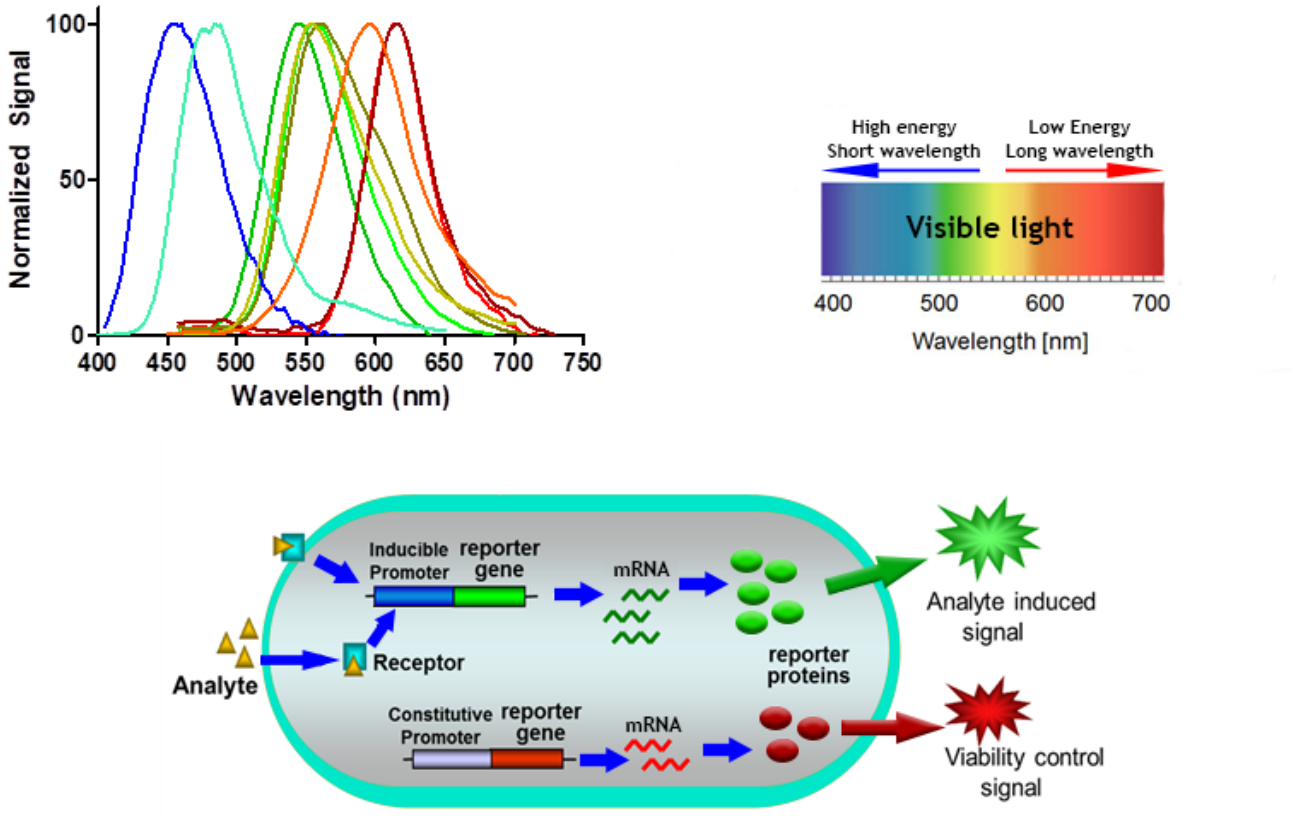

Fig. 8: Emission spectra of different bioluminescent reporters and example of a whole-cell biosensor having two reporters: one specific for the analyte and one used as internal viability control.

The main limitations of reporter gene-based biosensors are the long assay time (several hours), which is required for the expression of the reporter protein, and scarce robustness due to changes of cell's viability. In fact, non-specific effects of sample or matrix, or changes in temperature and pH, may lead to altered viability, thus affecting the analytical signal. To this end luciferases and fluorescent reporter genes emitting at different wavelengths can be used to improve robustness by addition of an internal viability control. To separate the bioluminescent signals spectral resolution by use of suitable optical fields can be exploited. [86-87] (Fig. 8).

Another critical issue related to bioluminescence detection is the low level of light emitted by the cells which necessarily requires highly sensitive light detectors [88].

1.3.1 Bioluminescence

Bioluminescence is the naturally occurring process through which living organisms are able to emit light. The light emitted in the bioluminescent reaction is a cold light (less than 20% of the light generates thermal radiation or heat) and it is the result of an undergoing radiative decay of an excited intermediate. In bioluminescence, unlike other luminescent processes such us fluorescence, the electronic excited state is not photoinduced, but is rather the product of a chemical reaction catalysed by an enzyme, generally called luciferase [89]. In theory, one photon of light should be given off for each molecule of reactant, this is equivalent to Avogadro's number of photons per mole of reactant. In actual practice, direct chemical reactions seldom exceed a quantum yield of 10^{-3}-10^{-2}, while the bioluminescent reaction catalysed by the *Photinus pyralis* luciferase showed the highest quantum yield emission efficiency reported (i.e. 0.41 ± 0.074) [90-93].

This turns to be of great advantage for detecting analytes present at very low concentrations or when miniaturization for developing lab-on-a-chip platforms is required [94-95].

A large variety of marine and terrestrial organisms (bacteria, fungi, fish, insects, worms) express bioluminescent proteins, that are very different according to their evolutionary functions, reaction mechanisms, substrates used and bioluminescent properties (Fig. 9).

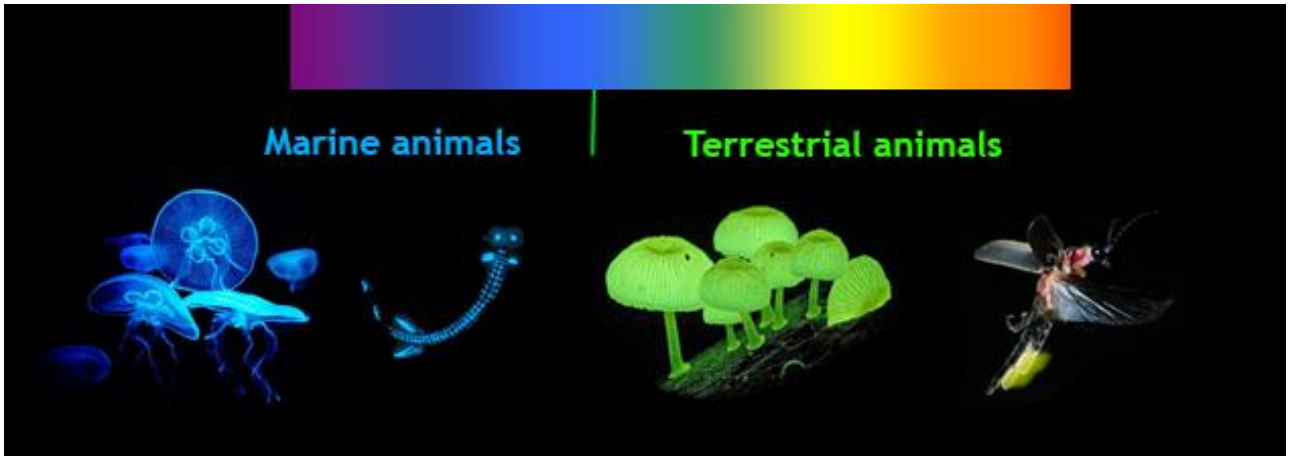

Fig. 9: Examples of naturally bioluminescent emitting organisms. From left to right*: Aequorea victoria, Bathophilus digitatus, Agaricus gardneri* and *Photinus pyralis*.

Interestingly, the BL emission spectra of naturally occurring BL systems cover all the visible range between 400 nm and 650 nm, while all bioluminescent substrates studied till now share the same luminophore: a peroxide bond –O–O– [96-97].

The most common biological functions of BL are: counterillumination camouflage, attraction, defense, warning, communication and mimicry. The naturally bioluminescent proteins can be grouped into two major categories: photoproteins and luciferases. Luciferases like firefly luciferase and click beetle luciferase catalyze oxidation of D-luciferin in the presence of ATP, Mg^{2+} and molecular oxygen (O_2). As it shown in figure 10, adenylation of luciferin is followed by, cyclization, and decarboxylation of the adenyl-luciferin complex, resulting in the emission of CO_2 and light [98-99]. Photoproteins such as *Aequorea victoria's* aequorin are calcium-regulated proteins in which light emission is initiated by upon calcium binding [100].

Although more than 30 kinds of luciferases have been identified in nature, there are only 9 natural luciferins reported up to date.

Firefly luciferase is the most common luciferase used in bioanalytical applications; it emits yellow-green light (λ_{em} = 557 nm at pH 7.8) with glow-type kinetics and a broad emission band.

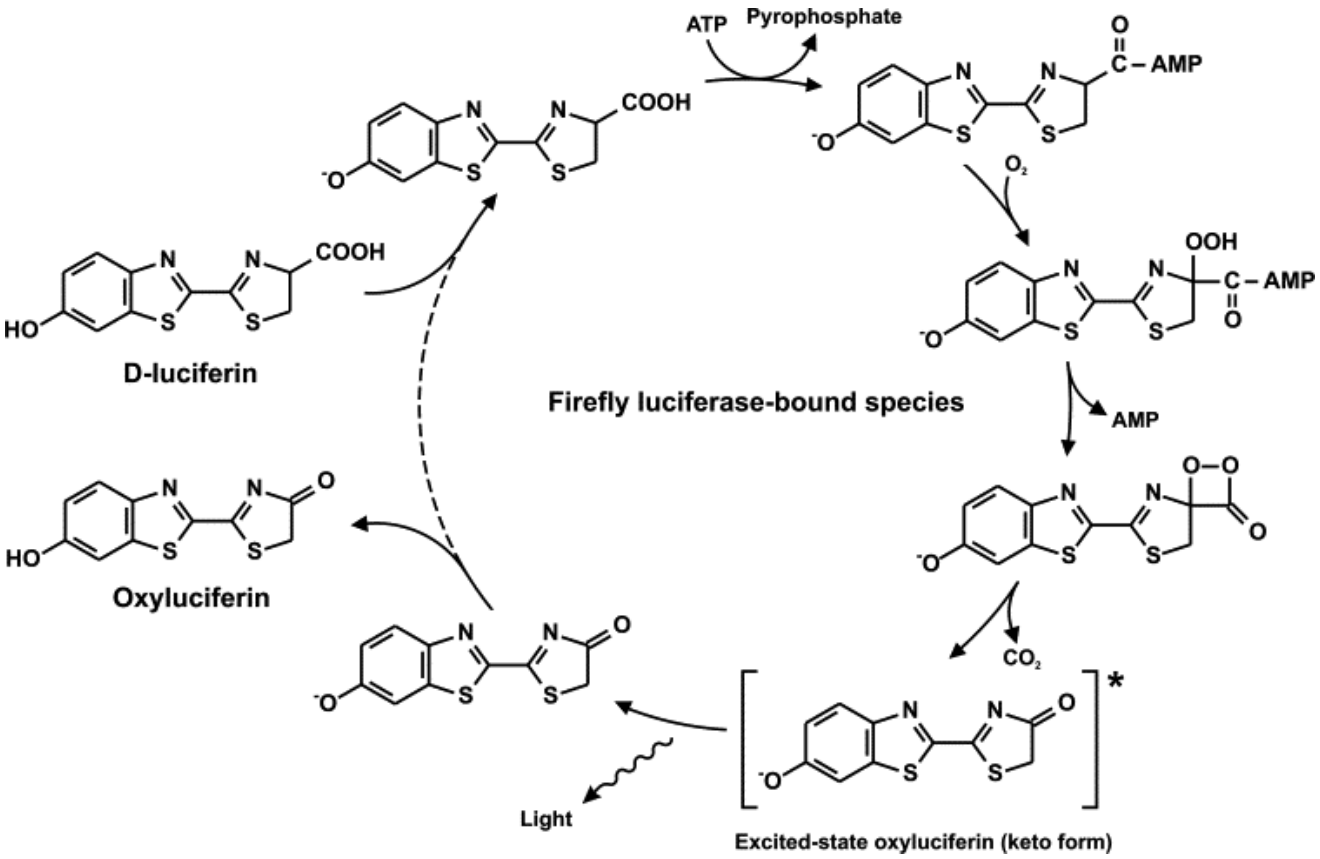

Fig. 10: Luciferase-catalyzed oxidation of D-luciferin [97]

Among luciferases, *Photinus pyralis* luciferase (PpyLuc) is by far the most investigated and employed in bioanalytical applications and biosensors development.[101-102] PpyLuc is a 61-kDa monomeric protein that does not require any post-translational modifications and it does not show any toxicity to cells even at high concentrations, being thus suitable for heterologous expression in both prokaryotic and eukaryotic systems.

PpyLuc bioluminescence is temperature and pH-sensitive, showing a remarkable red-shift at lower pH and higher temperatures.

Half-life of this luciferase expressed in mammalian cells was calculated to be in the range from 1 to 4 hours in the presence of protease inhibitors.

Firefly luciferin, among others, diffuses easily across biological membranes including cell membranes, the blood brain barrier and the blood placenta barrier. In particular, crossing of cell membranes is increased at low pH (e.g., 100 mM Na-citrate, pH 5.2) due to the protonation of the carboxyl group of D-luciferin [103-104]. Several studies evaluated luciferin cytotoxicity, showing no effect after 24 h [105].

D-luciferin must be stored in the dark as it is sensitive to light. It could be stored for long periods of time at -80°C and for 8-24 hours at 4°C [106].

Thanks to recent advances in genetic engineering and in silico studies, directed evolution of new semi-synthetic luciferases and luciferins have been made leading to improvement of thermostability, altered spectral emission and increased quantum yield emission [107-109].

For example, mutants emitting at 460 nm and 620 nm have been obtained changing the amino acid I288 from Isoleucine (nonpolar and neutral, MW= 131) to valine (nonpolar and neutral, MW= 117) and alanine (nonpolar and neutral, MW= 89) respectively. Because of this improvement, the luciferase reporter gene can be used for new applications, such as biosensors with multiplex capability, that allow to simultaneously measure more than one analyte. [99]

Also, multiplex detection can be performed, by exploiting spatial, temporal, spectral resolution or by selecting luciferases such us firefly and NanoLuc luciferase that require different substrates (Fig. 11) [110].

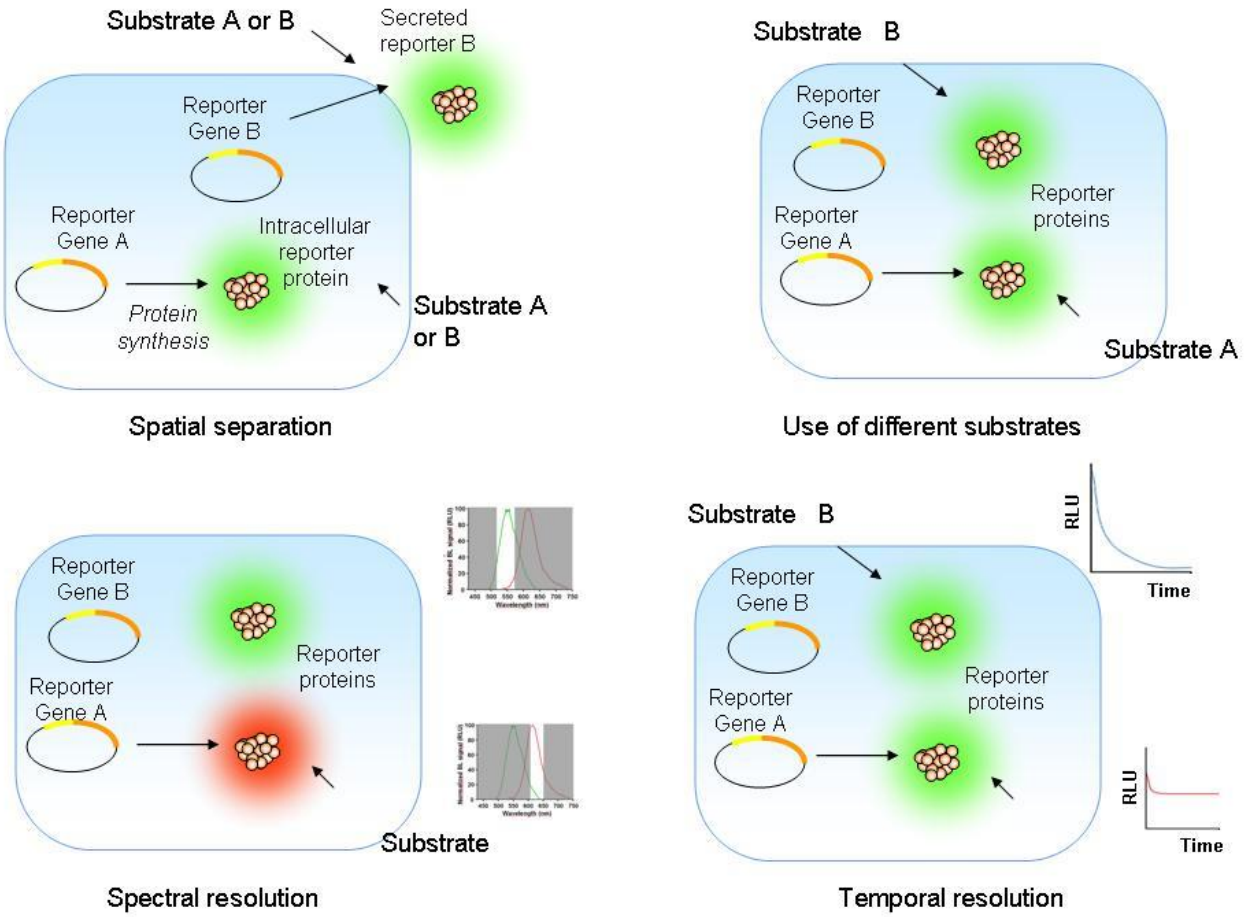

Fig. 11: Different strategies to develop multiplex cell-based assays relying on two different luciferases expressed in the same cell. [110]

Reproduced by permission of Springer Nature (License number 4697591282423).

NanoLuc luciferase is the newest semisynthetic luciferase available on market. The native luciferase from deep sea shrimp utilizes coelenterazine in an ATP-independent reaction to produce blue light (λmax= 454 nm) [111]. The native enzyme has a heteromeric stable structure consisting of two 35 kDa subunits and two 19 kDa subunits and high specific activity. Thanks to structural studies the bioluminescent activity was associated only with the smaller, but instable subunit (Oluc-19) [111-113].

Thanks to enzymatic evolution and substrate substitution the enzyme has been changed leading to a semisynthetic new enzyme with increased stability and improved bioluminescent properties.

The final enzyme results has a 10% of mutated aminoacids in comparison with the native primary structure with a brighter glow-type emission kinetics (claimed to be 150-fold brighter than firefly luciferase).

The small size of the enzyme and the absence of post translational modification enables rapid synthesis and folding of the reporter upon induction even in prokaryotic organisms (Fig. 12).

Meanwhile, the rapid protein degradation (through PEST sequence) avoids unnecessary overexpression and intracellular accumulation in cells that may lead to artefacts and toxicity [111].

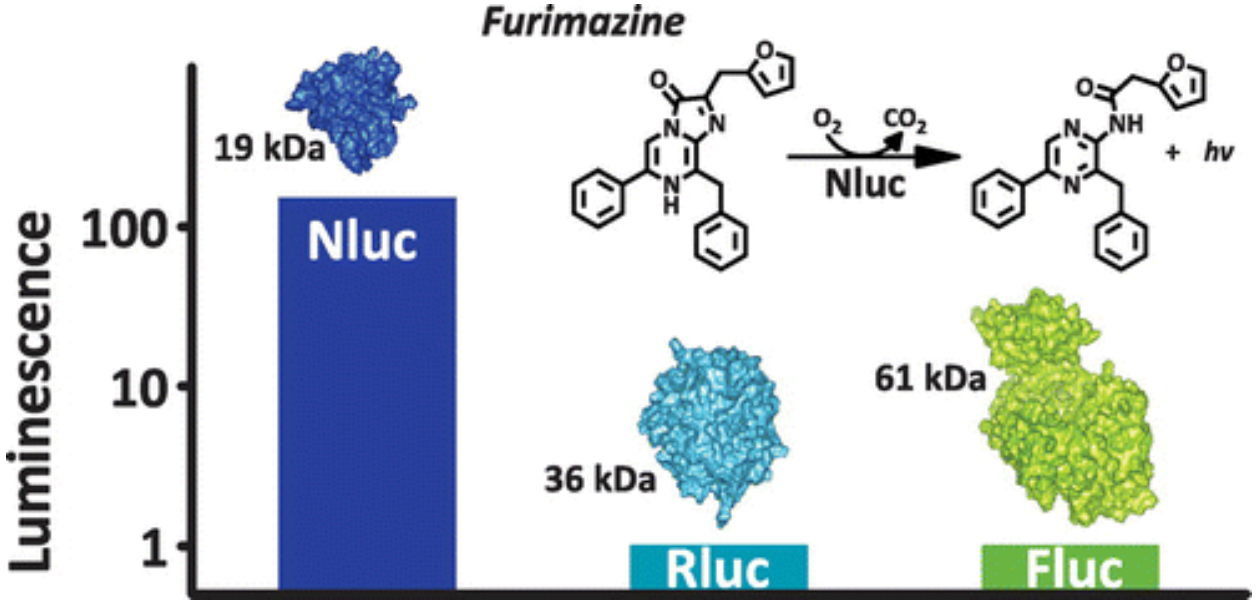

Fig. 12: Comparison between NanoLuc, Renilla and Firefly luciferase [111].

Reproduced with permission of ACS Publications (https://pubs.acs.org/doi/10.1021/cb3002478)

1.3.2 Fluorescence

Fluorescence is a luminescent phenomenon which describes the emission of photons by a compound after being illuminated with an electromagnetic radiation (i.e. visible light). (Fig.13) The first description of fluorescence occurs in 1852 by George Gabriel Stokes, when he observes the emission of visible light by calcium fluoride (CaF_2) after being irradiated by UV light [114]. Fluorescent compounds are generally classified into four categories small organic compounds, synthetic polymers, proteins and multi-component systems [115-116].

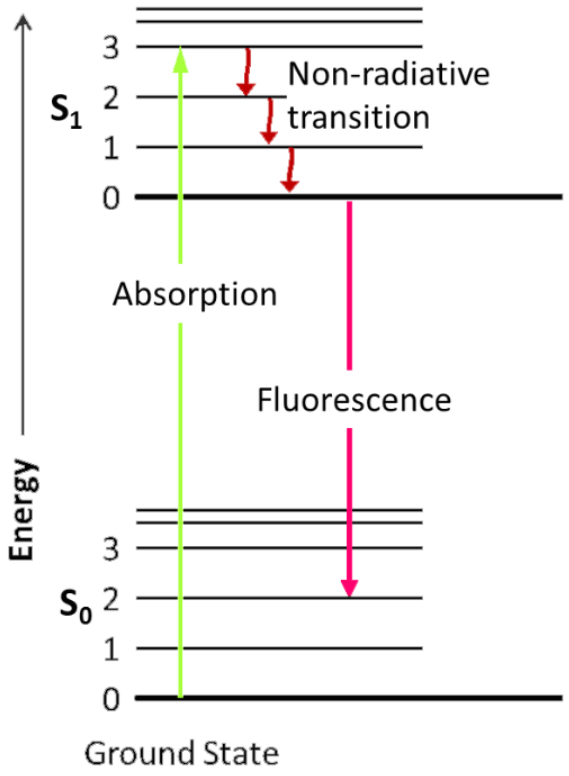

Fig. 13: Jablonski diagram [115-116].

Unlike phosphorescence, in fluorescence the electron spin is still paired with the ground state electron and the light emission stops nearly immediately when the radiation source stops (0.5 - 20 nanoseconds of lifetime) [117].

Fluorescence signal is linearly proportional to the concentration of the fluorescent molecule.

In most cases, the fluorescent emitted light has longer wavelength and therefore lower energy than the absorbed radiation. The difference between the maximum excitation and maximum emission wavelength is called Stokes shift. Different compounds showed different stokes shift and fluorescent properties. A narrower adsorption/emission band with higher Stokes shift is desirable, as it avoids the overlap of the absorption spectrum and emission spectrum (Fig.14) [118-120].

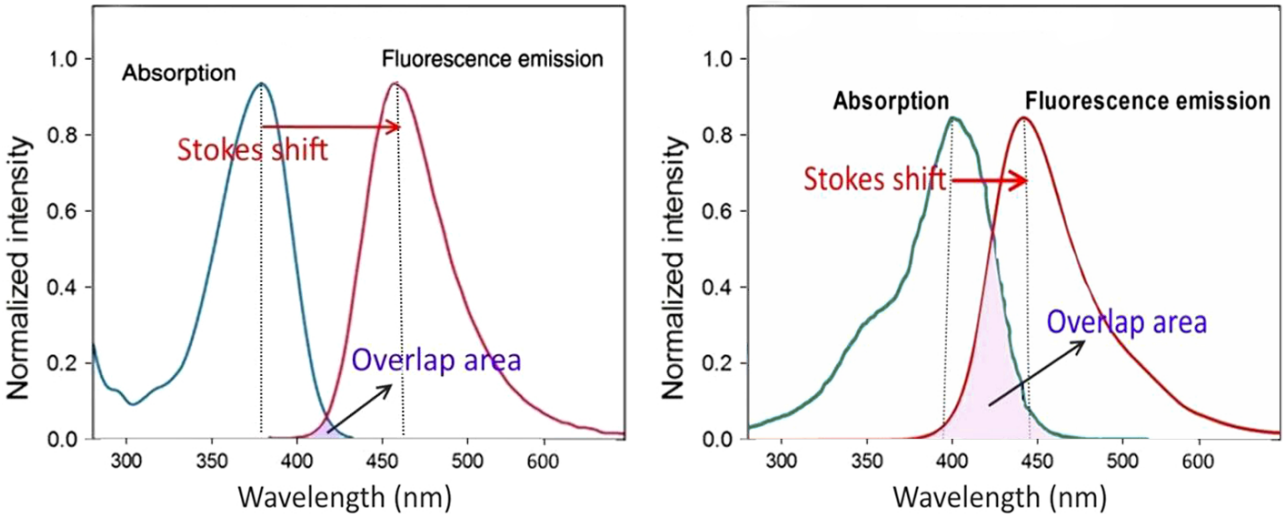

Fig. 14: Examples of different Stokes shift and overlap area between absorption and emission area [120].

Over the years, fluorescence molecules, in particular proteins and nanoparticles have been extensively used for different applications such as lamps, mineralogy studies, chemical sensors, cosmic-ray detection and biological detectors (labelling protein of interest and reporter gene technology) [121].

Several naturally fluorescent proteins have been studied and modified at the molecular level to enhance their property and expand their applications, as shown in figure above (Fig.15) [122-123]

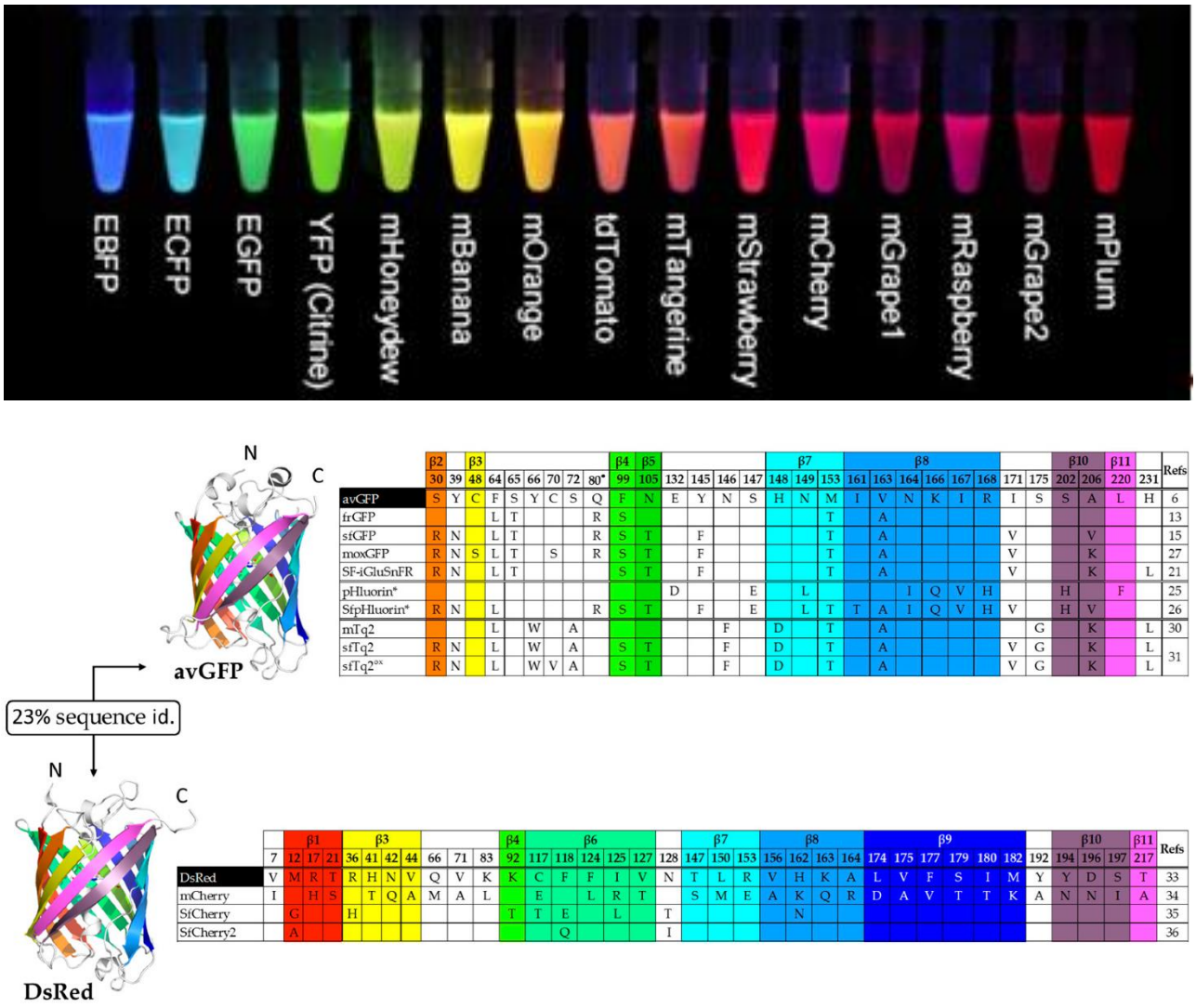

	β2		β3							β4	β5					β7			β8								β10		β11		Refs
	30	39	48	64	65	66	70	72	80*	99	105	132	145	146	147	148	149	153	161	163	164	166	167	168	171	175	202	206	220	231	
avGFP	S	Y	C	F	S	Y	C	S	Q	F	N	E	Y	N	S	H	N	M	I	V	N	K	I	R	I	S	S	A	L	H	6
frGFP				L	T				R	S								T		A											13
sfGFP	R	N		L	T				R	S	T		F					T		A					V			V			15
moxGFP	R	N	S	L	T		S		R	S	T		F					T		A					V			K			27
SF-iGluSnFR	R	N		L	T					S	T		F					T		A					V			K		L	21
pHluorin*												D			E		L				I	Q	V	H			H		F		25
SfpHluorin*	R	N		L					R	S	T		F		E		L	T	T	A	I	Q	V	H	V		H	V			26
mTq2				L		W		A						F		D		T		A						G		K		L	30
sfTq2	R	N		L		W		A		S	T			F		D		T		A					V	G		K		L	31
sfTq2^{ox}	R	N		L		W	V	A		S	T			F		D		T		A					V	G		K		L	

	β1			β3						β4		β6						β7			β8				β9								β10			β11	Refs
	7	12	17	21	36	41	42	44	66	71	83	92	117	118	124	125	127	128	147	150	153	156	162	163	164	174	175	177	179	180	182	192	194	196	197	217	
DsRed	V	M	R	T	R	H	N	V	Q	V	K	K	C	F	F	I	V	N	T	L	R	V	H	K	A	L	V	F	S	I	M	Y	Y	D	S	T	33
mCherry	I		H	S		T	Q	A	M	A	L		E		L	R	T		S	M	E	A	K	Q	R	D	A	V	T	T	K	A	N	N	I	A	34
SfCherry		G			H							T	T	E		L		T				N														35
SfCherry2		A												Q				I																			36

Fig. 15: Examples of fluorescent proteins used for reporter gene applications. Some fluorescent variants of the native proteins have been obtained with mutation of the aminoacidic structures [124-125].

1.4 Living cell Immobilization

Maintenance of cell viability and physiological cellular activity is crucial in whole-cell biosensing. To this end, several cell immobilizations approaches have been explored over the years, each one having peculiar advantages and limitations (Fig. 16). Both microbial and mammalian cells were successfully immobilized on different surfaces or entrapped into suitable matrixes, depending on the goal of the immobilization and the type of cell. When dealing with whole-cell biosensors, several factors should be taken into consideration during

cell immobilization; for example, opacity of some matrices, such as PVA, is not an issue for electrochemical biosensors while it could interfere with optical signal detection [126-127]. Nature-inspired approaches are the most promising and widely exploited techniques in cell preservation. Among the most employed matrices for cell biosensor's immobilization, three groups can be identified: ionic hydrogels, thermogels and synthetic polymers.

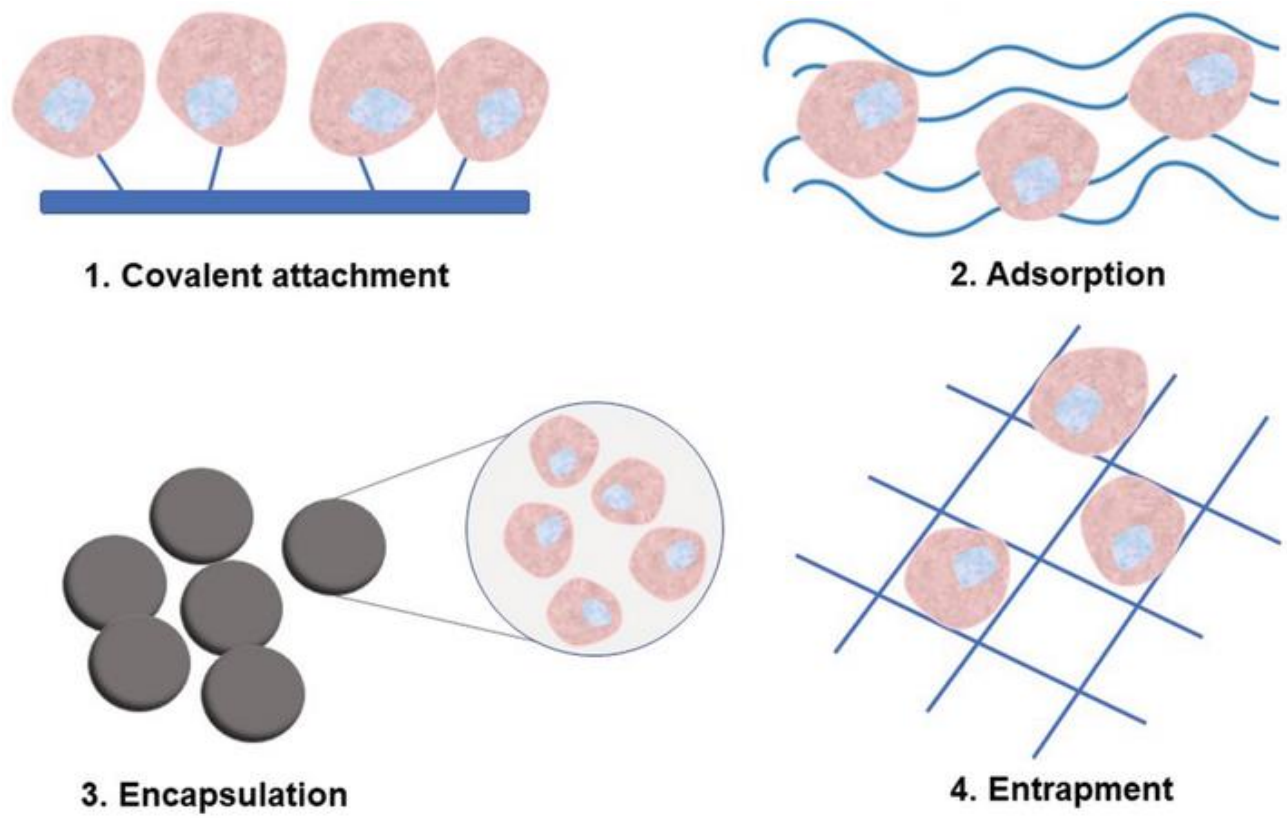

Fig. 16: Different immobilization techniques methods categories for whole-cell immobilization approaches for biosensing. [131]

Hydrogel entrapment, i.e. using agarose, acrylamide and alginate, represents the easiest and most exploited approach for cell biosensor immobilization [128-131]. In particular, bacteria and yeast entrapped into alginate beads or slices have been implemented into portable biosensing devices with intended use in remote area, showing possibility of long-term storage, low toxicity and good reproducibility [132-134]. However, several classes of positively charged surface coatings have been also employed such as polymers and

polyelectrolytes, to reduce the molecular crowding interactions between negatively charged bacteria.

One of the longest storage times for bacterial cells, up to 8 months, was achieved by spore-forming bacteria *Bacillus subtilis* and *Bacillus megaterium* for arsenic and zinc detection. Thanks to their amazing capability to survive to extreme conditions such as freezing temperatures, desiccation, dry and wet heat allowing easier storage and shipment even in remote area. Recently, spores were also exposed to extreme conditions, such us simulate Mars surface conditions, showing good survival rates [135-136].

Current trends in bacterial biosensors are focused on the achievement of fine control over cells, to enable their manipulation, thus providing a new strategy to concentrate cells and separate them from complex media before measurement of the analytical signal. This leads to a reduction of matrix effect an increased analytical performance [137].

Mammalian cell lines have several disadvantages compared with yeast and bacterial cell, however their implementation in immobilized conditions is highly valuable. Mammalian cell lines are also more effected by external factors and physico-chemical stressors. For these reasons, a suitable support is required to provide the cells not just an inert matrix for cell growth, but to confer them protection from external agents and to create of a suitable micro-environment (Tab. 3). Indeed, local concentration of cytokines and other soluble factors for paracrine signalling improves cell-to-cell communication and survival.

Over the years different materials have been exploited as matrices to optimize the immobilization of mammalian cells, and in some cases were used approaches similar to those explored for microbial cells. Among others, agarose, natural and synthetic hydrogels and gelatine are the most promising. However, the lack of optimal culture conditions during storage (i.e. temperature, humidity and CO_2) negatively affect cell metabolism and responsiveness leading to a rapid loss of their function. Up to now, the most promising strategy allows storage of mammalian cells with a 6-week viability during storage (in air, at room temperature) compared to 8 months obtained for microbial cells [138-143].

Table 3: Advantages and disadvantages of different techniques used to preserve cell viability.

PRESERVATION METHOD	ADVANTAGES	DISADVANTAGES
Freeze drying (lyophilization)	Proven industrial performance record Easily rehydrated product	Costly and complex technique Product sensitive to moisture
Vacuum drying	Yields potentially high survival rates and long-term stability Relatively low production costs Suitable alternative for freeze-sensitive microorganisms	Less well-proven performance record Harsher drying conditions than freeze drying
Encapsulation in organic polymers (e.g. hydrogels)	Provides physical shielding and isolation Allows solute diffusion	Biodegradable Bacterial growth may occur Opacity may hinder optical signal detection
Encapsulation in inorganic polymers (e.g. sol-gel)	Provides physical shielding and isolation Mechanical rigidity and good optical properties Allows solute diffusion Limits bacterial growth	Tested for a limited variety of microorganisms

1.5 3D-printing technologies

3D printing is the process of making layer-upon-layer a three-dimensional solid object from a computer-aided design (CAD). (Fig. 17) Thanks to the development of this technology combined with additive manufacturing and affordable micro/nano-fabrication technologies new supports for point-of-need biosensing are becoming available. Indeed, 3D printing enables the production of complex and well characterized shape with several materials, spanning from polymers to metals [144-145]. The easy tunability with the possibility of cheap and rapid in-house prototyping have favoured the rapid spread of this technology.

Fig. 17: 3D printer Makerbot Replicator 2X and Makerware software for 3D printing of microfabricated device.

There are different types of 3D printing depending on the mechanism by which materials are bonded together and the type of materials compatible with the technology. The most used categories for biosensors applications are photopolymerization, fused deposition modelling, powder bed fusion and material jetting [146]. The first applications of 3D printing technology for on-site biosensing have been related to the development of customized adaptor for biosensors integration into portable device using fused deposition modelling. Fused deposition technology is based on the depositing of layers of melted thermoplastic polymer such as acrylonitrile butadiene styrene (ABS) and polylactic acid (PLA). Several 3D printed devices have been made with this cheap and biocompatible polymer showing great advantages and versatility [42,146-148].

More recently, material jetting method is becoming more and more employed in this area as it allows to print multiple materials at the same time achieving unique properties in the final 3D-printed structure. This technique allows the creation of not only a simple inert scaffold but also functional material with tuneable advanced properties. Indeed, mammalian cells can be successfully deposited and directly printed onto a scaffold [149-150]. Increased storage, differentiation process and in vivo implants have been also exploited to obtain “living materials” [151].

In particular, a 3D fully interconnected porous architecture is an ideal requirement of a scaffold to ensure cell differentiation, nutrient exchange and removal of metabolic waste. Cells migration is followed by proliferation, maturation and differentiation to generate the tissue of interest (i.e. bone tissue formation). Increased performance of 3D-printed microorganisms has been also obtained in other fields including fermentation and bioremediation processes. For example, environmental impact and half-life have been improved with 3D printed hydrogel ink for *P. putida* and *A. xylinum* for pollutants identification and degradation as well as cellulose production. [152-153]

1.6 Portable light detectors

In a biosensor, the detector acquires and amplifies the signal produced by the interaction between the biological part and the analyte. Some detectors are also able to process the signal, others need an external system for data elaboration. Light detectors can be usually divided in laboratory-based instrumentation for highly sensitive detection (i.e. photomultiplier tubes) and compact instrumentation for on-field applications (i.e. photodiodes). Photodiodes and photomultiplier are semiconductor devices that convert incident light into an electrical signal. Unlike the photodiode, the photomultiplier tubes are characterized by an internal amplification system able to increase the acquired signal as well as increase the background noise. Accordingly, photodiodes are characterized by low background noise, low sensitivity and slower response time. Photomultipliers are extremely sensitive in particular in the ultraviolet, visible and near-infrared ranges, but they have high background noise and require a more powerful energy supplier.

During the last decade, a great effort has been made for the development of ultra-sensitive and miniaturised portable light detectors. Thanks to the recent development in this technology, new generation of silicon and organic photodiodes, complementary metal oxide semiconductors (CMOS) and charge-coupled devices (CCD) have been implemented into portable devices for on-field applications [154-156].

In particular, CCD and CMOS are the most promising light sensors for biosensing applications. Both sensors are pixelated metal oxide semiconductors that accumulate a signal charge in each pixel proportional to the local light intensity. In CCD, each pixel's charge packet is sent sequentially to a common output structure, where there is a common amplifier and charge converter. In CMOS, the amplification and conversion process take place in each pixel and the final signal is sent in a parallel mode instead of sequential one (Fig. 18). These differences have significant implications for sensor architecture [157].

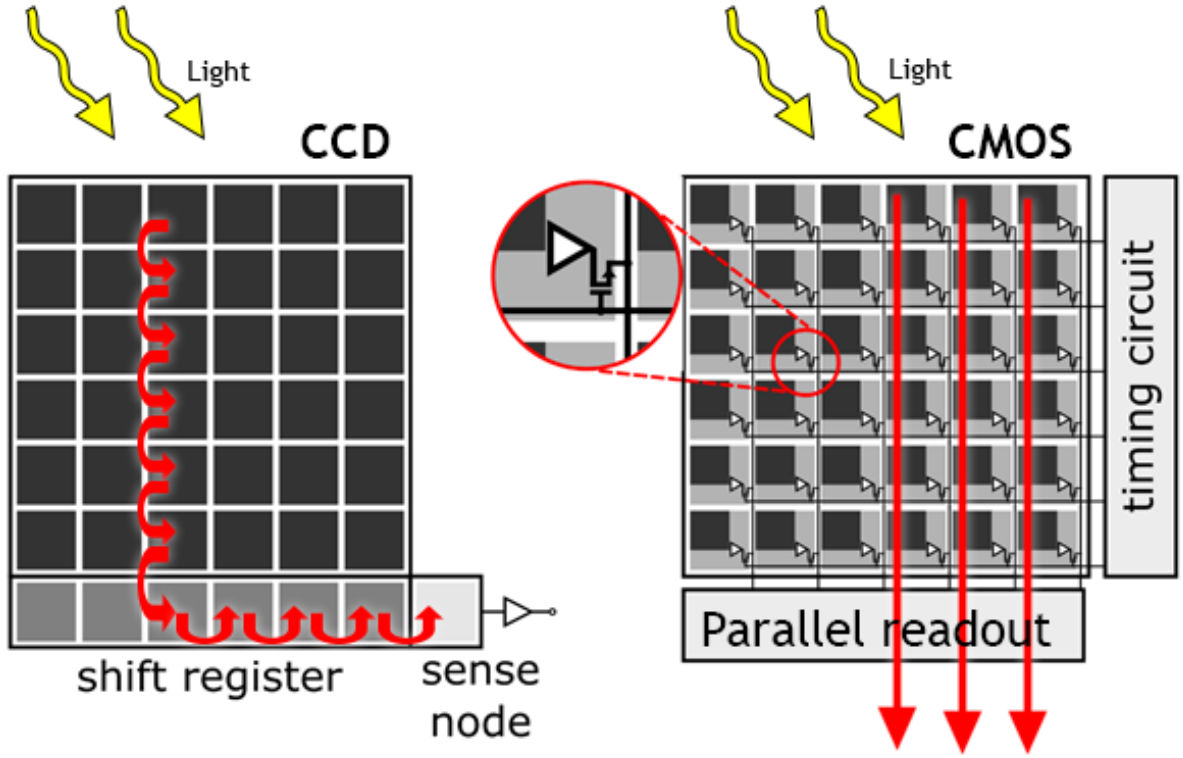

Fig. 18: Schematic representation of CCD and CMOS light transduction mechanism [157].

Among others, CMOS light detectors integrated into smartphone cameras have had a tremendous improvement due to the rapid diffusion of smartphones.

Indeed, this kind of technology provides a powerful, low cost tool for several applications, including personalized diagnosis and health monitoring in every day's life. These devices can transmit relevant data to experts such as physicians and can help self-management of common chronic diseases, such as diabetes and cardiovascular diseases. The same detector

can also be implemented for real-time *on-site* monitoring of pollutants in remote contaminated area where there are no equipped facilities. The use of smartphones for point-of-care analysis is highly appealing, however, there are lot of challenges such as clinical validation, reproducibility, robustness and rapidity that need to be solved before these devices could significantly improve healthcare delivery and provide better health management tools globally (Fig.19) [158-160].

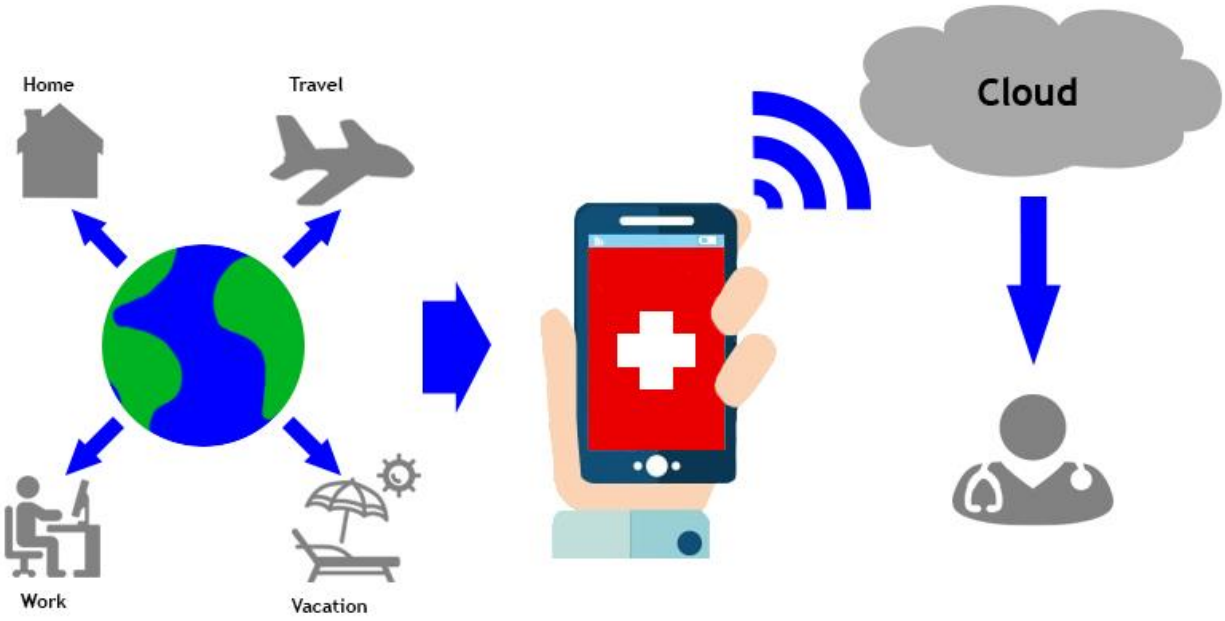

Fig.19: Smartphone as portable light detector for on-site biosensing and online data transfer.

Several analytical devices have been reported in the past implementing different portable light detector (CCD or CMOS) focusing on the different advantages of each technique. Side-by-side comparison have also been reported to evaluate the sensitivity of smartphone implementing a CMOS sensor with a low-light luminograph equipped with a thermoelectrically cooled CCD. As expected, a good correlation between light intensity and measured signal was reported for both systems; however, the signal-to-noise ratios (S/N) of the luminograph images were approximately three orders of magnitude higher than those obtained with the smartphone camera [161].

Several factors explain this lower detectability of the smartphone integrated camera, for instance the smaller pixel size and the absence of a sensor cooling system, which causes higher thermal noise. For every 6°C reduction in chip temperature the dark-current shot noise, which is the major source of noise, is cut approximately in half [162]. The variance due to dark current shot noise is described by the following equation:

$$\sigma_d^2 = 2qI_d\Delta f \qquad \textbf{(eq. 1)}$$

Where $\boldsymbol{\sigma_d^2}$ is the variance of shot noise, **q** is the charge of an electron, $\mathbf{I_d}$ is the amount of dark current, **Δf** is the electronic bandwidth of the sensing system. The implementation of cooled systems into portable devices is not straightforward, since additional components are required to avoid water vapor condensation on the camera window and also a larger power supply. The feasibility of using different portable CCD cameras as low-light detectors has been reported by cooling the sensor with a Peltier chamber down to -10 °C. This approach enabled the detection of different types of cells including magnetotactic bacteria and yeast; however, these approaches still require an external computer to handle the images and elaborate the signals [163-164].

Smartphone based biosensors potential for clinical applications have been widely demonstrated by imaging *P. falciparum*-infected red blood cells, detecting *M. tuberculosis*-infected sputum samples, performing immunoassays for urine analysis and prostate cancer diagnosis and quantitative analyses of lateral flow tests with electrochemical and colorimetric detection [165-167]. However, an important issue that need to be solved is related to the fact that each smartphone has a different (CMOS) camera with different performance. Several comparisons have been made between different Android and iOS smartphones and until now the best performance have been obtained with OnePlus devices [168-170].

1.7 References

[1] Turner A, Karube I, Wilson GS. Biosensors: fundamentals and applications. Oxford university press. 1987.

[2] Luka G, Ahmadi A, Najjaran H, Alocilja E, DeRosa M, Wolthers K, Malki A, Aziz H, Althani A, Hoorfar M. Microfluidics integrated biosensors: A leading technology towards lab-on-a-chip and sensing applications. Sensors. 2015; 15(12): 30011-31.

[3] Liu S, Zhaozhu Z, Xinyu L. Advances in pesticide biosensors: current status, challenges, and future perspectives. Anal Bioanal Chem. 2013; 405(1):63-90.

[4] Bănica FG. Chemical Sensors and Biosensors: Fundamentals and Applications. John Wiley & Sons. 2012

[5] Wang W, Zhao Q, Luo M, Li M, Wang D, Wang Y, Liu Q. Immobilization of firefly luciferase on PVA-co-PE nanofibers membrane as biosensor for bioluminescent detection of ATP. ACS appl. mat. Interf. 2015; 7(36): 20046-52.

[6] Pancrazio JJ, Whelan JP, Borkholder DA, Ma W, Stenger DA. Development and application of cell-based biosensors. Ann. Biomed. Engine. 1999; 27(6): 697-711.

[7] Chambers JP, Arulanandam BP, Matta LL, Weis A, Valdes JJ. Biosensor recognition elements. Texas Univ San Ant Dept Biology. 2008

[8] Barhoumi AH, Maaref A, Rammah M, Martelet C, Jaffrezic N, Mousty C, Vial S, and Forano C. Urea biosensor based on Zn3 Al-Urease layered double hydroxides nanohybrid coated on insulated silicon structures. Mat. Sci. Eng. C. 2006; 26:328–33.

[9] https://www.fda.gov/news-events/press-announcements/fda-approves-first-continuous-glucose-monitoring-system-fully-implantable-glucose-sensor-and

[10] Philippu A. In Vivo Neuropharmacology and Neurophysiology. Springer New York, ed. 2017.

[11] Liu H, Ge J, Ma E, Yang L. Advanced biomaterials for biosensor and theranostics. Biom. Trans. Med. Academic Press. 2019; 213-55.

[12] Vijayalakshmi AB, Sushrut A. Antibody-based biosensors for detection of veterinary viral pathogens. Adv. Anim. Vet. Sci. 2013; 1(4): 37-44.

[13] Estrela P, Sharma S, Byrne H, O'Kennedy R J. Antibodies and antibody-derived analytical biosensors. Ess biochem. 2016; 60:9-18.

[14] Lum J, Wang R, Lassiter K, Srinivasan B, Abi-Ghanem D, Berghman L**,** Hargisa B, Tung S, Lu H, Li Y. Rapid detection of avian influenza H5N1 virus using impedance measurement of immuno-reaction coupled with RBC amplification. Biosensors and Bioelectronics. 2012; 38(1): 67-73.

[15] Nguyen BT, Koh G, Lim HS, Chua AJ, Ng MM, Toh CS. Membrane-based electrochemical nanobiosensor for the detection of virus. Anal. Chem. 2019; 81(17):7226-34.

[16] Li D, Wang J, Wang R, Li Y, Abi–Ghanem D, Berghman L, Hargis B and Lu H. A nanobeads amplified QCM immunosensor for the detection of avian influenza virus H5N1. Biosens. Bioelectron. 2011; 26:4146 – 54.

[17] Bhattacharya M, Hong S, Lee D, Cui T, Goyal SM. Carbon nanotube based sensors for the detection of viruses. Sens. Act. B: Chem. 2011; 155(1): 67-74.

[18] Luo Y, Nartker S, Miller H, Hochhalter D, Wiederoder M, Wiederoder S**,** Setterington E, Lawrence TD, Alocilja EC. Surface functionalization of electrospun nanofibers for detecting *E. coli* O157: H7 and BVDV cells in a direct-charge transfer biosensor. Bios Bioel. 2010; 26(4): 1612-7.

[19] Sharma P, Sablok K, Bhalla V, Suri CR. A novel disposable electrochemical immunosensor for phenyl urea herbicide diuron. Bios. Bioel. 2011; 26(10); 4209-12.

[20] Valera E, Ramón-Azcón J, Barranco A, Alfaro B, Sánchez-Baeza F, Marco MP, Rodríguez Á. Determination of atrazine residues in red wine samples. A conductimetric solution. Food Chem. 2010; 122(3): 888-94.

[21] Cavalcanti IT, Guedes MI, Sotomayor MD, Yamanaka H, Dutra RF. A label-free immunosensor based on recordable compact disk chip for early diagnostic of the dengue virus infection. Bioc. Engine. Jour. 2012; 67; 225-30.

[22] HuyTQ, Hanh NTH, Thuy NT, Van Chung P, Nga PT, Tuan MA. A novel biosensor based on serum antibody immobilization for rapid detection of viral antigens. Talanta. 2011; 86:271-7.

[23] Hnaien M, Diouani MF, Helali S, Hafaid I, Hassen WM, Renault NJ, Ghram A, Abdelghani A. Immobilization of specific antibody on SAM functionalized gold electrode for rabies virus detection by electrochemical impedance spectroscopy. Bioc. Engin. Jour. 2008; 39(3): 443-9.

[24] Xu J, Wan JY, Yang ST, Zhang SF, Xu N, Li N, Li J, Wang H, Bai X, Liu WS. A surface plasmon resonance biosensor for direct detection of the rabies virus. Act Vet. 2012; 81(2): 107-11.

[25] Zeng GM, Zhang Y, Tang L, Chen LJ, Pang Y, Feng CL, Huang G, Niu CG. Sensitive and renewable picloram immunosensor based on paramagnetic immobilisation. Int. Jour. Env. Anal Chem. 2012; 92(6): 729-41.

[26] Li X, Li P, Zhang Q, Li R, Zhang W, Zhang Z, Ding X, Tang X. Multi-component immunochromatographic assay for simultaneous detection of aflatoxin B1, ochratoxin A and zearalenone in agro-food. Bios Bioel. 2013; 49: 426-32.

[27] Gan N, Zhou J, Xiong P, Hu F, Cao Y, Li T, Jiang, Q. An ultrasensitive electrochemiluminescent immunoassay for Aflatoxin M1 in milk, based on extraction by magnetic graphene and detection by antibody-labeled CdTe quantumn dots-carbon nanotubes nanocomposite. Toxins. 2013; 5(5): 865-83.

[28] Vidal JC, Bonel L, Ezquerra A, Duato P, Castillo JR. An electrochemical immunosensor for ochratoxin A determination in wines based on monoclonal antibody and paramagnetic microbeads. Anal Bioan. Chem. 2012; 403(6): 1585-93.

[29] Zhao Y, Wang P, Wang F, Zhou H, Li W, Yue J, Ha Y. A novel biosensor regulated by the rotator of F0F1–ATPase to detect deoxynivalenol rapidly. Bioc. Biop. Res. Com. 2012; 423(1): 195-9.

[30] Heinze BC, Song J, Lee C, Najam A, Yoon J. Microfluidic immunosensor for rapid and sensitive detection of bovine viral diarrhea virus. Sens. Act. B: Chem. 2009; 138:491 –6

[31] Yakes BJ, Papafragkou E, Conrad SM, Neill JD, Ridpath JF, Burkhardt W, Kulka M, Degrasse SL. Surface plasmon resonance biosensor for detection of feline calicivirus, a surrogate for norovirus. Int. J. Food Microbiol. 2013; 162: 152 –8

[32] Connelly J, Baeumner A. Biosensors for the detection of waterborne pathogens. Anal. Bioanal. Chem. 2012; 402: 117 –27.

[33] Kausaite-Minkstimiene A, Ramanavicius A, Ruksnaite J, Ramanaviciene A. A surface plasmon resonance immunosensor for human growth hormone based on fragmented antibodies. Anal. Met. 2013; 5(18): 4757-63.

[34] Namsoo K, Kim D, Cho Y. Development of indirect-competitive quartz crystal microbalance immunosensor for C-reactive protein. Sens. Act. B: Chem. 2009; 143(1):444-8.

[35] Luzi E, Minunni M, Tombelli S, Mascini M. New trends in affnity sensing – aptamers for ligand binding. Trend Anal.Chem. 2003; 22: 810–8

[36] Minunni M, Tombelli S, Gullotto A, Luzi E, Mascini M. Development of biosensors with aptamers as bio-recognition element: the case of HIV-1 Tat protein. Biosens. Bioelectron. 2004; 20:1149–56.

[37] Pfeiffer F, Mayer G. Selection and biosensor application of aptamers for small molecules. Front. Chem. 2016; 4: 25.

[38] LaVan DA, McGuire T, Langer R. Small-scale systems for in vivo drug delivery. Nat. Biotechnol. 2003; 21: 1184–91.

[39] Durand MJ, Hua A, Jouanneau S, Cregut M, Thouand G. Detection of Metal and Organometallic Compounds with Bioluminescent Bacterial Bioassays. Adv. Bioc. Eng. Biotec. 2015; 3:77-99.

[40] Gui Q, Lawson T, Shan S, Yan L, Liu Y. The application of whole-cell-based biosensors for use in environmental analysis and in medical diagnostics. Sensors. 2017; 17(7):1623.

[41] Wei H, Ze-Ling S, Le-Le C, Wen-Hui Z, Chuan-Chao D. Specific detection of bioavailable phenanthrene and mercury by bacterium reporters in the red soil. Int. Jour. Env. Sci. Tec. 2014; 11(3): 685-94.

[42] Cevenini L, Calabretta MM, Tarantino G, Michelini E, Roda A. Smartphone-interfaced 3D printed toxicity biosensor integrating bioluminescent “sentinel cells”. Sens. Act. B: Chem. 2016; 225: 249-57.

[43] Guedri H, Durrieu C. A self-assembled monolayers based conductometric algal whole-cell biosensor for water monitoring. Microc. Act. 2008; 163(3): 179-84

[44] Ivask A, Green T, Polyak B, Mor A, Kahru A, Virta M, Marks R. Fibre-optic bacterial biosensors and their application for the analysis of bioavailable Hg and As in soils and sediments from Aznalcollar mining area in Spain. Biosens Bioelectron 2007; 22(7): 1396-402.

[45] Kumar J, Jha SK, D'Souza SF. Optical microbial biosensor for detection of methyl parathion pesticide using Flavobacterium sp. whole-cells adsorbed on glass fiber filters as disposable biocomponent. Bios. Bioel. 2006; 21(11): 2100-5

[46] Silva N, Gil D, Karmali A, Matos M. Biosensor for acrylamide based on an ion-selective electrode using whole-cells of Pseudomonas aeruginosa containing amidase activity. Biocat. Biotrans. 2009; 27(2): 143-51.

[47] Valdman E, Gutz IGR. Bioluminescent sensor for naphthalene in air: cell immobilization and evaluation with a dynamic standard atmosphere generator. Sens Actuators B 2008; 133(2): 656-663.

[48] Kwok NY, Dong S, Lo W, Wong KY. An optical biosensor for multi-sample determination of biochemical oxygen demand (BOD). Sens. Act. B: Chem. 2005; 110 (2):289–98.

[49] Dhall P, Kumar A, Joshi A, Saxsena TK, Manoharan A, Makhijani SD, Kumar R. Quick and reliable estimation of BOD load of beverage industrial wastewater by developing BOD biosensor, Sens. Act. B: Chem. 2008; 133(2) 478–83.

[50] Chee GJ, Nomura Y, Ikebukuro K, Karube I. Optical fiber biosensor for the determination of low biochemical oxygen demand, Biosens. Bioelectron. 2000; 15(7): 371–6

[51] Tag K, Riedel K, Bauer H, Hanke G, Baronian KHR, Kunze G. Amperometric detection of Cu^{2+} by yeast biosensors using flow injection analysis (FIA). Sens. Act. B: Chem. 2007; 122(2): 403-9.

[52] Stolper P, Fabel S, Weller MG, Knopp D, Niessner R. Whole-cell luminescence-based flowthrough biodetector for toxicity testing, Anal. Bioanal. Chem. 2008; 390 (4):1181–7

[53] Fujimoto H, Wakabayashi M, Yamashiro H, Maeda I, Isoda K, Kondoh M, Kawase M,

Miyasaka H, Yagi K. Whole-cell arsenite biosensor using photosynthetic bacterium Rhodovulum sulfidophilum, Appl. Microbiol. Biotechnol. 2006; 73(2):332–338.

[54] Reshetilov AN, Semenchuk IN, Iliasov PV, Taranova LA. The amperometric biosensor for detection of sodium dodecyl sulfate. Anal Chim. Act. 1997; 347(1-2):19-26.

[55] Nomura Y, Ikebukuro K, Yokoyama K, Takeuchi T, Arikawa Y, Ohno S, Karube I. Application of a linear alkylbenzene sulfonate biosensor to river water monitoring. Bios. Bioel. 1998; 13(9): 1047-53.

[56] Petänen T, Romantschuk M. Use of bioluminescent bacterial sensors as an alternative method for measuring heavy metals in soil extracts. Anal. Chim. Act. 2002; 456(1): 55-61.

[57] Arora S, Pastorella G, Byrne B, Marsili E, O'Kennedy R. Microbial Cells and Biosensing: A Dual Approach-Exploiting Antibodies and Microbial Cells as Analytical/Power Systems. Rev. Pharm. Biom. Anal. 2010; 63-75.

[58] Saini R, Hegde K, Brar SK, Verma M. Advances in whole-cell-based biosensors in environmental monitoring. Tool Tec. Prot. Mon. Env. Cont. 2019; 263-84

[59] Alpat Ş, Alpat SK, Çadırcı BH, Yaşa İ, Telefoncu A. A novel microbial biosensor based on Circinella sp. Modified carbon paste electrode and its voltammetric application. Sens. Act. B: Chem. 2008; 134(1):175-81.

[60] Michelini E, Roda A. Staying alive: new perspectives on cell immobilization for biosensing purposes. Anal. Bioan. Chem. 2012; 402(5): 1785-97.

[61] Roberts MAJ, Cranenburgh RM, Stevens MP, Oyston PCF. Synthetic biology: biology by design. Microbiol. 2013; 159(7): 1219.

[62] Choffnes ER, Relman DA, Pray L. The science and applications of synthetic and systems biology: workshop summary. Nat. Acad. Press. 2011.

[63] Laurent JM, Young JH, Kachroo AH, Marcotte EM. Efforts to make and apply humanized yeast. Brief. Fun. Gen. 2015; 15(2): 155-63.

[64] Radhika V, Proikas-Cezanne T, Jayaraman M, Onesime D, Ha JH, Dhanasekaran DN. Chemical sensing of DNT by engineered olfactory yeast strain. Nat. Chem. Biol. 2007; 3(6): 325.

[65] Bereza-Malcolm LT, Mann G, Franks AE. Environmental sensing of heavy metals through whole-cell microbial biosensors: a synthetic biology approach. ACS Synt. Biol. 2014; 4(5): 535-46.

[66] Saito H. Regulation of cross-talk in yeast MAPK signaling pathways. Cur. Op. Microbiol. 2010; 13(6): 677-83.

[67] Zhang C, Parrello D, Brown PJ, Wall JD, Hu Z. A novel whole-cell biosensor of Pseudomonas aeruginosa to monitor the expression of quorum sensing genes. App. Microbiol. Biotech. 2018; 102(14):6023-38.

[68] Wan X, Ho TY, Wang B. Engineering Prokaryote Synthetic Biology Biosensors. Handbook Cell Bios. 2019; 1-37.

[69] Wan X, Volpetti F, Petrova E, French C, Maerkl SJ, Wang B. Cascaded amplifying circuits enable ultrasensitive cellular sensors for toxic metals. Nat. Chem. Biol. 2019; 15(5):540.

[70] Schwille P. Bottom-up synthetic biology: engineering in a tinkerer's world. Science. 2011; 333:1252-4.

[71] Fanalista F, Birnie A, Maan R, Burla F, Charles K, Pawlik G, Deshpande S, Dekker C. Shape and Size Control of Artificial Cells for Bottom-Up Biology. ACS nano. 2019

[72] Hodgman CE, Jewett MC. Cell-free synthetic biology: thinking outside the cell. Met. Eng. 2012; 14(3):261-9.

[73] Voyvodic PL, Pandi A, Koch M, Conejero I, Valjent E, Courtet P, Renard E, Faulon JL, Bonnet, J. Plug-and-play metabolic transducers expand the chemical detection space of cell-free biosensors. Nat Com. 2019; 10(1):1697.

[74] Alam J, Cook JL. Reporter genes: application to the study of mammalian gene transcription. Anal. Bioc. 1990; 188(2):245-54.

[75] Jawed A, Cook JL. Reporter genes: application to the study of mammalian gene transcription. Anal bioc. 1990; 188(2):245-54.

[76] Nordgren IK, Tavassoli A. A bidirectional fluorescent two-hybrid system for monitoring protein–protein interactions.Mol. BioSys. 2014; 10(3):485-90.

[77] Welsh S, and Kay SA. Reporter gene expression for monitoring gene transfer. Cur Opin. Biotec. 1997; 8(5):617-22.

[78] Cevenini L, Calabretta MM, Lopreside A, Branchini BR, Southworth TL, Michelini E, Roda A. Bioluminescence Imaging of Spheroids for High-throughput Longitudinal Studies on 3D Cell Culture Models. Pho. Photobiol. 2017; 93(2); 531-5.

[79] Smith AM, Mancini MC, Nie S. Bioimaging: second window for in vivo imaging. Nat. Nanotec. 2009; 4(11):710.

[80] Han S, Samanta A, Xie X, Huang L, Peng J, Park SJ, Loong DBT, Choi Y, Chang YT, Homayoun AA, Yang Y, Xing B, Yang Y. Gold and hairpin DNA functionalization of upconversion nanocrystals for imaging and in vivo drug delivery. Adv. Mat. 2017; 29(18):1700244.

[81] Pinner S, Sahai E. Imaging amoeboid cancer cell motility in vivo. Jour. Micros. 2018; 231(3):441-5.

[82] Legler J, Zeinstra LM, Schuitemaker F, Lanser PH, Bogerd J, Brouwer A, Brouwer A, Vethaak AD, de Voogt P, Murk AJ, van der Burg B. Comparison of in vivo and in vitro reporter gene assays for short-term screening of estrogenic activity. Env. Sci. Tec. 2002; 36(20):4410-5.

[83] Li Z, Suzuki Y, Huang M, Cao F, Xie X, Connolly A J, Yang PC, Wu J. C. Comparison of reporter gene and iron particle labeling for tracking fate of human embryonic stem cells and differentiated endothelial cells in living subjects. Stem cells. 2008; 26(4):864-73.

[84] Yamasaki K, Takeyoshi M, Yakab, Y, Sawaki M, Imatanaka N, Takatsuki M. Comparison of reporter gene assay and immature rat uterotrophic assay of twenty-three chemicals." Toxicology. 2002; 170(2):21-30.

[85] Muramatsu T, Mizutani Y, Ohmori Y, Okumura JI. Comparison of three nonviral transfection methods for foreign gene expression in early chicken embryosin ovo. Bioc. Biop. Res. Com. 1997; 230(2):376-80.

[86] Park JY, Kricka LJ. Prospects for the commercialization of chemiluminescence-based point-of-care and on-site testing devices. Anal Bioanal Chem 2014; 406(23): 5631-7.

[87] Michelini E, Cevenini L, Mezzanotte L, Ablamsky D, Southworth T, Branchini B, Roda A. Spectral-resolved gene technology for multiplexed bioluminescence and high-content screening. Anal. Chem. 2008; 80(1); 260-7.

[88] Michelini E, Cevenini L, Calabretta MM, Spinozzi S, Camborata C, Roda A. Field-deployable whole-cell bioluminescent biosensors: so near and yet so far. Anal. Bioanal Chem. 2013; 405(19); 6155-63.

[89] Houston PL, Kable SH. Photodissociation of acetaldehyde as a second example of the roaming mechanism. Proc. Nat. Acad. Sci. 2006; 103(44):16079-82.

[90] Niwa K, Ichino Y, Kumata S, Nakajima Y, Hiraishi Y, Kato DI, Viviani VR, Ohmiya Y. Quantum yields and kinetics of the firefly bioluminescence reaction of beetle luciferases. Photoc. Photobiol. 2010; 86(5): 1046-9.

[91] Thouand G, Marks R, Bioluminescence: Fundamentals and Applications in Biotechnology. eds. 2014; 2.

[92] Nakatsu T, Ichiyama S, Hiratake J, Saldanha A, Kobashi N, Sakata K, Kato H. Structural basis for the spectral difference in luciferase bioluminescence. Nature. 2006; 440(7082): 372-6.

[93] [BRACHINI] Branchini BR, Southworth TL, Fontaine DM, Davis AL, Behney CE, Murtiashaw MH. A Photinus pyralis and Luciola italica chimeric firefly luciferase produces enhanced bioluminescence. Biochem. 2014; 53(40), 6287-9.

[94] Scott D, Dikici E, Ensor M, Daunert S. Bioluminescence and its impact on bioanalysis. Ann Rev. Anal. Chem. 2011; 4;297-319.

[95] Roda A, Guardigli M, Michelini E, Mirasoli M, Pasini, P. Peer reviewed: analytical bioluminescence and chemiluminescence. 2003.

[96] McElroy WD, Seliger HH, White EH. Mechanism of bioluminescence, chemi-luminescence and enzyme function in the oxidation of firefly luciferin. Photoc. Photobiol. 1969; 10(3):153-70.

[97] Marquette CA. Chemiluminescent and bioluminescent biosensors. In: Chemiluminescence and Bioluminescence: Past, Present and Future. Royal Soc. Chem. Ed 2012

[98] Hosseinkhani S. Molecular enigma of multicolor bioluminescence of firefly luciferase. Cell. Mol. Life Sci. 2011; 68(7):1167-82.

[99] Rowe L, Dikici E, Daunert S. Engineering bioluminescent proteins: expanding their analytical potential. 2009; 8662-8.

[100] Shimomura O. Regeneration of the photoprotein aequorin. Nature. 1975; 236–8.

[101] Branchini BR, Ablamsky DM, Murtiashaw MH, Uzasci L, Fraga H, Southworth TL. Thermostable red and green light-producing firefly luciferase mutants for bioluminescent reporter applications. Anal Biochem. 2007; 361(2): 253-62.

[102] Santaniello E, Meroni G. Color-tuning of firefly luciferase bioluminescence by modification of enzyme and substrate structure: new opportunities for optical imaging. Minerva Biotec. 2009; 21(2): 77.

[103] Saito R, Kuchimaru T, Higashi S, Lu SW, Kiyama M, Iwano S, Maki SA. Synthesis and luminescence properties of near-infrared N-heterocyclic luciferin analogues for in vivo optical imaging. Bul. Chem. Soc. 2019; 92(3):608-18.

[104] Koksharov MI, Ugarova NN. Thermostabilization of firefly luciferase by in vivo directed evolution. Prot. Eng. Des. Sel. 2011. 24(11): 835-44.

[105] Teow SY, Liew K, Mat MFC, Marzuki M, Aziz NA, Chu TL, Ahmad M, Khoo ASB. Development of a luciferase/luciferin cell proliferation (XenoLuc) assay for real-time measurements of Gfp-Luc2-modified cells in a co-culture system. BMC. Biotec. 2019; 19(1): 34.

[106] Van Leeuwen W, Hagendoorn MJ, Ruttink T, Van Poecke R, Van Der Plas LH, Van Der Krol AR. The use of the luciferase reporter system for in planta gene expression studies. Plant Mol Biol Rep. 2000. 18(2): 143-4.

[107] Nakatsu T. Structural basis for the spectral difference in luciferase bioluminescence. Nature. 2006; 372-6.

[108] Branchini BR, Southworth TL, Khattak NF, Michelini E, Roda A. Red-and green-emitting firefly luciferase mutants for bioluminescent reporter applications. Anal Biochem. 2005; 345(1): 140-8.

[109] Rowe L, Dikici E, Daunert S. Engineering bioluminescent proteins: expanding their analytical potential. 2009; 8662-8.

[110] Cevenini L, Calabretta MM, Calabria D, Roda A, Michelini E. Luciferase genes as reporter reactions: how to use them in molecular biology?. Biol: Fund. Appl. 2015; 3:3-17.

[111] Eggers CT, Valley MP, Klaubert DH, Unch J, Encell LP, Wood KV, Hall MP, Benink HA, Otto P, Zimmerman K, Vidugiris G, Machleidt T, Robers MB, Benink HA, Eggers CT, Slater MR, Meisenheimer PL, Klaubert DH, Fan F, Encell LP, Wood KV. Engineered luciferase reporter from a deep sea shrimp utilizing a novel imidazopyrazinone substrate. ACS chem. Biol. 2012; 7(11):1848-57.

[112] England CG, Ehlerding EB, Cai W. NanoLuc: a small luciferase is brightening up the field of bioluminescence. Biocon. Chem. 27(5); 1175-87.

[113] Saito K, Nagai T. Recent progress in luminescent proteins development. Cur Op Chem Biol. 2015; 27:46-51.

[114] Stokes GG. On the change of refrangibility of light. Phil trans Royal Soc Lon. 1852: 142; 463-562.

[115] Liu J, Liu C, He W. Fluorophores and Their Applications as Molecular Probes in Living Cells. Curr Org Chem. 2013; 17(6): 564–79.

[116] Stockert JC, Blázquez-Castro A. Chapter 4 Fluorescent Labels. Fluo. Mic. Life. Sci. 2017; 96–134.

[117] Ranson RM, Evangelou E, & Thomas CB. Modeling the fluorescent lifetime of Y 2 O 3: Eu. App Phys Let. 1998; 72(21): 2663-4.

[118] Hou J, Cai P, Wang C, Shen Y. A novel fluorescent probe with a large stokes shift for cysteine based on dicyanoisophorone. Tetra Let, 2018; 59(26); 2581-5.

[119] Jiang M, Gu X, Lam JW, Zhang Y, Kwok RT, Wong KS, Tang BZ. Two-photon AIE bio-probe with large Stokes shift for specific imaging of lipid droplets. Chem Scie. 2017; 8(8): 5440-6.

[120] Bavali A, Parvin P, Tavassoli M, Mohebbifar MR. Angular distribution of laser-induced fluorescence emission of active dyes in scattering media. Appl. Opt. 2018; 57(7):32-8.

[121] Valeur B. Molecular fluorescence. Digital Enc App Phys. 2003;477-531.

[122] Markwardt ML, Kremers GJ, Kraft CA, RayK, Cranfill PJ, Wilson KA, Rizzo MA. An improved cerulean fluorescent protein with enhanced brightness and reduced reversible photoswitching. PloS One: 2011;6(3):e17896.

[123] Shen Y, Chen Y, Wu J, Shaner NC, Campbell RE. Engineering of mCherry variants with long Stokes shift, red-shifted fluorescence, and low cytotoxicity. PLoS. One. 2017; 12(2): e0171257.

[124] Pedelacq JD, Cabantous S. Development and Applications of Superfolder and Split Fluorescent Protein Detection Systems in Biology. Inter. Jour. Mol. Sci. 2019; 20(14):3479.

[125] Hollister EB, Brooks JP, Gentry TJ. Nucleic Acid-Based Methods of Analysis. Env. Microbiol. 2015; 271-305

[126] Houbertz R, Domann G, Cronauer C, Schmitt A, Martin H, Park J-U, Fröhlich L, Buestrich R, Popall M, Streppel U, Dannberg P, Wächter C, Bräuer A. Inorganic-organic hybrid materials for application in optical devices. Thin Solid Films. 2003; 442:194–200.

[127] Charrier T, Durand MJ, Jouanneau S, Dion M, Pernetti M, Poncelet D, Thouand G. A multi-channel bioluminescent bacterial biosensor for the on-line detection of metals and toxicity. Part I: design and optimization of bioluminescent bacterial strains. Anal. Bioana.l Chem. 2011; 400(4):1051-60.

[128] Barin M, Otadi M, Khorasheh F, Kheirolomoom A. Effect of cell concentration on the acylation of penicillin G enzymatic reaction in immobilized cells. Sci. Iran. Trans. C Chem. Chem. Eng. 2009; 16.

[129] Ruan B, Wu P, Chen M, Lai X, Chen L, Yu L, Gong B, Kang C, Dang Z, Shi Z, Liu Z. Immobilization of Sphingomonas sp. GY2B in polyvinyl alcohol–alginate–kaolin beads for efficient degradation of phenol against unfavorable environmental factors. Ecotox. Environ. Saf. 2018; 162:103-111.

[130] Mbeunkui F, Richaud C, Etienne AL, Schmid RD, Bachmann TT. Bioavailable nitrate detection in water by an immobilized luminescent cyanobacterial reporter strain. Appl. Microbiol. Biotechnol. 2002; 60:306-12.

[131] Borin GP, de Melo RR, Crespim E, Sato HH, Contesini FJ. An Overview on Polymer Gels Applied to Enzyme and Cell Immobilization. In Polymer Gels. Springer. 2018.

[132] Jouanneau S, Durand-Thouand MJ, & Thouand G. Design of a toxicity biosensor based on *Aliivibrio fischeri* entrapped in a disposable card. Env. Sci. Pol. Res. 2016. 23(5), 4340-5.

[133] Belkin S, Yagur-Kroll S, Kabessa Y, Korouma V, Septon T, Anati Y, Zohar-Perez C, Rabinovitz Z, Nussinovitch A, Agranat AJ. Remote detection of buried landmines using a bacterial sensor. Nat. Biotec. 2017; 35:308.

[134] Cevenini L, Lopreside A, Calabretta MM, D'Elia M, Simoni P, Michelini E, Roda A . A novel bioluminescent NanoLuc yeast-estrogen screen biosensor (nanoYES) with a compact

wireless camera for effect-based detection of endocrine-disrupting chemicals. Anal. Bioan. Chem. 2018; 410:1237-46.

[135] Cortesão M, Fuchs FM, Commichau FM, Eichenberger P, Schuerger AC, Nicholson WL, Setlow P, Moeller R. Bacillus subtilis Spore Resistance to Simulated Mars Surface Conditions. Front Microbiol. 2019; 10:333.

[136] Date A, Pasini P, Daunert S. Construction of spores for portable bacterial whole-cell biosensing systems. Anal Chem. 2007. 79(24): 9391-7.

[137] Ranmadugala D, Ebrahiminezhad A, Manley-Harris M, Ghasemi Y, Berenjian A. Magnetic immobilization of bacteria using iron oxide nanoparticles. Biotec. Let. 2018; 40: 237-48.

[138] Lin CC, Anseth KS. Cell–cell communication mimicry with poly (ethylene glycol) hydrogels for enhancing β-cell function. Proc Nat. Ac. Sci. 2011; 108(16):6380-5.

[139] Cevenini L, Calabretta MM, Lopreside A, Tarantino G, Tassoni A, Ferri M, Roda A, Michelini E. Exploiting NanoLuc luciferase for smartphone-based bioluminescence cell biosensor for (anti)-inflammatory activity and toxicity. Anal Bioanal. Chem. 2016; 408(30): 8859-68.

[140] Xu Y, Mawatari K, Konno T, Kitamori T, Ishihara K. Spontaneous packaging and hypothermic storage of mammalian cells with a cell-membrane-mimetic polymer hydrogel in a microchip. ACS Appl. Mater. 2015;(7):23089–97.

[141] Michelini E, Calabretta MM, Cevenini L, Lopreside A, Southworth T, Fontaine DM, Simoni P, Branchini BR, Roda A. Smartphone-based multicolor bioluminescent 3D spheroid biosensors for monitoring inflammatory activity. Bios. Bioelect. 2019; 123:269-77.

[142] Baraniak PR, Cooke MT, Saeed R, Kinney MA, Fridley KM, McDevitta TC. Stiffening of human mesenchymal stem cell spheroid microenvironments induced by incorporation of gelatin microparticles. Journ. Mec. Behav. Biom. Mat. 2012; 11:63-71.

[143] Cruz-Acuña R, Quirós M, Huang S, Siuda D, Spence JR, Nusrat A, García AJ. PEG-4MAL hydrogels for human organoid generation, culture, and in vivo delivery. Nat. Protoc. 2018; 13(9):2102.

[144] Bishop GW, Satterwhite-Warden JE, Kadimisetty K, Rusling JF. 3D-printed bioanalytical devices. Nanotec. 2016; 27:e284002.

[145] Sharafeldin M, Jones A, Rusling JF. 3D-Printed Biosensor Arrays for Medical Diagnostics. Micromac. 2018; 9(8): e394

[146] Palenzuela CLM, Pumera M. (Bio) Analytical chemistry enabled by 3D printing: Sensors and biosensors. TrAC Trends Anal Chem. 2018; 103:110-8.

[147] Gowers SA, Curto VF, Seneci CA, Wang C, Anastasova S, Vadgama P, Yang GZ, Boutelle MG. 3D printed microfluidic device with integrated biosensors for online analysis of subcutaneous human microdialysate. Anal. Chem. 2015; 87(15); 7763-70.

[148] Roda A, Guardigli M, Calabria D, Calabretta MM, Cevenini L, Michelini E. A 3D-printed device for a smartphone-based chemiluminescence biosensor for lactate in oral fluid and sweat. Analyst. 2014; 139(24): 6494-501.

[149] Xu T, Jin J, Gregory C, Hickman JJ, Boland T. Inkjet printing of viable mammalian cells. Biomat. 2005; 26:93–9.

[150] Wüst S, Müller R, Hofmann S. Controlled positioning of cells in biomaterials—approaches towards 3D tissue printing. J. Funct. Biomat. 2011; 2:119–54.

[151] Liu Y, Li T, Ma H, Zhai D, Deng C, Wang J, Zhuo S, Chang J, Wu C. 3D-printed scaffolds with bioactive elements-induced photothermal effect for bone tumor therapy. Act. Biomater. 2018; 73:531-46.

[152] Schaffner M, Rühs PA, Coulter F, Kilcher S, Studart AR. 3D printing of bacteria into functional complex materials. Sci Adv. 2017; 3(12):e6804

[153] Kyle S. 3D Printing of Bacteria: The Next Frontier in Biofabrication. Trends Biot. 2018; 36:340-1.

[154] Srinivasan B, Tung S. Development and applications of portable biosensors. Jour. Labor. Autom. 2015; 20(4): 365-89.

[155] Lai S, Caboni A, Loi D, Barbaro M. A CMOS biocompatible charge detector for biosensing applications. IEEE Trans. Elec. Dev. 2012; 59(9):2512-19.

[156] Golden J.P, Ligler FS. A comparison of imaging methods for use in an array biosensor. Bios. Bioelec. 2002; 17(9):719-25.

[157] Litwiller D. CCD vs. CMOS. Photon. Spec. 2001; 35(1): 154-8.

[158] Scott Kruse C, Karem P, Shifflett K, Vegi L, Ravi K, Brooks M. Evaluating barriers to adopting telemedicine worldwide: A systematic review. Jour. Tel. Telec. 2018; 24(1):4-12.

[159] Sauers-Ford HS, Hamline MY, Gosdin MM, Kair LR, Weinberg GM, Marcin JP, Rosenthal JL. Acceptability, Usability, and Effectiveness: A Qualitative Study Evaluating a Pediatric Telemedicine Program. Ac. Emerg. Med. 2019; 26(9):1022-33.

[160] Mehrotra A, Jena AB, Busch AB., Souza J, Uscher-Pines L, Landon BE. Utilization of telemedicine among rural Medicare beneficiaries. Jam. 2016, 315(18): 2015-6.

[161] Roda A, Michelini E, Cevenini L, Calabria D, Calabretta MM, Simoni P. Integrating biochemiluminescence detection on smartphones: mobile chemistry platform for point-of-need analysis. Anal. Chem. 2014; 86:7299-304.

[162] Christensen DA, Herron JN. Optical System Design for Biosensors Based on CCD Detection. Bios. Biodetec. Methods Mol. Biol. eds 2009; 503.

[163] Roda A, Cevenini L, Borg S, Michelini E, Calabretta MM, Schüler D. Bioengineered bioluminescent magnetotactic bacteria as a powerful tool for chip-based whole-cell biosensors. Lab Chip. 2013; 13(24):4881-9.

[164] Roda A, Cevenini L, Michelini E, Branchini BR. A portable bioluminescence engineered cell-based biosensor for on-site applications. Bios. Bioel. 2011; 26(8):3647-53.

[165] Drakeley C, Reyburn H. Out with the old, in with the new: the utility of rapid diagnostic tests for malaria diagnosis in Africa. Trans. Royal Soc. Trop. Med. Hyg. 2009; 103(4):333-7.

[166] You DJ, Park TS, Yoon JY. Cell-phone-based measurement of TSH using Mie scatter optimized lateral flow assays. Bios. Bioel. 201340(1): 180-5.

[167] Mudanyali O, Dimitrov S, Sikora U, Padmanabhan S, Navruz I, Ozcan A. Integrated rapid-diagnostic-test reader platform on a cellphone. Lab Chip. 2012; 12(15):2678-86.

[168] Kim H, Awofeso O, Choi S, Jung Y, Bae E. Colorimetric analysis of salivaealcohol test strips by smartphone-based instruments using machine-learning algorithms. Appl. Opt. 2017; 56:8492.

[169] Kim H, Jung Y, Doh IJ, Lozano-Mahecha RA, Applegate B, Bae E. Smartphone-based low light detection for bioluminescence application. Sci. Rep. 2017; 9(7):40203

[170] Lopreside A, Calabretta MM, Montali L, Ferri M, Tassoni A, Branchini BR, Southworth T, D'Elia M, Michelini E. Prêt-à-porter nanoYESα and nanoYESβ bioluminescent cell biosensors for ultrarapid and sensitive screening of endocrine-disrupting chemicals. Anal. Bioanal. Chem. 2019; 1-13.

2

Aim of the Thesis

2 Aim of the Thesis

The goal of this PhD project has been the development and optimization of bioengineered whole-cell biosensors for point-of-need applications.

Thanks to synthetic biology tools combined with genetic engineering and reporter gene technology whole-cells have been tailored at the molecular level to respond to specific analytes by the generation of measurable and quantitative dose-dependent signals. These tools have been also used to improve the analytical performance of the new developed biosensors, in terms of limit of detection, response time and dynamic range. The development of ready to use cartridges with immobilized and responsive whole-cell biosensors that could be stored for long time have been also exploited.

In chapter 3, several optical reporter genes (fluorescent, bioluminescent and colorimetric) have been exploited for whole-cell biosensing thanks to their high sensitivity and straightforward procedure. In order to identify the best reporter gene in terms of sensitivity, response time and limit of detection, a battery of standardized whole-cell and cell-free biosensors have been developed. The analytical performance of eight reporters from the three reporter categories have been profiled for bought whole-cell and cell-free biosensors systems. Two representative bacterial biosensors for mercury and quorum sensing molecule have been selected as the monitoring of these compound in water is important for health of human and environment. The lowest detectable concentration of analytes and the fastest responses were achieved with bioluminescent NanoLuc luciferase. Notably, a LOD ≤ 50.0 fM $HgCl_2$ for the mercury whole-cell biosensors and a LOD ≤ 0.38 pM of $3OC_6HSL$ for quorum sensing biosensors were achieved with just 30 min of induction.

NanoLuc luciferase and other bioluminescent reporters were therefore selected as reporter genes for the development of other whole-cell biosensors during this PhD.

Whole-cell biosensors based on bacteria cells are important for environmental monitoring as they are easier to be used and more robust. But, cellular responses to some molecules are different in prokaryotes from those in eukaryotes and this limits their application in

toxicity evaluation and drug screening. While, other microorganisms like yeast provide the robustness of bacteria cell with the predictivity of eukaryotic cell pathways.

During this PhD I have worked on the development of whole-cell biosensors based on yeast cell for the identification and quantification of (anti)estrogen-like compounds. In chapter 4 and 5, *S. cerevisiae* yeast cells have been exploited as chassis for the recombinant expression of human estrogen receptors (hERα and hERβ), combined with the properties of bioluminescent NanoLuc luciferase. Thanks to synthetic biology tools and genetic engineering all genetics components have been optimized and a fast and sensitive biosensor have been developed. Indeed, even after 5 min a dose-response curve was obtained showing a LOD of 1.08 ± 0.02 nM and 0.015 ± 0.001 nM for hERα and hERβ, respectively. The best response was obtained with only 30 min of incubation time, showing a LOD of 0.016 ± 0.001 nM and an EC_{50} of 1.47 ± 0.06 nM for the ERα strain, while a LOD of 0.0011 ± 0.0002 nM and EC_{50} of 0.10 ± 0.01 nM were found for the ERβ strain.

New straightforward immobilization procedures and 3D printer adaptors have been also developed to prove the feasibility of integrating these new biosensors into portable devices for on-field application. Thanks to the new immobilization procedure a longer storage time and higher bioluminescent signal were achieved. While, thanks to 3D printer technology adaptors for biosensors integration with low-cost and user-friendly device have been developed. In particular, a Go-Pro Hero 5 camera and a OnePlus 5 smartphone have been used for image acquisition. Showing a limit of detection only 10 time higher compared to conventional laboratory instrumentations, which are much more expensive and cannot be used in on-field setting and need a trained user to carry out all the necessary procedure for signal acquisition.

In chapter 5, a viability control strain was also developed based on a chimeric green-emitting luciferase, PLG2, expressed for the first time in *S. cerevisiae*. The integration of this viability control strain into the same portable device together with yeast reporter strains harbouring hERα and hERβ allowed a more reproducible and repeatable response about (anti)estrogenic activity via human estrogen receptor, as well as sample toxicity information.

All biosensors based on microorganisms, like yeast and bacteria, are characterised by many features like rapid growth on a broad range of substrates, ease of handling and are very cheap. Also, thanks to their high robustness they can be “easily” integrated into portable devices for on-field application. Yeast, being eukaryotic cells, can be used for obtaining a good predictivity, however some complex intracellular pathways can not be successfully reproduced into this cell. To this end, during this PhD I have also worked on the development of a portable device for on-field application based on human cell lines.

In chapter 6, 3D cell cultures of human embryonic kidney (HEK293T) cell line were genetically engineered for monitoring NF-κB signal transduction pathway with a bright red-emitting luciferase (PpyRE-TS).

Ready-to-use cartridges with 3D bioluminescent whole-cell biosensors for (anti)inflammatory activity monitoring were developed and a proof-of-principle device integrated with smartphone was obtained for point-of-care applications. In order to increase the reproducibility of mammalian cell biosensors an internal viability control was introduced with a green-emitting luciferase (PpyGR-TS), under the control of a weak constitutive promoter. The inducible and constitutive promoters were successfully expressed into the same cell, to further improve the biosensors robustness by correcting the specific analytical signal according to non-specific effects on cell viability as well as small variations in spheroid number and dimension. Nevertheless, the simultaneous detection of multiple colors emitted from the same well represented a challenge for a smartphone-based filterless device. Several luciferases have been tested and pH and thermostable mutant luciferases with a well separated emission spectra have been selected.

Accordingly, the developed biosensor provides a green signal in absence of NF-κB activity, while emits red light which intensity is proportional to inflammatory stimuli. In optimized conditions, the biosensor gives a LOD of 0.15 ±0.05 ng/mL and an EC_{50} of 1.0 ±0.1 ng/mL with TNFα as model analyte.

3

Comprehensive profiling of diverse genetic reporters with application to whole-cell and cell-free biosensors

Reproduced from: “Comprehensive profiling of diverse genetic reporters with application to whole-cell and cell-free biosensors”

Antonia Lopreside, Xinyi Wan, Elisa Michelini, Aldo Roda and Baojun Wang

Analytical Chemistry,2019; 91(23), 15284-92.

(https://pubs.acs.org/doi/10.1021/acs.analchem.9b04444)

analytical chemistry

Article

Cite This: Anal. Chem. 2019, 91, 15284−15292

pubs.acs.org/ac

Comprehensive Profiling of Diverse Genetic Reporters with Application to Whole-Cell and Cell-Free Biosensors

Antonia Lopreside,[†,‡] Xinyi Wan,[†,§] Elisa Michelini,[‡] Aldo Roda,[‡] and Baojun Wang*[,†,§]

[†]School of Biological Sciences and [§]Centre for Synthetic and Systems Biology, University of Edinburgh, Edinburgh EH9 3FF, U.K.
[‡]Department of Chemistry "G. Ciamician", Alma Mater Studiorum, University of Bologna, 40126 Bologna, Italy

Supporting Information

ABSTRACT: Whole-cell and cell-free transcription-translation biosensors have recently become favorable alternatives to conventional detection methods, as they are cost-effective, environmental friendly, and easy to use. Importantly, the biological responses from the biosensors need to be converted into a physicochemical signal for easy detection, and a variety of genetic reporters have been employed for this purpose. Reporter gene selection is vital to a sensor performance and application success. However, it was largely based on trial and error with very few systematic side-by-side investigations reported. To address this bottleneck, here we compared eight reporters from three reporter categories, i.e., fluorescent (*gfpmut3*, *deGFP*, *mCherry*, *mScarlet-I*), colorimetric (*lacZ*), and bioluminescent (*luxCDABE* from *Aliivibrio fischeri* and *Photorhabdus luminescens*, *NanoLuc*) reporters, under the control of two representative biosensors for mercury- and quorum-sensing molecules. Both whole-cell and cell-free formats were investigated to assess key sensing features including limit of detection (LOD), input and output dynamic ranges, response time, and output visibility. For both whole-cell biosensors, the lowest detectable concentration of analytes and the fastest responses were achieved with NanoLuc. Notably, we developed, to date, the most sensitive whole-cell mercury biosensor using NanoLuc as reporter, with an LOD ≤ 50.0 fM $HgCl_2$ 30 min postinduction. For cell-free biosensors, overall, *NanoLuc* and *deGFP* led to shorter response time and lower LOD than the others. This comprehensive profile of diverse reporters in a single setting provides a new important benchmark for reporter selection, aiding the rapid development of whole-cell and cell-free biosensors for various applications in the environment and health.

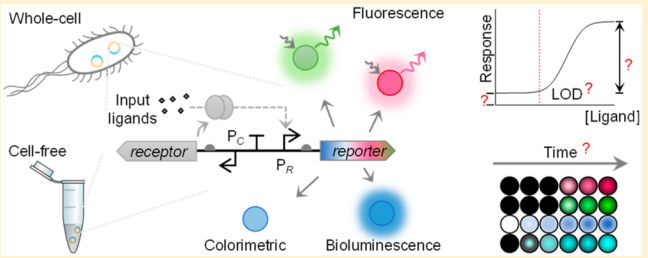

Whole-cell biosensors are cells that detect and report a target or condition of interest.[1−4] Due to being renewable, environmental friendly, and cost-effective, they have drawn increasing attention as viable alternatives to electronic or chemical sensors over the last three decades.[2,3] Notably, in the rising era of synthetic biology, a growing number of engineered whole-cell biosensors have been researched for a broad range of applications, such as environmental assessment,[3,5−7] clinical diagnosis[8,9] and biotherapy,[10,11] controlled bioprocessing,[12,13] mineral surveying,[14] and landmine clearing.[15]

Meanwhile the cell-free transcription-translation (TX-TL) system is becoming a favorable technology for *in vitro* synthetic biology study due to its capability of flexibility, stability, portability, and fast prototyping as well as creating a minimal cellular environment.[16−19] Because the cell-free system (CFS) contains no cells but only the basic biological machineries and energy sources required for TX-TL,[20] it has been proposed as a feasible solution to circumvent the biosafety issues associated with whole-cell biosensing.[19] Hence, a number of cell-free biosensors have been developed recently to detect heavy metals,[21] antibiotics,[22] and pathogens.[23,24]

Both whole-cell and cell-free biosensors share a similar architecture comprising a sensing module, a computing module, and an output actuating module.[1−3] Many reporter proteins that produce light,[8,25,26] fluorescence,[5,15] colors,[23,27] electrons,[28] or gas vesicles[29] can be used as genetic reporters in the output module.

Like other genetic devices or gene expression studies,[17,30] many biosensors were first built with fluorescent reporters as the output actuator,[3,5,15,24] thus simplifying their characterization in laboratory settings. Fluorescent proteins are relatively stable and take a short time to mature, and their light emission can be readily measured by a fluorimeter under specific light excitation. In addition, they can be used to study sensor cells at single cell level by fluorescence microscopy or fluorescence activated cell sorting.

Colorimetric reporters are often used to allow direct visualization of sensor output by the naked eye, which can drive down the operating costs of readout machines. As the first enzyme used to produce colorimetric output in engineered biosensors,[31] β-galactosidase (i.e., LacZ) from *Escherichia coli lac* operon is the most popular enzyme used for both whole-cell and cell-free biosensors.[19,21,23] The LacZ-catalyzed

Received: September 29, 2019
Accepted: November 6, 2019
Published: November 6, 2019

hydrolysis is fast,[19] but many bacterial strains contain an intact *lac* operon, which will increase the background of the colorimetric output.

Bioluminescent reporters are also based on biochemical reactions which produce light without the need of an excitation light source. Among them, bacterial (LuxCDABE or LuxAB)[8,32] and firefly (LucFF)[33] luciferases are often used in whole-cell or cell-free biosensors. Owing to its high luminescent activity and small size (19 kDa), the recently engineered NanoLuc luciferase has become a favored bioluminescent reporter for whole-cell biosensors.[25,34] Many of these bioluminescent biosensors have been coupled with portable devices for field testing or on-site diagnosis.[8,25,35] However, unless the whole luciferase cassette is present, an external substrate such as D-luciferin, coelenterazine, or furimazine is required, limiting their applications for continuous monitoring.

Although a variety of genetic reporters have been thoroughly studied, their selections for biosensor engineering were more based on one's experience rather than systematic side-by-side investigations. A few prior studies have been carried out to compare a couple of reporter categories; however, they were either not from the view of biosensor applications or not in directly comparable settings.[7,36−38] To facilitate biosensor engineering, it is of great importance to compare different reporter categories systemically while evaluating their contributions to sensing performance. To this end, here we characterized and compared three widely used reporter categories, i.e., fluorescent, colorimetric, and bioluminescent reporters, under two representative biosensors of mercury- and quorum-sensing molecule within two different sensor settings, i.e., whole-cell and cell-free contexts. We investigated their properties in terms of contributions to analytical performance and key sensing features including limit of detection (LOD), input and output dynamic ranges, response time, and output visibility. Such a comprehensive profile provides a new benchmark reference for reporter gene selection, which will aid the rapid development of whole-cell and cell-free biosensors for various applications.

EXPERIMENTAL SECTION

Strains, Chemicals, and Reagents. Plasmid cloning and *in vivo* genetic circuit characterization were all performed in *E. coli* TOP10. Cells were cultured in Lysogeny broth (LB) medium (10 g L^{-1} peptone, 5 g L^{-1} NaCl, 5 g L^{-1} yeast extract), with appropriate antibiotics. The antibiotic concentrations used were 50 μg mL^{-1} for both kanamycin and ampicillin (for low copy number plasmid) or 100 μg mL^{-1} for ampicillin (for high copy number plasmid). Antibiotics and inducers (i.e., mercury(II) chloride ($HgCl_2$) and *N*-(β-ketocaproyl)-L-homoserine lactone ($3OC_6HSL$)) were analytical grade and purchased from Sigma-Aldrich. They were dissolved in ddH_2O or nuclease free H_2O (W4502, Sigma-Aldrich) and were then filtered using 0.22 μm syringe filters (SLGP033RS, Millipore).

LacZ substrate 5-bromo-4-chloro-3-indolyl β-D-galactopyranoside (X-gal) (MB1001, Melford) was dissolved in dimethyl sulfoxide (DMSO) (D8418, Sigma-Aldrich) to make 2% or 5% (w/v) stock solutions. Substrate furimazine for NanoLuc luciferase was from Nano-Glo Luciferase Assay System (N1110, Promega).

Plasmid Circuit Construction. Standard molecular biology techniques were used to construct plasmids containing mercury- and quorum-sensing molecule-responsive genetic circuits. All plasmids were constructed via BioBrick assembly[39] and standard PCR. BioBrick vectors pSB1A3, pSB4A3, and pSB3K3 were used for plasmids cloning, and pSB3K3 was used for sensor circuit characterization (http://biobricks.org). Plasmid maps and detailed configurations are provided in relevant figures and summarized in Figure S1. Sequence details and sources of relevant parts are listed in Table S1. All primers used in this study, listed in Table S2, were purchased from Sigma-Aldrich. All plasmids constructed in this study have been confirmed by Sanger sequencing (Source BioScience). Detailed plasmid construction procedures are described in Supporting Information.

Reporter Gene Expression Assay *in Vivo*. For *in vivo* reporter gene characterization, engineered *E. coli* with constructed sensor plasmids were induced with $HgCl_2$ or $3OC_6HSL$, and the reporter signals were measured using a plate reader (BMG FLUOstar) post 30, 60, 90,120, 180, 240, 300, and 360 min induction and incubation. NanoLuc-conducted bioluminescent and LacZ-conducted colorimetric measurements were acquired in lysing and nonlysing conditions using the same concentration of substrates (X-gal = 0.04 mg mL^{-1} from 2% X-gal stock solution and 0.2 μL of furimazine stock solution per 200 μL of culture). NanoLuc-derived bioluminescent kinetics were measured for 30 min after substrate addition, and the highest signal was chosen for data analysis. Colorimetric signal measurement was preceded by 30 min incubation at 37 °C, with orbital shaking at 300 rpm in the plate reader. To determine the cell density, absorbance (A_{600}) was also read prior to each reporter measurement. For the *lux* operon reporter, the bioluminescent signal was measured immediately after absorbance measurement without the addition of substrates. Unless indicated otherwise, each reporter within different sensors was tested with three biological replicates. All the data shown are mean values with standard deviation as error bars. Detailed experimental procedures, data analysis, and instrument settings for reporter measurements and visualization are described in Supporting Information.

Reporter Gene Expression Assay *in Vitro*. The cell-free reactions were performed using *E. coli* S30 Extract System for Circular DNA (L1020, Promega) according to the manufacturer's protocol. Each reaction contained 40% (v/v) S30 premix, 10% (v/v) amino acid mix, 30% (v/v) S30 extract, and 2% (v/v) inducer. The remaining 18% (v/v) contained DNA template with or without substrates. A 9.6 nM DNA template was used for each reporter within the mercury-sensing circuit and for the negative control (reaction with empty pSB3K3). A 9.2 nM DNA template was used for each reporter within the quorum-sensing molecule-responsive circuit. Fluorescent and colorimetric reporters within each sensor were measured continuously using BMG FLUOstar plate reader after induction. For LacZ reporter characterization, 5% X-gal was supplied into cell-free mixture before incubation (with 0.042% X-gal as the final concentration). For NanoLuc reporter characterization, 0.5 μL of furimazine stock solution was added to each well of the cell-free mixture after 20, 40, 60, 120, 180, and 240 min incubation. Unless indicated otherwise, all the reporters within different sensors were tested in two independent experiments and each with three technical replicates. All the data shown are mean values with standard deviation as error bars. Detailed experimental procedures, data analysis, and instrument settings for reporter measurements are

DOI: 10.1021/acs.analchem.9b04444
Anal. Chem. 2019, 91, 15284−15292

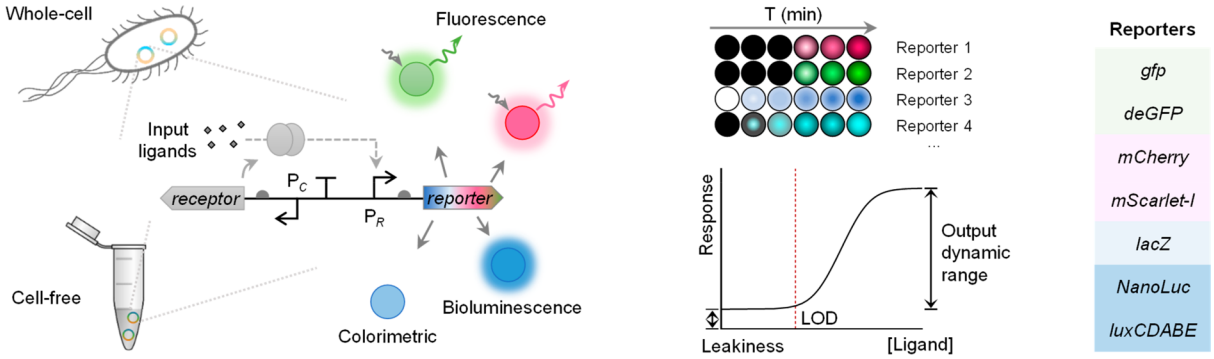

Figure 1. Comprehensive profiling of diverse genetic reporters in whole-cell and cell-free expression biosensor systems. Three categories of genetic reporters are selected to compare their profiles when applied in whole-cell and cell-free biosensors: (1) green fluorescent reporters (i.e., *gfp* and *deGFP*) and red fluorescent reporters (i.e., *mCherry* and *mScarlet-I*), (2) colorimetric reporter (i.e., *lacZ*), and (3) bioluminescent reporters (i.e., *NanoLuc* and *lux* operons from *A. fischeri* and *P. luminescens*). Response time, limit of detection (LOD), output dynamic range, and basal expression (leakiness) are tested for those reporters within both the mercury- and quorum-sensing molecule-responsive sensors.

described in Supporting Information. Calculation of sensor detection limit, mathematical modeling, and data fitting for both whole-cell and cell-free biosensors are described in Supporting Information.

RESULTS AND DISCUSSION

Design and Standardization of Reporter Expression Characterization for Biosensors. We characterized eight different genetic reporters to compare their main advantages and limitations contributing to the sensing performance of both whole-cell and cell-free biosensors. Fluorescent reporter genes *gfp* (*gfpmut3*), *deGFP*, *mCherry*, and *mScarlet-I*, luciferase genes *NanoLuc* and *lux* operons from *Aliivibrio fischeri* and *Photorhabdus luminescens*, and colorimetric output gene *lacZ* have been selected and profiled within the same biosensor settings both *in vivo* and *in vitro* (Figure 1).

Two biosensing systems for the mercury ion and $3OC_6HSL$ quorum-sensing molecule have been designed and standardized to characterize and compare the selected reporters (Figure S1). The medium copy number plasmid pSB3K3 (10−12 copies per cell[40]) was used for characterizing all reporters to limit the metabolic burden. The output actuating modules coupled with selected reporters were placed in opposite directions to the sensing modules to prevent potential transcriptional read-through to the reporter from the sensing module. All reporters within the two sensing systems were tested under the same condition either in *E. coli* TOP10 or in *E. coli* S30 CFS. LOD, input and output dynamic ranges, response time, and output visibility were profiled for each reporter.

***In Vivo* Characterization and Comparison of Genetic Reporters.** We first tested all chosen genetic reporters within a sensitive mercury sensor (i.e., J23109-*merR*-P_{merT}).[41] This sensor has a constitutive promoter (J23109) that drives the expression of the mercury receptor MerR, which would derepress its cognate promoter P_{merT} upon mercury (Hg^{2+}) binding and trigger the expression of the downstream reporter gene (Figure 2A).[42] Cell phone images, induction fold, and dose−response curves were obtained postinduction of mercury ($HgCl_2$) at various concentrations and different incubation times (Figure 2B−E, Figures S2−S4).

Comparing among the red fluorescent proteins (Figure 2B), we reported an induction fold over the control of 59.2 and 14.6 for mScarlet-I and mCherry, respectively (Figure S3), and LOD of 15.63 nM mercury for mCherry and 7.81 nM mercury for mScarlet-I (Figure S4), suggesting that mScarlet-I performs better than mCherry as a reporter. We deem this could be due to faster maturation and higher brightness of mScarlet than mCherry.[43] Comparing GFP and deGFP (Figure 2C), we reported that GFP had a higher fold of induction (51.3 vs 17.3), lower LOD (7.81 nM vs 125.00 nM of $HgCl_2$, Figure S4), and faster response (Figures S2,S3).

Both colorimetric reporter LacZ and bioluminescent reporter NanoLuc under the mercury sensor were monitored with lysed and nonlysed cells (see Experimental Section). Both reporters' performance was improved in cell lysing conditions in terms of response time, LOD, output dynamic range, and output visibilities (Figure 2D,E, Figures S2−S4), suggesting that the cell membrane could limit diffusion and transport of the substrates. For LacZ, the best LOD (0.49 nM of $HgCl_2$) with cell lysis was achieved 60 min postinduction, while the best LOD without cell lysis was 7.81 nM $HgCl_2$ (16-fold higher) after 6 h induction (Figure S4). For NanoLuc, the best LOD (5.00×10^{-5} nM $HgCl_2$) with cell lysis was obtained 30 min postinduction, while the best LOD without cell lysis was three orders higher (0.05 nM $HgCl_2$) and was observed 3 h postinduction and postincubation.

As concerns *lux* operons from *A. fischeri* and *P. luminescens*, only the *lux* operon from *P. luminescens* showed notable output upon mercury induction (Figure 2E, Figure S6). In addition, the *P. luminescens* luciferase contributed to a lower LOD (5.00×10^{-4} nM of $HgCl_2$) at early stage after induction (30−90 min), and higher output dynamic range at intermediate stage (90−120 min) (Figures S4 and S6). However, its overall performance was not comparable to that of NanoLuc with cell lysis. Compared to the NanoLuc without cell lysis, it remains a good bioluminescent reporter due to no requirement of adding substrates and lysing cells. Similar results were observed when testing the two operons under the quorum-sensing molecule sensor (Figures S6 and S7). Previous studies have shown that the luciferase from *A. fischeri* was thermolabile, with enzyme denaturation occurring above 30 °C, while the luciferase from *P. luminescens* was thermostable.[44] As all the experiments were performed at 37 °C, the activity of the luciferase from *A. fischeri* may have been inhibited due to denaturation. This was confirmed by characterizing the luciferase reporter under different temperatures, where the *A. fischeri* luciferase showed better activity at lower temperature in LB (Figure S7).

DOI: 10.1021/acs.analchem.9b04444
Anal. Chem. 2019, 91, 15284−15292

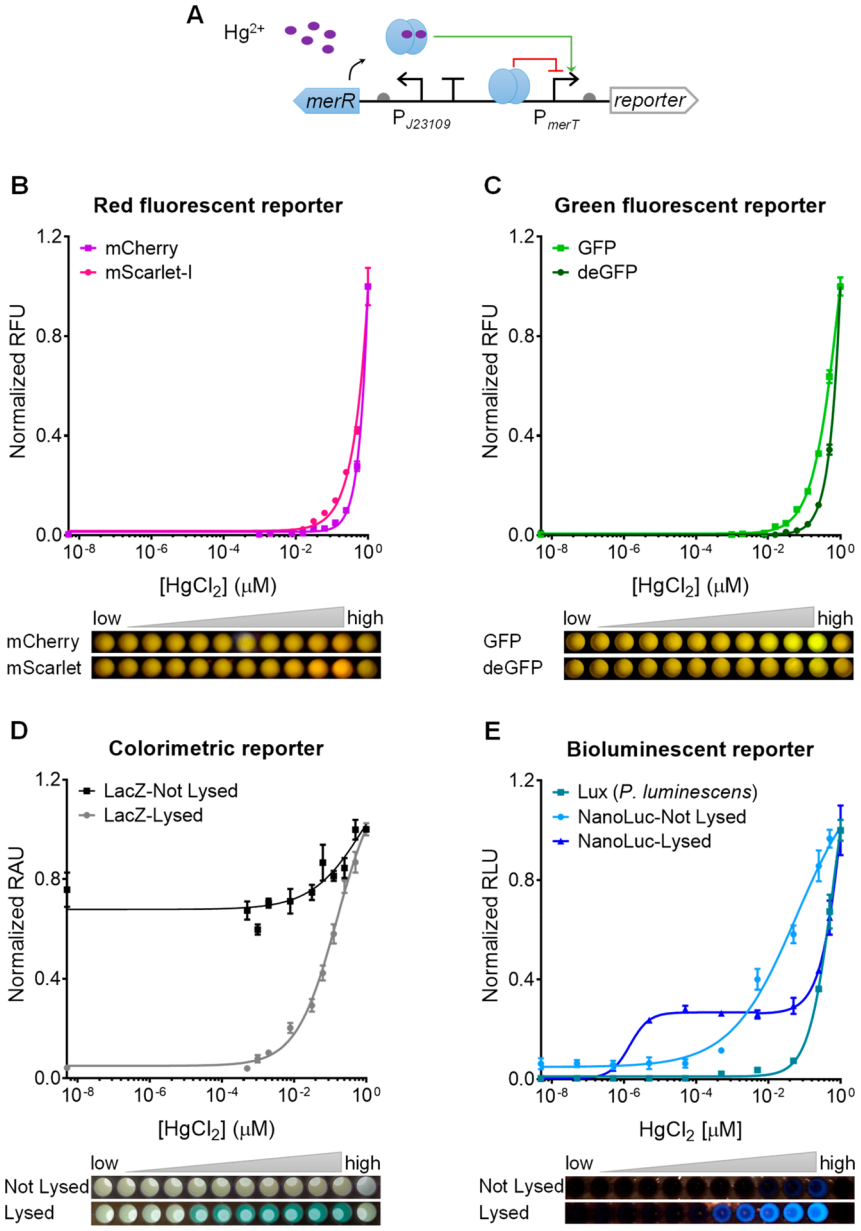

Figure 2. Characterization of diverse genetic reporters within a mercury-responsive whole-cell biosensor. (A) Schematic of a mercury-responsive sensor module (J23109-*merR*-P_{merT}) coupled to a genetic reporter. (B–E) Dose–response curves and cell phone images of the mercury sensor with red fluorescent reporters mCherry and mScarlet-I (B), green fluorescent reporters GFP and deGFP (C), colorimetric reporter LacZ with the cells lysed or not lysed (D), and bioluminescent reporters NanoLuc with cells lysed or not lysed and LuxCDABE from *P. luminescens* (E). The last well in each cell phone image shows the reporter-free negative control cultures. Data were collected 360 min postinduction for B and C, and 90 min postinduction for D and E. Values are mean ± SD (n = 3 biologically independent experiments).

Different media (i.e., M9 with glycerol or glucose as carbon source) were also tested, indicating that salt and glucose levels could affect the two luciferases' activities (Figure S7).[45]

Pros and Cons of Different Reporter Categories Acting *in Vivo*. mScarlet-I, GFP, LacZ (with cell lysis), and NanoLuc (with cell lysis) were selected for further analyses and investigation, as they showed superior performance in response time, LOD, and output dynamic range when compared to other reporters within their own categories.

We first compared the four reporters under the mercury sensor (Figure 3A). The best dose–responses for each reporter and the cognate fold of induction were analyzed (Figure 3B,C). The sensors with mScarlet-I and GFP reporter showed similar LOD and induction fold, both of which were improved with longer incubation time (Figure 3C, Figure S4). However, we observed high background level, especially for green fluorescence, due to autofluorescence from bacterial cells and LB medium, limiting their use for direct visualization (Figure S2). In contrast, LacZ and NanoLuc showed very low background, facilitating their direct visualization by the naked eye. Moreover, they contributed to faster response (30 min for LacZ and NanoLuc vs 60 min for GFP and mScarlet-I), much lower LOD (16-fold lower for LacZ and 5 orders of magnitude lower for NanoLuc) and broader input dynamic ranges than the fluorescent reporters, which indicates the fast enzymatic reaction-based reporters are preferable for sensors requiring a short and sensitive response. This observation is consistent with previous studies.[7,36,38] Nevertheless, both

DOI: 10.1021/acs.analchem.9b04444
Anal. Chem. 2019, 91, 15284–15292

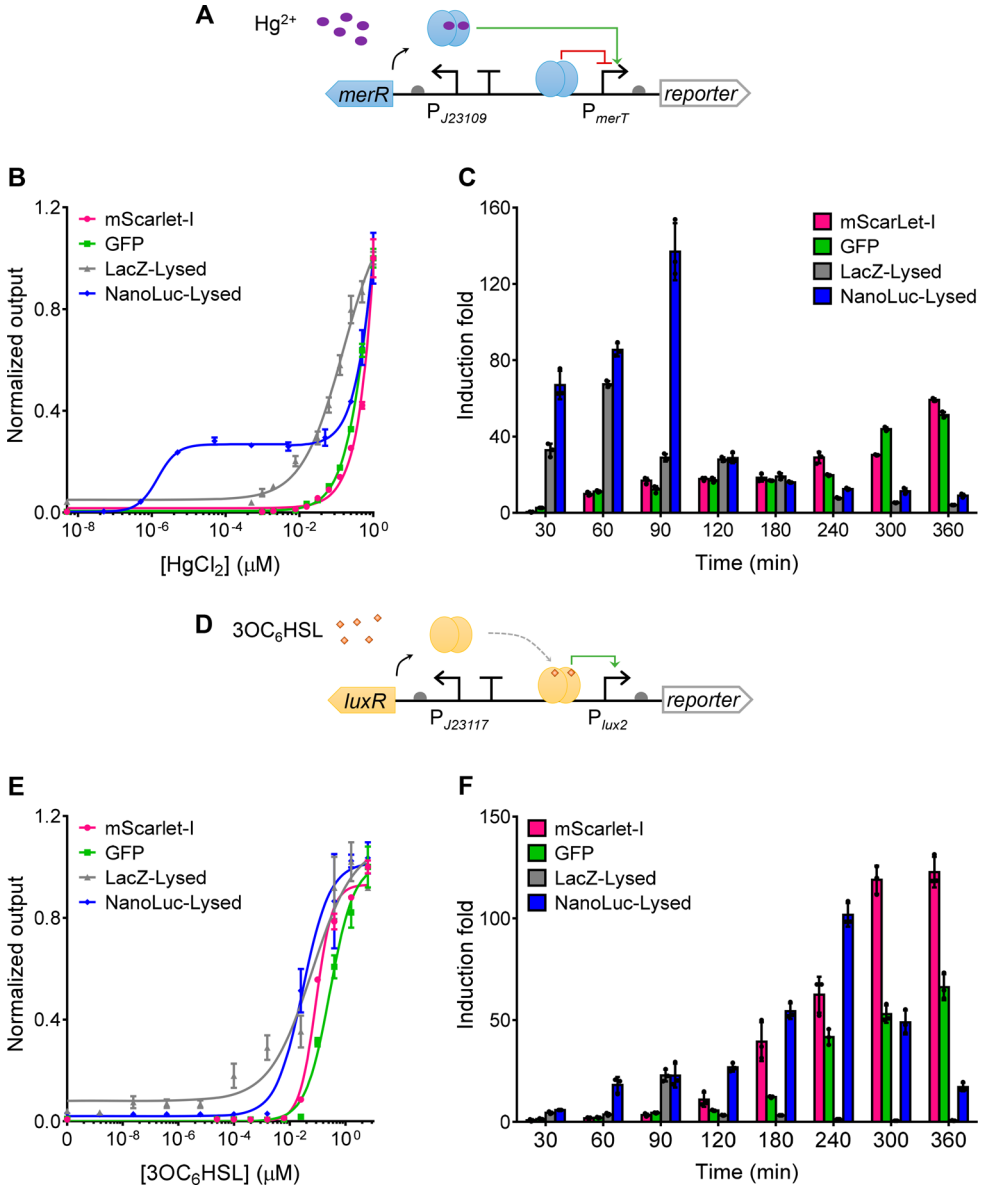

Figure 3. Comparing diverse genetic reporters within mercury and quorum-sensing molecule whole-cell biosensors. (A, D) Schematics showing the mercury- or quorum-sensing molecule sensor module (J23109-*merR*-P_{merT} or J23117-*luxR*-P_{lux2}) coupled to an output genetic reporter. (B, E) Dose−response of the mercury- and quorum-sensing molecule sensors with different reporters. For mScarlet-I and GFP, data were collected 360 min postinduction and postincubation. For LacZ and NanoLuc, data were collected 90 min postinduction. Dose−responses for the sensors at different time points are shown in Figures S4 and S5, and the relevant cell phone images are shown in Figures S2 and S8. (C, F) Fold of induction over time of the mercury- or quorum-sensing molecule sensors with different reporters responding to 0.1 μM $HgCl_2$ (C) and 0.04 μM $3OC_6HSL$ (F) respectively. Induction fold was calculated using the output with induction divided by the output without induction. Values are mean ± SD (n = 3 biologically independent experiments).

reporters with cell lysis are only suitable for disposable sensors with single-time-point readout. In addition, short time incubation will be required to obtain the best LOD and output dynamic range (Figure 3C, Figure S4) due to background activity induced by the sensor's leakiness, which is more sensitive toward amplified enzymatic reactions than fluorescent reporters (Figure S2).

To test the generality of the aforementioned reporters' performance, we next characterized the same set of reporters under a different sensing system, i.e., a quorum-sensing molecule ($3OC_6HSL$)-responsive sensor (J23117-*luxR*-P_{lux2}, Figure 3D−F).[46] In this sensing system, a constitutive promoter (J23117) drives the expression of the $3OC_6HSL$-responsive LuxR receptor which activates its cognate promoter P_{lux2} when bound to $3OC_6HSL$ (Figure 3D).[46] Similar to the performance of reporters under the mercury sensor, GFP and mScarlet-I under the quorum-sensing molecule sensor showed similar dose−response curves and LOD, and both their LOD and induction fold were improved with longer incubation time (Figure 3E,F, Figure S5). Similarly, LacZ and NanoLuc showed much lower LOD (3−4 orders of magnitude lower than the fluorescent reporters) and faster responses (30 min for LacZ and NanoLuc vs 60 min for GFP and mScarlet-I) than the fluorescent reporters. Notably, NanoLuc provided the lowest LOD (3.81×10^{-4} nM of $3OC_6HSL$) among all reporters characterized (Figure S5). Similar high background

DOI: 10.1021/acs.analchem.9b04444
Anal. Chem. 2019, 91, 15284−15292

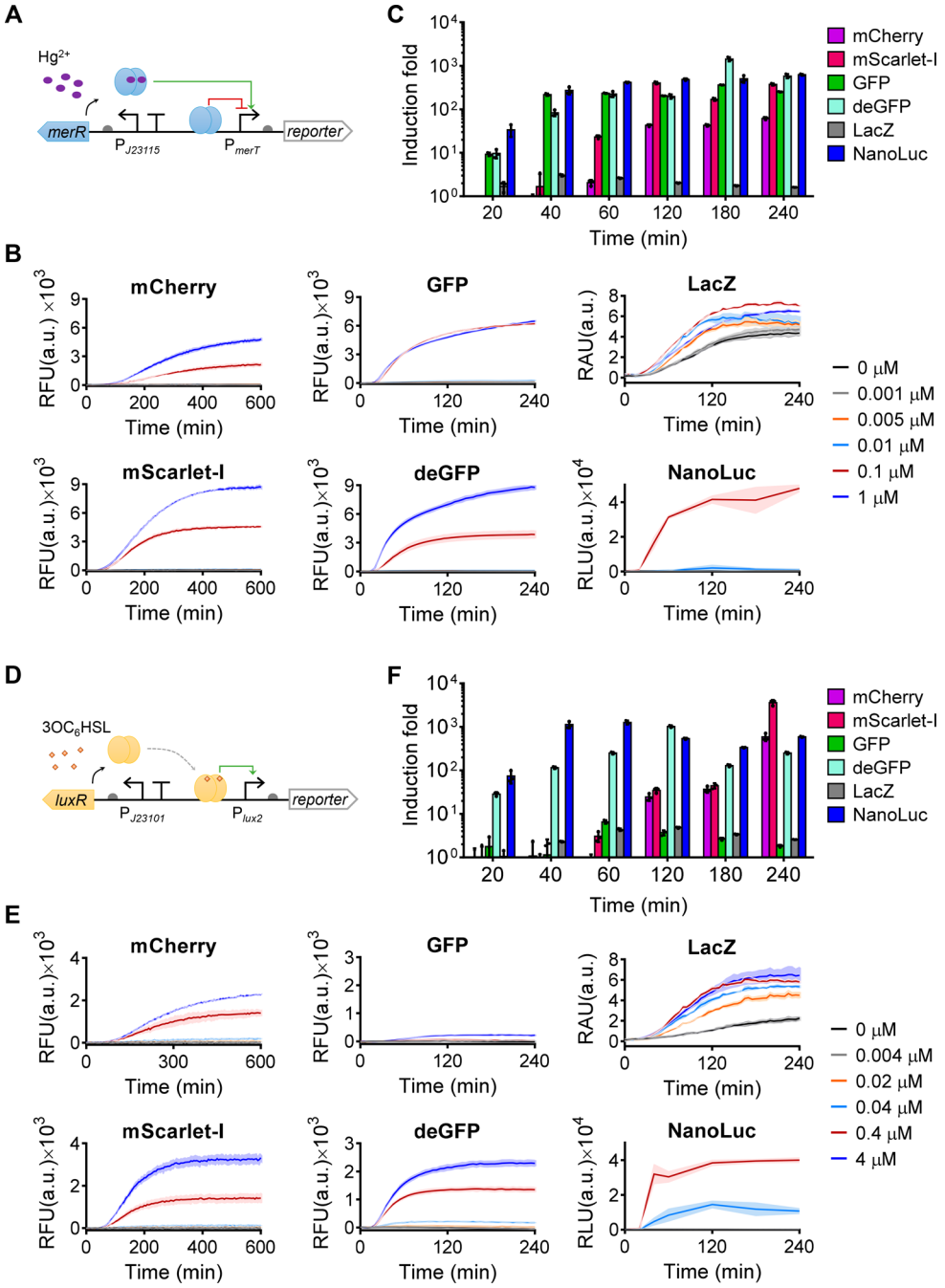

Figure 4. Profiling diverse genetic reporters within cell-free biosensors. (A, D) Schematics showing the mercury- or quorum-sensing molecule sensor (J23115-*merR*-P_{merT} or J23101-*luxR*-P_{lux2}) coupled to diverse genetic reporters. (B, E) Dynamic output responses of the sensors responding to varying concentrations of $HgCl_2$ (B) or $3OC_6HSL$ (E). (C, F) Fold of induction over time of the mercury- or quorum-sensing molecule cell-free sensors of different reporters responding to 0.1 μM $HgCl_2$ (C) and 0.4 μM $3OC_6HSL$ (F), respectively. Induction fold was calculated using the sensor output with induction divided by the sensor output without induction. Values are mean ± SD (n = 3 technical replicates). a.u., arbitrary units.

leakiness and decreasing induction fold across time were observed under the quorum-sensing molecule sensor (Figure 3F, Figure S8). In contrast to reporters under the mercury sensor, the best induction folds of LacZ and NanoLuc under the quorum-sensing molecule sensor were observed at longer incubation time. However, it is worth noting that the induction levels for the two types of sensors are not comparable and their output kinetics are different.

Interestingly, we observed a biphasic dose−response curve for the mercury sensor particularly with the NanoLuc reporter with cell lysis (Figures 2E,3B). Such a response curve was not observed for the quorum-sensing molecule sensor, suggesting the biphasic dose−response is largely due to the intrinsic sensing behavior of the mercury-sensing system. Unlike the transcriptional activator LuxR, MerR is a repressor-activator.[42] Moreover, previous studies suggested that with only one Hg^{2+} binding to the MerR homodimer, the MerR could activate transcription but at a moderate rate, while the MerR homodimer bound with two Hg^{2+} could fully activate the transcription.[42] Therefore, the mercury sensor may respond to

DOI: 10.1021/acs.analchem.9b04444
Anal. Chem. 2019, 91, 15284−15292

low mercury induction at a moderate rate while the response may be significantly increased in the presence of high mercury. This may explain why the biphasic dose−response curve occurred for the mercury sensor, particularly using NanoLuc reporter with cell lysis (Figures 2E and 3B). If the biphasic dose−response curve is not preferred, the data can be collected at an earlier time point postinduction and postincubation to eliminate such response behavior while maintaining similar high sensitivity (Figure S4A).

Characterization and Comparison of Genetic Reporters in TX-TL CFS. To provide a more comprehensive profiling of the different genetic reporters for biosensing, we compared the same reporters in an *in vitro* TX-TL CFS using cell-free biosensors. The CFS can be either based on crude cell extract[47] or a system of purified recombinant elements (PURE) necessary for transcription-translation.[48] The former is cheaper, easier to produce and more widely used in the field and therefore was selected for the reporter characterization in this study. Mercury- and quorum-sensing molecule sensors were also used for the *in vitro* test to provide a comparable context to their *in vivo* performance (Figure 4). To generate the same sensing activities for each sensor with different genetic reporters in the CFS, the same molar concentration of the sensory plasmids for each sensor was tested. Time-course response curves (Figure 4B,E), fold of induction (Figure 4C,F) and dose−responses (Figures S9 and S10) were analyzed for both sensors of different reporters. The experiments have been repeated at least twice independently (Figure S11).

Overall, the sensors with green fluorescent reporters or enzymatic reporters responded faster (20 min) and were more sensitive than the sensors with red fluorescent reporters (60 min) (Figure 4C,F, Figures S9, S10, and S11C,F). This meets our expectation, as the green fluorescent reporters generally mature faster than the red fluorescent reporters,[49] and the enzymatic reactions are usually more sensitive and can amplify the sensor's output signals. However, additional substrates are required for the enzymatic reaction, which is costly and unstable, whereas the high autofluorescence from the cell-free reagent could affect the measurement of the green fluorescent reporters. The LacZ substrate X-gal is more stable and cheaper than the NanoLuc substrate furimazine and can be added into the cell-free mixture at the beginning of induction. Nevertheless, cell-free sensors with LacZ reporter have low induction fold due to the sensors' high background caused by leakiness and hence low output dynamic range of the cognate color change. In addition, the commercial CFS we used was made from a *lacZ+* cell strain and hence already contains some background level of LacZ, thus increasing the background leakiness and reducing the output dynamic range. Using a LacZ-free CFS or a more sensitive LacZ substrate may improve this reporter's performance *in vitro*.

Surprisingly, both green fluorescent reporters and NanoLuc provided the best LOD among all the reporters (Figures S9 and S10) but with a shorter incubation time for the latter (Figure S10B). For the mercury sensor, the GFP reporter contributed to an LOD < 1.0×10^{-3} μM mercury, making it the most sensitive one among all cell-free mercury sensors constructed to date. For the quorum-sensing molecule sensor, both deGFP (4 h) and NanoLuc (40 min) contributed to an LOD < 4.0×10^{-3} μM $3OC_6HSL$, 5−10 times lower than the rest of reporters.

When each reporter category was compared, mScarlet-I was superior to mCherry in terms of response time and induction fold (Figure 4C,F, Figure S11C,F), similar to their performance *in vivo*. However, the comparison of GFP and deGFP was less conclusive. The fluorescence output of deGFP was much higher than that of GFP under the quorum-sensing molecule sensor (Figure 4E, Figure S11E) while it was only true for the mercury sensor under high mercury induction levels (Figure 4B, Figure S11B). deGFP was designed to be more translatable in CFS than its original eGFP,[50] but its performance against GFPmut3 (i.e., the GFP we tested here) has not been studied previously. Because deGFP worked well for both mercury- and quorum-sensing molecule sensors, it may be a more reliable reporter for regular cell-free biosensors. Further investigation would aid an in-depth comparison of their performance as a reporter, for example, by measuring the reporters' fluorescent intensity, maturation, and transcription and translation efficiency in different genetic contexts.

CONCLUSIONS

In summary, we provided a comprehensive profiling of eight different genetic reporters from three commonly used reporter categories (i.e., fluorescent, colorimetric, and bioluminescent detection) within two representative sensor systems both *in vivo* and *in vitro*. The selected reporters have been frequently used in either whole-cell or cell-free biosensors but barely compared systematically in terms of their contributions to sensing features, limiting the biosensors' development and applications. NanoLuc luciferase is a noticeable reporter due to its small size and high luminescent activity. Our study for the first time showed its characteristics in bacterial whole-cell biosensors and cell-free biosensors and indicated its superior reporting performance in both sensing systems. Overall, we reported that enzymatic reporters (especially bioluminescent reporter NanoLuc) provided the fastest response and lowest LOD *in vivo*. Both green fluorescent reporters and the enzymatic reporters contributed to the fastest response and lowest LOD *in vitro*. Considering the drastic differences and wide representation of the two sensor systems tested, similar conclusions obtained from the two sensor systems indicate the generality of our findings regarding the performance of these different genetic reporters. Therefore, these results can be reasonably applied to and inform the development of biosensors for other targets. However, the choice of sensor reporters also need to take into account several other important factors pertinent to their real world application requirements, such as the background signal level (green fluorescent reporter has the highest background activity), cost, and stability of the substrates for enzymatic reporters, whether an end-point data acquisition is sufficient or a continuous monitoring is preferred, and whether the cells can be lysed or not. This study provides new important benchmark for biosensor reporter gene selection, which will aid the rapid development of different whole-cell and cell-free biosensors for a variety of applications in the environment and health.

ASSOCIATED CONTENT

Supporting Information

The Supporting Information is available free of charge on the ACS Publications website at DOI: 10.1021/acs.analchem.9b04444.

Experimental procedures, plasmid maps, cell phone images, dose−response curves over time for *in vivo* and *in vitro* analyses, list of LOD, *lux* operon character-

DOI: 10.1021/acs.analchem.9b04444
Anal. Chem. 2019, 91, 15284−15292

ization, independent replicates of *in vitro* assay, list of genetic parts and sequences, list of oligonucleotides, and list of abbreviations (PDF)

AUTHOR INFORMATION

Corresponding Author

*E-mail: baojun.wang@ed.ac.uk.

ORCID

Baojun Wang: 0000-0002-4858-8937

Author Contributions

X.W. and A.L. contributed equally to this work. B.W. conceived and led the study. B.W., A.L., and X. W. designed the experiments. X.W., A.L., E.M., and A.R. designed and optimized the bioluminescent assays. X.W. and A.L. performed all the experiments and data analysis. All authors took part in the interpretation of results and preparation of materials for the manuscript. X.W., A.L., and B.W. wrote the manuscript with inputs from all authors.

Notes

The authors declare no competing financial interest.

ACKNOWLEDGMENTS

We thank Shimshon Belkin (Hebrew University of Jerusalem) for providing the plasmids comprising the *lux* operons. This work was supported by UK BBSRC grant [BB/N007212/1], Leverhulme Trust [RPG-2015-445], UKRI Future Leaders Fellowship [MR/S018875/1], Wellcome Trust Seed Award in Science [202078/Z/16/Z], and EPSRC/BBSRC Global Challenges Research Fund Awards to B.W. A.L., E.M., and A.R. were supported by the NATO Science for Peace and Security Programme under grant no. 985042.

REFERENCES

(1) Wang, B.; Buck, M. *Trends Microbiol.* **2012**, *20* (8), 376−384.
(2) van der Meer, J. R.; Belkin, S. *Nat. Rev. Microbiol.* **2010**, *8* (7), 511−522.
(3) Kim, H. J.; Jeong, H.; Lee, S. J. *Anal. Bioanal. Chem.* **2018**, *410* (4), 1191−1203.
(4) Hicks, M.; Bachmann, T. T.; Wang, B. *ChemPhysChem* **2019**, *20*, 1−14.
(5) Wang, B.; Barahona, M.; Buck, M. *Biosens. Bioelectron.* **2013**, *40* (1), 368−376.
(6) Cao, Y.; Feng, Y.; Ryser, M. D.; Zhu, K.; Herschlag, G.; Cao, C.; Marusak, K.; Zauscher, S.; You, L. *Nat. Biotechnol.* **2017**, *35* (11), 1087−1093.
(7) Stocker, J.; Balluch, D.; Gsell, M.; Harms, H.; Feliciano, J.; Daunert, S.; Malik, K. A.; van der Meer, J. R. *Environ. Sci. Technol.* **2003**, *37* (20), 4743−4750.
(8) Mimee, M.; Nadeau, P.; Hayward, A.; Carim, S.; Flanagan, S.; Jerger, L.; Collins, J.; McDonnell, S.; Swartwout, R.; Citorik, R. J.; et al. *Science* **2018**, *360* (6391), 915−918.
(9) Courbet, A.; Endy, D.; Renard, E.; Molina, F.; Bonnet, J. *Sci. Transl. Med.* **2015**, *7* (289), 289ra83.
(10) Ho, C. L.; Tan, H. Q.; Chua, K. J.; Kang, A.; Lim, K. H.; Ling, K. L.; Yew, W. S.; Lee, Y. S.; Thiery, J. P.; Chang, M. W. *Nat. Biomed. Eng.* **2018**, *2* (1), 27−37.
(11) Chen, J. X.; Steel, H.; Wu, Y. H.; Wang, Y.; Xu, J.; Rampley, C. P. N.; Thompson, I. P.; Papachristodoulou, A.; Huang, W. E. *Appl. Environ. Microbiol.* **2019**, *85* (6), e02959.
(12) Zhang, F.; Carothers, J. M.; Keasling, J. D. *Nat. Biotechnol.* **2012**, *30* (4), 354−359.
(13) Dekker, L.; Polizzi, K. M. *Curr. Opin. Chem. Biol.* **2017**, *40*, 31−36.
(14) Cerminati, S.; Soncini, F. C.; Checa, S. K. *Biotechnol. Bioeng.* **2011**, *108* (11), 2553−2560.
(15) Belkin, S.; Yagur-Kroll, S.; Kabessa, Y.; Korouma, V.; Septon, T.; Anati, Y.; Zohar-Perez, C.; Rabinovitz, Z.; Nussinovitch, A.; Agranat, A. J. *Nat. Biotechnol.* **2017**, *35* (4), 308−310.
(16) Garamella, J.; Marshall, R.; Rustad, M.; Noireaux, V. *ACS Synth. Biol.* **2016**, *5* (4), 344−355.
(17) Niederholtmeyer, H.; Sun, Z. Z.; Hori, Y.; Yeung, E.; Verpoorte, A.; Murray, R. M.; Maerkl, S. J. *eLife* **2015**, *4*, e09771.
(18) Rampley, C. P. N.; Davison, P. A.; Qian, P.; Preston, G. M.; Hunter, C. N.; Thompson, I. P.; Wu, L. J.; Huang, W. E. *Sci. Rep.* **2017**, *7* (1), 7261.
(19) Pardee, K.; Green, A. a; Ferrante, T.; Cameron, D. E.; Daleykeyser, A.; Yin, P.; Collins, J. J. *Cell* **2014**, *159* (4), 940−954.
(20) Perez, J. G.; Stark, J. C.; Jewett, M. C. *Cold Spring Harbor Perspect. Biol.* **2016**, *8* (12), a023853.
(21) Didovyk, A.; Tonooka, T.; Tsimring, L.; Hasty, J. *ACS Synth. Biol.* **2017**, *6* (12), 2198−2208.
(22) Duyen, T. T. M.; Matsuura, H.; Ujiie, K.; Muraoka, M.; Harada, K.; Hirata, K. *J. Biosci. Bioeng.* **2017**, *123* (1), 96−100.
(23) Pardee, K.; Green, A. A.; Takahashi, M. K.; Braff, D.; Lambert, G.; Lee, J. W.; Ferrante, T.; Ma, D.; Donghia, N.; Fan, M.; et al. *Cell* **2016**, *165* (5), 1255−1266.
(24) Wen, K. Y.; Cameron, L.; Chappell, J.; Jensen, K.; Bell, D. J.; Kelwick, R.; Kopniczky, M.; Davies, J. C.; Filloux, A.; Freemont, P. S. *ACS Synth. Biol.* **2017**, *6* (12), 2293−2301.
(25) Lopreside, A.; Calabretta, M. M.; Montali, L.; Ferri, M.; Tassoni, A.; Branchini, B. R.; Southworth, T.; D'Elia, M.; Roda, A.; Michelini, E. *Anal. Bioanal. Chem.* **2019**, *411* (19), 4937−4949.
(26) Michelini, E.; Calabretta, M. M.; Cevenini, L.; Lopreside, A.; Southworth, T.; Fontaine, D. M.; Simoni, P.; Branchini, B. R.; Roda, A. *Biosens. Bioelectron.* **2019**, *123*, 269−277.
(27) Watstein, D. M.; Styczynski, M. P. *ACS Synth. Biol.* **2018**, *7* (1), 267−275.
(28) Webster, D. P.; TerAvest, M. a; Doud, D. F. R.; Chakravorty, A.; Holmes, E. C.; Radens, C. M.; Sureka, S.; Gralnick, J. a; Angenent, L. T. *Biosens. Bioelectron.* **2014**, *62*, 320−324.
(29) Bourdeau, R. W.; Lee-Gosselin, A.; Lakshmanan, A.; Farhadi, A.; Kumar, S. R.; Nety, S. P.; Shapiro, M. G. *Nature* **2018**, *553* (7686), 86−90.
(30) Wang, B.; Kitney, R. I.; Joly, N.; Buck, M. *Nat. Commun.* **2011**, *2* (1), 508.
(31) Quillardet, P.; Huisman, O.; D'Ari, R.; Hofnung, M. *Proc. Natl. Acad. Sci. U. S. A.* **1982**, *79* (19), 5971−5975.
(32) King, J. M. H.; DiGrazia, P. M.; Applegate, B.; Burlage, R.; Sanseverino, J.; Dunbar, P.; Larimer, F.; Sayler, G. S. *Science* **1990**, *249* (4970), 778−781.
(33) Pellinen, T.; Huovinen, T.; Karp, M. *Anal. Biochem.* **2004**, *330* (1), 52−57.
(34) Eggers, C. T.; Valley, M. P.; Klaubert, D. H.; Unch, J.; Encell, L. P.; Wood, K. V.; Hall, M. P.; Benink, H. A.; Otto, P.; Zimmerman, K.; et al. *ACS Chem. Biol.* **2012**, *7* (11), 1848−1857.
(35) Siegfried, K.; Endes, C.; Bhuiyan, A. F. M. K.; Kuppardt, A.; Mattusch, J.; van der Meer, J. R.; Chatzinotas, A.; Harms, H. *Environ. Sci. Technol.* **2012**, *46* (6), 3281−3287.
(36) Huang, C. W.; Yang, S. H.; Sun, M. W.; Liao, V. H. C. *Environ. Sci. Pollut. Res.* **2015**, *22* (13), 10206−10213.
(37) Garcia, H. G.; Lee, H. J.; Boedicker, J. Q.; Phillips, R. *Biophys. J.* **2011**, *101* (3), 535−544.
(38) Hakkila, K.; Maksimow, M.; Karp, M.; Virta, M. *Anal. Biochem.* **2002**, *301* (2), 235−242.
(39) Shetty, R. P.; Endy, D.; Knight, T. F. *J. Biol. Eng.* **2008**, *2*, 5.
(40) Liu, Q.; Schumacher, J.; Wan, X.; Lou, C.; Wang, B. *ACS Synth. Biol.* **2018**, *7* (2), 553−564.
(41) Wan, X.; Volpetti, F.; Petrova, E.; French, C.; Maerkl, S. J.; Wang, B. *Nat. Chem. Biol.* **2019**, *15* (5), 540−548.
(42) Chang, C. C.; Lin, L. Y.; Zou, X. W.; Huang, C. C.; Chan, N. L. *Nucleic Acids Res.* **2015**, *43* (15), 7612−7623.

DOI: 10.1021/acs.analchem.9b04444
Anal. Chem. 2019, 91, 15284−15292

(43) Bindels, D. S.; Haarbosch, L.; Van Weeren, L.; Postma, M.; Wiese, K. E.; Mastop, M.; Aumonier, S.; Gotthard, G.; Royant, A.; Hink, M. A.; et al. *Nat. Methods* **2017**, *14* (1), 53−56.
(44) Manukhov, I. V.; Eroshnikov, G. E.; Vyssokikh, M. Y.; Zavilgelsky, G. B. *FEBS Lett.* **1999**, *448* (2−3), 265−268.
(45) Waters, P.; Lloyd, D. *Microbiology* **1985**, *131* (11), 2865−2869.
(46) Wang, B.; Barahona, M.; Buck, M. *Nucleic Acids Res.* **2015**, *43* (3), 1955−1964.
(47) Kim, D. M.; Kigawa, T.; Choi, C. Y.; Yokoyama, S. *Eur. J. Biochem.* **1996**, *239* (3), 881−886.
(48) Shimizu, Y.; Inoue, A.; Tomari, Y.; Suzuki, T.; Yokogawa, T.; Nishikawa, K.; Ueda, T. *Nat. Biotechnol.* **2001**, *19* (8), 751−755.
(49) Balleza, E.; Kim, J. M.; Cluzel, P. *Nat. Methods* **2018**, *15* (1), 47−51.
(50) Shin, J.; Noireaux, V. *J. Biol. Eng.* **2010**, *4*, 8.

DOI: 10.1021/acs.analchem.9b04444
Anal. Chem. 2019, 91, 15284−15292

Supporting Information

Comprehensive profiling of diverse genetic reporters with application to whole-cell and cell-free biosensors

Antonia Lopreside[1,2], Xinyi Wan[1,3], Elisa Michelini[2], Aldo Roda[2] and Baojun Wang[1,3]*

[1]School of Biological Sciences, University of Edinburgh, Edinburgh EH9 3FF, UK

[2]Department of Chemistry "G. Ciamician", Alma Mater Studiorum, University of Bologna, Italy

[3]Centre for Synthetic and Systems Biology, University of Edinburgh, Edinburgh EH9 3FF, UK

**Correspondence can be addressed to BW (baojun.wang@ed.ac.uk)*

Table of Contents

Experimental Procedure

Plasmid circuit construction

Compared to previously studied plasmids pBW316J101-luxR[1] and pXWJ109Hg-gfp[2], the constitutive promoters with receptors were inverted and oriented in the opposite direction to the inducible promoters and reporters by PCR and BioBrick™ assembly. For tuning the intracellular receptor densities, the constitutive promoters that drive the expression of the mercury receptor MerR and the quorum sensing molecule receptor LuxR were replaced via PCR.

mCherry was amplified from BioBrick™ part BBa_J06504 by PCR with addition of a ribosome binding site (RBS) BBa_B0030. *mScarlet-I* with BBa_B0030 was synthesized through Integrated DNA Technologies (gBlocks® Gene Fragments) and was amplified by PCR. *gfp* was amplified from a previously studied plasmid pXWJ109Hg-gfp[2] by PCR. *deGFP* was amplified from plasmid Pr-deGFP (#67743, Addgene) by PCR with addition of BBa_B0030. *lacZ* was amplified from *E. coli* MG1655 genome by PCR with addition of BBa_B0030. *NanoLuc* was amplified from plasmid pCDNA-NanoLuc[3] with addition of BBa_B0030. *lux* operons from *P. luminescens* and *A. fischeri* were amplified from the gift plasmids provided by Prof Belkin Shimshon (Hebrew University of Jerusalem).

Reporter gene expression assay *in vivo*

For reporter gene characterization, the engineered *E. coli* were first inoculated from a single colony on a freshly streaked solid LB plate to 5 mL LB medium, and cultured overnight at 37°C with shaking (160 rpm). Then the cells were diluted 100-fold from the overnight culture into fresh LB medium. For liquid culture induction, the diluted culture was loaded into a 96-well 2.0 mL deepwell plate with round bottom (E2896-2110, Starlab), and induced with 40 μL inducers to a final volume of 1.6 mL per well. The microplate was sealed with an air permeable film (AXY2006, SLS), and incubated in a shaker incubator (MB100-4A, Allsheng) with continuous shaking (1,000 rpm, 37°C). After 30, 60, 90,120, 180, 240, 300 and 360 min incubation, 200 μL of induced culture were dispensed in 96-well microplates with clear-bottom (655096, Greiner Bio-One). A plate reader (BMG FLUOstar) was used to measure fluorescence (bottom reading), absorbance and bioluminescence (top reading). 485 nm excitation and 520 ± 10 nm emission wavelengths were used for measuring green fluorescent reporters with Gain = 1,000. For red fluorescent reporters measurement, 584 nm excitation and 620 ± 10 nm emission wavelengths with Gain = 2,000 were used. Bioluminescent signal was acquired with 0.1 s of signal integration for each well and Gain = 1,500. Colorimetric signal was acquired by absorbance measurement of A_{650}. NanoLuc-conducted bioluminescent and LacZ-conducted colorimetric measurements were acquired in lysing and non-lysing conditions using the same concentration of substrates (X-gal = 0.04 mg mL^{-1} from 2% X-gal stock solution and 0.2 μL of furimazine stock solution per 200 μL culture). B-PER™ Bacterial Protein Extraction Reagent (78243, ThermoFisher Scientific) and PBS (K813-500ML, VWR) were used in lysing and non-lysing

conditions respectively to dilute the substrate. A 50 μL-volume of diluted substrate was added in each well with a final volume of 250 μL. NanoLuc-derived bioluminescent kinetics were measured for 30 min after substrate addition and the highest signal was chosen for data analysis. Colorimetric signal measurement was preceded by 30 min incubation at 37°C, with orbital shaking at 300 rpm in the plate reader. To determine the cell density, absorbance (A_{600}) was also read prior to each reporter measurement. For *lux* operon reporter, the bioluminescent signal was measured immediately after absorbance measurement without the addition of substrates.

The plate reader data acquired using Omega MARS 3.20 R2 were exported to Microsoft Excel 2013 and GraphPad Prism 6.01 for data analysis and presentation. The medium backgrounds of fluorescence, absorbance or luminescence were determined from blank wells loaded with LB medium and were subtracted from the readings of other wells. The relative fluorescence, absorbance or luminescence unit (RFU, RAU or RLU) at different time points for a sample culture was determined by the blank corrected output signal divided by A_{600}, and after subtracting its triplicate-averaged counterpart of the negative control cultures (reporter-free) at the same time. Unless indicated otherwise, each reporter within different sensors was tested with three biological replicates. All the data shown are mean values with standard deviation as error bars.

Fluorescent, bioluminescent and colorimetric signals were also acquired with a cell phone (OnePlus5) integrated camera (1/2.8" 16MP Sony IMX 398 sensor, 1.12 μm pixel size and F1.7 aperture). The microplates with cultured cells after each measurement were placed onto the surface of a Safe Imager™ (S37102, Invitrogen) blue-light transilluminator, and were covered with an amber filter in a dark environment. Fluorescent signals were acquired with the blue light on while the bioluminescent signals were acquired with the light off. The images with fluorescent or bioluminescent signals were captured with 30 s integration time.

Reporter gene expression assay *in vitro*

E. coli S30 Extract System for Circular DNA (L1020, Promega) was used for *in vitro* characterization of different reporters. Engineered *E. coli* with different reporters were first inoculated from a single colony on a freshly streaked solid LB plate to 2 mL terrific broth (TB) medium (12 g L^{-1} peptone, 24 g L^{-1} yeast extract, 12.54 g L^{-1} K_2HPO_4, 2.31 g L^{-1} KH_2PO_4, 4 mL L^{-1} glycerol), and cultured for 8 h at 37°C with shaking (160 rpm). Then 75 μL of each culture was diluted into 30 mL of fresh TB, and was incubated overnight at 37°C with shaking (160 rpm). The cultured cells were used for plasmid extraction. The plasmids were purified using ZymoPURE II™ Plasmid Midiprep Kit (D4201, Zymo Research) following the manufacturers' protocols, and then were further purified using Monarch® PCR & DNA Cleanup Kit (T1030S, NEB). The plasmids were eluted in nuclease free H_2O.

All cell-free reactions were prepared in a black 384-well microplate with clear bottom (for fluorescence and absorbance measurement, 788096, Greiner Bio-One) or a white 384-well microplate with clear bottom (for bioluminescence measurement, 788095, Greiner Bio-One) on ice, with 4 μL cell-free mixture topped with 5 μL of Chill-Out Liquid Wax (CHO1411, Bio-Rad) in each well. The plate was sealed with a transparent EASYseal plate sealer (676001, Greiner Bio-One) for fluorescence (bottom reading) and absorbance measurement, or covered with a transparent lid for bioluminescence measurement (bottom reading) to ease the addition of the substrate furimazine. The plate was incubated and measured continuously by BMG FLUOstar plate reader at 37˚C without shaking. The settings for measuring the fluorescence and bioluminescence were the same as for the *in vivo* characterization. Absorbance (A_{670}) was used for measuring the colorimetric reporter.

The plate reader data were processed using Omega MARS 3.20 R2, Microsoft Excel 2013 and GraphPad Prism 6.01. To calculate the RFU, RAU and RLU at different time points, the background of output signals was subtracted from each cell-free reaction by using its triplicate-averaged counterpart of the negative control (reporter-free) at the same time. All the data shown are mean values with standard deviation as error bars.

Calculation of sensor detection limit

The limit of detection (LOD) is the lowest analyte concentration likely to be reliably distinguished from the basal signal and at which detection is feasible.[4] The calculation has been described previously.[2]

Mathematical modelling and data fitting

Biochemical models were developed for individual transcription factor receptor modules to abstract their ligand-dependent dose response behaviors. The ordinary differential equation-based deterministic model was used for accurately modelling the gene regulation and expression across the full input or output range of the sensor systems.[5] It has been described previously.[1]

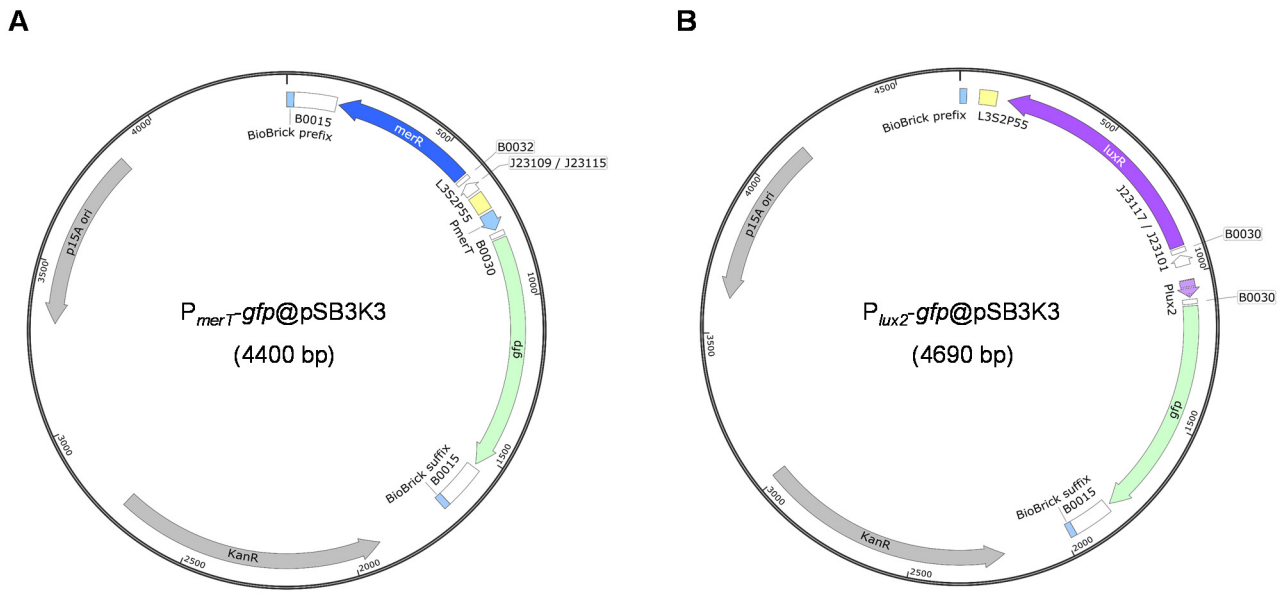

Figure S1: Representative plasmid maps for the sensor genetic circuits constructed and tested *in vivo* and *in vitro* in this study.

Plasmids maps showing the mercury (A) and quorum sensing molecule (B) sensor circuits with *gfp* as the output reporter. For the sensors with other reporters (except *lux* operon), *gfp* was replaced by *mCherry*, *mScarlet-I*, *degfp*, *lacZ* or *NanoLuc*. For the sensors using *lux* operon as output reporter, *gfp* with its RBS was replaced by the *lux* operon with RBS. Sequence details are listed in Table S1.

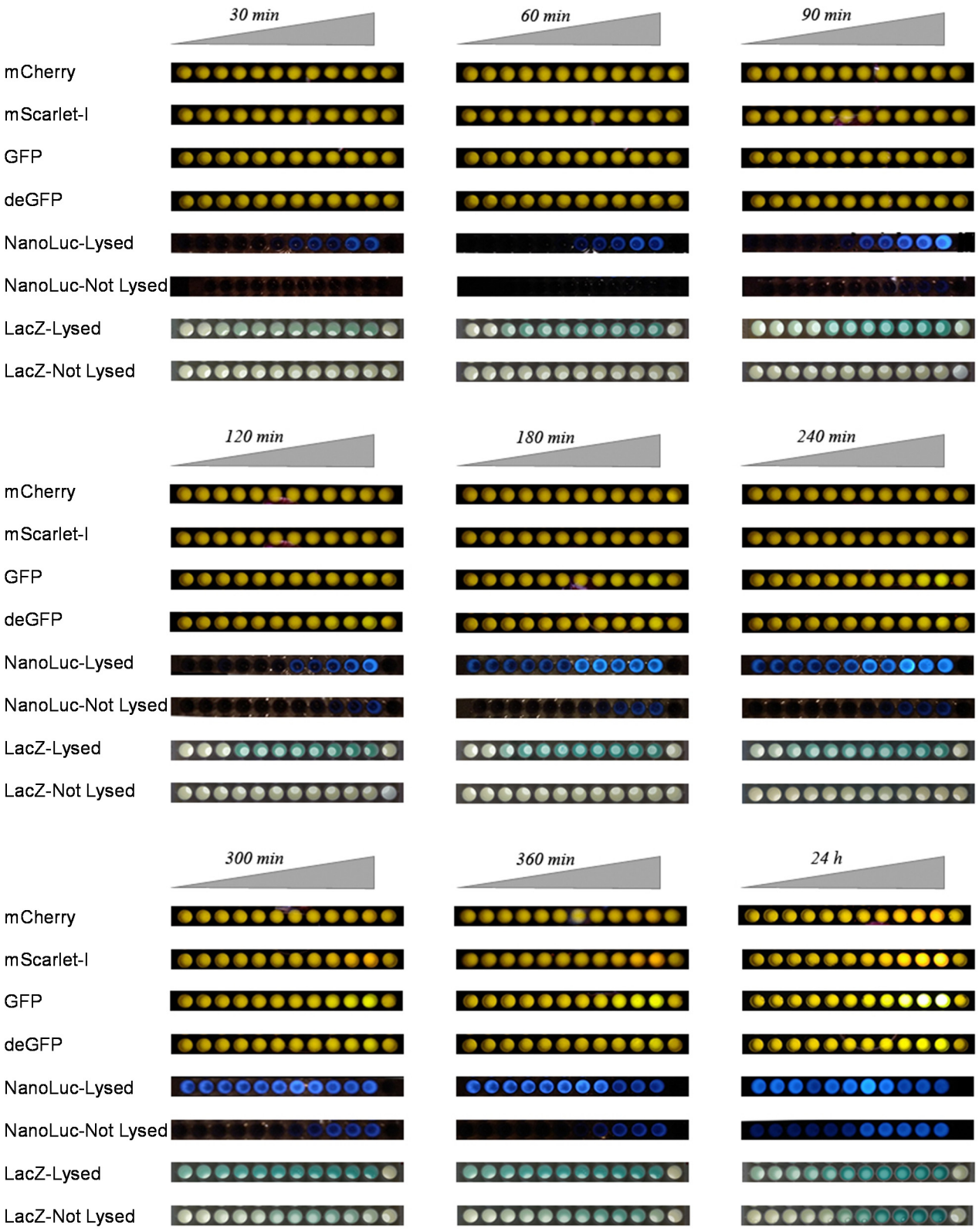

Figure S2: Cell phone images of diverse reporters within whole-cell mercury sensor. Related to Figures 2 and 3B–C.

The last well in each cell phone image shows the reporter-free negative control cultures.

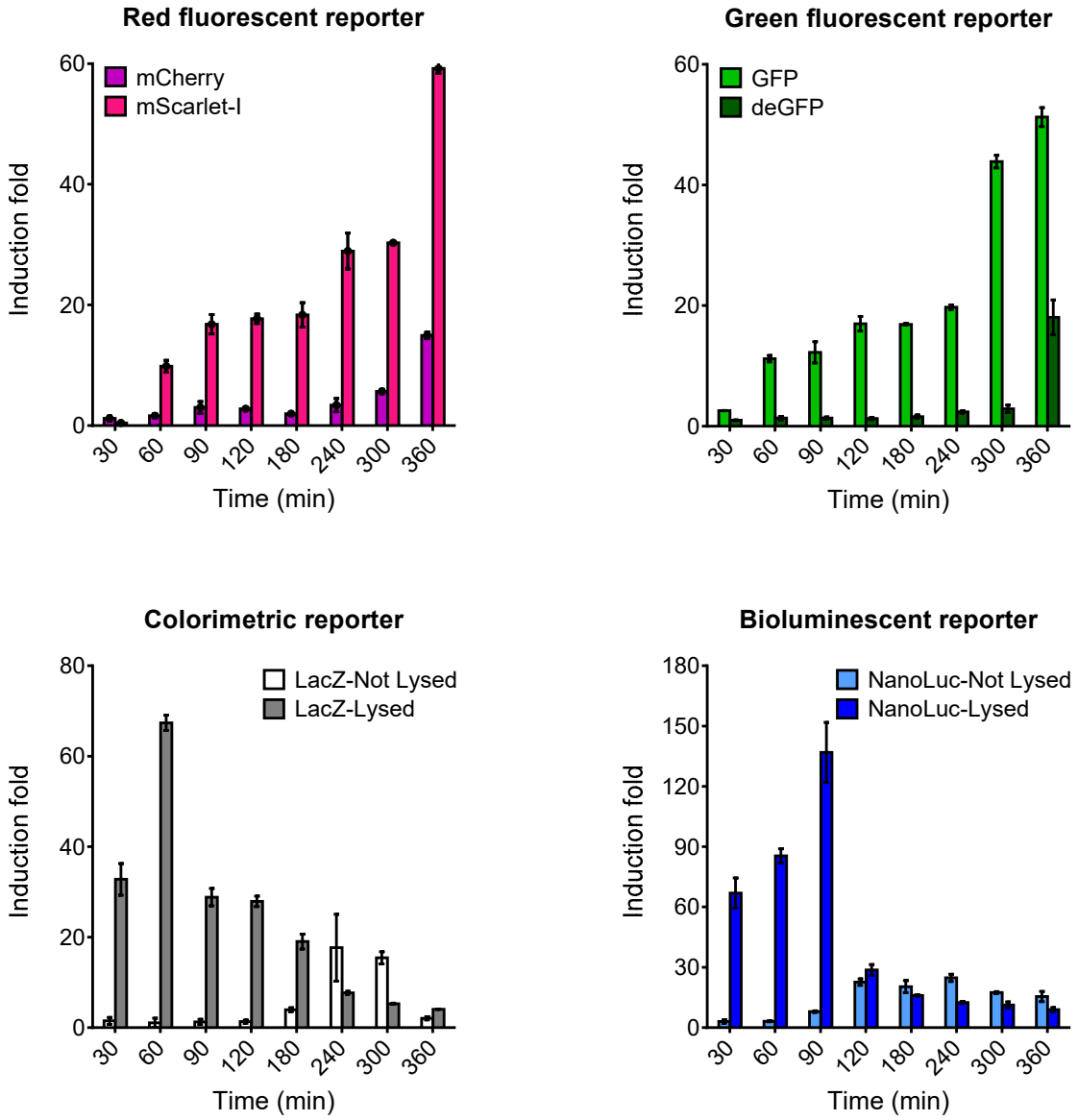

Figure S3: Induction fold of different reporters within whole-cell mercury sensor. Related to Figures 2 and 3B–C.

The mercury sensors with different reporters were induced with 0.1 μM $HgCl_2$. Values are mean ± s.d. (n = 3 biologically independent experiments).

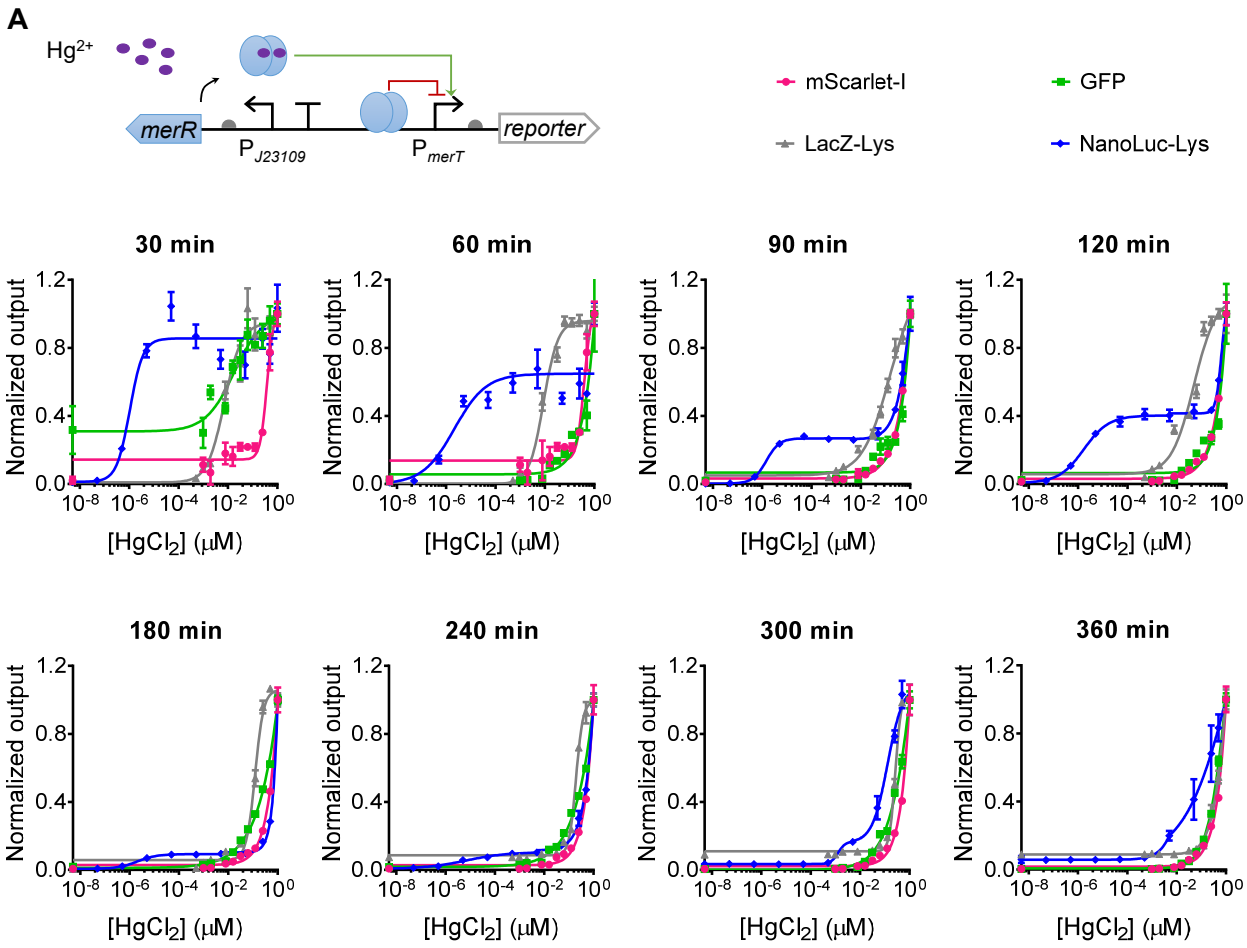

B

	30 min	60 min	90 min	120 min	180 min	240 min	300 min	360 min
mCherry	–	250.00	250.00	125.00	125.00	125.00	125.00	15.63
mScarlet-I	–	15.63	15.63	7.81	7.81	7.81	7.81	7.81
GFP	–	15.63	15.63	15.63	7.81	7.81	7.81	7.81
deGFP	–	500.00	250.00	250.00	250.00	250.00	250.00	125
NanoLuc-Lysed	5.00×10^{-5}	5.00×10^{-5}	5.00×10^{-5}	5.00×10^{-4}	5.00×10^{-4}	5.00×10^{-4}	0.50	0.50
NanoLuc-Not Lysed	–	0.50	0.50	0.50	0.05	0.50	5.00	5.00
LuxCDABE	5.00×10^{-4}	5.00×10^{-4}	5.00×10^{-4}	5.00×10^{-3}	5.00×10^{-3}	0.05	0.05	0.05
LacZ-Lysed	1.95	0.49	0.49	0.49	0.49	7.81	7.81	31.25
LacZ-Not Lysed	–	–	–	–	250.00	125.00	125.00	7.81

All data shown have the same unit of nM $HgCl_2$.
–: LOD cannot be calculated due to no significant difference observed between the mercury induced and non-induced samples.

Figure S4: Dose-response curves of whole-cell mercury sensor with diverse genetic reporters. Related to Figures 2 and 3B–C.

(A) Dose-response curves of whole-cell mercury sensor with diverse output genetic reporters. Top left, schematic of the mercury sensor. Values are mean ± s.d. (n = 3 biologically independent experiments). (B) Limits of detection (LOD) of whole-cell mercury sensors with different reporters.

A

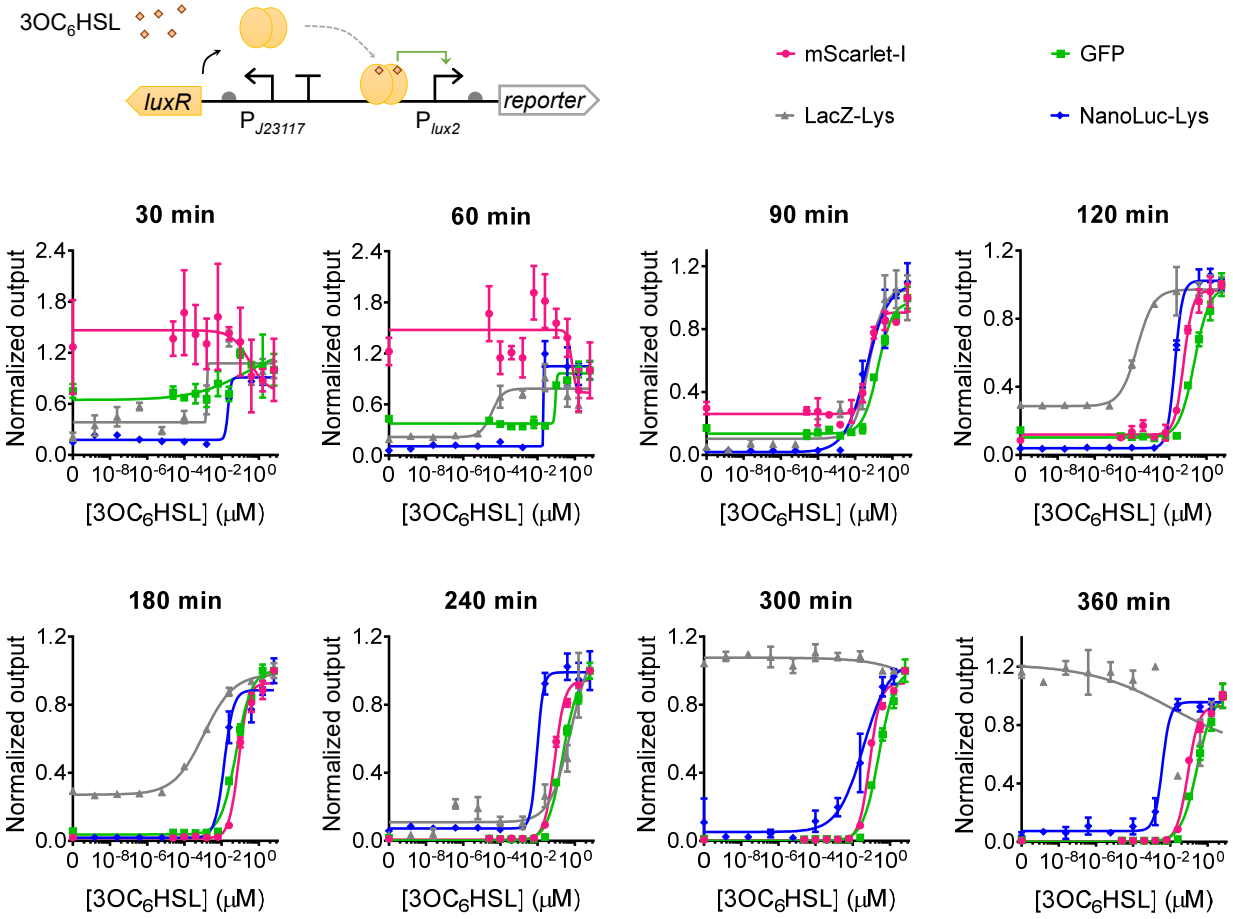

B

	30 min	60 min	90 min	120 min	180 min	240 min	300 min	360 min
mScarlet-I	–	100.00	100.00	25.00	25.00	6.25	6.25	6.25
GFP	–	100.00	100.00	10.00	25.00	25.00	25.00	6.25
NanoLuc-Lysed	3.81×10^{-4}	3.81×10^{-4}	6.10×10^{-3}	9.77×10^{-2}	1.56	1.56	25.00	25.00
LacZ-Lysed	1.56	6.10×10^{-3}	9.77×10^{-2}	9.77×10^{-2}	1.56	1.56	1.56	–

All data shown have the same unit of nM $3OC_6HSL$.
–: LOD cannot be calculated due to no significant difference observed between the $3OC_6HSL$ induced and non-induced samples.

Figure S5: Dose-response curves of whole-cell quorum sensing molecule sensor with diverse output genetic reporters. Related to Figure 3E–F.

(A) Dose-response curves of whole-cell quorum sensing molecule sensor with diverse output genetic reporters. Top left, schematic of the quorum sensing molecule sensor. Values are mean ± s.d. (n = 3 biologically independent experiments). (B) Limits of detection (LOD) of whole-cell quorum sensing molecule sensors with different reporters.

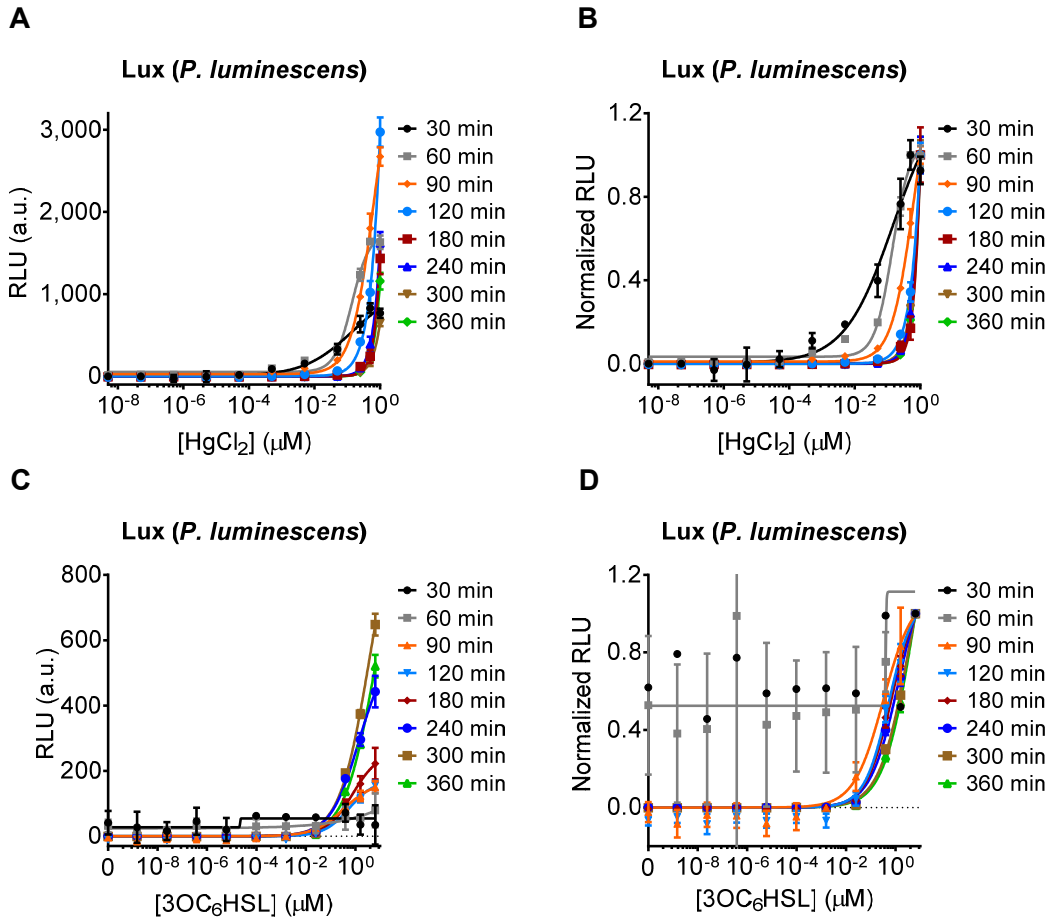

Figure S6: Dose-response curves of sensors *in vivo* with *lux* operon as reporter.

(A,B) Dose response curves (A) and normalized response curves (B) of a mercury sensor with *lux* operon from *P. luminescens* as output reporter. (C,D) Dose response curves (C) and normalized response curves (D) of a quorum sensing molecule sensor with *lux* operon from *P. luminescens* as output reporter. Values are mean ± s.d. (n = 3 biologically independent experiments). a.u., arbitrary units.

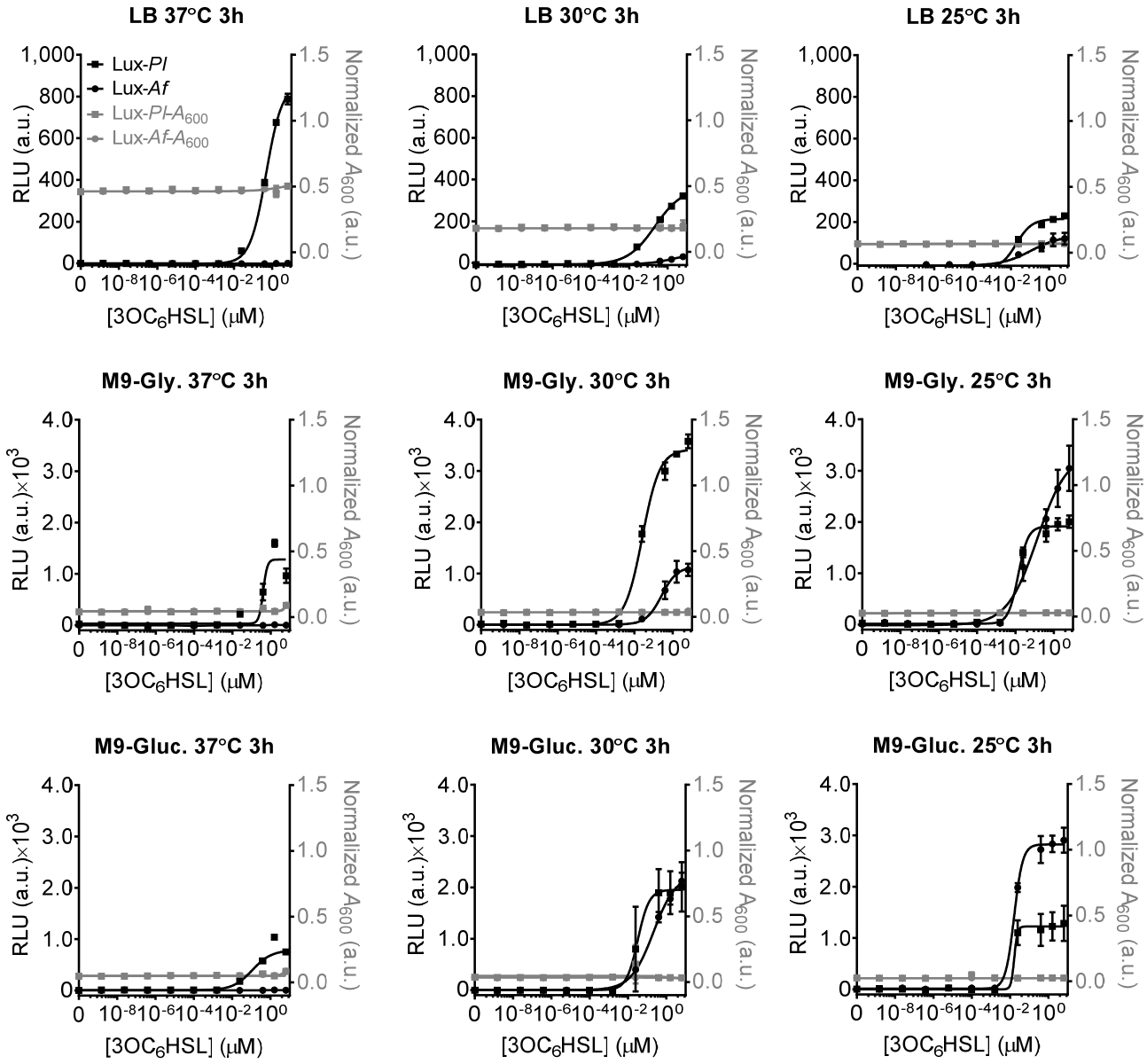

Figure S7: Characterization of *lux* operon within quorum sensing molecule sensor using different media and incubation temperature.

Lux-*Pl*, LuxCEABE from *P. luminescens*. Lux-*Af*, LuxCEABE from *A. fischeri*. M9-Gly., M9 medium with glycerol as carbon source. M9-Gluc., M9 medium with glucose as carbon source. All data were collected 3 h post induction and incubation. Values are mean ± s.d. (n = 2 biologically independent experiments). a.u., arbitrary units.

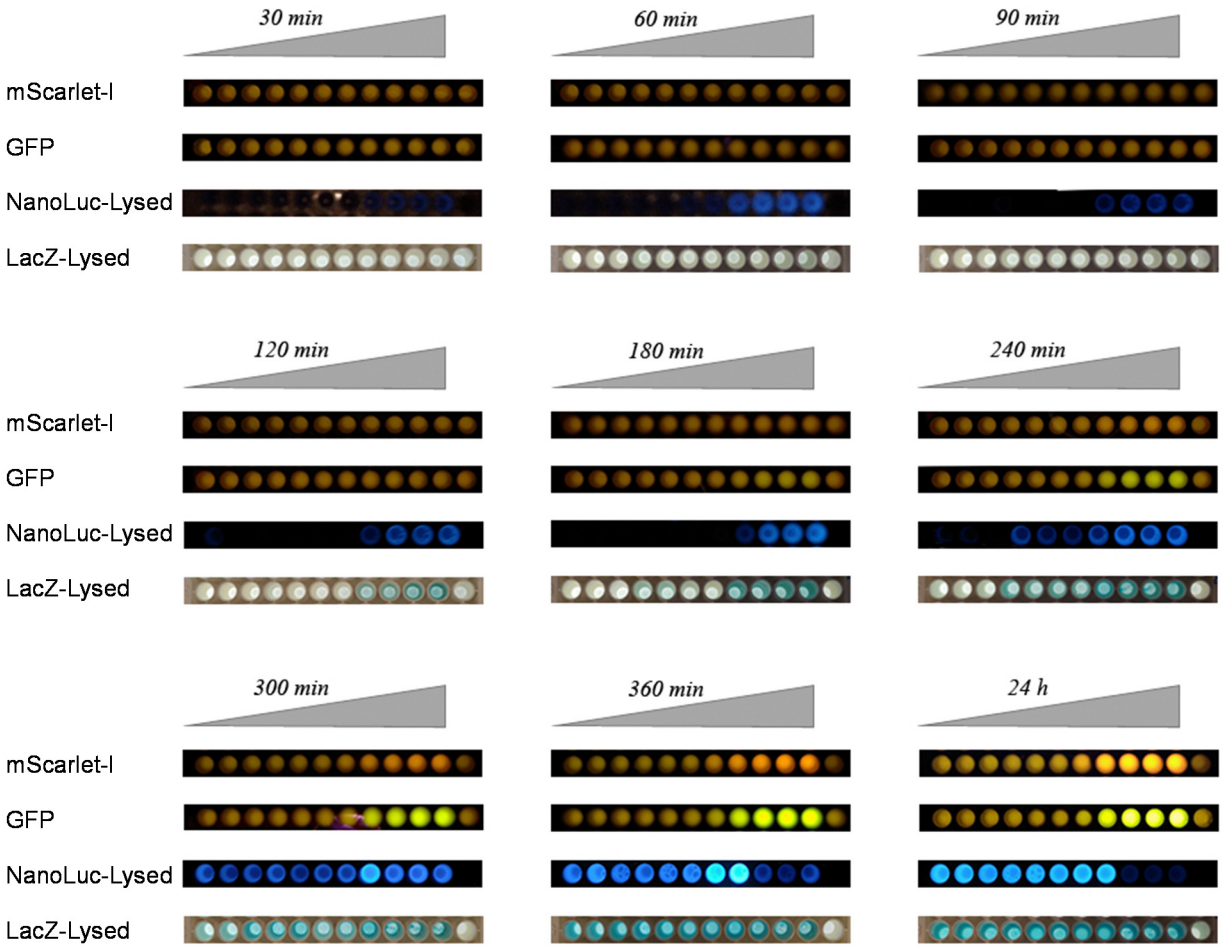

Figure S8: Cell phone images of diverse reporters within whole-cell quorum sensing molecule sensor. Related to Figure 3E–F.

The last well in each cell phone image shows the reporter-free negative control cultures.

A

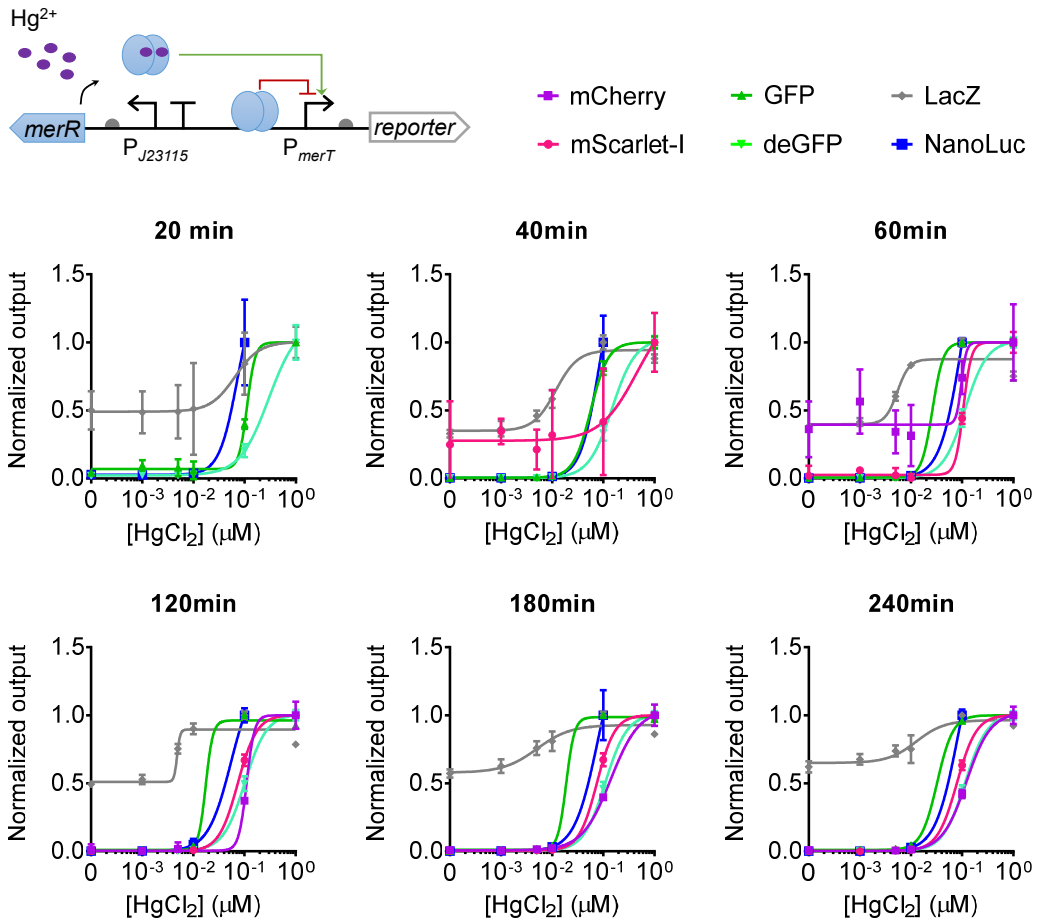

B

Reporters	20 min	40 min	60 min	120 min	180 min	240 min
mCherry	–	–	–	0.01 – 0.10	0.01 – 0.10	0.01 – 0.10
mScarlet-I	–	–	0.01 – 0.10	0.01 – 0.10	0.01 – 0.10	5.00×10^{-3} – 0.01
GFP	0.01 – 0.10	5.00×10^{-3} – 0.01	1.00×10^{-3} – 5.00×10^{-3}	1.00×10^{-3} – 5.00×10^{-3}	< 1.00×10^{-3}	< 1.00×10^{-3}
deGFP	0.01 – 0.10	5.00×10^{-3} – 0.01	1.00×10^{-3} – 5.00×10^{-3}	5.00×10^{-3} – 0.01	1.00×10^{-3} – 5.00×10^{-3}	1.00×10^{-3} – 5.00×10^{-3}
LacZ	0.10 – 1.00	1.00×10^{-3} – 5.00×10^{-3}	1.00×10^{-3} – 5.00×10^{-3}	1.00×10^{-3} – 5.00×10^{-3}	1.00×10^{-3} – 5.00×10^{-3}	0.01 – 0.10
NanoLuc	0.01 – 0.10	1.00×10^{-3} – 0.01	1.00×10^{-3} – 0.01	0.01 – 0.10	1.00×10^{-3} – 0.01	1.00×10^{-3} – 0.01

All data shown have the same unit of μM $HgCl_2$.
–: LOD cannot be calculated due to no significant difference observed between the mercury induced and non-induced samples.

Figure S9: Dose-response curves of cell-free mercury sensor with diverse output genetic reporters. Related to Figure 4B–C.

(A) Schematic and normalized dose-response curves of cell-free mercury sensors. Values are mean ± s.d. (n = 3 technical replicates). (B) Limit of detection (LOD) of the sensor tested in A. As only a few concentrations of mercury were tested, the LOD were shown as a range.

A

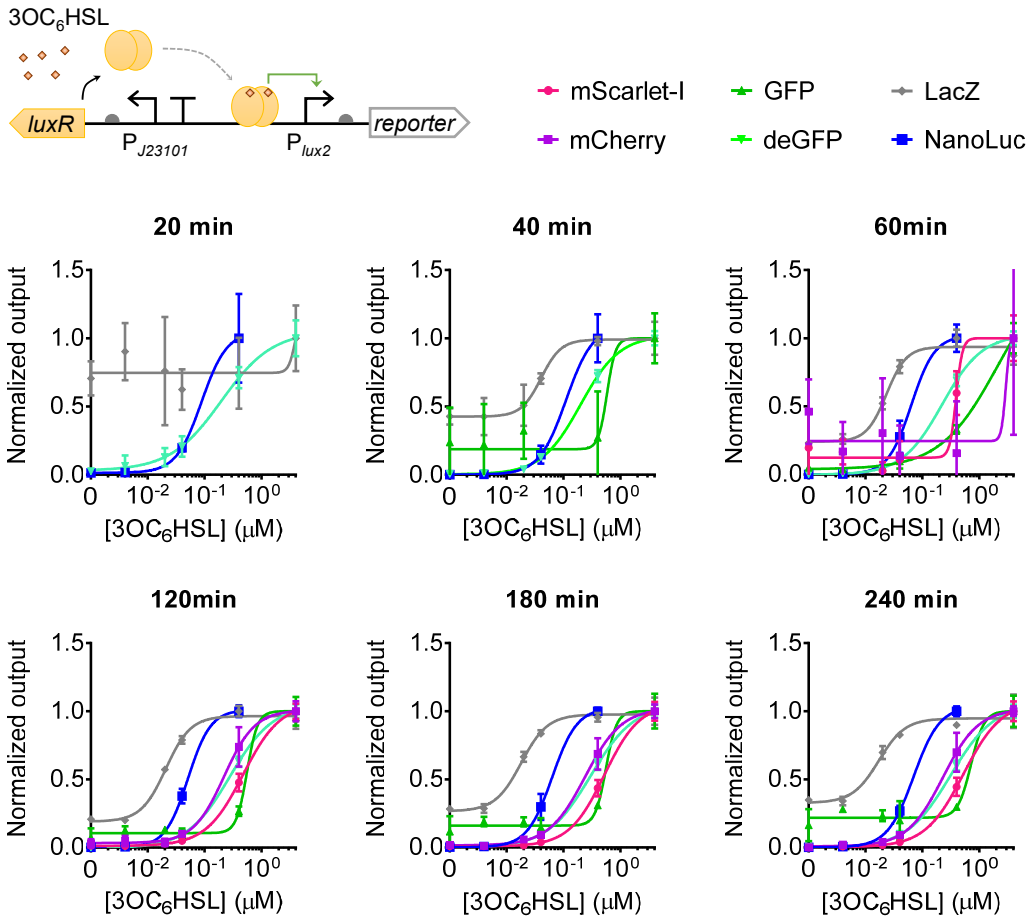

B

Reporters	20 min	40 min	60 min	120 min	180 min	240 min
mCherry	–	–	–	0.04 – 0.40	0.02 – 0.04	0.02 – 0.04
mScarlet-I	–	–	0.40 – 4.00	0.04 – 0.40	0.02 – 0.04	4.00×10^{-3} – 0.02
GFP	–	0.40 – 4.00	0.04 – 0.40	0.04 – 0.40	0.40 – 4.00	0.40 – 4.00
deGFP	0.02 – 0.04	4.00×10^{-3} – 0.02	4.00×10^{-3} – 0.02	4.00×10^{-3} – 0.02	4.00×10^{-3} – 0.02	$< 4.00 \times 10^{-3}$
LacZ	–	0.02 – 0.04	4.00×10^{-3} – 0.02	4.00×10^{-3} – 0.02	4.00×10^{-3} – 0.02	4.00×10^{-3} – 0.02
NanoLuc	4.00×10^{-3} – 0.04	$< 4.00 \times 10^{-3}$	$< 4.00 \times 10^{-3}$	$< 4.00 \times 10^{-3}$	4.00×10^{-3} – 0.04	$< 4.00 \times 10^{-3}$

All data shown have the same unit of μM $3OC_6HSL$.
–: LOD cannot be calculated due to no significant difference observed between the $3OC_6HSL$ induced and non-induced samples.

Figure S10: Dose-response curves of cell-free quorum sensing molecule sensor with diverse output genetic reporters. Related to Figure 4E–F.

(A) Schematic and normalized dose-response curves of cell-free quorum sensing molecule sensors. Values are mean ± s.d. (n = 3 technical replicates). (B) Limit of detection (LOD) of the sensor tested in A. As only a few concentrations of $3OC_6HSL$ were tested, the LOD were shown as a range.

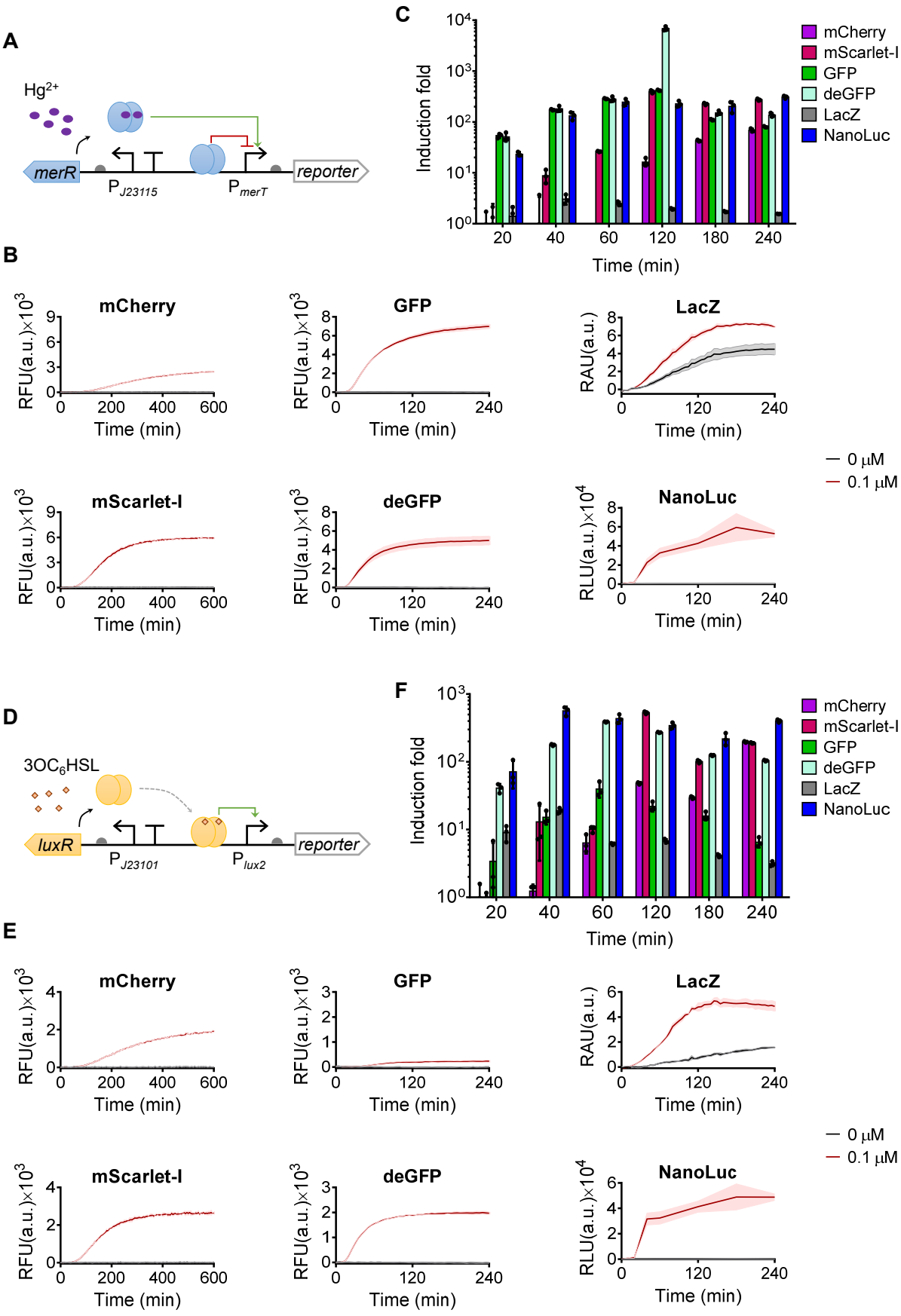
A
Hg2+
merR
P J23115
P merT
reporter
B
mCherry
GFP
LacZ
mScarlet-I
deGFP
NanoLuc
RFU(a.u.)×10^3
RAU(a.u.)
RLU(a.u.)×10^4
Time (min)
0 μM
0.1 μM
C
Induction fold
mCherry
mScarlet-I
GFP
deGFP
LacZ
NanoLuc
Time (min)
D
3OC6HSL
luxR
P J23101
P lux2
reporter
E
F

Figure S11: Characterization of diverse genetic reporters within mercury and quorum sensing molecule cell-free biosensors. Related to Figure 4.

(A,D) Schematics of the mercury or quorum sensing molecule sensor modules (J23115-*merR*-P_{merT} or J23101-*luxR*-P_{lux2}) coupled to diverse genetic reporters. (B,E) Dynamic output responses of the sensors responding to two concentrations of $HgCl_2$ (B) or $3OC_6HSL$ (E). (C,F) Fold of induction over time of the mercury or quorum sensing cell-free sensors with different reporters responding to 0.1 μM $HgCl_2$ (C) and 0.4 μM $3OC_6HSL$ (F) respectively. Induction fold was calculated using the output with induction divided by the output without induction. Values are mean ± s.d. (n = 3 technical replicates). a.u., arbitrary units.

Table S1: List of genetic parts and sequences used in this study

Underlined sequences indicate –35 and –10, or –24 and –12 promoter regions. Sequences in blue are MerR binding sites, sequences in yellow are LuxR binding sites.

Name	Type	DNA sequence (5'-3')
J23101	Constitutive promoter[1]	TTTACAGCTAGCTCAGTCCTAGGTATTATGCTAGC
J23109	Constitutive promoter[2]	TTTACAGCTAGCTCAGTCCTAGGGACTGTGCTAGC
J23115	Constitutive promoter[1]	TTTATAGCTAGCTCAGCCCTTGGTACAATGCTAGC
J23117	Constitutive promoter[1]	TTGACAGCTAGCTCAGTCCTAGGGATTGTGCTAGC
P_{merT}	Inducible promoter[6]	TTCCATATCGCTTGACTACGTACATGAGTACGGAAGTAAGGTTACGCTATCCAATCC
P_{lux2}	Inducible promoter[1]	AGACCTGTAGGATCGTACAGGTTTACGCAAGAAAATGGTTTGTTACTTTCGAATAAA
B0030	RBS[5]	ATTAAAGAGGAGAAA
R0032	RBS[5]	TCACACAGGAAAG
B0015	Terminator[7]	CCAGGCATCAAATAAAACGAAAGGCTCAGTCGAAAGACTGGGCCTTTCGTTTTATCTGTTGTTTGTCGGTGAACGCTCTCTACTAGAGTCACACTGGCTCACCTTCGGGTGGGCCTTTCTGCGTTTATA
L3S2P55	Terminator[8]	CTCGGTACCAAAGACGAACAATAAGACGCTGAAAAGCGTCTTTTTTCGTTTTGGTCC
merR	Gene[6]	ATGGAAAATAATTTGGAAAACCTGACCATTGGCGTTTTTGCCAAGGCGGCCGGGGTCAACGTGGAGACAATCCGCTTCTATCAGCGCAAGGGCCTGTTGCGGGAACCGGACAAGCCTTACGGCAGCATCCGCCGCTATGGGGAGGCGGACGTGGTTCGGGTGAAATTCGTGAAATCGGCACAGCGGCTGGGGTTCAGTCTGGACGAGATTGCCGAGCTGTTGCGGCTCGACGATGGCACCCACTGCGAGGAGGCCAGCAGCCTGGCCGAACACAAGCTCAAGGACGTGCGCGAGAAGATGGCCGACTTGGCGCGCATGGAAACCGTGCTGTCTGAACTCGTGTGCGCCTGCCATGCACGAAAGGGGAATGTTTCCTGCCCGTTGATCGCGTCACTACAGGGCGAAGCAGGCCTGGCAAGGTCAGCTATGCCTTAG
luxR	Gene[1]	ATGAAAAACATAAATGCCGACGACACATACAGAATAATTAATAAAATTAAAGCTTGTAGAAGCAATAATGATATTAATCAATGCTTATCTGATATGACTAAAATGGTACATTGTGAATATTATTTACTCGCGATCATTTATCCTCATTCTATGGTTAAATCTGATATTTCAATCCTAGATAATTACCCTAAAAAATGGAGGCAATATTATGATGACGCTAATTTAATAAAATATGATCCTATAGTAGATTATTCTAACTCCAATCATTCACCAATTAATTGGAATATATTTGAAAACAATGCTGTAAATAAAAAATCTCCAAATGTAATTAAAGAAGCGAAAACATCAGGTCTTATCACTGGGTTTAGTTTCCCTATTCATACGGCTAACAATGGCTTCGGAATGCTTAGTTTTGCACATTCAGAAAAAGACAACTATATAGATAGTTTATTTTTACATGCGTGTATGAACATACCATTAATTGTTCCTTCTCTAGTTGATAATTATCGAAAAATAAATATAGCAAATAATAAATCAAACAACGATTTAACCAAAAGAGAAAAAGAATGTTTAGCGTGGGCATGCGAAGGAAAAAGCTCTTGGGATATTTCAAAAATATTAGGTTGCAGTGAGCGTACTGTCACTTTCCATTTAACCAATGCGCAAATGAAACTCAATACAACAAACCGCTGCCAAAGTATTTCTAAAGCAATTTTAACAGGAGCAATTGATTGCCCATACTTTAAAAATTAATAA
mCherry	Gene*	ATGGTGAGCAAGGGCGAGGAGGATAACATGGCCATCATCAAGGAGTTCATGCGCTTCAAGGTGCACATGGAGGGCTCCGTGAACGGCCACGAGTTCGAGATCGAGGGCGAGGGCGAGGGCCGCCCCTACGAGGGCACCCAGACCGCCAAGCTGAAGGTGACCAAGGGTGGCCCCCTGCCCTTCGCCTGGGACATCCTGTCCCCTCAGTTCATGTACGGCTCCAAGGCCTACGTGAAGCACCCCGCCGACATCCCCGACTACTTGAAGCTGTCCTTCCCCGAGGGCTTCAAGTGGGAGCGCGTGATGAACTTCGAGGACGGCGGCGTGGTGACCGTGACCCAGGACTCCTCCTTGCAGGACGGCGAGTTCATCTACAAGGTGAAGCTGCGCGGCACCAACTTCCCCTCCGACGGCCCCGTAATGCAGAAGAAGACCATGGGCTGGGAGGCCTCCTCCGAGCGGATGTACCCCGAGGACGGCGCCCTGAAGGGCGAGATCAAGCAGAGGCTGAAGCTGAAGGACGGCGGCCACTACGACGCTGAGGTCAAGACCACCTACAAGGCCAAGAAGCCCGTGCAGCTGCCCGGCGCCTACAACGTCAACAT

		CAAGTTGGACATCACCTCCCACAACGAGGACTACACCATCGTGGAACAGTACGAA CGCGCCGAGGGCCGCCACTCCACCGGCGGCATGGACGAGCTGTACAAGTAA
mScarlet-I	Gene[9]	ATGGTGAGTAAAGGAGAAGCTGTGATTAAAGAGTTCATGCGCTTCAAAGTTCACA TGGAGGGTTCTATGAACGGTCACGAGTTCGAGATCGAAGGCGAAGGCGAGGGCCG TCCGTATGAAGGCACCCAGACCGCCAAACTGAAAGTGACTAAAGGCGGCCCGCTG CCTTTTTCCTGGGACATCCTGAGCCCGCAATTTATGTACGGTTCTAGGGCGTTCA TCAAACACCCAGCGGATATCCCGGACTATTATAAGCAGTCTTTTCCGGAAGGTTT CAAGTGGGAACGCGTAATGAATTTTGAAGATGGTGGTGCCGTGACCGTCACTCAG GACACCTCCCTGGAGGATGGCACCCTGATCTATAAAGTTAAACTGCGTGGTACTA ATTTTCCACCTGATGGCCCGGTGATGCAGAAAAAGACGATGGGTTGGGAGGCGTC TACCGAACGCTTGTATCCGGAAGATGGTGTGCTGAAAGGCGACATTAAAATGGCC CTGCGCCTGAAAGATGGCGGCCGCTATCTGGCTGACTTCAAAACCACGTACAAAG CCAAGAAACCTGTGCAGATGCCTGGCGCGTACAATGTGGACCGCAAACTGGACAT CACCTCTCATAATGAAGATTATACGGTGGTAGAGCAATATGAGCGCTCCGAGGGT CGTCATTCTACCGGTGGCATGGATGAACTATACAAA
gfp	Gene[7]	ATGCGTAAAGGAGAAGAACTTTTCACTGGAGTTGTCCCAATTCTTGTTGAATTAG ATGGTGATGTTAATGGGCACAAATTTTCTGTCAGTGGAGAGGGTGAAGGTGATGC AACATACGGAAAACTTACCCTTAAATTTATTTGCACTACTGGAAAACTACCTGTT CCATGGCCAACACTTGTCACTACTTTCGGTTATGGTGTTCAATGCTTTGCGAGAT ACCCAGATCATATGAAACAGCATGACTTTTTCAAGAGTGCCATGCCCGAAGGTTA TGTACAGGAAAGAACTATATTTTTCAAAGATGACGGGAACTACAAGACACGTGCT GAAGTCAAGTTTGAAGGTGATACCCTTGTTAATAGAATCGAGTTAAAAGGTATTG ATTTTAAAGAAGATGGAAACATTCTTGGACACAAATTGGAATACAACTATAACTC ACACAATGTATACATCATGGCAGACAAACAAAAGAATGGAATCAAAGTTAACTTC AAAATTAGACACAACATTGAAGATGGAAGCGTTCAACTAGCAGACCATTATCAAC AAAATACTCCAATTGGCGATGGCCCTGTCCTTTTACCAGACAACCATTACCTGTC CACACAATCTGCCCTTTCGAAAGATCCCAACGAAAAGAGAGACCACATGGTCCTT CTTGAGTTTGTAACAGCTGCTGGGATTACACATGGCATGGATGAACTATACAAAT AA
degfp	Gene[10]	ATGGAGCTTTTCACTGGCGTTGTTCCCATCCTGGTCGAGCTGGACGGCGACGTAA ACGGCCACAAGTTCAGCGTGTCCGGCGAGGGCGAGGGCGATGCCACCTACGGCAA GCTGACCCTGAAGTTCATCTGCACCACCGGCAAGCTGCCCGTGCCCTGGCCCACC CTCGTGACCACCCTGACCTACGGCGTGCAGTGCTTCAGCCGCTACCCCGACCACA TGAAGCAGCACGACTTCTTCAAGTCCGCCATGCCCGAAGGCTACGTCCAGGAGCG CACCATCTTCTTCAAGGACGACGGCAACTACAAGACCCGCGCCGAGGTGAAGTTC GAGGGCGACACCCTGGTGAACCGCATCGAGCTGAAGGGCATCGACTTCAAGGAGG ACGGCAACATCCTGGGGCACAAGCTGGAGTACAACTACAACAGCCACAACGTCTA TATCATGGCCGACAAGCAGAAGAACGGCATCAAGGTGAACTTCAAGATCCGCCAC AACATCGAGGACGGCAGCGTGCAGCTCGCCGACCACTACCAGCAGAACACCCCCA TCGGCGACGGCCCCGTGCTGCTGCCCGACAACCACTACCTGAGCACCCAGTCCGC CCTGAGCAAAGACCCCAACGAGAAGCGCGATCACATGGTCCTGCTGGAGTTCGTG ACCGCCGCCGGGATCTAA
NanoLuc	Gene[11]	ATGGTCTTCACACTCGAAGATTTCGTTGGGGACTGGCGACAGACAGCCGGCTACA ACCTGGACCAAGTCCTTGAACAGGGAGGTGTGTCCAGTTTGTTTCAGAATCTCGG GGTGTCCGTAACTCCGATCCAAAGGATTGTCCTGAGCGGTGAAAATGGGCTGAAG ATCGACATCCATGTCATCATCCCGTATGAAGGTCTGAGCGGCGACCAAATGGGCC AGATCGAAAAAATTTTTAAGGTGGTGTACCCTGTGGATGATCATCACTTTAAGGT GATCCTGCACTATGGCACACTGGTAATCGACGGGGTTACGCCGAACATGATCGAC TATTTCGGACGGCCGTATGAAGGCATCGCCGTGTTCGACGGCAAAAAGATCACTG TAACAGGGACCCTGTGGAACGGCAACAAAATTATCGACGAGCGCCTGATCAACCC CGACGGCTCCCTGCTGTTCCGAGTAACCATCAACGGAGTGACCGGCTGGCGGCTG TGCGAACGCATTCTGGCGTAA
LacZ	Gene (Amplified from *E. coli* MG1655 by PCR)	ATGACCATGATTACGGATTCACTGGCCGTCGTTTTACAACGTCGTGACTGGGAAA ACCCTGGCGTTACCCAACTTAATCGCCTTGCAGCACATCCCCCTTTCGCCAGCTG GCGTAATAGCGAAGAGGCCCGCACCGATCGCCCTTCCCAACAGTTGCGCAGCCTG AATGGCGAATGGCGCTTTGCCTGGTTTCCGGCACCAGAAGCGGTGCCGGAAAGCT GGCTGGAGTGCGATCTTCCTGAGGCCGATACTGTCGTCGTCCCCTCAAACTGGCA GATGCACGGTTACGATGCGCCCATCTACACCAACGTGACCTATCCCATTACGGTC AATCCGCCGTTTGTTCCCACGGAGAATCCGACGGGTTGTTACTCGCTCACATTTA ATGTTGATGAAAGCTGGCTACAGGAAGGCCAGACGCGAATTATTTTTGATGGCGT TAACTCGGCGTTTCATCTGTGGTGCAACGGGCGCTGGGTCGGTTACGGCCAGGAC

		AGTCGTTTGCCGTCTGAATTTGACCTGAGCGCATTTTTACGCGCCGGAGAAAACC GCCTCGCGGTGATGGTGCTGCGCTGGAGTGACGGCAGTTATCTGGAAGATCAGGA TATGTGGCGGATGAGCGGCATTTTCCGTGACGTCTCGTTGCTGCATAAACCGACT ACACAAATCAGCGATTTCCATGTTGCCACTCGCTTTAATGATGATTTCAGCCGCG CTGTACTGGAGGCTGAAGTTCAGATGTGCGGCGAGTTGCGTGACTACCTACGGGT AACAGTTTCTTTATGGCAGGGTGAAACGCAGGTCGCCAGCGGCACCGCGCCTTTC GGCGGTGAAATTATCGATGAGCGTGGTGGTTATGCCGATCGCGTCACACTACGTC TGAACGTCGAAAACCCGAAACTGTGGAGCGCCGAAATCCCGAATCTCTATCGTGC GGTGGTTGAACTGCACACCGCCGACGGCACGCTGATTGAAGCAGAAGCCTGCGAT GTCGGTTTCCGCGAGGTGCGGATTGAAAATGGTCTGCTGCTGCTGAACGGCAAGC CGTTGCTGATTCGAGGCGTTAACCGTCACGAGCATCATCCTCTGCATGGTCAGGT CATGGATGAGCAGACGATGGTGCAGGATATCCTGCTGATGAAGCAGAACAACTTT AACGCCGTGCGCTGTTCGCATTATCCGAACCATCCGCTGTGGTACACGCTGTGCG ACCGCTACGGCCTGTATGTGGTGGATGAAGCCAATATTGAAACCCACGGCATGGT GCCAATGAATCGTCTGACCGATGATCCGCGCTGGCTACCGGCGATGAGCGAACGC GTAACGCGAATGGTGCAGCGCGATCGTAATCACCCGAGTGTGATCATCTGGTCGC TGGGGAATGAATCAGGCCACGGCGCTAATCACGACGCGCTGTATCGCTGGATCAA ATCTGTCGATCCTTCCCGCCCGGTGCAGTATGAAGGCGGCGGAGCCGACACCACG GCCACCGATATTATTTGCCCGATGTACGCGCGCGTGGATGAAGACCAGCCCTTCC CGGCTGTGCCGAAATGGTCCATCAAAAAATGGCTTTCGCTACCTGGAGAGACGCG CCCGCTGATCCTTTGCGAATACGCCCACGCGATGGGTAACAGTCTTGGCGGTTTC GCTAAATACTGGCAGGCGTTTCGTCAGTATCCCCGTTTACAGGGCGGCTTCGTCT GGGACTGGGTGGATCAGTCGCTGATTAAATATGATGAAAACGGCAACCCGTGGTC GGCTTACGGCGGTGATTTTGGCGATACGCCGAACGATCGCCAGTTCTGTATGAAC GGTCTGGTCTTTGCCGACCGCACGCCGCATCCAGCGCTGACGGAAGCAAAACACC AGCAGCAGTTTTTCCAGTTCCGTTTATCCGGGCAAACCATCGAAGTGACCAGCGA ATACCTGTTCCGTCATAGCGATAACGAGCTCCTGCACTGGATGGTGGCGCTGGAT GGTAAGCCGCTGGCAAGCGGTGAAGTGCCTCTGGATGTCGCTCCACAAGGTAAAC AGTTGATTGAACTGCCTGAACTACCGCAGCCGGAGAGCGCCGGGCAACTCTGGCT CACAGTACGCGTAGTGCAACCGAACGCGACCGCATGGTCAGAAGCCGGGCACATC AGCGCCTGGCAGCAGTGGCGTCTGGCGGAAAACCTCAGTGTGACGCTCCCCGCCG CGTCCCACGCCATCCCGCATCTGACCACCAGCGAAATGGATTTTTGCATCGAGCT GGGTAATAAGCGTTGGCAATTTAACCGCCAGTCAGGCTTTCTTTCACAGATGTGG ATTGGCGATAAAAAACAACTGCTGACGCCGCTGCGCGATCAGTTCACCCGTGCAC CGCTGGATAACGACATTGGCGTAAGTGAAGCGACCCGCATTGACCCTAACGCCTG GGTCGAACGCTGGAAGGCGGCGGGCCATTACCAGGCCGAAGCAGCGTTGTTGCAG TGCACGGCAGATACACTTGCTGATGCGGTGCTGATTACGACCGCTCACGCGTGGC AGCATCAGGGGAAAACCTTATTTATCAGCCGGAAAACCTACCGGATTGATGGTAG TGGTCAAATGGCGATTACCGTTGATGTTGAAGTGGCGAGCGATACACCGCATCCG GCGCGGATTGGCCTGAACTGCCAGCTGGCGCAGGTAGCAGAGCGGGTAAACTGGC TCGGATTAGGGCCGCAAGAAAACTATCCCGACCGCCTTACTGCCGCCTGTTTTGA CCGCTGGGATCTGCCATTGTCAGACATGTATACCCCGTACGTCTTCCCGAGCGAA AACGGTCTGCGCTGCGGGACGCGCGAATTGAATTATGGCCCACACCAGTGGCGCG GCGACTTCCAGTTCAACATCAGCCGCTACAGTCAACAGCAACTGATGGAAACCAG CCATCGCCATCTGCTGCACGCGGAAGAAGGCACATGGCTGAATATCGACGGTTTC CATATGGGGATTGGTGGCGACGACTCCTGGAGCCCGTCAGTATCGGCGGAGTTTC AGCTGAGCGCCGGTCGCTACCATTACCAGTTGGTCTGGTGTCAAAAATAA
lux operon (*P. luminescens*)	Gene with RBS**	AGGAGGGGCAAATATGACTAAAAAAATTTCATTCATTATTAACGGCCAGGTTGAA ATCTTTCCCGAAAGTGATGATTTAGTGCAATCCATTAATTTTGGTGATAATAGTG TTTACCTGCCAATATTGAATGACTCTCATGTAAAAAACATTATTGATTGTAATGG AAATAACGAATTACGGTTGCATAACATTGTCAATTTTCTCTATACGGTAGGGCAA AGATGGAAAAATGAAGAATACTCAAGACGCAGGACATACATTCGTGACTTAAAAA AATATATGGGATATTCAGAAGAAATGGCTAAGCTAGAGGCCAATTGGATATCTAT GATTTTATGTTCTAAAGGCGGCCTTTATGATGTTGTAGAAAATGAACTTGGTTCT CGCCATATCATGGATGAATGGCTACCTCAGGATGAAAGTTATGTTCGGGCTTTTC CGAAAGGTAAATCTGTACATCTGTTGGCAGGTAATGTTTCATTATCTGGGATCAT GTCTATATTACGCGCAATTTTAACTAAGAATCAGTGTATTATAAAAACATCGTCA ACCGATCCTTTTACCGCTAATGCATTAGCGTTAAGTTTTATTGATGTAGACCCTA ATCATCCGATAACGCGCTCTTTATCTGTTATATATTGGCCCCACCAAGGTGATAC ATCACTCGCAAAAGAAATTATGCGACATGCGGATGTTATTGTCGCTTGGGGAGGG CCAGATGCGATTAATTGGGCGGTAGAGCATGCGCCATCTTATGCTGATGTGATTA AATTTGGTTCTAAAAAGAGTCTTTGCATTATCGATAATCCTGTTGATTTGACGTC

CGCAGCGACAGGTGCGGCTCATGATGTTTGTTTTTACGATCAGCGAGCTTGTTTT
TCTGCCCAAAACATATATTACATGGGAAATCATTATGAGGAATTTAAGTTAGCGT
TGATAGAAAAACTTAATCTATATGCGCATATATTACCGAATGCCAAAAAAGATTT
TGATGAAAAGGCGGCCTATTCTTTAGTTCAAAAAGAAAGCTTGTTTGCTGGATTA
AAAGTAGAGGTGGATATTCATCAACGTTGGATGATTATTGAGTCAAATGCAGGTG
TGGAATTTAATCAACCACTTGGCAGATGTGTGTACCTTCATCACGTCGATAATAT
TGAGCAAATATTGCCTTATGTTCAAAAAAATAAGACGCAAACCATATCTATTTTT
CCTTGGGAGTCATCATTTAAATATCGAGATGCGTTAGCATTAAAAGGTGCGGAAA
GGATTGTAGAAGCAGGAATGAATAACATATTTCGAGTTGGTGGATCTCATGACGG
AATGAGACCGTTGCAACGATTAGTGACATATATTTCTCATGAAAGGCCATCTAAC
TATACGGCTAAGGATGTTGCGGTTGAAATAGAACAGACTCGATTCCTGGAAGAAG
ATAAGTTCCTTGTATTTGTCCCATAATAGGTAAAAAGTATGGAAAATGAATCAAA
ATATAAAACCATCGACCACGTTATTTGTGTTGAAGGAAATAAAAAAATTCATGTT
TGGGAAACGCTGCCAGAAGAAAACAGCCCAAAGAGAAAGAATGCCATTATTATTG
CGTCTGGTTTTGCCCGCAGGATGGATCATTTTGCTGGTCTGGCGGAATATTTATC
GCGGAATGGATTTCATGTGATCCGCTATGATTCGCTTCACCACGTTGGATTGAGT
TCAGGGACAATTGATGAATTTACAATGTCTATAGGAAAGCAGAGCTTGTTAGCAG
TGGTTGATTGGTTAACTACACGAAAAATAAATAACTTCGGTATGTTGGCTTCAAG
CTTATCTGCGCGGATAGCTTATGCAAGCCTATCTGAAATCAATGCTTCGTTTTTA
ATCACCGCAGTCGGTGTTGTTAACTTAAGATATTCTCTTGAAAGAGCTTTAGGGT
TTGATTATCTCAGTCTACCCATTAATGAATTGCCGGATAACCTAGATTTTGAAGG
CCATAAATTGGGTGCTGAAGTCTTTGCGAGAGATTGTCTTGATTTTGGTTGGGAA
GATTTAGCTTCTACAATTAATAACATGATGTATCTTGATATACCGTTTATTGCTT
TTACTGCAAATAACGATAATTGGGTCAAGCAAGATGAAGTTATCACATTGTTATC
AAATATTCGTAGTAATCGATGCAAGATATATTCTTTGTTAGGAAGTTCGCATGAC
TTGAGTGAAAATTTAGTGGTCCTGCGCAATTTTTATCAATCGGTTACGAAAGCCG
CTATCGCGATGGATAATGATCATCTGGATATTGATGTTGATATTACTGAACCGTC
ATTTGAACATTTAACTATTGCGACAGTCAATGAACGCCGAATGAGAATTGAGATT
GAAAATCAAGCAATTTCTCTGTCTTAAAATCTATTGAGATATTCTATCACTCAAA
TAGCAATATAAGGACTCTCTATGAAATTTGGAAACTTTTTGCTTACATACCAACC
TCCCCAATTTTCTCAAACAGAGGTAATGAAACGTTTGGTTAAATTAGGTCGCATC
TCTGAGGAGTGTGGTTTTGATACCGTATGGTTACTGGAGCATCATTTCACGGAGT
TTGGTTTGCTTGGTAACCCTTATGTCGCTGCTGCATATTTACTTGGCGCGACTAA
AAAATTGAATGTAGGAACTGCCGCTATTGTTCTTCCCACAGCCCATCCAGTACGC
CAACTTGAAGATGTGAATTTATTGGATCAAATGTCAAAAGGACGATTTCGGTTTG
GTATTTGCCGAGGGCTTTACAACAAGGACTTTCGCGTATTCGGCACAGATATGAA
TAACAGTCGCGCCTTAGCGGAATGCTGGTACGGGCTGATAAAGAATGGCATGACA
GAGGGATATATGGAAGCTGATAATGAACATATCAAGTTCCATAAGGTAAAAGTAA
ACCCCGCGGCGTATAGCAGAGGTGGCGCACCGGTTTATGTGGTGGCTGAATCAGC
TTCGACGACTGAGTGGGCTGCTCAATTTGGCCTACCGATGATATTAAGTTGGATT
ATAAATACTAACGAAAAGAAAGCACAACTTGAGCTTTATAATGAAGTGGCTCAAG
AATATGGGCACGATATTCATAATATCGACCATTGCTTATCATATATAACATCTGT
AGATCATGACTCAATTAAAGCGAAAGAGATTTGCCGGAAATTTCTGGGGCATTGG
TATGATTCTTATGTGAATGCTACGACTATTTTTGATGATTCAGACCAAACAAGAG
GTTATGATTTCAATAAAGGGCAGTGGCGTGACTTTGTATTAAAAGGACATAAAGA
TACTAATCGCCGTATTGATTACAGTTACGAAATCAATCCCGTGGGAACGCCGCAG
GAATGTATTGACATAATTCAAAAAGACATTGATGCTACAGGAATATCAAATATTT
GTTGTGGATTTGAAGCTAATGGAACAGTAGACGAAATTATTGCTTCCATGAAGCT
CTTCCAGTCTGATGTCATGCCATTTCTTAAAGAAAAACAACGTTCGCTATTATAT
TAGCTAAGGAGAAAGAAATGAAATTTGGATTGTTCTTCCTTAACTTCATCAATTC
AACAACTGTTCAAGAACAAAGTATAGTTCGCATGCAGGAAATAACGGAGTATGTT
GATAAGTTGAATTTTGAACAGATTTTAGTGTATGAAAATCATTTTTCAGATAATG
GTGTTGTCGGCGCTCCTCTGACTGTTTCTGGTTTTCTGCTCGGTTTAACAGAGAA
AATTAAAATTGGTTCATTAAATCACATCATTACAACTCATCATCCTGTCCGCATA
GCGGAGGAAGCTTGCTTATTGGATCAGTTAAGTGAAGGGAGATTTATTTTAGGGT
TTAGTGATTGCGAAAAAAAAGATGAAATGCATTTTTTTAATCGCCCGGTTGAATA
TCAACAGCAACTATTTGAAGAGTGTTATGAAATCATTAACGATGCTTTAACAACA
GGCTATTGTAATCCAGATAACGATTTTTATAGCTTCCCTAAAATATCTGTAAATC
CCCATGCTTATACGCCAGGCGGACCTCGGAAATATGTAACAGCAACCAGTCATCA
TATTGTTGAGTGGGCGGCCAAAAAAGGTATTCCTCTCATCTTTAAGTGGGATGAT
TCTAATGATGTTAGATATGAATATGCTGAAAGATATAAAGCCGTTGCGGATAAAT
ATGACGTTGACCTATCAGAGATAGACCATCAGTTAATGATATTAGTTAACTATAA

		CGAAGATAGTAATAAAGCTAAACAAGAGACGCGTGCATTTATTAGTGATTATGTT CTTGAAATGCACCCTAATGAAAATTTCGAAAATAAACTTGAAGAAATAATTGCAG AAAACGCTGTCGGAAATTATACGGAGTGTATAACTGCGGCTAAGTTGGCAATTGA AAAGTGTGGTGCGAAAAGTGTATTGCTGTCCTTTGAACCAATGAATGATTTGATG AGCCAAAAAAATGTAATCAATATTGTTGATGATAATATTAAGAAGTACCACATGG AATATACCTAATAGATTTCGAGTTGCAGCGAGGCGGCAAGTGAACGAATCCCCAG GAGCATAGATAACTATGTGACTGGGGTGAGTGAAAGCAGCCAACAAAGCAGCAGC TTGAAAGATGAAGGGTATAAAAGAGTATGACAGCAGTGCTGCCATACTTTCTAAT ATTATCTTGAGGAGTAAAACAGGTATGACTTCATATGTTGATAAACAAGAAATTA CAGCAAGCTCAGAAATTGATGATTTGATTTTTTCGAGCGATCCATTAGTGTGGTC TTACGACGAGCAGGAAAAAATCAGAAAGAAACTTGTGCTTGATGCATTTCGTAAT CATTATAAACATTGTCGAGAATATCGTCACTACTGTCAGGCACACAAAGTAGATG ACAATATTACGGAAATTGATGACATACCTGTATTCCCAACATCGGTTTTTAAGTT TACTCGCTTATTAACTTCTCAGGAAAACGAGATTGAAAGTTGGTTTACCAGTAGC GGCACGAATGGTTTAAAAAGTCAGGTGGCGCGTGACAGATTAAGTATTGAGAGAC TCTTAGGCTCTGTGAGTTATGGCATGAAATATGTTGGTAGTTGGTTTGATCATCA AATAGAATTAGTCAATTTGGGACCAGATAGATTTAATGCTCATAATATTTGGTTT AAATATGTTATGAGTTTGGTGGAATTGTTATATCCTACGACATTTACCGTAACAG AAGAACGAATAGATTTTGTTAAAACATTGAATAGTCTTGAACGAATAAAAAATCA AGGGAAAGATCTTTGTCTTATTGGTTCGCCATACTTTATTTATTTACTCTGCCAT TATATGAAAGATAAAAAAATCTCATTTTCTGGAGATAAAAGCCTTTATATCATAA CCGGAGGCGGCTGGAAAAGTTACGAAAAAGAATCTCTGAAACGTGATGATTTCAA TCATCTTTTATTTGATACTTTCAATCTCAGTGATATTAGTCAGATCCGAGATATA TTTAATCAAGTTGAACTCAACACTTGTTTCTTTGAGGATGAAATGCAGCGTAAAC ATGTTCCGCCGTGGGTATATGCGCGAGCGCTTGATCCTGAAACGTTGAAACCTGT ACCTGATGGAACGCCGGGGTTGATGAGTTATATGGATGCGTCAGCAACCAGTTAT CCAGCATTTATTGTTACCGATGATGTCGGGATAATTAGCAGAGAATATGGTAAGT ATCCCGGCGTGCTCGTTGAAATTTTACGTCGCGTCAATACGAGGACGCAGAAAGG GTGTGCTTTAAGCTTAACCGAAGCGTTTGATAGTTGATATCCTTTGCCTAATTGT AAGTGGAATGCTTGCGTTATATAAATCTGAATGACATCTACACTTTACAAAATTC TCCAAAACATCCACATTTGGGTACTTGATAGAGGTTTATGGGGTTGGCTTAACAT TGTTCTCATTGTTATTATTGGCTCAAAGCAAAAGGAGATAACATGAAAAAATTGG CAGTTATGCTTGCATTGGGAATGATTAGCTTTGGTGCAATGGCAGTTGATGGGTA TAAAGATGCAAAGTTTGGCATGACAGAAGAAGAGTTTCTTTCGAAGAGGTTATGT GATTTTGAAAAATTTGAGGGAGATTCTCGAATAGAAGAAGTATCACTTTATTCAT GTTCTGACTTTTCGTTTGCTAACAAAAAGCGTGAAGCAATGGCATTTTTTTTAAA TGGGAAATTTAAAAGATTAGAGATTAATATTGGCAGACTTGTGAAGCCAGTAAGC AAATCGTTAACGAAAAAGTACGGAGATGGATCATCGTATCCATCAAAAGAAGAAT TTGAGAACGCGCTAAAATACAATGGAACTATGTCTATAGGTTATGATAATAATAC GGTATTAGTTGATATACATATAATATGTGGCAAAGAAGGCATAGAAACCAGTCAA CTGATTTATACGAGTCCAGATGTTTATACGCTCCCAGATTTCGGAGAAAAAATCC AGGAATTAAAGGGATTAAAGGAATTTGCCCTATAG
lux operon (*A. fischeri*)	Gene with RBS**	AGGAGGGGCAAATATGAATAAATGTATTCCAATGATAATTAATGGAATGATTCAA GATTTTGATAATTATGCATATAAAGAAGTTAAACTAAATAATGATAATAGAGTAA AATTATCTGTCATTACTGAAAGTTCAGTTTCAAAAACATTAAATATCAAAGATAG AATTAATCTAAATTTAAATCAGATTGTGAATTTTTTATATACCGTTGGTCAACGA TGGAAAAGTGAAGAATATAATCGGCGACGAACCTATATCCGTGAGTTAAAAACAT ATCTTGGTTATTCTGATGAAATGGCAAGATTAGAAGCGAATTGGATTGCAATGTT ATTGTGCTCTAAAAGTGCTTTGTATGACATTGTTAATTATGATTTGGGCTCTATA CACGTATTAGATGAATGGCTTCCACGTGGTGATTGCTATGTTAAAGCACAACCGA AAGGTGTTTCTGTTCACTTGTTAGCTGGTAATGTTCCATTATCAGGAGTGACATC TATTTTGCGTGCTATTTTAACAAAAAATGAGTGCATTATTAAAACTTCGTCTTCA GATCCTTTTACTGCAAACGCTTTAGTTTCCAGTTTTATTGATGTTAATGCAGACC ATCCAATAACCAAATCAATGTCTGTTATGTATTGGCCGCATGATGAAGATATGAC TCTATCTCAAAGAATAATGAATCATGCCGACGTGGTTATTGCTTGGGGTGGAGAC GAGGCGATTAAATGGGCGGTAAAATATTCACCACCGCATGTCGATATTCTGAAAT TTGGACCAAAGAAAAGCTTAAGTATTATTGAAGCTCCTAAAGATATAGAAGCCGC AGCAATGGGGGTTGCTCATGATATTTGTTTCTATGACCAGCAAGCCTGCTTCTCT ACTCAAGACGTTTATTATATAGGAGATAATTTACCTTTATTTTTAAATGAACTTG AAAAACAGCTAGATCGATACGCGAAAATTTTACCAAAAGGTTCAAATAGTTTTGA TGAAAAAGCGGCGTTTACTCTTACTGAAAAAGAAAGTCTATTTGCTGGATATGAA GTGAGAAAGGGAGATAAGCAAGCTTGGTTAATAGTCGTATCACCTACAAATAGCT

TTGGAAATCAACCGCTATCACGAAGTGTGTATGTTCATCAAGTATCTGATATTAA
AGAGATAATTCCTTTTGTTAATAAAAATAGAACACAAACTGTTTCTATTTATCCT
TGGGAAGCGTCATTAAAATATCGAGATAAATTAGCAAGAAGTGGAGTTGAAAGAA
TTGTTGAATCAGGCATGAATAATATTTTCAGAGTTGGAGGGGCTCATGATTCATT
ATCTCCTCTCCAGTACCTAGTTAGGTTTGTATCGCATGAGAGACCATTTAATTAT
ACGACAAAAGATGTTGCGGTTGAAATCGAACAAACACGTTACTTAGAGGAAGATA
AGTTTTTAGTTTTTGTCCCATAGTTAAAGGAAATTATATGAAAGATGAAAGTGCT
TTTTTTACGATTGATCACATCATCAAGCTTGATAATGGTCAGTCTATCCGAGTTT
GGGAAACACTCCCTAAAAAGAACGTACCAGAGAAAAAACATACAATACTTATTGC
TTCGGGTTTTGCTAGAAGAATGGATCATTTTGCAGGTCTTGCTGAGTATTTATCT
ACTAACGGTTTTCATGTCATTCGCTACGATTCTTTGCATCATGTTGGATTAAGCA
GTGGATGTATAAATGAATTTACGATGTCGATTGGAAAAAATAGCCTGCTTACAGT
CGTAGATTGGCTTACAGATCATGGTGTCGAACGAATAGGGCTGATTGCTGCTAGT
TTGTCAGCGAGAATCGCCTATGAGGTAGTAAATAAAATTAAATTATCATTTTTAA
TTACGGCCGTAGGTGTCGTTAATCTTAGAGATACATTAGAAAAAGCATTGGAGTA
TGACTATTTGCAATTACCTATTTCAGAGTTACCAGAAGATCTTGACTTTGAAGGT
CATAATTTAGGATCGGAGGTCTTTGTTACAGATTGCTTTAAACATAATTGGGACA
CGTTAGACTCGACACTTAATAGTGTTAAAGGATTAGCGATTCCATTTATTGCTTT
TACTGCAAACGATGATAGTTGGGTAAAGCAAAGTGAAGTTATAGAGCTCATTGAT
AGCATTGAATCTAGTAATTGTAAGCTCTATTCGCTAATTGGAAGTTCACATGATC
TTGGGGAAAATTTGGTTGTATTAAGAAATTTTTATCAATCAGTGACGAAGGCAGC
CTTAGCATTAGATGATGGTTTATTGGATTTAGAGATAGACATTATTGAACCTCGA
TTTGAGGACGTTACAAGTATTACTGTTAAGGAGCGTAGATTAAAAAATGAAATTG
AAAATGAATTATTAGAATTGGCTTAAATAAACAGAATCACCAAAAAGGAATAGAG
TATGAAGTTTGGAAATATTTGTTTTTCGTATCAACCACCAGGTGAAACTCATAAG
CAAGTAATGGATCGCTTTGTTCGGCTTGGTATCGCCTCAGAAGAGGTAGGGTTTG
ATACATATTGGACCTTAGAACATCATTTTACAGAGTTTGGTCTTACGGGAAATTT
ATTTGTTGCTGCGGCTAACCTGTTAGGAAGAACTAAAACATTAAATGTTGGCACT
ATGGGGGTTGTTATTCCGACAGCACACCCAGTTCGACAGTTAGAAGACGTTTTAT
TATTAGATCAAATGTCGAAAGGTCGTTTTAATTTTGGAACCGTTCGAGGGCTATA
CCATAAAGATTTTCGAGTATTTGGTGTTGATATGGAAGAGTCTCGAGCAATTACT
CAAAATTTCTACCAGATGATAATGGAAAGCTTACAGACAGGAACCATTAGCTCTG
ATAGTGATTACATTCAATTTCCTAAGGTTGATGTATATCCCAAAGTGTACTCAAA
AAATGTACCAACCTGTATGACTGCTGAGTCCGCAAGTACGACAGAATGGCTAGCA
ATACAAGGGCTACCAATGGTTCTTAGTTGGATTATTGGTACTAATGAAAAAAAAG
CACAGATGGAACTCTATAATGAAATTGCGACAGAATATGGTCATGATATATCTAA
AATAGATCATTGTATGACTTATATTTGTTCTGTTGATGATGATGCACAAAAGGCG
CAAGATGTTTGTCGGGAGTTTCTGAAAAATTGGTATGACTCATATGTAAATGCGA
CCAATATCTTTAATGATAGCAATCAAACTCGTGGTTATGATTATCATAAAGGTCA
ATGGCGTGATTTTGTTTTACAAGGACATACAAACACCAATCGACGTGTTGATTAT
AGCAATGGTATTAACCCTGTAGGCACTCCTGAGCAGTGTATTGAAATCATTCAAC
GTGATATTGATGCAACGGGTATTACAAACATTACATGCGGATTTGAAGCTAATGG
AACTGAAGATGAAATAATTGCTTCCATGCGACGCTTTATGACACAAGTCGCTCCT
TTCTTAAAAGAACCTAAATAAATTACTTATTTGATACTAGAGATAATAAGGAACA
AGTTATGAAATTTGGATTATTTTTTCTAAACTTTCAGAAAGATGGAATAACATCT
GAAGAAACGTTGGATAATATGGTAAAGACTGTCACGTTAATTGATTCAACTAAAT
ATCATTTTAATACTGCCTTTGTTAATGAACATCACTTTTCAAAAAATGGTATTGT
TGGAGCACCTATTACCGCAGCTGGTTTTTTATTAGGGTTAACAAATAAATTACAT
ATTGGTTCATTAAATCAAGTAATTACCACCCATCACCCTGTACGTGTAGCAGAAG
AAGCCAGTTTATTAGATCAAATGTCAGAGGGACGCTTCATTCTTGGTTTTAGTGA
CTGCGAAAGTGATTTCGAAATGGAATTTTTTAGACGTCATATCTCATCAAGGCAA
CAACAATTTGAAGCATGCTATGAAATAATTAATGACGCATTAACTACAGGTTATT
GTCATCCCCAAAACGACTTTTATGATTTTCCAAAGGTTTCAATTAATCCACACTG
TTACAGTGAGAATGGACCTAAGCAATATGTATCCGCTACATCAAAAGAAGTCGTC
ATGTGGGCAGCGAAAAAGGCACTGCCTTTAACATTTAAGTGGGAGGATAATTTAG
AAACCAAAGAACGCTATGCAATTCTATATAATAAAACAGCACAACAATATGGTAT
TGATATTTCGGATGTTGATCATCAATTAACTGTAATTGCGAACTTAAATGCTGAT
AGAAGTACGGCTCAAGAAGAAGTGAGAGAATACTTAAAAGACTATATCACTGAAA
CTTACCCTCAAATGGACAGAGATGAAAAAATTAACTGCATTATTGAAGAGAATGC
AGTTGGGTCTCATGATGACTATTATGAATCGACAAAATTAGCAGTGGAAAAAACA
GGGTCTAAAAATATTTTATTATCCTTTGAATCAATGTCCGATATTAAAGATGTAA
AAGATATTATTGATATGTTGAACCAAAAAATCGAAATGAATTTACCATAATAAAA

TTAAAGGCAATTTCTATATTAGATTGCCTTTTTAAATTTCTGTTGATATTAGGTA
TTACTGGAGAGGGTATGACTGTCCATACTGAATATAAAAGAAATCAAATCATTGC
TAGTTCAGAAATTGATGATCTTATCTTTATGACGAAACCACAAGAGTGGTCATTT
GAAGAGCAAAAAGAAATACGGGATAAATTAGTTCGTGAGGCTTTTTATTTTCACT
ACAATAGAAATGAAGAATATAGAAATTATTGTATCAATCAGCATGTGAGTGATAA
TTTACACACTATTGATGAAATACCCGTGTTTCCAACATCTGTTTTTAAATATAAG
AAATTACATACTGTCACAGCCGAGGACATTGAAAATTGGTATACAAGTAGTGGAA
CTCGTGGAGTAAAAAGTCATATTGCACGTGATCGTCTTAGCATTGAACGCTTGCT
TGGTTCTGTCAACTTCGGAATGAAATACGTTGGAGATTGGTTTGAGCATCAAATG
GAATTGATAAATTTAGGACCAGATAGATTCAATACAAATAATATTTGGTTTAAAT
ATGTCATGAGTTTGGTCGAGTTACTTTATCCGACTGAATTTACAGTTGATAATGA
CAAAATAGATTTTGAAAAAACAGTAAAACATCTATTTAGAATTAAGAATAGTAAA
AAAGACATTTGCTTAATTGGGCCACCATTTTTTGTGTATCTTTTGTGCCAATATA
TGAAAGAAAACAATATTGAATTTAAAGGAGGAGATAGAGTACATATTATTACTGG
TGGAGGATGGAAATCTAATCAGAATGACTCTTTAGATCGTGCTGATTTTAATCAA
TTATTAATGGATACTTTCCAACTCGACAAGATTAATCAAATTAGAGATACCTTTA
ATCAAGTTGAGCTTAATACTTGTTTTTTTGAAGATGAATTTCAAAGAAAACATGT
TCCACCGTGGGTATATGCTCGGGCTCTTGATCCTGAAACCTTGAAACCCGTAGCA
GATGGTGAGATCGGGTTGTTAAGTTATATGGACGCCTCATCAACTGCTTACCCTG
CTTTTATTGTTACTGATGATATCGGTATTGTAAAAGAAATTAGAGAACCAGATCC
TTACCCAGGGGTAACTGTTGAGATTGTTCGGCGCTTAAATACACGTGCGCAAAAA
GGATGCGCGCTCTCTATGGCTAATGTCATACAAAAGAATATCAAGGATTAAGTTA
TGATTGTTGATGGTAGAGTTTCAAAAATAGTATTAGCGTCAATAAGAAATAATAT
ATATAAGGTATTTATTACTGTAAATTCACCAATAAAGTTCATCGCTGGACAATTT
GTAATGGTCACGATTAATGGGAAAAAATGCCCTTTTTCAATTGCGAATTGCCCGA
CAAAAAATTACGAAATAGAATTGCATATTGGTAGTTCGAATAGAGACTGCTCATT
GGATATTATCGAATATTTTGTCGATGCTCTTGTTGAGGAAGTCGCAATTGAGTTA
GATGCTCCCCATGGAAACGCTTGGTTACGGTCTGAAAGTAATAACCCATTGCTAT
TAATTGCGGGAGGTACAGGTTTATCATATATAAATAGCATTCTAACAAATTGCTT
AAATAGGAATATACCTCAAGATATTTATCTTTACTGGGGAGTAAAAGACAGTTCT
CTTTTGTATGAAGATGAAGAGTTACTAAACTTATCACTAAACAACAAAAACTTTC
ATTATATTCCTGTTATTGAAGATAAAAGTGAAGAATGGATAGGGAGAAAAGGCAC
TGTTCTTGATGCTGTCATGGAAGATTTTACTGATCTTACTTATTTTGATATTTAT
GTTTGTGGACCCTTCATGATGGCTAAAACAGCAAAAGAAAAATTAATTGAAGAGA
AAAAAGCAAAGTCAGAACAGATGTTTGCCGATGCTTTTGCATACGTATAA

*: http://parts.igem.org/Part:BBa_J06504

**: gift from Prof Belkin Shimshon (Hebrew University of Jerusalem)

Table S2: List of oligonucleotides used in this study

Underlined sequences are the enzyme cutting site and the sequences in bold are the coding sequence regions of the reporter genes.

Primer (set)	Sequence (5'– 3')	Usage
mCherry_F	CGTCTAGAGATTAAAGAGGAGAAATACTAG**ATGGTGAGCAAGG**	To add XbaI cutting site and B0030 to the front of *mCherry*
mCherry_R	GCACTAGTATTA**TTACTTGTACAGCTCGTCCATGCCGC**	To add SpeI cutting site to the end of *mCherry*
ScarLet-I_F	CGTCTAGAGATTAAAGAGGAGAAATACTAG**ATGGTGAGTAAAGG**	To add XbaI cutting site and B0030 to the front of *mScarlet-I*
ScarLet-I_R	GCACTAGTATTA**TTAGTATAGTTCATCCATGCCACCTTAGTATAGTTCATCCATGCCACC**	To add SpeI cutting site to the end of *mScarlet-I*
GFP_F	CGGAATTCGCGGCCGCTCTAGAGATTAAAGAGGAGAAATACTAG**ATGGAGCTTTTCACTGGCGTTGTTCCC**	To insert BioBrick prefix and B0030 to the front of *gfp*
GFP_R	GCACTAGTATTA**TTAGATCCCGGCGGCGGTCACG**	To add SpeI cutting site to the end of *gfp*
deGFP_F	CGGAATTCGCGGCCGCTCTAGAGATTAAAGAGGAGAAATACTAG**ATGGAGCTTTTCACTGGCGTTGTTCCC**	To insert BioBrick prefix and B0030 to the front of *degfp*
deGFP_R	GCACTAGTATTA**TTAGATCCCGGCGGCGGTCACG**	To add SpeI cutting site to the end of *degfp*
NanoLuc_F	CGGAATTCGCGGCCGCTCTAGAGATTAAAGAGGAGAAATACTAG**ATGGTCTTCACACTCGAAGATTTCGTTGGG**	To insert BioBrick prefix and B0030 to the front of *NanoLuc*
NanoLuc_R	GCACTAGTATTA**TTACGCCAGAATGCGTTCGCACAGC**	To add SpeI cutting site to the end of *NanoLuc*
Rbs30_spacer_F	CTGGAATTCGCGGCCGCTTCTAGAGATTAAAGAGGAGAAATACTAG	To introduce B0030
Rbs30_spacer_R	ATTACCGCCTTTGAGTGAGC	
PmerT_J23115_F	GCTACTAGTATTTATAGCTAGCTCAGCCCTTGG	To introduce P_{merT}
PmerT_R	GGAATTCGCGGCCGCTTCTAGAGATATAAACGCAGAAAGGCCC	
PmerT_J23109_F	GCTACTAGTATTTACAGCTAGCTCAGTCCTAGG	
Additional B0015 Terminator	GCTTCTAGAGCTCGGTACCAAAGACGAACAATAAGACGCTGAAAAGCGTCTTTTTTCGTTTTGGTCCTACTAGAGTTCCATATCGCTTGACTACG	To introduce the additional B0015 terminator
mCherry_F	CGTCTAGAGATTAAAGAGGAGAAATACTAG**ATGGTGAGCAAGG**	To add XbaI cutting site and B0030 to the front of *mCherry*

mCherry_R	GCACTAGTATTA**TTACTTGTACAGCTCGTCCATGCCGC**	To add SpeI cutting site to the end of *mCherry*
J23101_fromJ23117_F	CCTAGGACTGAGCTAGCTGTAAATCACACTGGCTCACCTTC	To mutate J23117 to J23101 promoter by point mutation
J23101_fromJ23117_R	GCTAGCTCAGTCCTAGGTATTATGCTAGCTACTAGAGATTAAAGAGG	To mutate J23117 to J23101 promoter by point mutation
E_X_r30_lacZ_fwd	CCGGAATTCGCGGCCGCTTCTAGAGATTAAAGAGGAGAAATACTAG**ATGACCATGATTACGGATTCACTGGCC**	For amplifying *lacZ* from *E. coli* MG1655 genome
S_lacZ_rev	GCTACTAGTATTA**TTTTTGACACCAGACCAACTGGTAATGGTAGCGACCGGCGCTCAGCTGAAACTCCGCCGATACTGACGGGCTCC**	
GB_ORF8-B15_fwd2	**GCCCTATAG**TAATACTAGAGCCAGGC	For amplifying the sensor circuits and *lux* operon for AQUA cloning[12]
GB_Plux2_rev	ATTTGCCCCTCCTCTCTAGTTTTATTCGAAAG	
GB_PmerT_rev	ATTTGCCCCTCCTCTCTAGTAGGATTGGATAGCGTAACC	
GB_LuxC_fwd	ACT**AGAGAGGAGGGGCAAATATGACTAAAAAAATTTC**	
GB_ORF8_rev	CTCTAGTAT**TACTATAGGGCGAATTCCTTTAATC**	
GB_VFLuxC_fwd	ACTAGAGAGGAGGGGCAAAT**ATGAATAAATGTATTCCAATG**	
GB_VFLuxG_rev	CTCTAGTATTATTA**TACGTATGCAAAAGCATC**	
GB_VFLuxG-B15_fwd	**CATACGTA**TAATAATACTAGAGCCAGGC	
-XbaI_luxD_fwd	**TGCCGGATAACCTAGATTTTGAAGGC**	For removing the XbaI and EcoRI sites in the *lux* operon (*P. luminescens*) using AQUA cloning[12]
-XbaI_luxD_rev	**TGGCCTTCAAAATCTAGGTTATCCGGC**	
-EcoRI_ORF8_rev	**CTATAGGGCAAATTCCTTTAATCCC**	
-EcoRI_ORF8_fwd	**GGATTAAAGGAATTTGCCCTATAG**	

Table S3: List of abbreviations used in this study

Abbreviation	Full name / explanation
$3OC_6HSL$	N-(β-ketocaproyl)-L-homoserine lactone
CFS	cell-free system
deGFP	a GFP derived from an enhanced GFP with optimized translation ability in CFS
DMSO	dimethyl sulfoxide
fM	femtomolar
GFP	green fluorescent protein
GFPmut3	a GFP derived from *Aequorea victoria* with improved fluorescence emission at excitation 488 nm
$HgCl_2$	mercury (II) chloride
LacZ	β-galactosidase
LB	lysogeny broth
LOD	limit of detection
LucFF	firefly luciferase
LuxCDABE/LuxAB	bacterial luciferase operon
LuxR	quorum sensing molecule-responsive transcription activator
mCherry	a monomeric RFP derived from *Discosoma sp.*
MerR	mercury (II)-responsive transcription activator-repressor
mScarlet-I	a monomeric RFP derived from synthetic construct based on mCherry and multiple other naturally occurring RFPs and chromo proteins
NanoLuc	luciferase engineered by directed evolution from the deep sea shrimp *Oplophorus gracilirostris*
PBS	phosphate-buffered saline
PURE	purified recombinant elements
RFP	red fluorescent protein
TX-TL	transcription-translation
X-gal	5-Bromo-4-chloro-3-indolyl β-D-galactopyranoside

References

(1) Wang, B.; Barahona, M.; Buck, M. Amplification of Small Molecule-Inducible Gene Expression via Tuning of Intracellular Receptor Densities. *Nucleic Acids Res.* **2015**, *43* (3), 1955–1964.

(2) Wan, X.; Volpetti, F.; Petrova, E.; French, C.; Maerkl, S. J.; Wang, B. Cascaded Amplifying Circuits Enable Ultrasensitive Cellular Sensors for Toxic Metals. *Nat. Chem. Biol.* **2019**, *15* (5), 540–548.

(3) Cevenini, L.; Calabretta, M. M.; Lopreside, A.; Tarantino, G.; Tassoni, A.; Ferri, M.; Roda, A.; Michelini, E. Exploiting NanoLuc Luciferase for Smartphone-Based Bioluminescence Cell Biosensor for (Anti)-Inflammatory Activity and Toxicity. *Anal. Bioanal. Chem.* **2016**, *408* (30), 8859–8868.

(4) Armbruster, D. A.; Pry, T. Limit of Blank, Limit of Detection and Limit of Quantitation. *Clin. Biochem. Rev.* **2008**, *29 Suppl 1* (August), S49-52.

(5) Wang, B.; Kitney, R. I.; Joly, N.; Buck, M. Engineering Modular and Orthogonal Genetic Logic Gates for Robust Digital-like Synthetic Biology. *Nat. Commun.* **2011**, *2* (1), 508.

(6) Wang, B.; Barahona, M.; Buck, M. A Modular Cell-Based Biosensor Using Engineered Genetic Logic Circuits to Detect and Integrate Multiple Environmental Signals. *Biosens. Bioelectron.* **2013**, *40* (1), 368–376.

(7) Wang, B.; Barahona, M.; Buck, M. Engineering Modular and Tunable Genetic Amplifiers for Scaling Transcriptional Signals in Cascaded Gene Networks. *Nucleic Acids Res.* **2014**, *42* (14), 9484–9492.

(8) Chen, Y. J.; Liu, P.; Nielsen, A. A. K.; Brophy, J. A. N.; Clancy, K.; Peterson, T.; Voigt, C. a. Characterization of 582 Natural and Synthetic Terminators and Quantification of Their Design Constraints. *Nat. Methods* **2013**, *10* (7), 659–664.

(9) Bindels, D. S.; Haarbosch, L.; Van Weeren, L.; Postma, M.; Wiese, K. E.; Mastop, M.; Aumonier, S.; Gotthard, G.; Royant, A.; Hink, M. A.; et al. MScarlet: A Bright Monomeric Red Fluorescent Protein for Cellular Imaging. *Nat. Methods* **2016**, *14* (1), 53–56.

(10) Siegal-Gaskins, D.; Tuza, Z. A.; Kim, J.; Noireaux, V.; Murray, R. M. Gene Circuit Performance Characterization and Resource Usage in a Cell-Free “Breadboard.” *ACS Synth. Biol.* **2014**, *3* (6), 416–425.

(11) Eggers, C. T.; Valley, M. P.; Klaubert, D. H.; Unch, J.; Encell, L. P.; Wood, K. V.; Hall, M. P.; Benink, H. A.; Otto, P.; Zimmerman, K.; et al. Engineered Luciferase Reporter from a Deep Sea Shrimp Utilizing a Novel Imidazopyrazinone Substrate. *ACS Chem. Biol.* **2012**, *7* (11), 1848–1857.

(12) Beyer, H. M.; Gonschorek, P.; Samodelov, S. L.; Meier, M.; Weber, W.; Zurbriggen, M. D. AQUA Cloning: A Versatile and Simple Enzyme-Free Cloning Approach. *PLoS One* **2015**, *10* (9), e0137652.

4

A novel bioluminescent NanoLuc yeast-estrogen screen biosensor (nanoYES) with a compact wireless camera for effect-based detection of endocrine-disrupting chemicals

Reproduced from: “A novel bioluminescent NanoLuc yeast-estrogen screen biosensor (nanoYES) with a compact wireless camera for effect-based detection of endocrine-disrupting chemicals”

Luca Cevenini, Antonia Lopreside, Maria Maddalena Calabretta, Marcello D’Elia, Patrizia Simoni, Elisa Michelini, Aldo Roda

Analytical and Bioanalytical Chemistry, 2018, 410.4: 1237-46.

Anal Bioanal Chem (2018) 410:1237–1246
DOI 10.1007/s00216-017-0661-7

RESEARCH PAPER

A novel bioluminescent NanoLuc yeast-estrogen screen biosensor (nanoYES) with a compact wireless camera for effect-based detection of endocrine-disrupting chemicals

Luca Cevenini[1] · Antonia Lopreside[1] · Maria Maddalena Calabretta[1] · Marcello D'Elia[2] · Patrizia Simoni[3] · Elisa Michelini[1,4,5] · Aldo Roda[1,4]

Received: 28 July 2017 / Revised: 8 September 2017 / Accepted: 19 September 2017 / Published online: 30 September 2017

Abstract The presence of chemicals with estrogenic activity in surface, groundwater, and drinking water poses serious concerns for potential threats to human health and aquatic life. At present, no sensitive portable devices are available for the rapid monitoring of such contamination. Here, we propose a cell-based mobile platform that exploits a newly developed bioluminescent yeast-estrogen screen (nanoYES) and a low-cost compact camera as light detector. *Saccharomyces cerevisiae* cells were genetically engineered with a yeast codon-optimized variant of NanoLuc luciferase (yNLucP) under the regulation of human estrogen receptor α activation. Ready-to-use 3D-printed cartridges with immobilized cells were prepared by optimizing a new procedure that enables to produce alginate slices with good reproducibility. A portable device was obtained exploiting a compact camera and wireless connectivity enabling a rapid and quantitative evaluation (1-h incubation at room temperature) of total estrogenic activity in small sample volumes (50 μL) with a LOD of 0.08 nM for 17β-estradiol. The developed portable analytical platform was applied for the evaluation of water samples spiked with different chemicals known to have estrogen-like activity. Thanks to the high sensitivity of the newly developed yeast biosensor and the possibility to wireless connect the camera with any smartphone model, the developed configuration is more versatile than previously reported smartphone-based devices, and could find application for on-site analysis of endocrine disruptors.

Published in the topical collection *Microbial Biosensors for Analytical Applications* with guest editor Gérald Thouand

Electronic supplementary material The online version of this article (https://doi.org/10.1007/s00216-017-0661-7) contains supplementary material, which is available to authorized users.

✉ Elisa Michelini
elisa.michelini8@unibo.it

✉ Aldo Roda
aldo.roda@unibo.it

[1] Department of Chemistry "G. Ciamician", Alma Mater Studiorum, University of Bologna, via Selmi 2, 40126 Bologna, Italy

[2] Gabinetto Regionale di Polizia Scientifica per l'Emilia Romagna, Via Volto Santo 3, 40123 Bologna, Italy

[3] Department of Medical and Surgical Sciences, Alma Mater Studiorum, University of Bologna, Via Massarenti 9, 40138 Bologna, Italy

[4] INBB, Istituto Nazionale di Biostrutture e Biosistemi, Viale delle Medaglie d'Oro 305, 00136 Rome, Italy

[5] Health Sciences and Technologies-Interdepartmental Center for Industrial Research (HST-ICIR), University of Bologna, via Tolara di Sopra 41/E 40064, Ozzano dell'Emilia, Bologna, Italy

Keywords Bioluminescence · NanoLuc luciferase · Endocrine disruptors · Effect-based analysis · Estrogenic activity · Yeast-based biosensor

Introduction

The monitoring of micropollutants in the aquatic environment represents both a key technical and regulatory challenge that has been addressed in the EU Directive 2008/105/EC (the Environmental Quality Standards Directive, EQSD), later amended with the Directive 2013/39/EU under the European WFD [1]. In particular, several environmental contaminants are known to affect endocrine functions resulting in adverse health effects in humans and wildlife. These compounds, falling under the umbrella of endocrine-disrupting chemicals (EDCs), interfere

at different levels with the endocrine system, e.g., by binding to the receptors of several hormones (e.g., estrogens, androgens and progestogens, corticosteroids, and thyroid hormones). Different unrelated molecules have been classified as EDCs, including synthetic hormones, polycyclic aromatic hydrocarbons (PAHs), polychlorinated biphenyls (PCBs), dioxins, dibenzofurans, and alkylphenols [2]. This high heterogeneity in chemical structure and physicochemical properties poses significant technical issues for the development of analytical methods and for the identification of a harmonized regulatory framework [3, 4]. Although there are no legal discharge limits in the environment, some micropollutants have been recently prioritized at EU level according to their suspected health risks and to the current unavailability of adequate monitoring methods [5]. In 2015, the Joint Research Center published a technical report with the first Watch List containing the following substances: diclofenac, 17β-estradiol (E2), Estrone (E1), 17α-ethinylestradiol (EE2), oxadiazon, methiocarb, 2,6-ditert-butyl-4-methylphenol, triallate, imidacloprid/thiacloprid/thiamethoxam/clothianidin/acetamiprid, erythromycin/clarithromycin/azithromycin, and 2-ethylhexyl 4-methoxycinnamate. Of these ten substances, three compounds, i.e., E2, E1, and EE2, share the same mechanism of action, i.e., via activation of estrogen receptor α (ERα) [6]. The monitoring of these chemicals is challenging and only expensive and sophisticated laboratory equipment (e.g., mass spectrometry) can provide suitable detection limits for their detection.

An approach complementary to chemical analysis is represented by effect-based analysis, relying on the evaluation of actual biological activity of a sample, measured as the ability to activate receptors or other molecular targets [7–9]. Receptor-mediated effects are generally measured with bioassays or cell-based assays in which cells are re-programmed to express a reporter protein as a consequence of activation of a specific receptor. Cell-based assay have proven highly valuable tools to understand the level of estrogenic contamination in water bodies [3, 10] and for eco-toxicological studies [11, 12]. In particular, assays based on both human cell lines and yeasts have been developed by engineering living cells with the human estrogen α or β receptor, whose activation drives the expression of a reporter protein such as a luciferase or a green fluorescent protein [13–22].

As an alternative to reporter gene technology, [23] achieved detection at sub-ppb levels of estradiol and ppm levels of bisphenol A by engineering *Escherichia coli* cells to express on the surface native estrogen receptors and exploiting impedance. These assays are able to assess the effective biological activity of a sample taking into account mixture effects and even the presence of unidentified and unknown chemicals. Such information is crucial in the analysis of complex samples containing a high number of chemicals, for example to rapidly detect tap water contamination. Other biosensing approaches have been also explored to develop new tools able to measure estrogenic activity in environmental samples; for example, [24] proposed receptor-based optical biosensors that can be reused for up to 300 sensing cycles.

Among cell-based assays for estrogen-like activity, the most applied are ER-CALUX based on human U2-OS osteosarcoma cell line [25], E-SCREEN based on MCF-7 human breast adenocarcinoma cell line [26], and the yeast estrogen screen (YES) developed by Routledge and Sumpter [27]. In particular, YES assay is based on a recombinant *Saccharomyces cerevisiae* yeast strain expressing the human estrogen receptor hER and a reporter plasmid carrying the reporter gene lac-Z encoding the enzyme β-galactosidase for colorimetric detection.

Despite their widespread use in laboratory settings, these assays have not yet been implemented in portable formats. The availability of new methods enabling the on-site analysis would be an extremely helpful tool for routine screening and for providing a rapid alert in case of accidental disasters in order to rapidly undertake proper countermeasures [6].

We previously reported proof-of-principle devices integrating yeast cells for endocrine disruptors, nevertheless the low bioluminescence (BL) emission of the cells required highly sensitive light detectors such as cooled charge-coupled device (CCD) cameras for astrophotography [28]. We recently reported the obtainment of general toxicity cell biosensors exploiting the smartphone-integrated camera as detector [29, 30]. Yet these biosensors integrated mammalian cell lines, with the well-known limitations related to cell handling and shelf-life. A 3D-printed cartridge was fabricated to integrate cells with a smartphone, simplifying the device itself but limiting its applicability to a single smartphone model. Considering the high number of commercial smartphones and their short lifespan, this represents a serious limitation for real-life applications. Therefore, taking advantage of our experience, we addressed main limitations of previous portable cell biosensors in terms of detectability, universality of the device, and shelf-life of the cells. To increase detectability, we developed a new yeast biosensor by exploiting NanoLuc luciferase [31] as reporter protein, to develop a device of general use we replaced the smartphone with a compact wireless camera that can be connected to any smartphone, and we optimized a novel strategy for obtaining reproducible ready-to-use alginate slices with embedded cells.

Materials and methods

Chemicals and reagents

All the reagents required for yeast cell culture maintenance were from Sigma-Aldrich (St. Louis, MO). Synthetic complete (SC) liquid medium was prepared by adding 6.7 g yeast nitrogen base w/o amino acids, 1.4 g yeast synthetic drop-out medium supplement, 10 mL adenine hemisulfate solution to 1 L of H_2O. The solution was autoclaved and then 40 mL of

glucose 50% *w*/*v* solution (0.22 μm filter sterilized) was added. SC-ura-trp-leu medium was prepared by supplementing SC medium with L-histidine (2 g/L). SC (-Ura-Trp-Leu-His) medium was supplemented with L-histidine (0.02 g/L), L-leucine (0.1 g/L), L-tryptophan (0.02 g/L), and uracil (0.02 g/L). 17β-estradiol (E2), 17α-ethynylestradiol (EE2), diethylstilbestrol (DES), estrone (E1), and bisphenol A (BPA) were from Sigma-Aldrich. Dialysis tubing cellulose membrane and the kit for plasmid extraction and purification were from Sigma-Aldrich. FastDigest restriction enzymes, FastAP, and T4 DNA Ligase required for cloning and yeast protein extraction reagent (YPER) were from Thermo Fisher Scientific (Waltham, MA, USA). The bioluminescent substrate furimazine was from Promega (Madison, WI, USA). All other chemicals were purchased form Sigma-Aldrich (St. Louis, MO, USA).

Obtainment of NanoLuc estrogen responsive *S. cerevisiae* strain

Yeast expression plasmid pRSII426 and pBEVY-L were form Addgene (Cambridge, Massachusetts, USA). The yeast codon optimized version of the NanoLuc-PEST luciferase (yNLucP) was a kind gift from Prof. C. Andréasson (Stockholm University, Sweden) [32]. The sequence encoding the human estrogen receptor was amplified with polymerase chain reaction (PCR) using pSP72hERα as template and cloned into pBEVY-L (Leu2 marker) vector under the control of constitutive ADH1 promoter, using *KpnI* and *EcoRI* sites. The generated vector was called pBEVY-L-ERα.

The reporter vector was created by cloning, into a pRSII426 plasmid (Ura3 marker), five copies of an ERE response element (-AGGTCAgagTGACCT-) [33] upstream of a minimal cytochrome C promoter (CYCmin) driving the expression of the yNLucP coding sequence, giving the plasmid pRSII426-ERE-yNLucP. The correctness of sequences and vectors was confirmed by restriction analysis and sequencing.

The yeast *S. cerevisiae* BMA64-1A (MATa, ura 3-52, trp1Δ2 leu2-3 112his3-11 ade2-1, can1-100) wild-type strain was used as recipient strain [34] and transformed with plasmids pBEVY-L-ERα and pRSII426-ERE-yNLucP using the LiAc/SS-DNA/PEG method [35]. Colonies harboring both vectors were selected in SC-ura-leu plates after incubation at 30 °C for 4 days. Fifteen percent glycerol stocks of the recombinant strain were prepared and stored at −80 °C.

Laboratory-based assay procedure and luminescence measurements

The novel NanoLuc yeast estrogen screen (nanoYES) assay was carried out in a type II laminar flow cabinet to reduce aerosol formation. Before running an assay, a single colony from an agar plate containing the selective medium was used to inoculate 3.0 mL of SC medium. This culture was grown overnight at 30 °C with orbital shaking at 200 rpm in selective SC medium.

Briefly, a 3 mL overnight yeast culture was diluted in fresh SC medium to optical density (OD_{600}) of 0.6 and grown for about 4 h until OD_{600} = 1 was reached. Then, 150 μL of culture was dispensed in 96-well microplates and incubated at 25 °C with different concentrations of E2 (from 0.001 to 100 nM) at 1% ethanol final concentration, for 1 h. Control wells (CTR) were incubated with 1% ethanol final concentration. BL emission kinetics were recorded using a Varioskan Flash multimode reader (5 min with 300 ms integration time) after addition of 50 μL of an optimized BL substrate containing 10 μM furimazine diluted in YPER reagent (YPER-Nano). Light emissions were expressed as relative light units (RLU). The detection limit is defined as the E2 concentration that corresponds to the blank signal plus three times the standard deviation. All experiments were performed in triplicate and repeated at least three times.

Fabrication of the mobile platform 3D-printed cartridges and GoProHero5 adaptors

The compact GoPro HERO 5 video camera (GoPro, Inc., San Mateo, CA, USA) was chosen as light detector. A cartridge of 60 × 40 mm, 7 mm high, containing an array of 16 square wells (5 mm wide and 5 mm deep each) was created with a desktop 3D printer (Makerbot Replicator 2X) using black and white thermoplastic polymer acrylonitrile butadiene styrene (ABS) (FormFutura, Nijmegen, NL) using the dual extrusion option. The GoProHero5 adaptors and dark-box were printed using black ABS. All pieces were printed at 300 μm layer resolution, 30% infill.

Preparation of cartridges with immobilized yeast biosensors.

An overnight culture of yeast cells was diluted in 30 mL of fresh medium to optical density (OD_{600}) of 0.6 and grown for about 4 h until an OD_{600} = 1 was reached. The culture was centrifuged and resuspended in 3 mL SC-ura-leu medium containing 10% trehalose and 1.5% sodium alginate.

This mixture was then poured into a dialysis tubing cellulose membrane (avg. flat width 10 mm, molecular weight cut-off = 14 kDa) and immersed in a 0.2 M $CaCl_2$ solution for 1 h at room temperature (25 °C) to allow the formation of the gel inside the membrane. Using a 3D-printed "microtome-like" device, that has a slot for a surgical blade placed at 2 mm from the edge, the obtained gel (about 12 cm length, avg. diameter 5 mm) was repeatedly cut in several slices, then placed into the wells of the 3D-printed cartridges. A 50 μL volume of SC medium was added to each well and the cartridges were covered with Parafilm M® and stored at 4 °C until use.

The stability of the yeast biosensor kept at 4 °C was daily tested by incubating the cells in duplicate with 10 nM E2 (50 μL) for 1-h incubation at room temperature; a 50 μL volume of YPER-Nano substrate was added to each well and image was acquired with the GoProHero5 in night mode (30 s, ISO 800) equipped with the 3D-printed black-box accessory. Images were analyzed with ImageJ software and data plotted using GraphPad Prism v.5 (GraphPad Software, Inc. La Jolla, CA). BL emission was normalized with respect to BL signal obtained at day 0 (freshly immobilized cells). All measurements were performed in duplicate and repeated at least three times with different cell cartridges.

Analytical performance of the GoPro-based yeast estrogen screen

The analytical performance of the developed platform was performed by incubating yeast estrogen biosensors with increasing concentrations (from 0.05 to 10 nM) of E2, selected as model estrogenic analyte. Briefly, a cell-cartridge containing immobilized yeast cells stored at 4 °C was equilibrated at room temperature for 15 min, then a 50 μL volume of E2 dilutions (1% ethanol final concentration) were added in duplicate wells. Control wells were incubated with 1% ethanol final concentration (50 μL). After 1-h incubation at room temperature, a 50 μL volume of YPER-Nano substrate was added to each well, then the cartridge was inserted into the 3D-printed black-box accessory, and BL emission was acquired with the GoProHero5 in night mode (30 s, ISO 800). Images were quantified with ImageJ software by selecting a square region of interest (ROI) around each well and measuring the BL emission of duplicate wells. E2 dose-response curves were obtained by calculating the fold response with respect to control and plotted using GraphPad Prism. Non-linear regression was performed by fitting the experimental data using a four-parameters sigmoidal curve, then the EC50 value for E2 was calculated as the effective concentration which produces the midpoint *y* value (50%) of the dose-response curve. All measurements were performed in duplicate and repeated three times with different cell cartridges.

Yeast-estrogen cartridge configuration for effect-based analysis

To obtain yeast-estrogen biosensors for real sample analysis, easy-to-use cartridges with immobilized cells were prepared as follows: half of the cartridge was used to test in duplicate the yeast bioreporter response to 0.5, 1, and 5 nM E2 or 1% EtOH as control, while the remaining wells were incubated in duplicate with tap water samples (25 μL) spiked with different concentrations of diethylstilbestrol (0.1 and 10 nM) and bisphenol A (10 nM). Sample wells were also co-incubated with 0.5 nM E2 (25 μL). Dilution of estrogenic compounds were prepared to provide a 1% ethanol final concentration in every well.

Cartridges were incubated for 1 h at room temperature, then a 50 μL volume of YPER-Nano substrate was added to each well and BL emission was acquired with the GoProHero5 as described above. Images were quantified with ImageJ software by selecting a square ROI around each well and measuring the mean BL emission of duplicate wells. BL signal were then normalized with respect to 0.5 nM E2 (selected as reference and set to 100%) and plotted using GraphPad Prism. All measurements were performed in duplicate and repeated three times with different cell cartridges.

Results and discussion

The possibility to use the smartphone camera to detect the BL emission from living whole-cell biosensors has been previously demonstrated by us exploiting genetically engineered mammalian cell lines [29, 30]. Despite adequate analytical performance, one of the main limitations of this approach is surely related to the short shelf life of mammalian cells when maintained outside an incubator with controlled temperature and humidity. In addition, considering the short life span of smartphones, mainly due to short battery life and software updates changes, the general applicability of such devices is questionable with the necessity of upgrading and fabricating new devices, with subsequent assay optimization and calibration, for each smartphone model.

In this scenario, a mobile platform based on the use of a compact camera, such as the GoProHero camera, and robust yeast cells as living biosensors could represent a suitable solution to overcome these issues. Indeed, yeast cells are particularly suitable for the development of whole-cell biosensors integrated into a portable mobile platform as they provide the analytical robustness typical of bacterial cells, with the possibility to express functional human receptors and regulatory elements to obtain predictive information about actual biological activity of samples [36].

The GoProHero5, optimized for sport and outdoor activities, represents a robust, waterproof CMOS camera (12 MP, UHD 4K) which can be directly controlled using the built-in touch-screen display or can be connected to any smartphone via dedicated GoPro-App (paired wireless network), making it a very versatile light sensor for the development of portable devices. In addition, the long exposure time (up to 30 s at ISO 800) makes this camera a powerful choice for low-light imaging applications, including bioluminescence measurements.

Development of a novel yeast-estrogen screen exploiting NanoLuc luciferase (nanoYES)

The novel yeast-estrogen strain (Fig. 1a) was obtained by genetically engineering *S. cerevisiae* cells with two vectors: (i) a plasmid for the expression of the human estrogen receptor α (hERα) under the control of the constitutive ADH1 promoter and (ii) a reporter plasmid containing five copies of an ERE response element (-AGGTCAgagTGACCT-) upstream of a minimal cytochrome C promoter (CYCmin) which drives the expression of the yeast codon-optimized NanoLuc luciferase coding sequence (yNLucP). Both vectors contain the 2 μ origin, thus ensuring consistent replication of the two plasmids during cell division and maintaining each plasmid at about 50 copies/cell. Due to the high copy number, the expression of the human estrogen receptor was placed under a weak promoter to avoid strong overexpression that may lead to artifacts in the biosensor response. Indeed, the high copy number of reporter vector allows consistent production of yNLucP reporter enzyme upon induction.

The small size (19 kDa) and the absence of post-translational modifications and disulfide bonds of NanoLuc luciferase enable its rapid synthesis and folding, thus reducing total assay time; moreover, the use of its destabilized version provides a half-life of 5 min in yeast, compared to 40 min of the yNluc [32], thus faithfully reflecting mRNA levels. Yeast cells were sequentially transformed with the two plasmids and single colonies screened for their responsiveness with 10 nM E2. A new BL substrate composition was formulated to optimize BL emission in yeast cells. The NanoGlo® substrate (containing a lysis buffer optimized for mammalian cells) showed suitable for yeast cells [32]. However, to increase light output, we formulated an alternative substrate by diluting furimazine (10 μM) in YPER buffer, a specific yeast-cell lysis reagent used for the extraction of functionally active solubilized proteins from yeast. The use of this formulation (YPER-Nano) provides both an increased BL emission (20%) and more stable emission kinetics (signal half-life > 20 min) compared to NanoGlo® substrate or furimazine alone (signal half-life < 2 min). Dose-response curve for E2 (0.001–100 nM) were obtained using liquid cultures of three positive clones in 96-well microplate format and benchtop luminometer. The yeast-estrogen biosensor incubated for 1 h with different concentrations of E2 shows a limit of detection of 0.010 ± 0.002 nM and an EC50 of 0.6 ± 0.1 nM (Fig. 1b). The nanoYES shows a LOQ of 0.020 ± 0.005 nM E2 and mean recovery rate of 93 ± 11%. The nanoYES response to other estrogenic compounds was also evaluated (Fig. 1b) and corresponding limit of detection and EC50s are shown in Table 1. The developed yeast estrogen bioassay shows comparable results in terms of ranking of estrogenic activity (E2 > EE2 > DES > E1) and EC50 values, obtained by previous works based on recombinant yeast cells [37, 38].

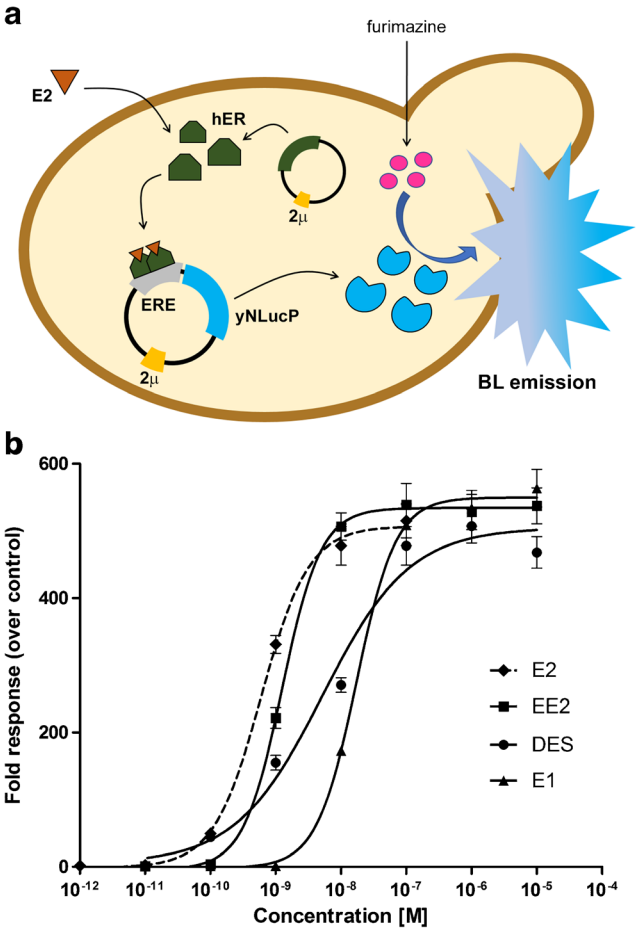

Fig. 1 **a** Schematic representation of the bioluminescent yeast-estrogen strain. *S. cerevisiae* cells were transformed with a plasmid for the expression of the human estrogen receptor α (hERα) under the control of the weak constitutive ADH1 promoter. Cells were also transformed with a vector containing five copies of estrogen response element (ERE) and the cDNA encoding for the yeast codon optimized NanoLuc luciferase destabilized variant (yNLucP). Both vectors contain a 2 μ replication origin for their propagation during yeast growth. The binding of estrogens such as 17β-estradiol (E2) to hERα activates the intracellular signaling pathway (receptor dimerization) which leads to the expression of yNLucP luciferase. Light emission is obtained after addition of an optimized substrate solution containing furimazine (2-furanylmethyl-deoxy-coelenterazine). **b** Dose-response curves for different estrogenic compounds (E2: 17β-estradiol; EE2: 17α-ethinylestradiol; DES: diethylstilbestrol; E1: estrone) obtained using the nanoYES performed in 96-well microplate format and benchtop instrumentation. Data represent the mean values ± the standard deviation (SD) obtained with three replicates and repeating the experiments three times

Design and 3D-printing fabrication of the mobile platform based on GoPro Hero camera

The mobile platform was designed to create an all-in-one device based on the GoPro Hero5 camera (see Electronic Supplementary Material (ESM) Fig. S1). A series of modular adaptors were fabricated with black ABS using a desktop 3D printer, providing a dark box of compact size (65 × 65 mm,

Table 1 nanoYES response to estrogenic compounds, obtained using liquid cultures, in 96-well plate format and benchtop luminometer

Compound	LOD (nM)	EC50 (nM)
17β-estradiol (E2)	0.010 ± 0.002	0.6 ± 0.1
17α-ethynylestradiol (EE2)	0.05 ± 0.01	1.2 ± 0.3
Diethylstilbestrol (DES)	0.019 ± 0.005	5.2 ± 0.5
Estrone (E1)	0.5 ± 0.1	17 ± 2

60 mm height) for the acquisition of BL emission. This accessory also includes a slot to insert a 3D-printed cell-cartridge containing the immobilized nanoYES. The multi-well cartridges (60 × 40 mm), containing 16 wells of 5 × 5 mm (150 μL volume each), were printed with white and black ABS using the dual extrusion option provided by the Makerbot Replicator 2X. In particular, the bottom of the wells was printed using white ABS, while black ABS was used for the remaining parts. This configuration allowed to increase the intensity of acquired BL signal by reflection while avoiding crosstalk between adjacent wells, outperforming cartridges printed with only white or black ABS that suffered of higher crosstalk and lower signals, respectively.

Immobilization procedure and stability of nanoYES

To obtain ready-to-use cartridges, the nanoYES was immobilized into alginate slices. Cells at OD = 1 (about 1.8×10^7 cells/mL) were tenfold concentrated in culture medium to achieve a sufficient BL emission for a sensitive detection with the GoPro camera. The immobilization medium also contains 10% *w/v* trehalose to increase the shelf life of yeast cells [39].

A straightforward procedure was developed to generate yeast-alginate slices of defined and reproducible dimension (2.1 ± 0.2 mm) (see ESM Fig. S2).

To evaluate the reproducibility of immobilized nanoYES, a whole cell-cartridge (Fig. 2a) was incubated with 10 nM E2 for 1 h, and BL image acquired with the GoPro camera (Fig. 2b). The quantification of BL emission of 16 slices provided a coefficient of variation (CV%) of 11%, which is comparable to previously reported whole-cell bioassays [40].

The efficacy of our procedure was compared to conventional method for obtaining alginate beads. A 50 μL volume nanoYES/alginate mixture, containing the same cell number for each slice, was added dropwise into a $CaCl_2$ solution and let to harden for 1 h. Individual beads of about 4.5 ± 0.3 mm diameter were obtained, placed into the cell-cartridge wells, and treated as for the slices, with 10 nM E2 for 1 h. The mean BL signal using alginate beads is 8.5 times lower and less reproducible than those obtained with slices, most probably due to a slower and non-uniform distribution of analyte and BL substrate inside the beads (see ESM Fig. S3).

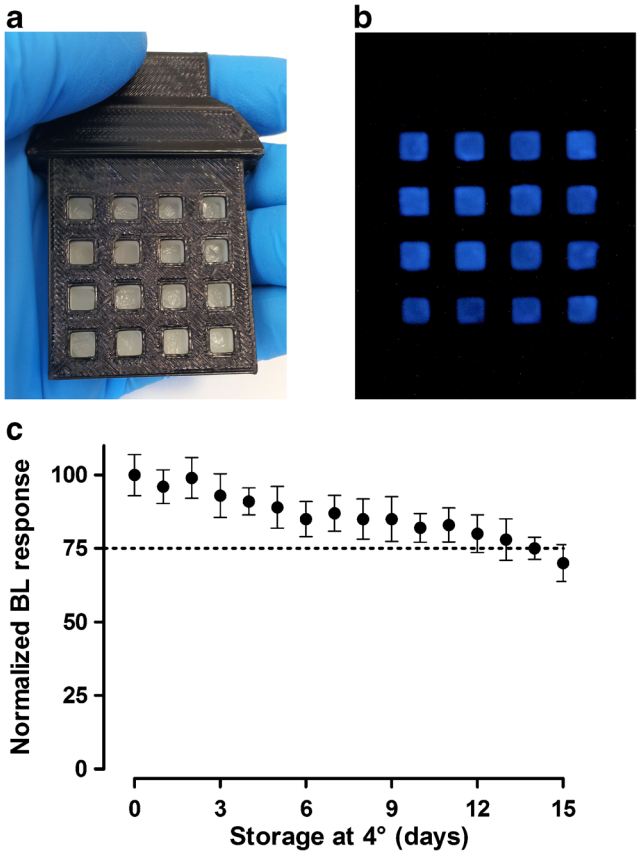

Fig. 2 **a** Picture of a 3D-printed cartridge containing 16 alginate slices of yeast-estrogen bioreporters. **b** BL image of 16 yeast-estrogen biosensors slices induced with 10 nM E2, acquired with the GoProHero5 camera in night mode (30 s at ISO 800), after addition of 50 μL YPERNano solution. **c** Responsiveness of immobilized yeast-bioreporters stored at 4 °C. Each day, duplicate wells were treated with 1 nM E2 and BL emissions were acquired with the GoPro camera. BL signals are normalized with respect to day 0 (freshly immobilized cells)

The stability and responsiveness of yeast-estrogen bioreporters immobilized into alginate slices stored at 4 °C in the 3D-printed cartridges was evaluated. Each day, duplicate wells were incubated with 1 nM E2 for 1 h and BL images were acquired with the GoPro camera. As shown in Fig. 2c, the nanoYES response was consistently maintained within 7 days (85% of initial response at day 7) and even after 2 weeks, the nanoYES maintains about 70% of the responsiveness obtained at day 0 (freshly immobilized cells). To guarantee good analytical performance in terms of LOD and sensitivity, we decided to use cell-cartridges not older than 10 days, which still provide a BL emission over the 75% of initial response (arbitrarily selected threshold).

Analytical performance of GoPro-based nanoYES

The assay in optimized conditions consists of incubation of 50 μL of E2 dilutions (concentration range from 0.05 to 10 nM) per each cartridge well containing (about 9.0×10^5

cells/slice) for 1 h at room temperature. Cell cartridge is then imaged with the GoProHero5 camera in night mode for 30 s at ISO 800, after addition of 50 μL YPER-Nano substrate (Fig. 3a). Since cells are lysed during BL emission acquisition, the cartridges are single-use. Figure 3b shows a detailed BL image corresponding to the dose-response curve for E2 acquired 10 min after substrate addition. Dose-response curves obtained with three different cartridges showed a LOD of 0.08 ± 0.02 nM and EC50 of 0.7 ± 0.1 nM E2 (Fig. 3c). In the GoPro-based platform, the limit of detection is about one order of magnitude higher compared to those obtained with the nanoYES using conventional benchtop luminometer while the EC50 is comparable (0.6 ± 0.2 nM E2). Conversely, the LOD is comparable to other previously reported yeast estrogen bioassays, such as those reported by Leskinen et al. (0.03 nM for E2) [15]. Also, the EC50 value is consistent with those obtained with similar yeast-based screening assays performed in laboratory settings, such as the conventional YES (EC50: 0.32 nM) [7]. These results confirmed the suitability of this configuration for the straightforward and quantitative detection of estrogenic activity in water samples.

GoPro-based nanoYES: analysis of spiked samples

As a proof of concept, tap water samples spiked with different concentrations of diethylstilbestrol (DES) and bisphenol A (BPA) were analyzed with the GoPro-based nanoYES to explore its actual feasibility for on-site testing, especially for monitoring of sites affected by high pollution such as downstream of industrial manufacturing plants and agricultural areas.

BPA was selected because of its ability to act as weak ER binder and interfere with the endogenous E2, causing severe effects on the reproductive system [41, 42] while DES is a synthetic nonsteroidal estrogen widely encountered in influents and effluents from municipal water treatment plants with concentrations levels in the range of 4–12 ng/L for primary influents [43, 44]. BPA is present at relatively high concentrations in several site areas, for example according to a recent review BPA concentrations in groundwater vary between 1 ng/L and 20 μg/L [45]. Each disposable cartridge also contains a calibration curve obtained by inducing the nanoYES with 0.5, 1, and 5 nM E2 allowing a rapid evaluation and subsequent interpolation of estrogenic activity of the samples (Fig. 4a). Control wells (CTR) were also included and incubated with 1% EtOH final concentration. Sample-wells were also induced with 0.5 nM E2, a concentration near the EC50, to evaluate both estrogenic and anti-estrogenic activity of samples.

Mean BL emission of each sample was quantified and normalized with respect to 0.5 nM E2, set to 100% (Fig. 4b). Sample no. 1, which contains 10 nM BPA (simulating a high contaminated sample), shows a remarkable decrease (35%) of BL emission. At this concentration, BPA (a weak hERα binder) interferes with the transactivation induced by 0.5 nM E2, thus decreasing BL emission. Acting as partial agonist, BPA competes with E2 (full agonist) for receptor occupancy, thus producing a net decrease in the receptor activation compared to that observed with the E2 alone.

Sample no. 2, which contains a very high concentration of a potent estrogen (10 nM DES), shows a remarkable increase compared to 0.5 nM E2 and was selected to simulate a strong estrogenic effect as in samples containing mixtures of

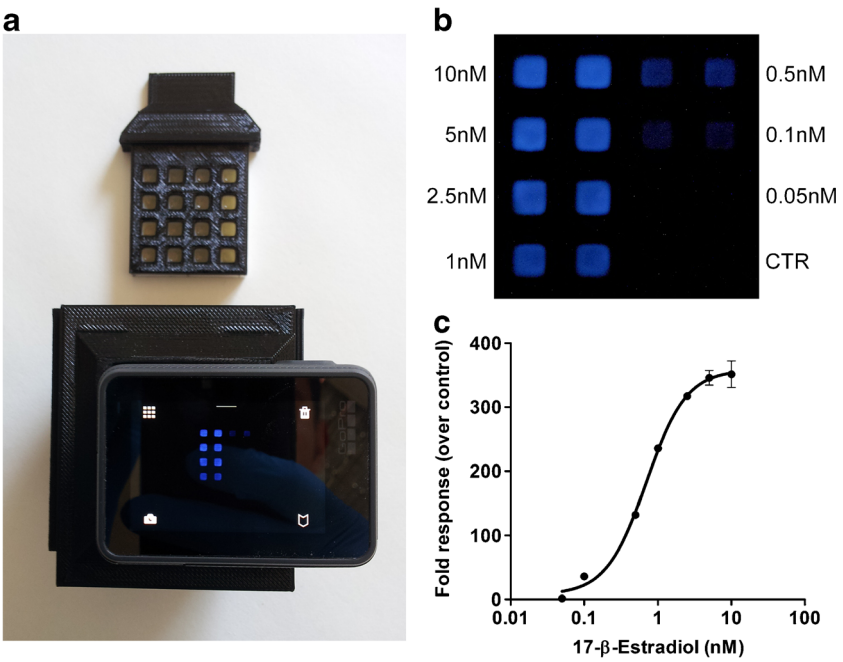

Fig. 3 **a** Picture of a typical yeast estrogen assay performed by incubating the cell-cartridge containing immobilized yeast bioreporters with 50 μL of sample and by acquiring BL emission with a GoProHero5 camera in night mode (30 s at ISO 800), after addition of 50 μL YPERNano solution. **b** BL image obtained by incubating the yeast-bioreporters with 17β-estradiol (concentration range from 0.05 to 10 nM) and **c** corresponding dose-response curve for 17β-estradiol obtained after quantification of BL emission with ImageJ software. Data are plotted as fold response with respect to control (1% EtOH)

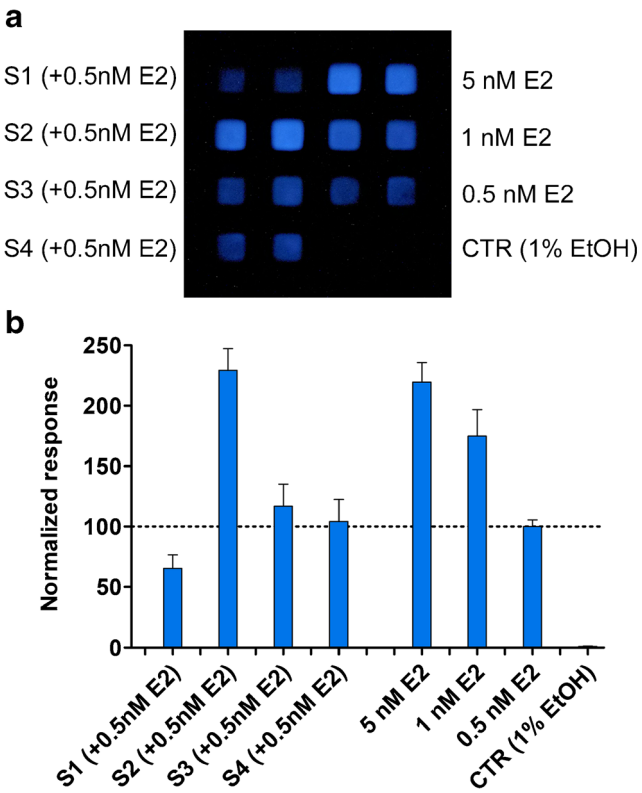

Fig. 4 **a** BL Image of a proof-of-concept analysis of spiked water samples and **b** quantitative elaboration where BL emissions were normalized with respect to 0.5 nM E2 set at 100. The configuration of the cell-cartridge allows to test the estrogenic activity of four samples in duplicate. The response of nanoYES to 0.5, 1, and 5 nM E2 was also included in each cartridge, allowing a quick evaluation and quantification of estrogenic activity. Sample wells are co-incubated with 0.5 nM E2 to detect both pro- and anti-estrogenic activity. As a proof-of-concept, three tap water samples were analyzed: sample no. 1 (S1) was spiked with 10 nM bisphenol A (BPA) shows anti-estrogenic activity. BPA (which does not produce a detectable BL signal at this concentration) is able to bind to the estrogen receptor thus interfering with the transactivation induced by 0.5 nM E2. Sample no. 2 (S2) which contains 10 nM diethylstilbestrol (DES) shows a remarkable increase compared to 0.5 nM E2 (comparable to BL signal obtained in the presence of 5 nM E2). Sample no. 3 (S3) was spiked with 0.1 nM diethylstilbestrol (DES); this concentration does not produce any estrogenic effect. Sample no. 4 (S4) contains only 50 μL tap water and has no estrogenic effect. All measurements were performed in duplicate and repeated with three different cell cartridges

estrogenic compounds. Sample no. 3, spiked with 0.1 nM DES (whose concentration does not produce a significantly increased BL signal), and sample no. 4, containing only tap water, do not show any alteration with respect to 0.5 nM E2-induced transactivation.

It must be pointed out that the envisaged application of the platform is for rapid monitoring of effluents of wastewater and critical areas, such as agricultural and industrial sites, in which a high concentration of EDCs is expected. Moreover, future studies will be aimed at evaluating the analytical performance of the nanoYES in the presence of EDCs mixtures.

Conclusion

In this work, we proposed a mobile platform for effect-based analysis of endocrine disruptors, based on bioluminescent yeast estrogen biosensors and a compact wireless camera as light detector.

The newly developed yeast estrogen biosensors exploit a yeast codon optimized variant of Nanoluc luciferase to achieve rapid and sensitive detection of estrogen-like compounds within 1 h. A straightforward procedure to immobilize the yeast biosensors into 3D-printed cartridges was also developed, obtaining reproducible ready-to-use disposable cartridges that can stored for 10 days at 4 °C without significant decrease in analytical performance.

The GoPro camera proved suitable for the sensitive detection of light emission from bioluminescent yeast biosensors, using the night mode setup with 30-s integration time. In addition, thanks to the possibility to connect this sensor with any smartphone model via dedicated GoProApp, the developed configuration results in a more standardized and versatile platform, compared to smartphone-based devices. A custom application (APP) running on different operative systems could be developed to either provide instructions to the user and for the quantification of BL images to obtain immediate results about estrogenic activity of samples.

In the proposed configuration, the mobile platform, containing robust microbial bioluminescent whole-cell bioreporters, allows a rapid evaluation of estrogenic activity in water samples and could find application for on-site analysis of EDCs.

Acknowledgements This research was sponsored in part by PRIN 2015 “Securing and ensuring sustainable use of agriculture waste, co- and by-products: an integrated analytical approach combining mass spectrometry with health effect-based biosensing” (Prot. 2015FFY97L), PRIN 2015 “Multifunctional nanotools for advanced cancer diagnostics” (Prot. 2015TWP83Z), and the NATO Science for Peace and Security Programme under Grant No. 985042.

Compliance with ethical standards

Conflict of interest The authors declare that they have no conflict of interest.

References

1. http://eur-lex.europa.eu/legal-content/EN/TXT/HTML/?uri=CELEX:32013L0039&from=IT (last accessed 26 July 2017).
2. Watson R. European Commission tables scientific criteria for endocrine disruptors. BMJ. 2016;353:i3459.
3. Kunz PY, Simon E, Creusot N, Jayasinghe BS, Kienle C, Maletz S, et al. Effect-based tools for monitoring estrogenic mixtures: evaluation of five in vitro bioassays. Water Res. 2017;110:378–88.
4. Ewence A, Brescia S, Johnson I, Rumsby PC. An approach to the identification and regulation of endocrine disrupting pesticides. Food Chem Toxicol. 2015;78:214–20.

5. Barbosa MO, Moreira NF, Riberio AR, Pereira MF, Silva AM. Occurrence and removal of organic micropollutants: an overview of the watch list of EU Decision 2015/495. Water Res. 2016;94: 257–79.
6. Tiedeken EJ, Tahar A, McHugh B, Rowan NJ. Monitoring, sources, receptors, and control measures for three European Union watch list substances of emerging concern in receiving waters—a 20 year systematic review. Sci Total Environ. 2017;574:1140–63.
7. Escher BI, Neale PA, Leusch FD. Effect-based trigger values for in vitro bioassays: reading across from existing water quality guideline values. Water Res. 2015;81:137–48.
8. Mertl J, Kirchnawy C, Osorio V, Grininger A, Richter A, Bergmair J, et al. Characterization of estrogen and androgen activity of food contact materials by different in vitro bioassays (YES, YAS, ERα and AR CALUX) and chromatographic analysis (GC-MS, HPLC-MS). PLoS One. 2014;9:e100952.
9. Gauglitz G. ABC Spotlight on effect-directed analysis—dose instead of concentration. Anal Bioanal Chem. 2015;407:3261–3.
10. Fang TY, Praveena SM, deBurbure C, Aris AZ, Ismail SN, Rasdi I. Analytical techniques for steroid estrogens in water samples—a review. Chemo 2016;165:358–368.
11. Roda A, Mirasoli M, Michelini E, Magliulo M, Simoni P, Guardigli M, et al. Analytical approach for monitoring endocrine-disrupting compounds in urban waste water treatment plants. Anal Bioanal Chem. 2006;385:742–52.
12. Comtois-Marotte S, Chappuis T, Vo Duy S, Gilbert N, Lajeunesse A, Taktek S, et al. Analysis of emerging contaminants in water and solid samples using high resolution mass spectrometry with a Q Exactive orbital ion trap and estrogenic activity with YES-assay. Chemosphere. 2017;166:400–11.
13. Wang S, Bovee TFH. Estrogen receptor agonists and antagonists in the yeast estrogen bioassay. Methods Mol Biol. 2016;1366:337–42.
14. Bovee TF, Heskamp HH, Hamers AR, Hoogenboom RL, Nielen MW. Validation of a rapid yeast estrogen bioassay, based on the expression of green fluorescent protein, for the screening of estrogenic activity in calf urine. Analytica chim acta. 2005;529:57–64.
15. Leskinen P, Michelini E, Picard D, Karp M, Virta M. Bioluminescent yeast assays for detecting estrogenic and androgenic activity in different matrices. Chemosphere. 2005;61:259–66.
16. Chu WL, Shiizaki K, Kawanishi M, Kondo M, Yagi T. Validation of a new yeast-based reporter assay consisting of human estrogen receptors alpha/beta and coactivator SRC-1: application for detection of estrogenic activity in environmental samples. Environ Toxicol. 2009;2:513–21.
17. Escande A, Pillon A, Servant N, Cravedi JP, Larrea F, Muhn P, et al. Evaluation of ligand selectivity using reporter cell lines stably expressing estrogen receptor alpha or beta. Biochem Pharmacol. 2006;71:1459–69.
18. Gutendorf B, Westendorf J. Comparison of an array of in vitro assays for the assessment of the estrogenic potential of natural and synthetic estrogens, phytoestrogens and xenoestrogens. Toxicology. 2001;166:79–89.
19. Gaido KW, Leonard LS, Lovell S, Gould JC, Babaï D, Portier CJ, et al. Evaluation of chemicals with endocrine modulating activity in a yeast-based steroid hormone receptor gene transcription assay. Toxicol Appl Pharmacol. 1997;143:205–12.
20. Klein KO, Baron J, Colli MJ, McDonnell DP, Cutler GB Jr. Estrogen levels in childhood determined by an ultrasensitive recombinant cell bioassay. J Clin Invest. 1994;94:2475–80.
21. Leusch FD, de Jager C, Levi Y, Lim R, Puijker L, Sacher F, et al. Comparison of five in vitro bioassays to measure estrogenic activity in environmental waters. Environ Sci Technol. 2010;44:3853–60.
22. Coldham NG, Dave M, Sivapathasundaram S, McDonnell DP, Connor C, Sauer MJ. Evaluation of a recombinant yeast cell estrogen screening assay. Environ Health Perspect. 1997;105:734–42.
23. Furst AL, Hoepker AC, Francis MB. Quantifying hormone disruptors with an engineered bacterial biosensor. ACS Cent Sci. 2017;3:110–6.
24. Liu L, Zhou X, Lu Y, Shan D, Xu B, He M, et al. Facile screening of potential xenoestrogens by an estrogen receptor-based reusable optical biosensor. Biosens Bioelectron. 2017;97:16–20.
25. Sonneveld E, Jansen HJ, Riteco JA, Brouwer A, van der Burg B. Development of androgen- and estrogen-responsive bioassays, members of a panel of human cell line-based highly selective steroid-responsive bioassays. Toxicol Sci. 2005;83:136–48.
26. Soto AM, Sonnenschein C, Chung KL, Fernandez MF, Olea N, Serrano FO. The E-SCREEN assay as a tool to identify estrogens: an update on estrogenic environmental pollutants. Environ Health Perspect. 1995;103:113–22.
27. Routledge EJ, Sumpter JP. Estrogenic activity of surfactants and some of their degradation products assessed using a recombinant yeast screen. Environ Toxicol Chem. 1996;15:241–8.
28. Roda A, Cevenini L, Michelini E, Branchini BR. A portable bioluminescence engineered cell-based biosensor for on-site applications. Biosens Bioelectron. 2011;26:3647–53.
29. Cevenini L, Calabretta MM, Lopreside A, Tarantino G, Tassoni A, Ferri M, et al. Exploiting NanoLuc luciferase for smartphone-based bioluminescence cell biosensor for (anti)-inflammatory activity and toxicity. Anal Bioanal Chem. 2016;408:8859–68.
30. Cevenini L, Calabretta MM, Tarantino G, Michelini E, Roda A. Smartphone-interfaced 3D printed toxicity biosensor integrating bioluminescent "sentinel cells". Sens Act B Chem. 2016;225: 249–57.
31. Hall MP, Unch J, Binkowski BF, Valley MP, Butler BL, Wood MG, et al. Engineered luciferase reporter from a deep sea shrimp utilizing a novel imidazopyrazinone substrate. ACS Chem Biol. 2012;7: 1848–57.
32. Masser AE, Kandasamy G, Kaimal JM, Andréasson C. Luciferase NanoLuc as a reporter for gene expression and protein levels in Saccharomyces cerevisiae. Yeast. 2016;33:191–200.
33. Mattingly KA, Ivanova MM, Riggs KA, Wickramasinghe NS, Barch MJ, Klinge CM. Estradiol stimulates transcription of nuclear respiratory factor-1 and increases mitochondrial biogenesis. Mol Endocrinol. 2008;22:609–22.
34. Baudin-Bailleu A, Guillemet E, Cullin C, Lacroute F. Construction of a yeast strain deleted for the TRP1 promoter and coding region that enhances the efficiency of the polymerase chain reaction disruption method. Yeast. 1996;30:353–6.
35. Sambrook EF, Fristch EF, Maniatis T. Molecular Cloning: A Laboratory Manual. 2nd ed. New York: Cold Spring Harbor Laboratory Press; 1989.
36. Jarque S, Bittner M, Blaha L, Hilscherova K. Yeast biosensors for detection of environmental pollutants: current state and limitations. Trends Biotechnol. 2016;34:408–19.
37. Céspedes R, Petrovic M, Raldúa D, Saura U, Piña B, Lacorte S, et al. Integrated procedure for determination of endocrine-disrupting activity in surface waters and sediments by use of the biological technique recombinant yeast assay and chemical analysis by LC-ESI-MS. Anal Bioanal Chem. 2004;378:697–708.
38. Bergamasco AM, Eldridge M, Sanseverino J, Sodré FF, Montagner CC, Pescara IC, et al. Bioluminescent yeast estrogen assay (BLYES) as a sensitive tool to monitor surface and drinking water for estrogenicity. J Environ Monit. 2011;13:3288–93.
39. Kim DH, Lee SB, Park HD. Effect of air-blast drying and the presence of protectants on the viability of yeast entrapped in calcium alginate beads with an aim to improve the survival rate. Appl Microbiol Biotechnol. 2017;101:93–102.
40. Balsiger HA, de la Torre R, Lee WY, Cox MB. A four-hour yeast bioassay for the direct measure of estrogenic activity in wastewater without sample extraction, concentration, or sterilization. Sci Total Environ. 2010;408:1422–9.

41. Cao H, Wang F, Liang Y, Wang H, Zhang A, Song M. Experimental and computational insights on the recognition mechanism between the estrogen receptor α with bisphenol compounds. Arch Toxicol. 2017;91:1–16.
42. FitzGerald RE, Wilks MF. Bisphenol A—why an adverse outcome pathway framework needs to be applied. Toxicol Lett. 2014;230:368–74.
43. Frye CA, Bo E, Calamandrei G, Calzà L, Dessì-Fulgheri F, Fernández M, et al. Endocrine disrupters: a review of some sources, effects, and mechanisms of actions on behaviour and neuroendocrine systems. J Neuroendocrinol. 2012;24:144–59.
44. Jin S, Yang F, Liao T, Hui Y, Xu Y. Seasonal variations of estrogenic compounds and their estrogenicities in influent and effluent from a municipal sewage treatment plant in China. Environ Toxicol Chem. 2008;27:146–53.
45. Careghini A, Mastorgio AF, Saponaro S, Sezenna E. Bisphenol A, nonylphenols, benzophenones, and benzotriazoles in soils, groundwater, surface water, sediments, and food: a review. Environ Sci Pollut Res Int. 2015;22:5711–41.

Analytical and Bioanalytical Chemistry

Electronic Supplementary Material

A novel bioluminescent NanoLuc yeast-estrogen screen biosensor (nanoYES) with a compact wireless camera for effect-based detection of endocrine-disrupting chemicals

Luca Cevenini, Antonia Lopreside, Maria Maddalena Calabretta, Marcello D'Elia, Patrizia Simoni, Elisa Michelini, Aldo Roda

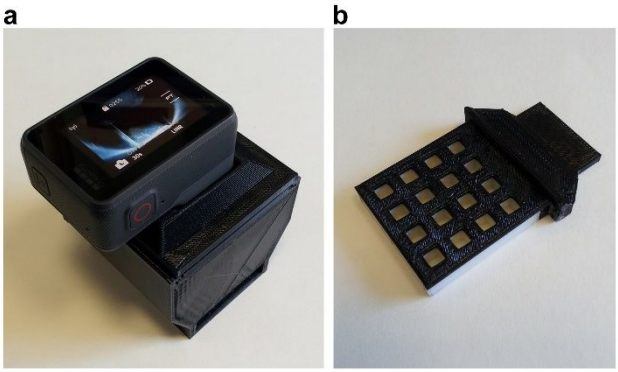

Fig. S1 a) 3D printed accessory designed to hold a GoPro Hero5 creating a self-supporting device. The adaptor (65 x 65 mm, 60 mm height) provides a dark box for acquisition of bioluminescent emission and integrates a slot to house the cell-cartridge. **b**) Multi-well cartridge (60 x 40 mm) printed with white and black ABS containing 16 wells of 5 x 5 mm (150 µL volume each) to house the cell-alginate slices

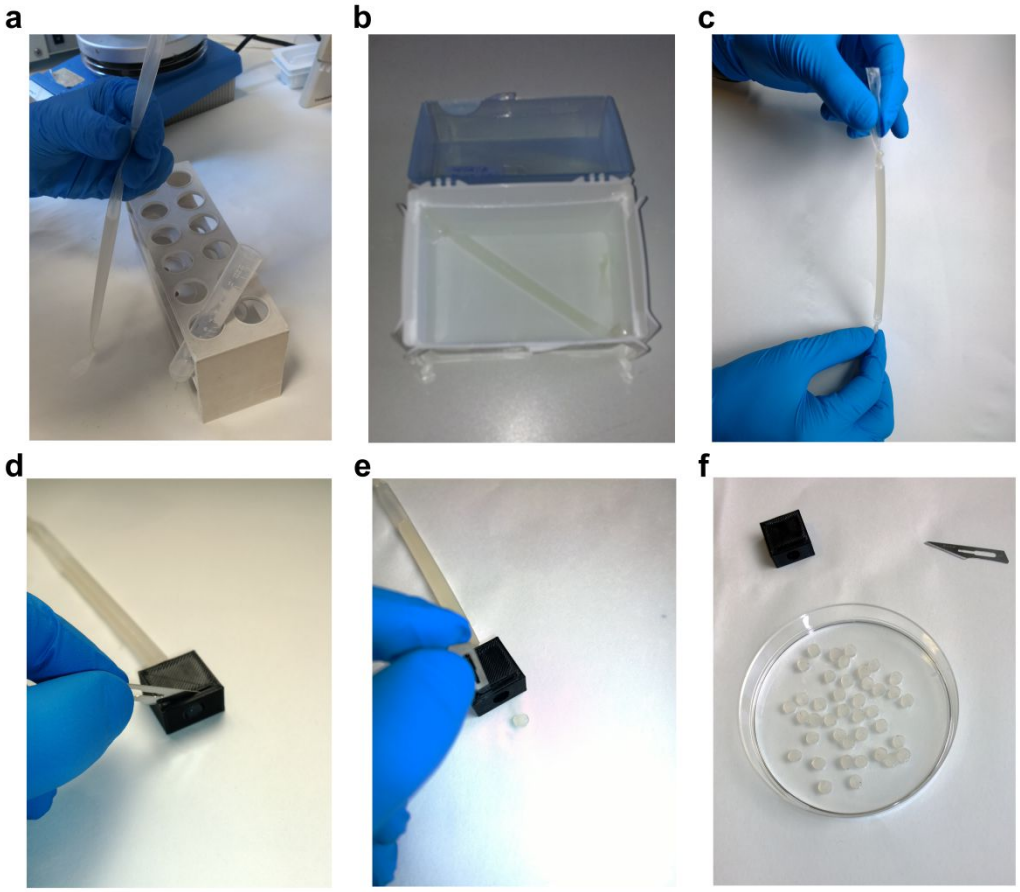

Fig. S2 Immobilization of nanoYES in alginate slices. **a**) Yeast cultures at OD_{600}=1 (about $1.8x10^7$ cells/mL) were concentrated 10X in culture medium containing trehalose (10% w/v) and poured (3 mL of yeast culture) into a dialysis tubing cellulose membrane (avg. flat width 10 mm, molecular weight cut-off = 14 KDa). **b**) The membrane was then immersed into a $CaCl_2$ solution to allow the formation of the gel inside the membrane. **c**) After 1 h incubation at room temperature (25°C) the yeast-bioreporter are immobilized into calcium alginate matrix and ready for the next steps. **d**) The obtained gel (about 12 cm length, avg. diameter 5mm) is inserted in a 3D printed "microtome-like" device fabricated for the straightforward production of slices with defined dimension. **e**) The microtome has a slot for a surgical blade placed at 2 mm from the edge, allowing to repeatedly cut the gel by simply realigning it to the edge after each slice. **f**) Using this technique about 48 slices of 2.1±0.2 mm were obtained, which are sufficient for the production of three cartridges

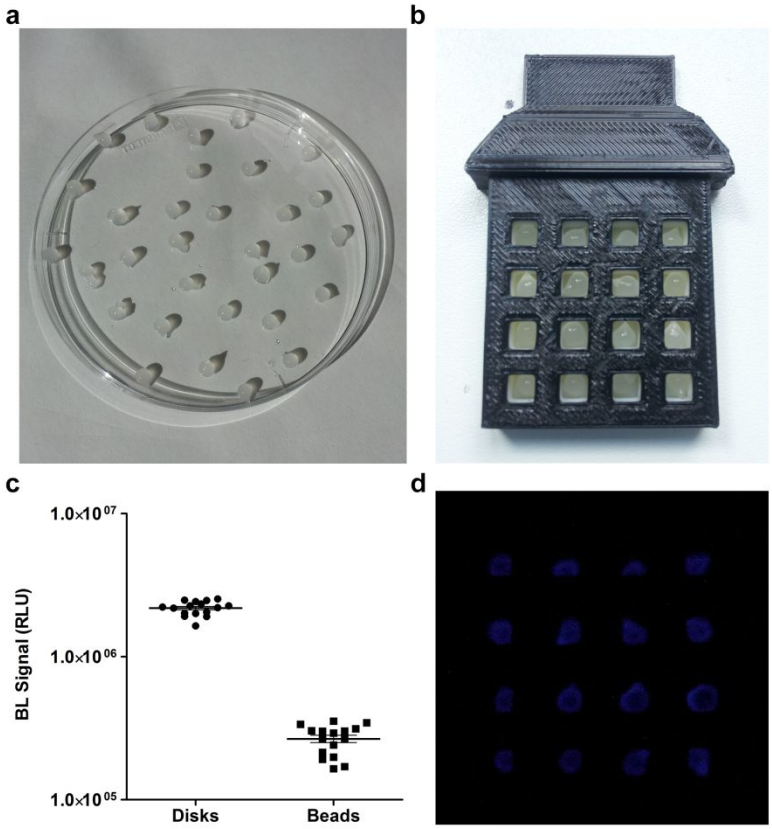

Fig. S3 Comparison with yeast immobilized in alginate beads. **a**) Picture of alginate beads obtained with the conventional procedure by dripping 50 µL of nanoYES-alginate mixture into a 0.1 M $CaCl_2$ agitated solution. **b**) Picture of the alginate beads (avg. diameter 4.5 mm) into a 3D printed cartridge. **c**) BL emission intensities and distribution of nanoYES immobilized in alginate slices or beads and induced with 10 nM E2. **d**) BL image of nanoYES immobilized in alginate beads and induced with 10 nM E2

5

Prêt-à-porter nanoYESα and nanoYESβ bioluminescent cell biosensors for ultrarapid and sensitive screening of endocrine disrupting chemicals

Reproduced from: "Prêt-à-porter nanoYESα and nanoYESβ bioluminescent cell biosensors for ultrarapid and sensitive screening of endocrine disrupting chemicals"

Antonia Lopreside, Maria Maddalena Calabretta, Laura Montali, Maura Ferri, Annalisa Tassoni, Bruce R Branchini, Tara Southworth, Marcello D'Elia, Aldo Roda, Elisa Michelini

Analytical and Bioanalytical Chemistry, 2019, 1-13.

Analytical and Bioanalytical Chemistry (2019) 411:4937–4949
https://doi.org/10.1007/s00216-019-01805-2

RESEARCH PAPER

Prêt-à-porter nanoYESα and nanoYESβ bioluminescent cell biosensors for ultrarapid and sensitive screening of endocrine-disrupting chemicals

Antonia Lopreside[1] · Maria Maddalena Calabretta[1] · Laura Montali[1] · Maura Ferri[2,3] · Annalisa Tassoni[2] · Bruce R. Branchini[4] · Tara Southworth[4] · Marcello D'Elia[5] · Aldo Roda[1,6] · Elisa Michelini[1,6,7]

Received: 21 December 2018 / Revised: 19 February 2019 / Accepted: 25 March 2019 / Published online: 10 April 2019

Abstract

Cell-based assays utilizing reporter gene technology have been widely exploited for biosensing, as they provide useful information about the bioavailability and cell toxicity of target analytes. The long assay time due to gene transcription and translation is one of the main drawbacks of cell biosensors. We report the development of two yeast biosensors stably expressing human estrogen receptors α and β and employing NanoLuc as the reporter protein to upgrade the widely used yeast estrogen screening (YES) assays. A viability control strain was also developed based on a chimeric green-emitting luciferase, PLG2, expressed for the first time in *Saccharomyces cerevisiae*. Thanks to their brightness, NanoLuc and PLG2 provided excellent sensitivity, enabling the implementation of these biosensors into low-cost smartphone-based devices. The developed biosensors had a rapid (1 h) response and reported on (anti)estrogenic activity via human estrogen receptors α and β as well as general sample toxicity. Under optimized conditions, we obtained LODs of 7.1 ± 0.4 nM and 0.38 ± 0.08 nM for E2 with nanoYESα and nanoYESβ, respectively. As a proof of concept, we analyzed real samples from plants showing significant estrogenic activity or known to contain significant amounts of phytoestrogens.

Keywords Bioluminescence · Biosensor · Luciferase · Smartphone · Estrogen receptor

Introduction

Endocrine-disrupting compounds (EDCs) are chemicals able to disrupt normal endocrine function, thus causing adverse effects on human and animal health [1]. Many of these compounds, either of natural and synthetic origin, affect the hormone systems of living organisms through very different mechanisms of action. Long-term exposure to these substances, even at low

Published in the topical collection *Young Investigators in (Bio-)Analytical Chemistry* with guest editors Erin Baker, Kerstin Leopold, Francesco Ricci, and Wei Wang.

Electronic supplementary material The online version of this article (https://doi.org/10.1007/s00216-019-01805-2) contains supplementary material, which is available to authorized users.

✉ Elisa Michelini
elisa.michelini8@unibo.it

[1] Department of Chemistry "G. Ciamician", University of Bologna, Via Selmi 2, 40126 Bologna, Italy

[2] Department of Biological Geological and Environmental Sciences (BIGeA), University of Bologna, Via Irnerio 42, 40126 Bologna, Italy

[3] Department of Civil, Chemical, Environmental and Materials Engineering, University of Bologna, Via Terracini 28, 40131 Bologna, Italy

[4] Department of Chemistry, Connecticut College, 270 Mohegan Ave., New London, CT 06320, USA

[5] Gabinetto Regionale di Polizia Scientifica per l'Emilia-Romagna, Via Volto Santo 3, 40123 Bologna, Italy

[6] INBB, Istituto Nazionale di Biostrutture e Biosistemi, Viale delle Medaglie d'Oro, 305, 00136 Rome, Italy

[7] Health Sciences and Technologies-Interdepartmental Center for Industrial Research (HST-ICIR), University of Bologna, via Tolara di Sopra 41/E, 40064 Ozzano dell'Emilia, Bologna, Italy

doses, may lead to severe pathological conditions including obesity, endometriosis, infertility, and cancer [2]. Several pathways are involved, including androgens, estrogens, and thyroid axes. In particular, interaction of EDCs with the estrogenic receptors ERα and ERβ alters the normal hormone biosynthesis, signaling, or metabolism, affecting the growth and differentiation of many organs such as the ovary, mammary gland, prostate, nervous system, cardiovascular system, and bones [3]. The cost of EDC-associated diseases in the European Union was estimated to be in the range of € 81–269 billion per year. The most considerable costs were associated with IQ loss and intellectual disability after prenatal organophosphate exposure and adult obesity attributed to phthalate exposure [4].

Therefore, there is a growing demand for new, fast, and reliable methods suitable for EDC detection both in laboratory settings and for on-site analyses [5]. Many analytical methods such as high-performance liquid chromatography associated with mass spectrometry (HPLC-MS) have been used in recent years, providing low limits of detection and high reproducibility. However, these techniques require sophisticated equipment and extensive sample processing. Furthermore, they do not provide information about bioactivity of the detected substances and are unsuitable for real-time, cost-effective on-field testing [6].

Such information can be obtained using biosensors employing a properly chosen biological recognition element [7]. Indeed, whole-cell biosensors relying on living cells provide information about the bioavailability of analytes or classes of analyte that is the fraction of analyte that is able to permeate the cell membrane and interact with specific molecular targets. Cell-based assays or bioassays are able to measure receptor-mediated effects due to the reprogramming of cells to express a reporter protein after activation of a specific receptor. Several bioluminescent (BL) bioassays and biosensors have been developed by genetically engineering cells with reporter proteins, providing a BL signal proportional to the activation of the target molecular pathway [8]. Furthermore, advances in light detection technology have made it possible to integrate these BL biosensors into portable analytical devices [9–12] suitable for environmental monitoring, food control, and anti-doping screening [13–16].

Moreover, such systems are able to detect chemicals according to their mechanism of action, irrespective of their chemical structure, and also to provide information on their combined effect (synergistic and/or antagonist and toxicity). This capability is highly valuable considering that new molecules are added every year to the watch list of EDCs, with many compounds still unclassified. Also, the US Environmental Protection Agency (EPA) highlighted the importance of high-throughput screening (HTS) with the Toxicity ForeCaster (ToxCast™) Program, obtaining data about thousands of chemicals in hundreds of mammalian-based HTS assays [17].

Mammalian-based HTS are formidable tools to provide data about toxicity and biological activity; however, it is well known that these assays can be highly demanding in terms of assay cost and time. Laboratories need to be equipped with cell culture facilities and incubation times from 5 to 48 h may be necessary for the production of reporter protein [18]. Although mammalian cells provide highly valuable data, yeast cells have many advantages, such as increased robustness, low cost of reagent, absence of endogenous estrogen receptor, and easier handling. Yeast-based assays and biosensors for EDCs generally show lower sensitivity with limits of detection about one order of magnitude higher than those of analogous assays using vertebrate cells [19]. Extraction and pre-concentration of the samples is thus generally required for EDC monitoring in environmental samples with yeast-based assays. Inevitably, this pre-analytical step increases the assay time and may cause higher aspecific cytotoxicity that, if not correctly assessed, could cause artifacts.

We tried to address these limitations in terms of the sensitivity, portability, and response time of yeast biosensors for EDCs by exploiting a newly developed luciferase, NanoLuc, to obtain a set of robust biosensors capable of detecting EDCs acting on estrogen receptors α and β. The applicability of a yeast codon–optimized variant of NanoLuc luciferase (yNLucP) as a reporter protein for yeast biosensors has been previously demonstrated [20, 21]. We immobilized the yeast biosensors in a 3D-printed cartridge and implemented the assay in a portable configuration by exploiting a compact camera as the detector [20]. Here, we report on the development of a new engineered strain expressing the yNLucP under the regulation of ERβ. We also engineered a second reporter strain with a chimeric luciferase, named PLG2, containing the N-domain of *Photinus pyralis* luciferase joined to the C-domain of *Luciola italica* luciferase [22]. PLG2 is a thermostable luciferase that produces a bright BL signal and is resistant to low pH shifting, making it well suited for cell-based assays. The second reporter strain constitutively expressing PLG2 luciferase was used as a viability reporter to correct the analytical signal according to cell viability.

We demonstrated the suitability of these recombinant strains for high-throughput sensitive analysis both inside and outside the laboratory using a luminometer and a mobile phone camera as detectors. We obtained good analytical performance and very rapid response times with incubation times ranging from 30 min to 1 h. The suitability of these biosensors for the analysis of real samples was also investigated using soybean and alfalfa extracts. Estrogenic activity of plant extracts determined with the smartphone biosensor well correlated with estrogenic activity measured with benchtop instrumentation.

Materials and methods

Chemicals and reagents

All the reagents required for yeast cell culture maintenance were purchased from Sigma-Aldrich (St. Louis, MO). Synthetic complete (SC) liquid medium was prepared containing 6.7 g/L yeast nitrogen base w/o amino acids, 1.4 g/L yeast synthetic drop-out medium supplement, and 10 mL/L adenine hemisulfate solution. The solution was autoclaved and then 40 mL/L of glucose 50% *w*/*v* solution (0.22-μm filter sterilized) was added. SC medium was supplemented with the required amino acids L-histidine (2 g/L), L-leucine (0.1 g/L), L-tryptophan (0.02 g/L), and uracil (0.02 g/L). The chemicals required for validation, all of analytical grade, and all reagents required for bacterial cell culture, the kit for plasmid extraction, and *Escherichia coli* (JM-109)-competent cell were purchased from Sigma-Aldrich (St. Louis, MO). FastDigest restriction enzymes, FastAP, and T4 DNA ligase required for cloning and yeast protein extraction reagent (YPER) were from Thermo Fisher Scientific (Waltham, MA, USA). The bioluminescent substrate furimazine was from Promega (Madison, WI, USA). All other chemicals were purchased from Sigma-Aldrich.

NanoLuc estrogen α and β responsive *Saccharomyces cerevisiae*

The reporter vector pRSII426-ERE-yNLucP containing five copies of an ERE response element (-AGGTCAgagTGACCT-) upstream of a minimal cytochrome C promoter (CYCmin) driving the expression of the yNLucP coding sequence has been described elsewhere [20]. The yeast expression plasmid pBEVY-L (Leu2 marker) was from Addgene (Cambridge, MA, USA). The sequence encoding the human estrogen receptor β was amplified with polymerase chain reaction (PCR) using the template pSG5hERβ [23]. The sequence was cloned into pBEVY-L vector under the control of constitutive ADH1 promoter, using *KpnI* and *EcoRI* sites. The generated vector was called pBEVY-ERβ-L.

The yeast codon–optimized version of the NanoLuc-PEST luciferase (yNLucP) has been previously described in [21]. The sequences were confirmed by restriction analysis and sequencing. The yeast *S. cerevisiae* BMA64-1A (MATa, ura3-52, trp1Δ2, leu2-3, 112his3-11, ade2-1, can1-100) wild-type strain [24] was transformed with plasmids pRSII426-ERE-yNLucP and pBEVY-ERβ-L using the LiAc/SS-DNA/PEG method [25]. Colonies were selected in SC-ura-leu plates after incubation at 30 °C for 4 days; 15% glycerol stocks of the recombinant strain were prepared and stored at − 80 °C. The procedure for obtaining *S. cerevisiae* harboring plasmids pBEVY-L-ERα and pRSII426-ERE-yNLucP is described elsewhere [20]. The NanoLuc yeast estrogen screen α and β strains were named nanoYESα and nanoYESβ, respectively.

Laboratory-based nanoYESα and nanoYESβ assays

For the nanoYESα and nanoYESβ assays, an overnight culture of a single colony was used to inoculate 5 mL SC medium containing the selected amino acids to optical density (OD_{600}) of 0.6. This culture was grown at 30 °C with orbital shaking at 200 rpm for about 4 h until $OD_{600} = 1$ was reached. Then, 160 μL of the culture was dispensed in 96-well microplates and incubated at 30 °C with different concentrations of E2 (from 0.001 to 100 nM) at 1% ethanol final concentration. One percent ethanol final concentration was used as control (CTR). Different incubation times (from 5 to 120 min) were tested. Then, 50 μL of YPER-Nano BL substrate [20] was added and BL emission kinetics were recorded using a Varioskan Flash multimode reader (300-ms integration time). Light emission was expressed as relative light units (RLU). The detection limit is defined as the E2 concentration that corresponds to the blank signal plus three times the standard deviation. All experiments were performed in triplicate and repeated at least three times.

In-house validation of nanoYESα and nanoYESβ assays

The Endocrine Disruptor Screening Program Test Guidelines from the EPA (https://www.regulations.gov/document?D=EPA-HQ-OPPT-2009-0576-0006) were used as guidelines for in-house validation. We tested 17β-estradiol (50-28-2; ≥ 97%), 17α-estradiol (57-91-0; ≥ 98%), 17α-methyltestosterone (58-18-4; ≥ 97.0%), diethylstilbestrol (56-53-1; 99.5%), 17α-ethinylestradiol (57-63-6; ≥ 98%), hexestrol (84-16-2; ≥ 98%), genistein (446-72-0; ≥ 98%), estrone (53-16-7; ≥ 99%), butyl paraben (94–26-8; ≥ 99%), 1,3,5-Tris(4-hydroxyphenyl)benzene (15797-52-1; 97%), dibutyl phthalate (84-74-2; 99%), atrazine (1912-24-9; 97.4%), and tamoxifen (10540-29-1; ≥ 99%).

Stock solutions of all reagents required for validation were prepared in ethanol (final vehicle concentration 1%) directly before use. Each plate contains wells treated with 1-nM final concentration of 17β-estradiol as positive controls, and a negative control (CTR) of 1% ethanol (final concentration). For the anti-estrogenic activity screening, chemicals were co-incubated with 1 nM of 17β-estradiol. All chemicals were tested as shown above, with an incubation time of 30 min. The detection limit is defined as the concentration that corresponds to the blank signal plus three times the standard deviation. All experiments were performed in triplicate and repeated at least three times.

Construction of BL *S. cerevisiae* strain constitutively expressing PLG2

The yeast expression plasmid pRSII425 (Leu2 marker) and p405TEF1 were from Addgene (Cambridge, MA, USA). The TEF1 promoter was cloned from p405TEF1 into pRSII425 with *Sac*I and *Xba*I. PLG2 luciferase was amplified by polymerase chain reaction (PCR) and cloned into pRSII425 using *BamHI* and *XhoI*. The final vector was named pRSII425-TEF1-PLG2. The sequences and vectors were confirmed by restriction analysis and sequencing. Yeast *S. cerevisiae* BMA64-1A (MATa, ura3-52, trp1Δ2, leu2-3, 112his3-11, ade2-1, can1-100) wild-type strain was used as the recipient strain [24] and transformed with plasmid pRSII425-TEF1-PLG2 using the LiAc/SS-DNA/PEG method. Colonies were selected from SC-leu plates after incubation at 30 °C for 4 days, and 15% glycerol stocks of the recombinant strain were prepared and stored at − 80 °C. The obtained strain was named ToxYLuc.

Laboratory-based toxicity assay with ToxYluc

An overnight culture from a single colony was used to inoculate SC-leu medium at an optical density (OD_{600}) of 0.6. This culture was grown at 30 °C with orbital shaking at 200 rpm for about 4 h until $OD_{600} = 1$ was reached. Then, 160 μL of cell culture was incubated with different concentrations of all chemicals at 30 °C for 30 min, in 96-black well microplates. The BL signal was acquired using a Varioskan Flash multimode reader (5 min with 300-ms integration time) after the addition of 50 μL of YPER-Bright-Glo™ BL substrate, containing 500 μL of Bright-Glo™ diluted in 500 μL of YPER lysing reagent (YPER-Glo). Light emissions were expressed as RLU. All experiments were performed in triplicate and repeated at least three times.

Smartphone-based biosensor with 3D-printed cell minicartridge and smartphone adaptor fabrication

The minicartridge and smartphone adaptors were fabricated using a desktop 3D printer Makerbot Replicator 2X (Makerbot, Boston, MA, USA) using thermoplastic acrylonitrile butadiene styrene (ABS) polymer as previously described [20]. The open-source Tinkercad browser-based 3D design platform (Autodesk, Inc.) was used to create 3D models. MakerWare v. 2.4 software was used to set up printing options. The cartridge contains an array of 16 wells of 50 μL each (3.5 mm × 3.5 mm × 4.5 mm). The adaptor, providing a dark box to avoid ambient light interference, was designed to fit the OnePlus 5 smartphone (OnePlus, Shenzhen, China).

Smartphone-based biosensor procedure

The OnePlus 5-based platform have been used for integration of nanoYESα, nanoYESβ, and ToxYluc into a portable device for ultrarapid on-field analysis. Briefly, nanoYESα, nanoYESβ, and ToxYluc overnight cultures were diluted in the morning to optical density (OD_{600}) of 0.6 and grown for about 4 h until an $OD_{600} = 1$ was reached. To prepare a cartridge integrating nanoYESα, nanoYESβ, and ToxYluc, the cultures were centrifuged and concentrated 10× in SC medium. Subsequently, 90 μL of cell suspension (about 9.0×10^5 cells/well) and 10 μL of samples (0.1% ethanol final concentration) were added in each well and incubated for 1 h at room temperature (24 °C). A 50-μL volume of YPER-Nano was added to wells containing nanoYESα, nanoYESβ, and a 50-μL volume of YPER-Glo substrate was added to wells containing ToxYluc. BL emission was acquired with OnePlus 5 camera for 30 s, ISO 3200. ImageJ software was used for BL signal measurement by selecting square regions of interest (ROI) around each well.

Analytical performance of the developed platform was assessed by incubating yeast estrogen biosensors α and β with increasing concentrations (from 0.001 to 40 nM) of E2, selected as the model estrogenic analyte. All measurements were performed in duplicate and repeated at least three times with different cell cartridges.

Real samples

Nine plant samples were analyzed for (anti)estrogenic activity with nanoYESα and nanoYESβ.

Five were soybean (*Glycine max* L.) samples: A, 95% methanol (*v*/*v*) extract of the same liquid cell culture previously analyzed by Sansanelli et al. [26] (2014); B, 95% methanol (*v*/*v*) extract analogues of a freshly grown liquid cell culture; C, 95% methanol (*v*/*v*) extract of callus culture grown on solid media; SE, industrial water-based seed extract, and DSE, industrial water-based digested seed extract (Phenbiox Srl, Bologna, Italy), treated for 24 h at room temperature with xylanase, α-amylase and glucosidase, as previously reported [26].

In addition, four alfalfa (*Medicago sativa* L.) samples were obtained from an industrial alfalfa aqueous extraction obtained after a double-screw press and squeezing at high pressure (Alfavita Srl, Ravenna, Italy): D, not treated extract, incubated for 2 h at 60 °C; E, extract treated with 1% (g enzyme/g dry weight) Neutrase 0.8 L (Novozymes A/S, Denmark) for 2 h at 60 °C and pH 7.0; F, extract treated with 1% Alcalase 2.4 L (Novozymes A/S, Denmark) for 2 h at 60 °C and pH 7.0; and G, extract treated with 1% papain (Sigma-Aldrich, Milan, Italy) for 2 h at 60 °C and pH 7.0.

Estrogenic and anti-estrogenic activity of all samples were carried out both with the laboratory-based nanoYESα and

nanoYESβ assays and the smartphone biosensor with an incubation time of 30 min, at 30 °C. Sample toxicities were also evaluated using at least two dilutions for each sample (1:10 and 1:1000) as described in the "Laboratory-based toxicity assay with ToxYluc" section. Real samples analysis with smartphone-based platform was performed as described for E2 samples, in duplicate with nanoYESα, nanoYESβ, and ToxYluc. The toxicity strain was integrated with nanoYESα/nanoYESβ into the same cartridge for simultaneous evaluation of cell viability and (anti)estrogenic activity of real samples with co-incubation with 1 nM of E2.

Then, different concentrations of E2 were added to tap water to prepare the spiked samples with low, medium, and high E2 concentrations. The spiked samples were analyzed using both nanoYESα and nanoYESβ laboratory-based assays as previously described.

Data analysis

All calculations were performed using Microsoft Office Excel 2016 and plotted using GraphPad Prism v.5 (GraphPad Software, Inc. La Jolla, CA). Non-linear regression was performed by fitting the experimental data using a four-parameter sigmoidal curve; EC50 values were calculated by the software as the effective concentration that produces the midpoint y value (50%) of the dose-response curve. The detection limit was calculated as the concentration that corresponded to the blank signal plus three times the standard deviation.

The fold induction (FI) of the nanoYES by the sample was calculated as:

$$FI = BLS/BLB$$

where BLS and BLB are the bioluminescence of the nanoYES with sample and blank solvent, respectively (measured in at least three replicates). At least three independent experiments were used to calculate mean FI values. To consider aspecific effects on cell viability, and correct the analytical signal accordingly, a control strain, ToxYLuc, was developed and used to calculate a correction factor (CF):

$$CF = BB/BS$$

where BB is the BL of the control strain ToxYLuc with blank solvent (1% ethanol) and BS is the BL of the control strain with the sample. When CF was in the range 0.5–2.0, the induction coefficient of the nanoYES with the samples was corrected according to the formula:

$$CFI = CF \times FI$$

where corrected fold induction (CFI) is the fold induction corrected for sample toxicity.

When the CF was higher than 2.0, the sample toxicity was considered too high and an additional sample dilution was performed before the measurement All experiments were performed in quadruplicate and repeated at least three times.

Results and discussion

Luciferase selection and assay design

In the present work, we addressed some of the main drawbacks of yeast-based bioreporters for detection and monitoring of endocrine disruptors, i.e., assay time, sensitivity, and portability. This study was prompted by promising results obtained by a recently developed BL yeast-estrogen screen, named nanoYES [20]. Here, we exploited a low-cost, compact camera as a light detector and 3D-printed cartridges and report the development of two new BL yeast strains: a strain for detection of (anti)estrogenic compounds acting on ERβ and a viability control strain for correcting the analytical signal according to aspecific effects on cell viability.

The newly developed yeast-estrogen strain was obtained by genetically engineering *S. cerevisiae* with plasmid pBEVY-ERβ-L for constitutive expression of hERβ under the regulation of ADH1 promoter and pRSII426-ERE-yNLucP carrying the constitutive pRSII426-ERE-yNLucP containing five copies of an ERE response element upstream of minimal cytochrome C promoter (CYCmin) which drives the expression of the yeast codon-optimized NanoLuc luciferase coding sequence (yNLucP). The vectors contain the 2μ origin for high copy number replication during cell division (50 copies/cell) and consistent production of yNLucP and hERβ. To avoid unrelated toxicity and artifacts in the biosensor response, the expression of the human ERβ was placed under a weak promoter (ADH1) and the destabilized version of yNanoLuc luciferase was chosen as the reporter gene. The use of destabilized luciferases enables detection of rapid changes in gene expression (both increases and decreases) which may not be detectable with stable luciferases that accumulate in living cells due to their long half-life [27]. Therefore, yNanoLuc, which has a half-life of 5 min when expressed in yeast cells [21], and was previously demonstrated suitable for implementation into portable devices with mobile camera detection, was selected as the reporter protein. We then selected another bright luciferase, PLG2, as the constitutive reporter for the viability control strain. PLG2 contains amino acid changes providing activity enhancement in comparison to the chimeric PpyLit, partial protection against red-shifting at low pH, and extended glow emission kinetics. The PLG2 luciferase provided about 3.0-fold greater sensitivity than luciferase from *P. pyralis* when expressed in mammalian cell lines (Hek293); however, the expression of this luciferase has not been reported yet in yeast [22]. Figure 1 shows the bioluminescence emission spectrum and kinetics obtained in yeast cells in lysing and non-lysing conditions. A maximum

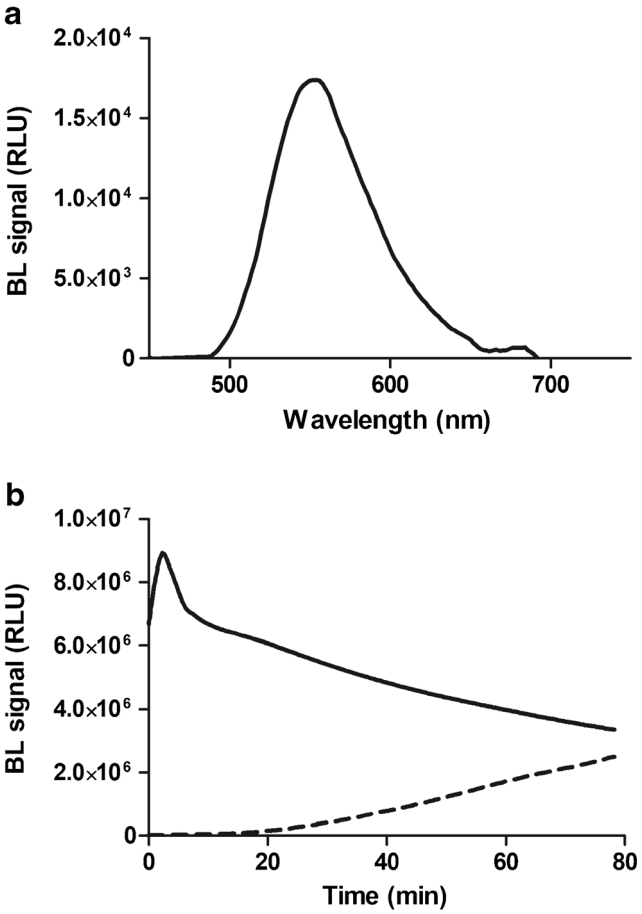

Fig. 1 **a** Bioluminescent emission spectrum obtained with *S. cerevisiae* expressing the PLG2 luciferase. **b** Emission kinetics of PLG2 constitutively expressed in *S. cerevisiae* obtained with YPER-Bright-Glo™ BL substrate (solid line) and Bright-Glo™ BL substrate (dotted line) (see the "Materials and methods" section for experimental details)

emission peak was obtained at 554 nm, consistent with previously reported characterization of this luciferase when expressed in other cell models. Using a commercially available Bright-Glo™ BL substrate, optimized for mammalian cell lines, the kinetic measurements showed non-optimal kinetics, whereas in lysing condition kinetics with a customized YPER-Bright-Glo™ substrate, we obtained a stable measurement that decreases about 50 min after substrate. An optimal acquisition time window was identified between 108 and 192 s, when the mean BL signal is 97 ± 3% of maximum emission.

Laboratory-based assay procedure analytical performance

Dose-response curves for 17β-estradiol (E2) (concentration range 0.0001 to 100 nM) were obtained with different incubation times, from 5 to 120 min, using nanoYESα and nanoYESβ, to identify the best assay conditions (Fig. 2 and Electronic Supplementary Material (ESM) Fig. S1). Unexpectedly, even after 5 min, a dose-response curve was obtained showing a LOD of 1.08 ± 0.02 nM and 0.015 ± 0.001 nM for nanoYESα and nanoYESβ, respectively. It was observed that dose-response curves after 30-min incubation provided similar LOD than those obtained with 120-min incubation with analyte. Longer incubation times lowered the EC_{50}, but did not provide better LOD. Under optimized assay conditions and 30-min incubation times, a LOD of 0.016 ± 0.001 nM and an EC_{50} of 1.47 ± 0.06 nM were obtained for the ERα strain, while a LOD of 0.0011 ± 0.0002 nM and EC_{50} of 0.10 ± 0.01 nM were found for the ERβ strain (Table 1). Values for ERα were similar to those obtained with analogous yeast-based assays. To the best of our knowledge, this response time is the fastest reported to date in yeast-based transactivation assays. In fact, the YES assay requires 72-h incubation at 32 °C with the analyte according to the original protocol based on colorimetric detection developed by Routledge and Sumpter [28] and modified by Rajapakse et al. [29]. Thanks to implementation of chemiluminescent β-galactosidase substrates, the sensitivity and timing of the assay were improved by Balsiger et al., leading to a 4-h assay with yeast bioreporters expressing ERα with a LOD for E_2 of 0.7 nM and an EC_{50} of 0.15 ± 0.01 nM [30]. Concerning yeast bioassays with ERα, recent yeast-based bioreporters based on bioluminescence (lux operon) or fluorescence detection provided similar LOD and EC_{50} values with incubation times ranging from 2.5 to 6 h [31–34].

With the nanoYESβ strain, we significantly improved the LOD in comparison with previously reported assays. Our results agree with those previously obtained by Bovee et al. who reported a maximal activation of the ERβ cytosensor of about 40% of that obtained with the analogous ERα cytosensor [31]. As a result, the EC_{50} values for E_2 decreased (0.06 nM in ref. [31]). The nanoYESβ sensitivity could be explained by the emission properties of the NanoLuc. The use of a customized substrate provided a 20% increase in BL emission when compared to furimazine, with glow-type kinetics (signal half-life > 20 min) compared to NanoGlo® substrate or furimazine alone (signal half-life < 2 min) [20].

Specificity of the nanoYESα and nanoYESβ

The analytical performance was first assessed by measuring the response of the nanoYES to E_2 and other molecules according to EPA Endocrine Disruptor Screening Program Test Guidelines (OPPTS 890.1300: Estrogen Receptor Transcriptional Activation - Human Cell Line HeLa 9903) (https://www.regulations.gov/document?D=EPA-HQ-OPPT-2009-0576-0006). Table S1 (see ESM) shows LOD and EC_{50} values for reference chemicals used in the proficiency test. For the acceptability criteria, we first analyzed positive and negative reference chemicals to verify the responsiveness of the nanoYESα and nanoYESβ using the appropriate

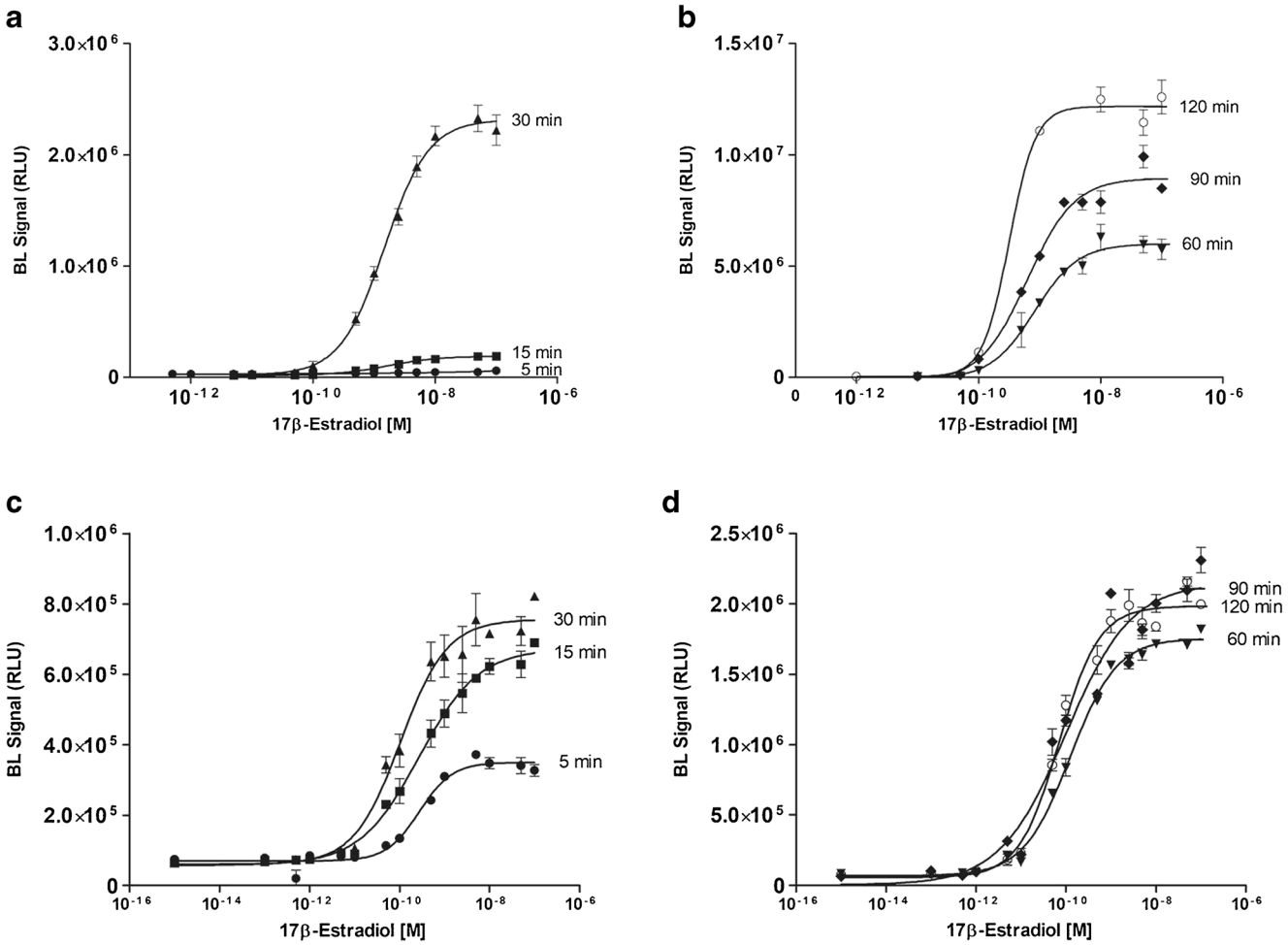

Fig. 2 Dose-response curves for 17β-estradiol obtained using the nanoYESα (**a**, **b**) and nanoYes β (**c**, **d**) at different incubation times (5, 15, 30, 60, 90, and 120 min). Experiments were performed in 96-black well microplate format and benchtop instrumentation using 160 μL of cells and 40 μL of 17β-estradiol solution (concentration range from 0.0001 to 100 nM). Data represent the mean values ± the standard deviation (SD) obtained with three replicates

concentrations of a strong estrogen E2, a weak estrogen (17α-estradiol), a very weak agonist (17α-methyltestosterone) and a negative compound (dibutyl phthalate).

We reported atypical response for some compounds like 1,3,5-Tris(4-hydroxyphenyl)benzene, whose activity, also according to the Endocrine Disruptor Screening Program [1], has a dual estrogenic/antagonistic behavior. Due to this activity, a non-conventional dose-response curve was obtained, and LOD and EC_{50} could not be calculated.

Obtained results (shown in Fig. 3) were within the acceptable range values of the guideline. We calculated the inter- and intra-assay variability (%CV) of the EC_{50} values from individual E2 standard curves and reported %CV of 23.9% and 17.4% for nanoYESα and nanoYESβ, respectively. Anti-estrogenic

Table 1 Limit of detection and half maximal effective concentration obtained with nanoYESα and nanoYESβ in a 96-black well plate format with a benchtop luminometer

Time	LOD	ERα (nM) EC_{50}	LOD	ERβ (nM) EC_{50}
5 min	1.08 ± 0.02	4.06 ± 0.03	0.015 ± 0.001	0.27 ± 0.03
10 min	0.71 ± 0.08	3.05 ± 0.5	0.012 ± 0.001	0.23 ± 0.02
15 min	0.038 ± 0.004	1.69 ± 0.09	0.0007 ± 0.0001	0.27 ± 0.03
30 min	0.016 ± 0.001	1.47 ± 0.06	0.001 ± 0.0001	0.1 ± 0.01
60 min	0.024 ± 0.003	0.83 ± 0.07	0.002 ± 0.0003	0.12 ± 0.01
90 min	0.021 ± 0.003	0.71 ± 0.06	0.0005 ± 0.0003	0.095 ± 0.011
120 min	0.01 ± 0.02	0.32 ± 0.06	0.0011 ± 0.0001	0.077 ± 0.006

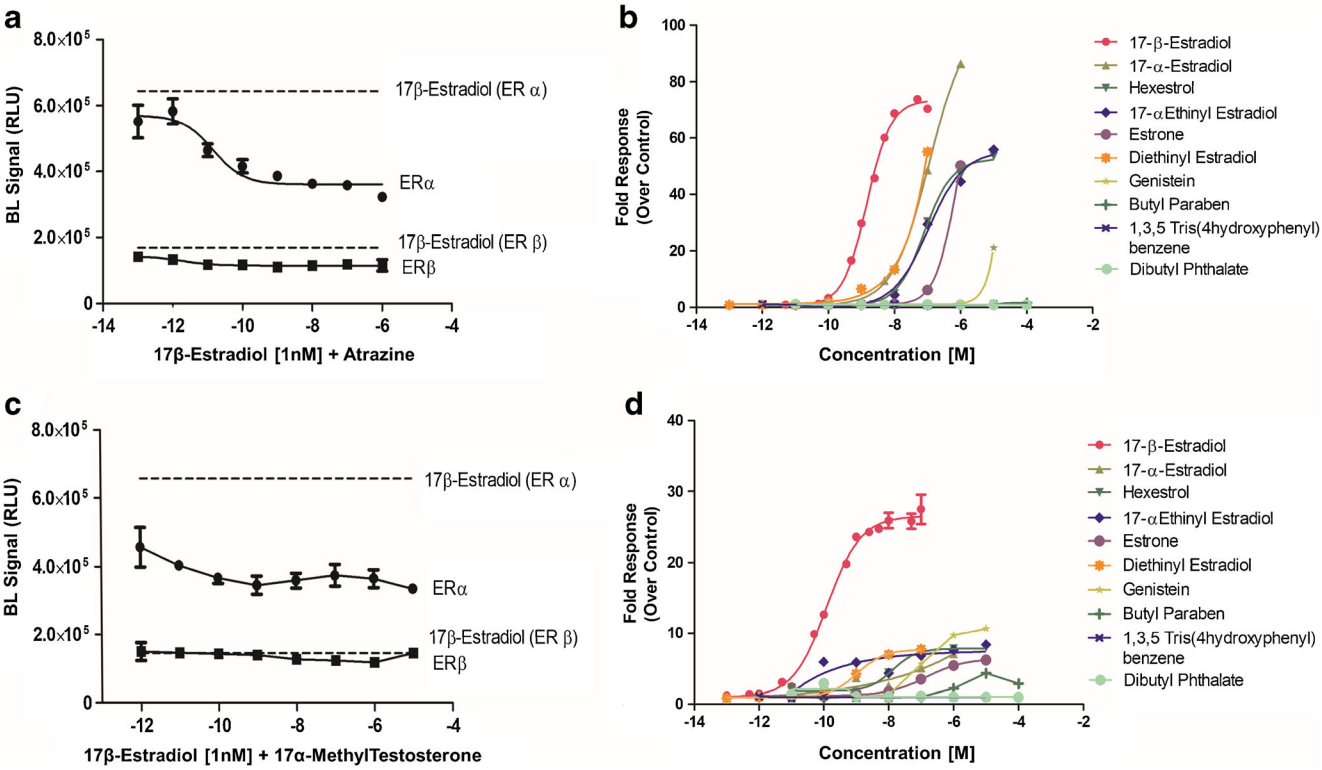

Fig. 3 Evaluation of anti-estrogenic activity of atrazine (**a**) and 17α-methyltestosterone (**c**) obtained by co-incubating nanoYESα and nanoYESβ in 96-black well plate with atrazine (from 0.0001 to 10^3 nM) and 17α-methyltestosterone (from 0.001 to 10^4 nM) with 1 nM of 17β-estradiol for 30 min. BL measurements were obtained after the addition of YPER-Nano BL substrate. Dose-response curves for different chemicals used for the validation of nanoYESα (**b**) and nanoYESβ (**d**) according to EPA Endocrine Disruptor Screening Program Test Guidelines

activity of some well-known anti-estrogenic compounds (i.e., atrazine and 17α-methyltestosterone) was also evaluated (as shown in Fig. 3a and c) by co-incubating nanoYESα and nanoYESβ with 1 nM of 17β-estradiol and different concentrations of the compounds. A decrease of the BL signal inversely proportional to the concentration of the anti-estrogenic compounds was reported for both strains, being more pronounced with nanoYESα. These results confirmed the potential applicability of nanoYESα and nanoYESβ for detecting anti-estrogenic compounds.

As shown in Fig. 3b and d, in agreement with previously published yeast bioassays biosensors, several compounds have different ERα or ERβ agonist activities, such as genistein, a phytoestrogen with a high affinity for estrogen receptor ERβ [35, 36]. We obtained a LOD for genistein of 849 ± 25 nM and 4.68 ± 0.08 nM with nanoYESα and nanoYESβ, respectively. For some chemicals, the relative potencies differed from previous reporter strains. Concerning estrone, which is included in the surface water watch list adopted by the European Commission, we reported a LOD of 7.1 ± 0.5 and 0.009 ± 0.001 with nanoYESα and nanoYESβ, respectively. As an example, we reported a REPβ, calculated as the ratio between the EC_{50} of E2 and the EC_{50} of the compound with ERβ strain, of 0.1 for diethylstilbestrol (ESM Table S1) whereas Bovee et al. reported a REPβ of 2.0 [31]. Despite these discrepancies, that are usually reported for cell-based assays, the LOD for E2 obtained with the nanoYESβ, i.e., 0.0011 ± 0.0002 nM (corresponding to 0.27 ng/L), corroborates the possible use of this biosensor as a rapid screening tool of pharmaceuticals in surface waters according to the European Directive 2013/39/EU, which included E2, estrone, and 17α-estradiol on the watch list. In fact, according to a recent proposal for amending the priority substance list (European Commission 2011), the proposed environmental quality standards (EQS) for E2 of inland surface water are 0.4 ng/L [37, 38].

Smartphone-based biosensor integrating nanoYESα, nanoYESβ, and ToxYLuc

The suitability of using the smartphone camera to detect the BL emitted by living cells has been previously reported by us and others with mammalian cells lines and bacteria [39–41]; however, to date, yeast biosensors have been integrated into devices with portable detectors (e.g., cooled CCD, GoProHero5 CMOS camera) but not coupled with smartphones. Despite yeast's great peculiarities, such as relatively short assay times and the possibility to analyze

environmental complex samples directly without extraction, sterilization, and/or concentration, their implementation in "prêt-à-porter" devices is still an open issue. Therefore, we focused our effort on the development of a very straightforward smartphone-based assay. We adapted a protocol previously developed with a biosensor exploiting the GoPro camera with some changes. The procedure includes incubation of 10 μL of sample (or E2 dilutions in the concentration range from 0.05 to 10 nM) per cartridge well containing 90 μL of cells (about 9.0×10^5 cells/well) for 1 h at room temperature. After the addition of 50 μL YPER-Nano substrate or YPER-Bright-Glo, the cartridge is snapped into the 3D-printed accessory and acquisition is performed with the OnePlus 5 integrated camera, a 1/2.8" 16-MP Sony IMX 398 sensor, using 3200 ISO sensitivity and 30-s acquisition (Fig. 4). We selected the OnePlus 5 smartphone because the shutter speed can be controlled over a longer period time (up to 30 s) and, with our in-house comparison of different smartphone cameras (data not shown), we were able to obtain the best results for low-light applications. This finding was in agreement with a recent inter-smartphone comparison performed by Kim et al. who reported a device and an imaging-processing algorithm to improve the sensitivity of smartphone cameras for low-light detection [40].

To demonstrate the biosensor capabilities and assess the feasibility of the smartphone-integrated CMOS for BL light detection, we integrated in the same cartridge the three strains: nanoYESα, nanoYESβ, and the viability control strain ToxYLuc. Under optimized conditions, we obtained a LOD of 7.1 ± 0.4 nM and 0.38 ± 0.08 nM for E2 with nanoYESα and nanoYESβ, respectively (Fig. 5a, b).

We assessed the reproducibility of the nanoYESα and nanoYESβ biosensors by testing the same concentration of E2 (1nM) and intra-assay variability of 18% and 13% was obtained using the same cartridge for nanoYESα and nanoYESβ, respectively, while an inter-assay variability of 25% and 18% was obtained with different cartridges prepared starting from different cultures.

Real sample analysis

To test the proposed smartphone-based biosensor integrating nanoYESα, nanoYESβ, and ToxYLuc on real samples, we assessed the estrogenic activity of industrial soybean seed extracts and cell suspensions (Fig. 5), previously characterized using the standard analytical technique HPLC–DAD [26], as well as alfalfa extracts.

Sansanelli et al. reported that soybean cell suspensions contain higher amounts of free isoflavones in comparison to seed extracts (i.e., 93.5% vs 16.8%) and they are more bioactive than the glycoside forms. Figure 6 shows results corrected for toxicity obtained with the nanoYESα and nanoYESβ using benchtop instrumentation. Toxicity effects used for correcting the estrogenic activity are shown in ESM Fig. S2. As an example, sample A, containing extract of soybean cell suspensions (dilution 1:100) with a prevalence of aglycones such as

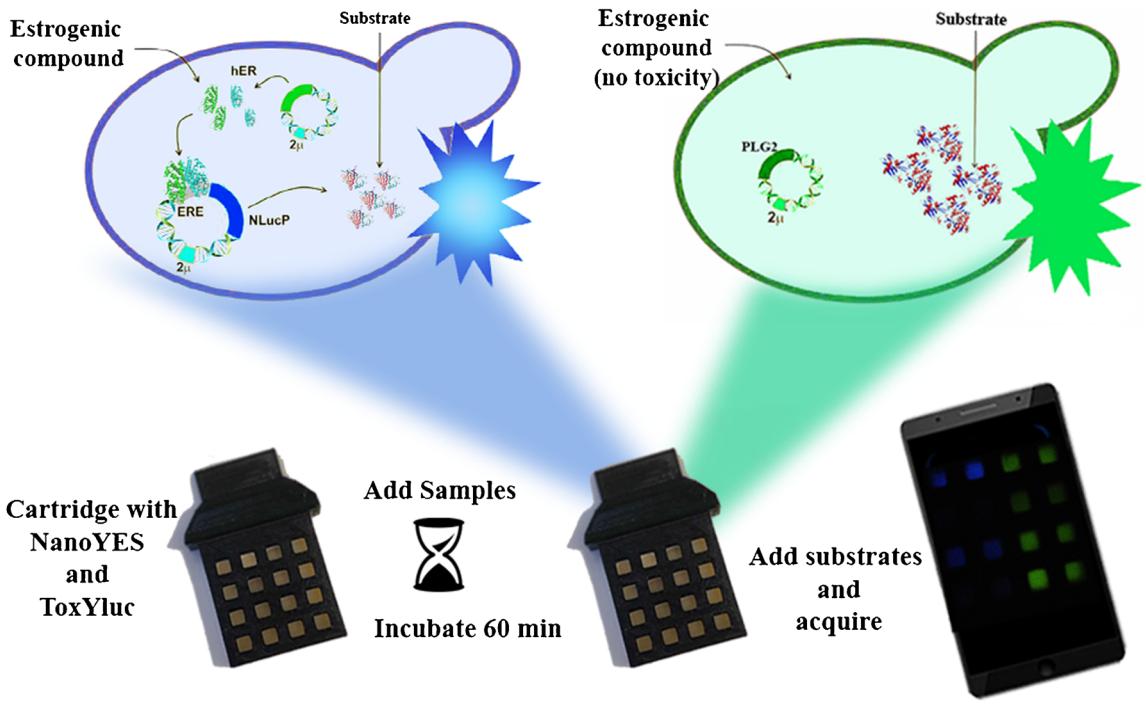

Fig. 4 Schematic representation of the smartphone biosensor principle. The 3D-printed cartridge integrates the three strains: nanoYESα, nanoYESβ expressing the reporter protein Nanoluc under the regulation of estrogen receptor α or estrogen receptor β activation, and the viability control strain ToxYLuc constitutively expressing the green-emitting PLG2 luciferase as reporter protein

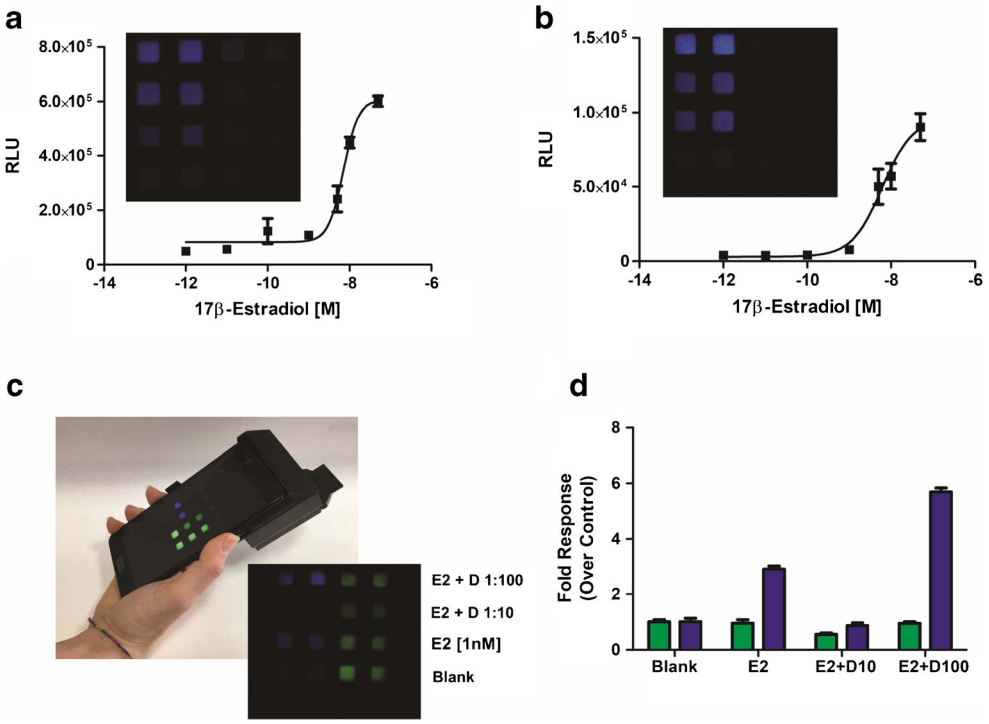

Fig. 5 Dose-response curves for 17β-estradiol with nanoYESα (**a**) and nanoYESβ (**b**) obtained after quantification of BL emissions with ImageJ software. BL images were obtained by incubating the cell-cartridge containing 90 μL of yeast bioreporters with 10 μL 17β-estradiol (concentration range from 0.001 to 100 nM) and by acquiring BL emission with OnePlus camera (30 s at ISO 3200), after addition of 50 μL YPERNano solution. Data are plotted as fold response with respect to control (1% EtOH). (**c**) Picture of assembled device composed by smartphone adaptor and cell cartridge comprising of yeast bioreporters nanoYESβ (in duplicate, left part of the cartridge) and ToxYLuc (in duplicate, right part of the cartridge). Yeast estrogen assays were performed by incubating the cell-cartridge containing 90 μL of nanoYESβ and ToxYLuc with 10 μL of sample. BL signals were obtained with a OnePlus camera acquiring for 30 s at ISO 3200, after addition of either 50 μL YPERNano substrate or YPERBrightGlo. (**d**) Graphical elaboration of sample analysis. Blank sample for estrogenic activity and for cell toxicity was obtained by incubating cells with 1% EtOH. Both BL signals of control wells were set at 1 to normalize results and enable both evaluation of estrogenic activity and toxicity

genistein and daidzein, showed a fold induction corrected for sample toxicity (CFI) of 11.0 ± 0.3 and 51.3 ± 0.3 for ERα and ERβ, respectively.

Conversely, alfalfa extracts (*Medicago sativa* L.) showed estrogenic activity towards both ERα and ERβ due to the presence of phytoestrogens in agreement to Boue et al. [42]. An interesting result was reported for the alfalfa sample digested with 1% Alcalase (Fig. 6b, sample F) which showed a significant increase in estrogenic activity with a CFI of 28.9 ± 0.7 and 28.4 ± 0.5 for ERα and ERβ in comparison to the non-digested extract (Fig. 6b, sample D). A possible explanation for the increase in estrogenic activity could be related to the generation of bioactive peptides, as previously reported for other plant derivatives and extracts with high biotechnological potential [43].

Unexpected results were obtained with some samples, i.e., B and DSE, for which lower dilutions provided higher estrogenic activity than more concentrated solutions, due to high variability in cell viability signals. For example, a normalized estrogenic activity corrected for cell viability of 0.68 ± 0.06 (ERα) and 1.01 ± 0.03 (ERβ) for sample B (1:100) and 1.45 ± 0.10 (ERα) and 2.10 ± 0.03 (ERβ) for sample B (1:1000) was reported. Although cell viability (see ESM) was taken into account for calculating the corrected normalized estrogenic activity, we believe that the high variability of sample B (1:1000) viability signal could have masked the expected decrease in estrogenic activity at higher dilution.

Moreover, to evaluate the ability of nanoYESα and nanoYESβ to detect unknown concentrations of estrogenic compounds, we performed recovery test of spiked 17β-estradiol as a reference compound in tap water samples. Table 2 reports the recovery values obtained when deionized water (blank) and different tap water samples, spiked with low, medium, and high 17β-estradiol concentrations, were analyzed with the nanoYESα and nanoYESβ strains. Satisfactory recoveries were obtained with nanoYESα showing average recovery values ranging from 95 to 116%, while the nanoYESβ from 80 to 90% (Table 2).

As concerns the results obtained with the new smartphone biosensor, a quantitative analysis for both (anti)estrogenic activity and cytotoxicity was obtained by co-incubating the samples with 1 nM E2. Figure 5c shows a typical cartridge used for analyzing two different dilutions (1:10 and 1:100) of sample D (alfalfa aqueous extract) in duplicate with nanoYESβ

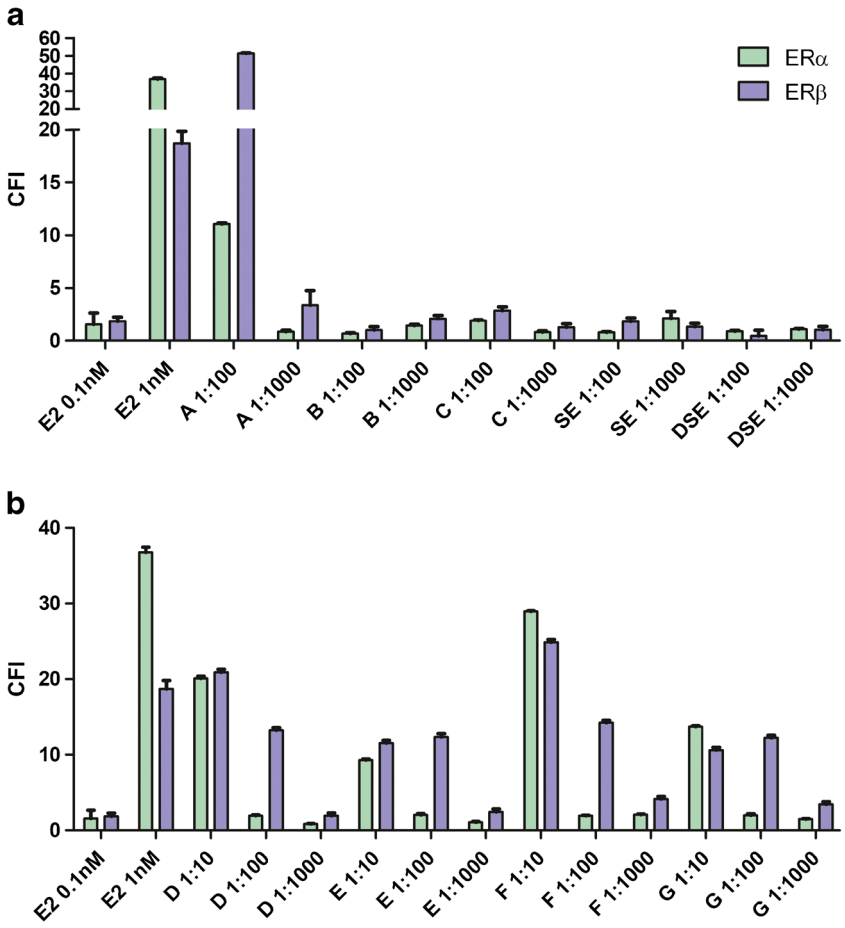

Fig. 6 (**a**) Evaluation of estrogenic activity of industrial soybean seed and (**b**) alfalfa (*Medicago sativa* L.) extracts incubated with nanoYESα (green) and nanoYESβ (violet) in 96-black well plates for 30 min. Data represent the mean values of CFI ± the standard deviation (SD) obtained with three replicates (details of data elaboration are in the "Materials and methods" section)

and ToxYLuc strain. The cartridge also included two reference samples in duplicate wells: 1 nM E2 and blank (vehicle), either water for aqueous extracts or 1% methanol for methanol extracts. The apparent anti-agonistic activity of sample D (1:10 dilution) was due to a significant loss in cell viability (55 ± 2%); conversely, a cell viability of 94 ± 4% was observed with incubation of sample D (1:100) dilution, with significant estrogenic activity (fold response 5.9 ± 0.1). Further characterizations will be required to better understand the bioactive molecules that are responsible for this activity.

These results confirm the importance of including the viability control strain in the same cartridge to correct the analytical signal and avoid artifacts due to sample or matrix-aspecific effects.

Conclusion

Here, we report the development and optimization of a rapid screening assay based on nanoYESα and nanoYESβ and its

Table 2 Recovery obtained by analyzing tap water samples spiked with low, medium, and high concentrations of 17β-estradiol using nanoYESα and nanoYESβ

Sample	Spiked concentration E2 (nM)	Detected concentration E2 (nM)		Recovery% E2 (nM)[a]	
		α	β	α	β
1	0	n.d.	n.d.	–	–
2	1.00×10^{-5}	n.d.	n.d.	–	–
3	1.00×10^{-3}	$1.16 \pm 0.03 \times 10^{-3}$	$0.90 \pm 0.06 \times 10^{-3}$	116%	90%
4	0.10	$0.11 \pm 0.01 \times 10^{-3}$	$0.08 \pm 0.02 \times 10^{-3}$	110%	80%
5	1.00	0.97 ± 0.07	0.81 ± 0.05	97%	81%
6	10.00	9.52 ± 0.09	8.78 ± 0.90	95%	88%

[a] Obtained by interpolating the corrected signal on a corrected dose-response curve for 17β-estradiol

implementation into a smartphone-based biosensor for on-site analysis. The low limit of detection allows the use of the developed yeast estrogen assay for the quantitative detection of estrogenic activity in complex biological samples and water samples. Those limits of detection and EC_{50} are comparable or better than those already reported for yeast estrogen bioassays. We integrated these three strains in a smartphone-based biosensing platform which could provide a first-level bioactivity and toxicity screening for rapid detection of EDCs in environmental and biological samples. Furthermore, those results were achieved with, as far as we know, the shortest incubation time ever used for a yeast biosensor. We envisage potential applications of such biosensor in different scenarios, such as for the analysis of environmental and food samples, and security applications for rapid monitoring of potentially harmful contaminants.

Acknowledgements We wish to thank Dr. Alessandro Filippini and Dr. Dario Zanichelli (Phenbiox Srl, Bologna, Italy) for providing soybean seed extracts, and Dr. Matteo Lamborghini (Alfavita Srl, Ravenna, Italy) for providing alfalfa plant extracts.

Funding information This research was sponsored in part by PRIN 2015 "Multifunctional nanotools for advanced cancer diagnostics" (Prot. 2015TWP83Z), PRIN 2015 "Securing and ensuring sustainable use of agriculture waste, co-and by-products: an integrated analytical approach combining mass spectrometry with health effect-based biosensing" (Prot. 2015FFY97L), the NATO Science for Peace and Security Programme under Grant No. 985042, Air Force Office of Scientific Research (FA9950-18-1-0017) and National Science Foundation (MCB-1410390).

Compliance with ethical standards

Conflict of interest The authors declare that they have no conflict of interest.

References

1. Browne P, Noyes PD, Casey WM, Dix DJ. Application of adverse outcome pathways to U.S. EPA's Endocrine Disruptor Screening Program. Environ Health Perspect. 2017;125:096001.
2. De Coster S, van Larebeke N. Endocrine-disrupting chemicals: associated disorders and mechanisms of action. J Environ Public Health. 2012;2012:713696.
3. Hotchkiss AK, Rider CV, Blystone CR, Wilson VS, Hartig PC, Ankley GT, et al. Fifteen years after "Wingspread"–environmental endocrine disrupters and human and wildlife health: where we are today and where we need to go. Toxicol Sci. 2008;105:235–59.
4. Trasande L, Zoeller RT, Hass U, Kortenkamp A, Grandjean P, Myers JP, et al. Estimating burden and disease costs of exposure to endocrine-disrupting chemicals in the European Union. J Clin Endocrinol Metab. 2015;100:1245–55.
5. Fang TY, Praveena SM, deBurbure C, Aris AZ, Ismail SNS, Rasdi I. Analytical techniques for steroid estrogens in water samples - a review. Chemosphere. 2016;165:358–68.
6. Sadik OA, Wanekaya AK, Andreescu S. Advances in analytical technologies for environmental protection and public safety. J Environ Monit. 2004;6:513–22.
7. Turner AP. Biosensors: sense and sensibility. Chem Soc Rev. 2013;42:3184–96.
8. Elad T, Belkin S. Reporter gene assays in ecotoxicology. Adv Biochem Eng Biotechnol. 2017;157:135–57.
9. Charrier T, Chapeau C, Bendria L, Picart P, Daniel P, Thouand G. A multi-channel bioluminescent bacterial biosensor for the on-line detection of metals and toxicity. Part II: technical development and proof of concept of the biosensor. Anal Bioanal Chem. 2011;400:1061–70.
10. Roda A, Cevenini L, Michelini E, Branchini BR. A portable bioluminescence engineered cell-based biosensor for on-site applications. Biosens Bioelectron. 2011;26:3647–53.
11. Ben-Yoav H, Melamed S, Freeman A, Shacham-Diamand Y, Belkin S. Whole-cell biochips for bio-sensing: integration of live cells and inanimate surfaces. Crit Rev Biotechnol. 2011;31:337–53.
12. Michelini E, Calabretta MM, Cevenini L, Lopreside A, Southworth T, Fontaine DM, et al. Smartphone-based multicolor bioluminescent 3D spheroid biosensors for monitoring inflammatory activity. Biosens Bioelectron. 2019;123:269–77.
13. Elad T, Belkin S. Whole-cell biochips for online water monitoring. Bioeng Bugs. 2012;3:124–8.
14. Zhang D, He Y, Wang Y, Wang H, Wu L, Aries E, et al. Whole-cell bacterial bioreporter for actively searching and sensing of alkanes and oil spills. Microb Biotechnol. 2012;5:87–97.
15. Jouanneau S, Durand MJ, Thouand G. Online detection of metals in environmental samples: comparing two concepts of bioluminescent bacterial biosensors. Environ Sci Technol. 2012;46:11979–87.
16. Cevenini L, Michelini E, D'Elia M, Guardigli M, Roda A. Dual-color bioluminescent bioreporter for forensic analysis: evidence of androgenic and anti-androgenic activity of illicit drugs. Anal Bioanal Chem. 2013;405:1035–45.
17. LaLone C, Villeneuve DL, Doering JA, Blackwell BR, Transue TR, Simmons CW, et al. Evidence for cross species extrapolation of mammalian-based high-throughput screening assay results. Environ Sci Technol. 2018. https://doi.org/10.1021/acs.est.8b04587 in press.
18. Michelini E, Cevenini L, Mezzanotte L, Coppa A, Roda A. Cell-based assays: fuelling drug discovery. Anal Bioanal Chem. 2010;398:227–38.
19. Jarque S, Bittner M, Blaha L, Hilscherova K. Yeast biosensors for detection of environmental pollutants: current state and limitations. Trends Biotechnol. 2016;34:408–19.
20. Cevenini L, Lopreside A, Calabretta MM, D'Elia M, Simoni P, Michelini E, et al. A novel bioluminescent NanoLuc yeast-estrogen screen biosensor (nanoYES) with a compact wireless camera for effect-based detection of endocrine-disrupting chemicals. Anal Bioanal Chem. 2018;410:1237–46.
21. Masser AE, Kandasamy G, Kaimal JM, Andréasson C. Luciferase NanoLuc as a reporter for gene expression and protein levels in Saccharomyces cerevisiae. Yeast. 2016;33:191–200.
22. Branchini BR, Southworth TL, Fontaine DM, Kohrt D, Talukder M, Michelini E, et al. An enhanced chimeric firefly luciferase-inspired enzyme for ATP detection and bioluminescence reporter and imaging applications. Anal Biochem. 2015;484:148–53.
23. Schena M, Picard D, Yamamoto KR. Vectors for constitutive and inducible gene expression in yeast. Methods Enzymol. 1991;194:389–98.
24. Baudin-Bailleu A, Guillemet E, Cullin C, Lacroute F. Construction of a yeast strain deleted for the TRP1 promoter and coding region that enhances the efficiency of the polymerase chain reaction disruption method. Yeast. 1996;30:353–6.
25. Sambrook EF, Fristch EF, Maniatis T. Molecular cloning: a laboratory manual. 2nd ed. New York: Cold Spring Harbor Laboratory Press; 1989.
26. Sansanelli S, Zanichelli D, Filippini A, Ferri M, Tassoni A. Production of free and glycosylated isoflavones in in vitro soybean

(Glycine max L.) hypocotyl cell suspensions and comparison with industrial seed extracts. Plant Cell Tissue Organ Cult. 2014;119: 301–11.
27. Leclerc GM, Boockfor FR, Faught WJ, Frawley LS. Development of a destabilized firefly luciferase enzyme for measurement of gene expression. Biotechniques. 2000;29(3):590–1 594-6, 598 passim.
28. Routledge EJ, Sumpter JP. Estrogenic activity of surfactants and some of their degradation products assessed using a recombinant yeast screen. Environ Toxicol Chem. 1996;15:241–8.
29. Rajapakse N, Ong D, Kortenkamp A. Defining the impact of weakly estrogenic chemicals on the action of steroidal estrogens. Toxicol Sci. 2001;60:296–304.
30. Balsiger HA, de la Torre R, Lee WY, Cox MB. A four-hour yeast bioassay for the direct measure of estrogenic activity in wastewater without sample extraction, concentration, or sterilization. Sci Total Environ. 2010;408:1422–9.
31. Bovee TF, Helsdingen RJ, Rietjens IM, Keijer J, Hoogenboom RL. Rapid yeast estrogen bioassays stably expressing human estrogen receptors alpha and beta, and green fluorescent protein: a comparison of different compounds with both receptor types. J Steroid Biochem Mol Biol. 2004;91:99–109.
32. Sanseverino J, Gupta RK, Layton AC, Patterson SS, Ripp SA, Saidak L, et al. Use of Saccharomyces cerevisiae BLYES expressing bacterial bioluminescence for rapid, sensitive detection of estrogenic compounds. Appl Environ Microbiol. 2005;71:4455–60.
33. Bergamasco AM, Eldridge M, Sanseverino J, Sodré FF, Montagner CC, Pescara IC, et al. Bioluminescent yeast estrogen assay (BLYES) as a sensitive tool to monitor surface and drinking water for estrogenicity. J Environ Monit. 2011;13(11):3288–93.
34. Leskinen P, Michelini E, Picard D, Karp M, Virta MP. Bioluminescent yeast assays for detecting estrogenic and androgenic activity in different matrices. Chemosphere. 2005;61:259–66.
35. Escande A, Pillon A, Servant N, Cravedi JP, Larrea F, Muhn P, et al. Evaluation of ligand selectivity using reporter cell lines stably expressing estrogen receptor alpha or beta. Biochem Pharmacol. 2006;71:1459–69.
36. Lee GS, Choi KC, Kim HJ, Jeung EB. Effect of genistein as a selective estrogen receptor beta agonist on the expression of calbindin-D9k in the uterus of immature rats. Toxicol Sci. 2004;82:451–7.
37. Hettwer K, Jähne M, Frost K, Giersberg M, Kunze G, Trimborn M, et al. Validation of Arxula yeast estrogen screen assay for detection of estrogenic activity in water samples: results of an international interlaboratory study. Sci Total Environ. 2018;621:612–25.
38. European Commission. Common implementation strategy for the Water Framework Directive (2000/60/EC) guidance on surface water chemical monitoring under the Water Framework Directive. Guidance Document No. 19; 2009–025.
39. Cevenini L, Calabretta MM, Lopreside A, Tarantino G, Tassoni A, Ferri M, et al. Exploiting NanoLuc luciferase for smartphone-based bioluminescence cell biosensor for (anti)-inflammatory activity and toxicity. Anal Bioanal Chem. 2016;408:8859–68.
40. Kim H, Jung Y, Doh IJ, Lozano-Mahecha RA, Applegate B, Bae E. Smartphone-based low light detection for bioluminescence application. Sci Rep. 2017;7:40203.
41. Cevenini L, Calabretta MM, Tarantino G, Michelini E, Roda A. Smartphone-interfaced 3D printed toxicity biosensor integrating bioluminescent "sentinel cells". Sensors Actuators B Chem. 2016;225:249–5.
42. Boué SM, Wiese TE, Nehls S, Burow ME, Elliott S, Carter-Wientjes CH, et al. Evaluation of the estrogenic effects of legume extracts containing phytoestrogens. J Agric Food Chem. 2003;51(8):2193–9.
43. Ferri M, Graen-Heedfeld J, Bretz K, Guillon F, Michelini E, Calabretta MM, et al. Peptide fractions obtained from rice by-products by means of an environment-friendly process show in vitro health-related bioactivities. PLoS One. 2017;12:e0170954.

Analytical and Bioanalytical Chemistry

Electronic Supplementary Material

Prêt-à-porter nanoYESα and nanoYESβ bioluminescent cell biosensors for ultrarapid and sensitive screening of endocrine disrupting chemicals

Antonia Lopreside, Maria Maddalena Calabretta, Laura Montali, Maura Ferri, Annalisa Tassoni, Bruce R Branchini, Tara Southworth, Marcello D'Elia, Aldo Roda, Elisa Michelini

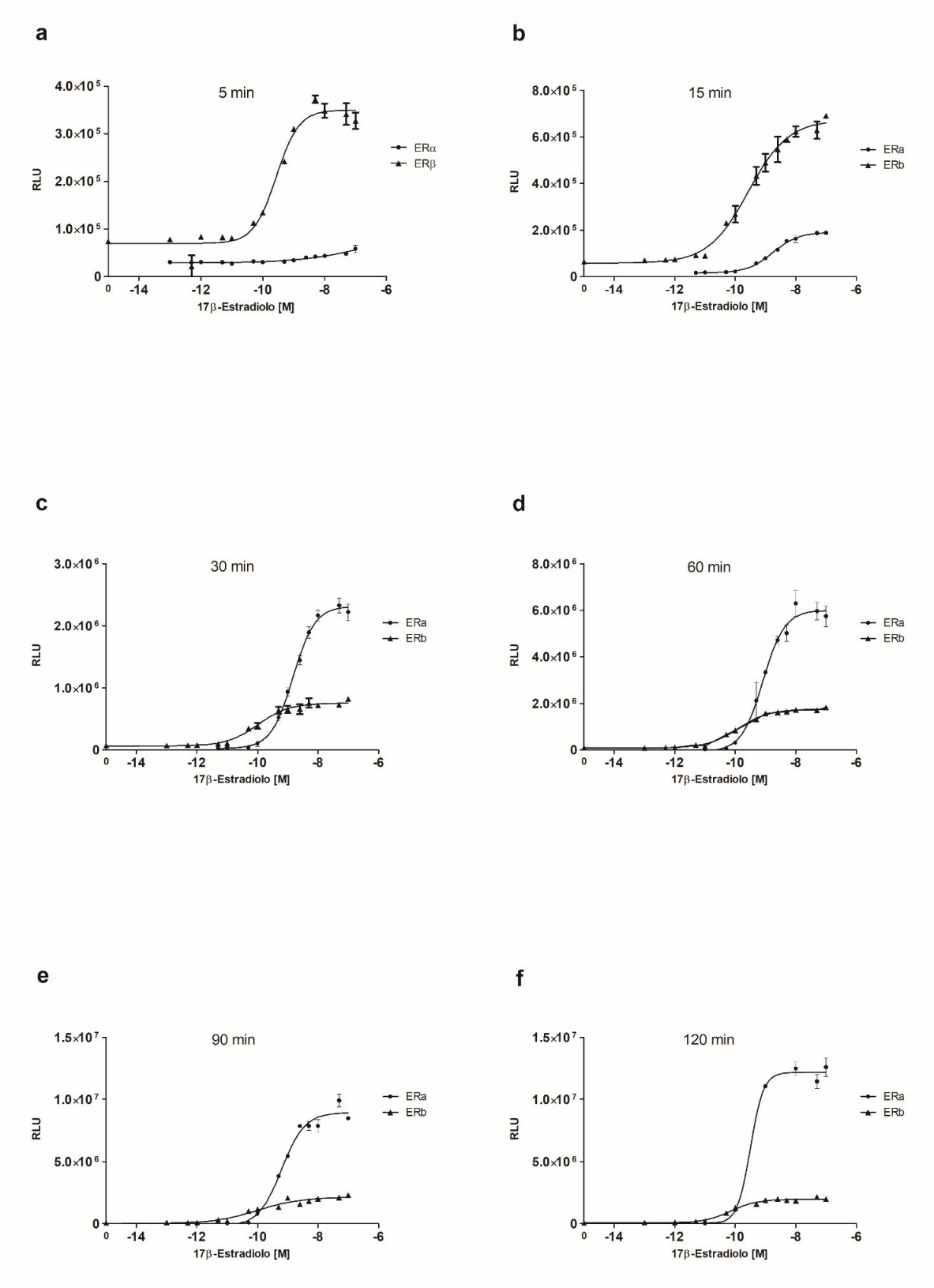

Fig. S1 Comparison, at different incubation times, between dose-response curves for 17β-estradiol obtained using nanoYESα and nanoYESβ: **a.** 5 min; **b.** 15 min; **c.** 30 min; **d.** 60 min; **e.** 90 min; **f.** 120 min. Experiments were performed in 96-black well microplate format and benchtop instrumentation using 180 µL of cells and 20 µL of 17β-estradiol solution (concentration range from 0.0001 nM to 100 nM). Data represent the mean values ± the standard deviation (SD) obtained with three replicates

Table S1 In house validation with proficiency chemicals. LOD and EC_{50} were calculated for a set of reference chemicals using nanoYESα and nanoYESβ in 96- black well plate format and a benchtop luminometer. Reference compounds to verify the responsiveness of the system include strong estrogenic compound (E2), a weak estrogen (17α-estradiol), a very weak agonist (17α-methyltestosterone) and a negative compound (corticosterone). Values represent mean ± SD of 3 separate experiments, each performed in triplicate

	ERα		**ERβ**		
	LOD (nM)	EC_{50} (nM)	LOD (nM)	EC_{50} (nM)	EPA Classification
17β-estradiol	0.016 ± 0.001	1.47 ± 0.06	0.001 ± 0.0002	0.12 ± 0.01	Strong
17α-estradiol	0.21 ± 0.03	95.9 ± 0.9	0.0031 ± 0.0003	537 ± 15	Weak
17α-methyltestosterone*	–	–	–	–	Very weak
Corticosterone*	–	–	–	–	Negative
Diethylstilbestrol	0.08 ± 0.01	7.4 ± 0.8	0.14 ± 0.02	1.1 ± 0.2	Positive
17α-ethinyl estradiol*	0.79 ± 0.07	108 ± 5	0.011 ± 0.007	–	Positive
Hexestrol	2.25 ± 0.08	80 ± 4	0.42 ± 0.01	13.3 ± 0.8	Positive
Genistein*	849 ± 25		4.68 ± 0.08	106 ± 7	Positive
Estrone	7.1 ± 0.5	1839 ± 44	0.009 ± 0.001	137 ± 11	Positive
Butyl Paraben	–	$1.5x10^4$ ± 0.1	270 ± 14	$1.0x10^3$ ± 0.04	Positive
1,3,5-Tris (4-hydroxyphenyl) Benzene*	–	–	–	–	Positive
Dibutyl phthalate*	–	–	–	–	Negative
Atrazine*	–	–	–	–	Negative
Tamoxifen*	–	–	–	–	Negative

*For some compounds, i.e., negative compounds and very weak estrogenic agonists LOD and EC_{50} were not calculated. All these chemicals were analyzed at the EPA test concentration range.

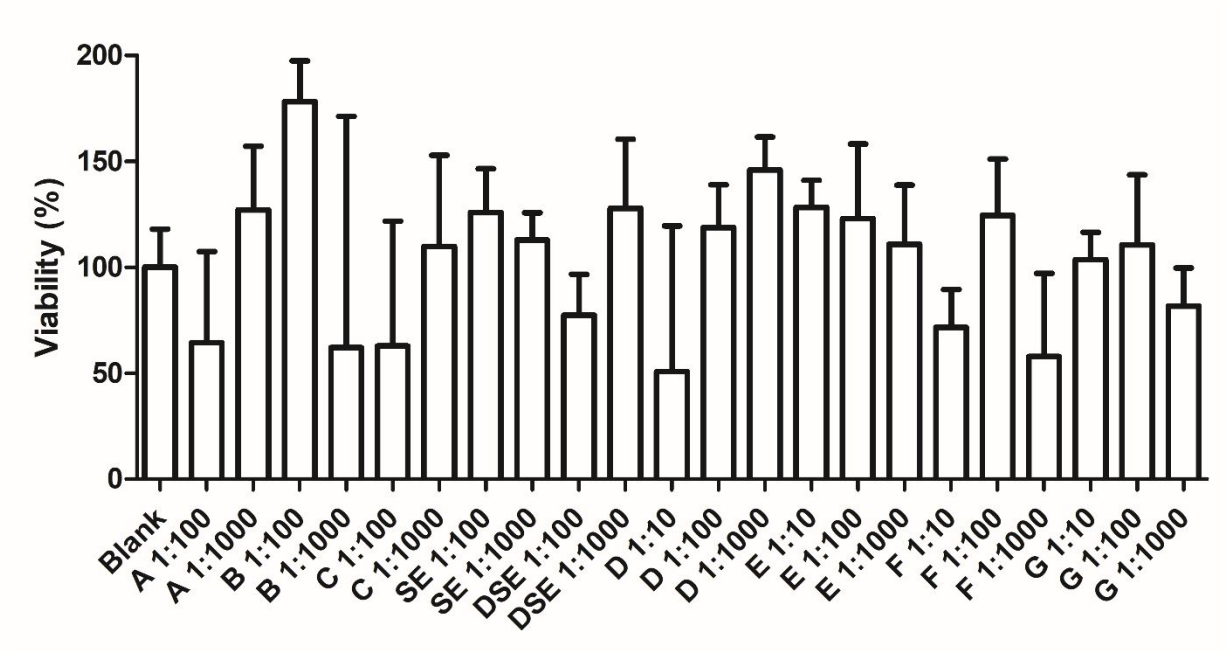

Fig. S2 Real samples toxicity evaluation with ToxYLuc biosensor with 30 min incubation time at 30°C

6

Smartphone-based multicolour bioluminescent 3D spheroid biosensors for monitoring inflammatory activity

Reproduced from: “Smartphone-based multicolor bioluminescent 3D spheroid biosensors for monitoring inflammatory activity”

Elisa Michelini, Maria Maddalena Calabretta, Luca Cevenini, Antonia Lopreside, Tara Southworth, Danielle D. Fontaine, Patrizia Simoni, Bruce R. Branchini, Aldo Roda

Biosensors and Bioelectronics, 123, 269-77.

Biosensors and Bioelectronics 123 (2019) 269–277

Contents lists available at ScienceDirect

Biosensors and Bioelectronics

journal homepage: www.elsevier.com/locate/bios

Smartphone-based multicolor bioluminescent 3D spheroid biosensors for monitoring inflammatory activity

Elisa Michelini[a,b,*], Maria Maddalena Calabretta[a], Luca Cevenini[a], Antonia Lopreside[a], Tara Southworth[c], Danielle M. Fontaine[c], Patrizia Simoni[d], Bruce R. Branchini[c], Aldo Roda[a,b,*]

[a] Department of Chemistry "G. Ciamician", University of Bologna, 40126 Bologna, Italy
[b] INBB, Istituto Nazionale di Biostrutture e Biosistemi, 00136 Rome, Italy
[c] Department of Chemistry, Connecticut College, New London, CT 06320, USA
[d] Department of Medical and Surgical Sciences (DIMEC), University of Bologna, Sant'Orsola Malpighi Hospital, Via Massarenti, 9, 40138 Bologna, Italy

ARTICLE INFO

Keywords:
Bioluminescence
Whole-cell biosensor
Luciferase
Smartphone
3D cell model

ABSTRACT

Whole-cell biosensors present many advantages, including being able to monitor the toxicity and bioavailability of chemicals; cells grown in traditional 2D cultures, however, do not reproduce the complexity of in vivo physiology. In the last years, 3D cell-culture models have garnered great attention due to their capability to better mimic in vivo cellular responses to external stimuli, providing excellent model living organisms. In order to obtain a predictive, sensitive, and robust yet low-cost 3D cell biosensor, we developed a smartphone-based bioluminescent 3D cell biosensor platform for effect-based analysis. We exploited the Nuclear Factor-kappa B (NF-kB) signal transduction pathway, which is induced by several types of stressors and is involved in the regulation of cell-cycle/growth, inflammation, apoptosis, and immunity. The smartphone-based biosensor relies on immobilized HEK293 spheroids genetically engineered with powerful red- and green-emitting luciferases utilized as inflammation and viability reporters. It provides a limit of detection for Tumor Necrosis Factor (TNFα) of 0.15 ± 0.05 ng/mL and could be a useful tool to initially screen environmental samples or other compounds on-site, especially for additional more accurate chemical analyses.

1. Introduction

The key idea in turning cells into biosensing systems is to convert molecular recognition events occurring at the cellular and molecular levels into measurable analytical signals (He et al., 2016; Thouand, 2018). In luminescent whole-cell biosensors, this is generally achieved by genetically engineering cells with reporter proteins whose expression is regulated by activation of specific molecular pathways. The expression of reporter proteins can be easily and quantitatively assessed by optical reading, e.g. fluorescence or bioluminescence (BL) (Raut et al., 2012; Roda et al., 2016a; Cevenini et al., 2014).

Thanks to their unusually high detectability, bioluminescent whole-cell biosensors have been used for on-site analysis by integrating cells into portable analytical devices (Michelini and Roda, 2012) exploiting portable light detectors such as charge-coupled devices (CCDs), video cameras, or complementary metal oxide semiconductors (CMOSs). These devices can be classified as true biosensors, since they incorporate entrapped cells as biological recognition elements integrated (or in intimate contact) with a transducer device (Turner, 2013). In the past years whole-cell biosensors, especially those based on robust microbial cells, were successfully applied in diverse fields, ranging from environmental monitoring to food quality assessment and safety analysis (Kim et al., 2018; Bazin et al., 2017; Cevenini et al., 2018; Kabessa et al., 2016; Roggo and van der Meer, 2017; Elad et al., 2010). Nevertheless, problems related to variability in cell growth and metabolism due to uncontrolled factors (e.g., matrix effects, temperature, pH variations) are still unsolved issues that hampered a widespread commercial diffusion of such biosensors.

More recently, portable light detectors have been replaced by smartphone-integrated CMOSs to obtain "instrument-free" detection. Smartphones offer several features that can be exploited for biosensor development, including high computational capability, powerful cameras, high coverage, and data-transmission speed (Zhang and Liu, 2016). Recently, optical microscopes, photometers, and other miniaturizable instrumentation were integrated in smartphones, exploiting 3D printing technology, to obtain reusable or disposable devices providing low-cost alternatives to conventional point-of-need and point-of-care solutions (Comina et al., 2016; Preechaburana et al., 2014; Sicard

* Corresponding authors at: Department of Chemistry "G. Ciamician", University of Bologna, 40126 Bologna, Italy.
E-mail addresses: elisa.michelini8@unibo.it (E. Michelini), aldo.roda@unibo.it (A. Roda).

https://doi.org/10.1016/j.bios.2018.09.012
Received 22 June 2018; Received in revised form 14 August 2018; Accepted 1 September 2018
Available online 04 September 2018
0956-5663/

et al., 2015). Despite its huge potential, the implementation of BL in smartphone-based platforms has been seldom explored (Arts et al., 2016; Cevenini et al., 2016a, 2016b; Ding et al., 2018; Kim et al., 2017; Roda et al., 2014a). It is well known that several advantages of BL are valuable for its implementation as a detection technique into compact portable devices, since no external light source and no geometry requirements for light detection are required (Roda et al., 2016b, 2013). However, it must be pointed out that, despite the excellent signal to noise ratio due to low background and high quantum yield of BL reactions catalyzed by luciferases (e.g., 0.4 for *P. pyralis* luciferase, Niwa et al., 2010), BL signals are generally very weak, challenging the detectors' sensitivity. For this reason, different strategies were undertaken, such as the selection of very bright luciferases (Arts et al., 2016; Ding et al., 2018), and the implementation of custom algorithms and hardware to maximize photon-capture efficiency (Kim et al., 2017).

Another important consideration is related to the type of cell that is used as the sensing element. Although microbial cells are usually robust and their integration into portable analytical devices is streamlined, they provide information that is less predictive of the effects on humans. Therefore, especially for toxicological studies, the use of mammalian cell lines is more advantageous. Interesting results were obtained with a cell biosensor smartphone platform for inflammation based on human embryonic kidney (HEK293T) cell lines genetically engineered to express the NanoLuc luciferase (Cevenini et al., 2016a). This platform provided adequate analytical performance; although, it lacked an internal viability control to correct the analytical signal according to cell toxicity. An external viability control was obtained by inclusion of wells containing cells engineered with a constitutive luciferase. This enabled parallel evaluation of nonspecific signal decays due to cell toxicity; however, an increase in signal variability due to cell-to-cell response variations was observed.

Moreover, to obtain more valuable information, e.g., in terms of the reliability of toxicity and bioactivity data, 3D cells can be developed to provide an environment that faithfully mimics the more structured in vivo physiological conditions (Dubiak-Szepietowska et al., 2016; Wittig et al., 2013). Several biosensors and prototypes were developed based on 3D multicellular cultures (spheroids), mainly relying on impedance measurements (Kloss et al., 2008; Lundstrom, 2017). The 3D cell culture systems that have been proposed to obtain spheroids that mimic the in vivo cellular microenvironment include the use of low-capacity plates, "hanging drop" systems, and rotary cell cultures (Choi et al., 2015). While all of these approaches have been optimized to obtain 3D cell cultures, their implementation into portable devices is not trivial.

Here, we report a smartphone-based platform, for quantitative effect-based analysis of analytes and complex samples having pro- or anti-inflammatory activity, relying on multicolor bioluminescent 3D cell biosensors. To the best of our knowledge, this is the first report of BL spheroid-based biosensing. We successfully applied this technology to evaluate inflammatory response induced by stressors via the NF-kB signal transduction pathway, which is induced by several types of stressors and is involved in the regulation of cell-cycle/growth, inflammation, apoptosis, and immunity (Inoue et al., 2007). Therefore, we developed and characterized a smartphone-based multicolor bioluminescent biosensor for inflammatory activity exploiting powerful red- and green-emitting luciferases. We selected luciferases with suitable emission properties for efficient spectral resolution exploiting the Bayer filter mosaic of smartphones.

The biosensor consists of immobilized spheroids of human cell lines engineered with a NFkB reporter plasmid driving the expression of a red-emitting luciferase and a second plasmid harboring a constitutively expressed green-emitting luciferase as a viability control (Fig. 1). We envisage potential applications of such an assay in different settings, such as the point-of-need analysis of environmental and food safety controls, evaluation of nutraceutical properties, and security applications for rapid monitoring of potentially harmful contaminants.

2. Experimental section

2.1. Chemical and reagents

Human embryonic kidney HEK293 cells were from ATCC (American Type Culture Collection [ATCC], Manassas, VA, USA) and cell culture reagents and materials were from Carlo Erba Reagents (Cornaredo, Milano, Italy). The enzymes required for cloning procedures were from Fermentas (Vilnius, Lithuania). The kits for plasmid extraction, beetle luciferin potassium salt (D-luciferin), and BrightGlo substrate were from Promega (Madison, WI, USA). Tumor Necrosis Factor-α (TNFα, purity higher than 95%), phorbol myristate acetate (PMA), poly(2-hydroxyethyl methacrylate) (poly-HEMA), gelatin from porcine skin type A, L-15 Medium (Leibovitz), isoproturon, naphthalene, aclonifen, hydrogen peroxide, and all other chemicals were purchased from Sigma-Aldrich (St. Louis, MO, USA). Polydimethylsiloxane (PDMS) Silgard 184 pre-polymer and curing agent were from Dow Corning (Midland, MI).

The mammalian expression plasmids pGL4.32_NFkB_Luc2P and pGL4.74[hRluc/TK] carrying Luc2P luciferase under the regulation of NFkB transcriptional regulation and hRLuc under Herpes simplex virus thymidine kinase promoter (TK) were from Promega. Plasmids PpyGR-TS and red-emitting mutant PpyRE-TS luciferase genes were previously described (Branchini et al., 2007). The reporter vectors pCMV_PpyGR-TS, pCMV_PpyRE-TS, pTK_PpyGR-TS, and pNFkB_PpyRE-TS were obtained by standard molecular cloning procedures.

2.2. 3D-printed microstructured cartridge and smartphone accessories

A cell cartridge containing 16 square wells (each 5 mm wide and 5 mm deep) was created with a desktop 3D printer (Makerbot Replicator 2 ×). The cartridge (40 × 40 mm, 7 mm height) was fabricated with black Polylactic Acid (PLA) at 210 °C, 300 μm resolution, 50% infill, printed over a customized round bottom resin film containing 500 μm microstructures with 400 μm depth, kindly provided by Elplasia™, Kuraray, Japan. Cartridges were then treated with a 30 mg/mL ethanol solution of poly-HEMA (40 μL/well) and let dry for 6 h at room temperature (25 °C) under the laminar flow hood. The cartridges were made using black PLA deposited over a microstructured sheet containing about 200 cone-shaped microspaces/cm^2 of 500 μm diameter and 400 μm depth. During the printing process, fused PLA enters into the microspaces sealing the bottom surface around each well. The 3D printed smartphone adaptors were fabricated with black acrylonitrile butadiene styrene (ABS) to provide a custom dark-box (65 × 65 mm, 60 mm high) weighting only 70 g. As the microspace film used as bottom for the cartridges is transparent, a mirror was inserted into the cartridge holder (Fig. 2e), to increase the light collected with the smartphone camera. The 3D printed parts simply snap together to form a self-supporting device (Fig. 2f). Smartphone adaptors and accessories were designed to fit the Nokia Lumia 1020 equipped with a high-performance back-side-illuminated (BSI) sensor (sensor size 1/1.5", 41MP, pixel size 1.1 μm), and printed using black ABS (at 230 °C, 300 μm resolution, 30% infill).

2.3. Bioluminescence characterization of HEK293 cells expressing green- and red-emitting luciferases with a smartphone

HEK293 cells were routinely grown in Dulbecco Modified Essential Medium (DMEM high glucose 4.5 g/L, GE Healthcare) supplemented with 10% fetal bovine serum, L-Glutamine 2 mM, 50 U/μL penicillin, and 50 μg/mL streptomycin. FuGENE HD transfection reagent (Promega) was used for transient transfections according to the manufacturer's instructions. Briefly, one day before transfection cells were plated on a 24-well plate at a density of 8 × 10^4 cells/well and transfected with 0.5 μg pCMV_PpyGR-TS or 0.5 μg pCMV_PpyRE-TS expression vector using a FuGENE®HD: DNA ratio of 3:1 and incubated at 37 °C with 5% CO_2 for 24 h. Cells were gently detached, counted, and

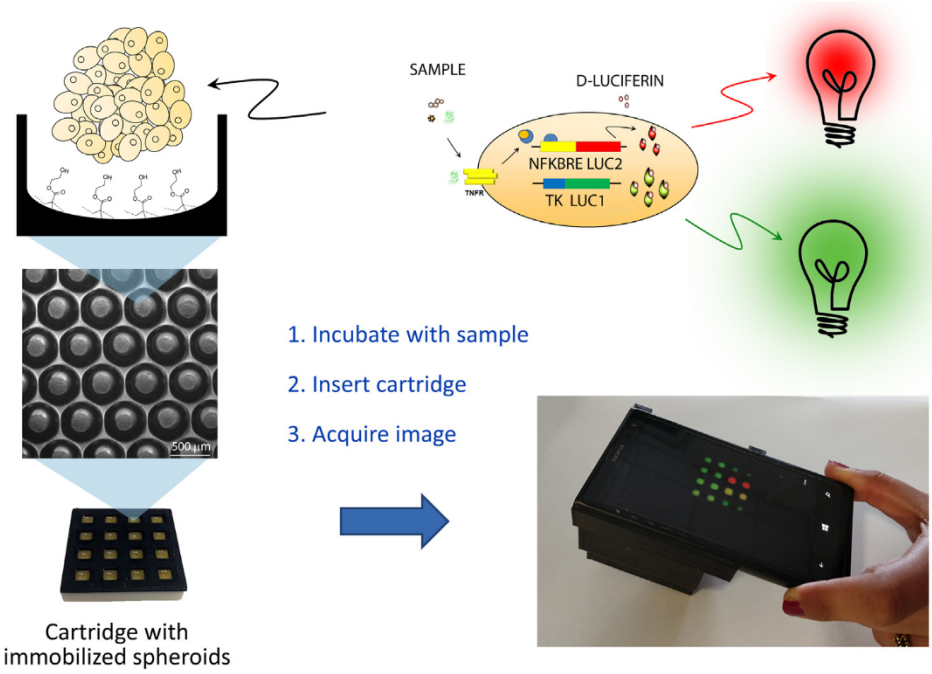

Fig. 1. Schematic representation of the genetically engineered bioluminescent cells and inflammation smartphone-based biosensor integrating dual-color bioluminescent 3D spheroids.

transferred in the 3D-printed cartridge at a density of 4.5×10^4 cells/well. Red- and green-emitting cells were diluted to a similar level of activity and imaged with the smartphone camera for 4 s using different sensitivity settings, from ISO 100 to ISO 4000, after addition of 50 µL BrightGlo substrate. The BL emission spectra (450–750 nm) and kinetics (5 min, 300 ms integration time) were acquired in a 96-well plate with a Varioskan Flash multimode reader (Thermo Fisher Scientific).

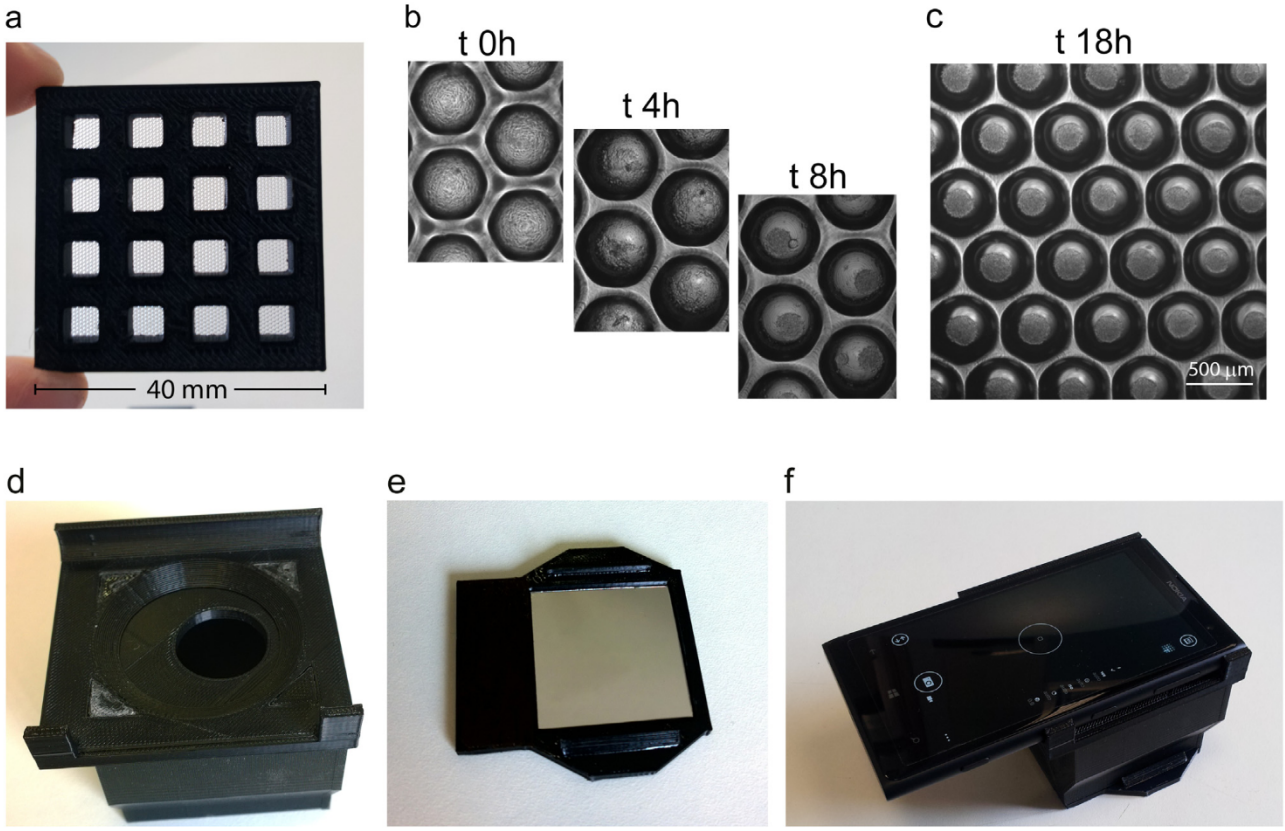

Fig. 2. 3D-printed smartphone accessories and spheroid formation; (a) Picture of the 3D printed cartridge made of PLA printed over a microspace bottom sheet; (b) HEK293-cells seeded into the cell cartridge and imaged at time 0 or after 4 h, 8 h, and 18 h overnight incubation (c); (d) Smartphone black-box accessory; (e) 3D printed cartridge holder comprising a mirror; (f) assembled smartphone-based device.

2.4. Preparation of a ready-to-use cartridge with immobilized spheroids

To develop a spheroid-biosensing platform for on-site analysis, we adopted several strategies to render the biosensor more simple and robust. A transparent PDMS lid was created using a monomer: curing agent ratio of 10:1. The solution was placed under vacuum for 40 min to remove bubbles and casted onto a 3D-printed master mold (replicating the cell-cartridge) to create the array of caps (5 × 5 mm, 2 mm height, each) that corresponded with the cell-cartridge wells. The PDMS was allowed to harden overnight at 50 °C, then gently removed from the mask and sprayed with 70% ethanol for disinfection. The spheroid biosensors were obtained by transfecting HEK293 cells with 0.1 μg pTK_PpyGR-TS and 0.4 μg pNFkB_PpyRE-TS in 24-well plates and were transferred (4.5×10^4 cells/well) into the 3D printed cell cartridge to enable spheroid formation. After overnight incubation at 37 °C, a 50 μL-volume of 5% w/v gelatin solution (in complete medium) was added to each well. The cell-cartridge was kept at room temperature (25 °C) to allow the gelatin to set and form a gel in the wells, then sealed with the PDMS lid. To control spheroid formation and optimize the protocol, spheroids were imaged with an inverted microscope (Olympus IX73) using a 4X objective (Olympus UPlanFLN).

Spheroid analysis was performed from bright-field images of HEK293 spheroids using ImageJ version 1.51d software to define for each spheroid's perimeter (P) and projected area (A). We calculated a sphericity factor Φ (Kelm et al., 2003) as follows:

$$\phi = \frac{\pi \sqrt[x]{\frac{4A}{\pi}}}{P} \quad (1)$$

2.5. Development of a smartphone-based dual-color inflammation spheroid biosensor

Different parameters were optimized in order to improve the 3D cell biosensor analytical performance in terms of selectivity, analysis time, and robustness. Thus, we changed different parameters including the choice of promoters, transfection ratio between different reporter plasmids, cell density at seeding (1.5×10^4, 3×10^4, and 4.5×10^4), and incubation time for achieving efficient and reproducible formation of spheroids (from 4 to 18 h). Briefly, under optimized conditions, HEK293 cells were transiently transfected in 24-well plates with 0.1 μg pTK_PpyGR-TS, for the constitutive expression of a green-emitting luciferase used as the viability control, and with 0.4 μg pNFkB_PpyRE-TS, a reporter vector in which a red-emitting luciferase is under the control of NFkB response elements (Fig. 1). At 24 h post-transfection, 40 μL of cells resuspended in DMEM (4.5×10^4 cells/well) were transferred into the 3D-printed cell cartridge and incubated at 37 °C for spheroid formation. After 18 h, a cartridge containing spheroids was treated in duplicate with 10 μL TNFα dilutions (concentration range 0.5–20 ng/mL from a stock solution of 10 μg/mL TNFα in phosphate-buffered saline solution) or culture medium, as a control (blank). After 5 h incubation, a 50 μL-volume of BrightGlo substrate was added to each well and BL images were acquired with the smartphone (4 s, ISO 800) assembled with the 3D printed accessories.

Images were analysed with ImageJ software (National Institutes of Health, Bethesda, MD) and GraphPad Prism v.5 (GraphPad Software, La Jolla, USA) was used to plot the data. Briefly, each image was split into RGB channels and the emission of PpyGR-TS and PpyRE-TS were quantified by selecting regions of interest (ROIs) on corresponding images to calculate the mean integrated density of duplicate wells. The dose-response curve for TNFα was obtained by calculating the red to green emission ratio for each concentration (corrected BL signals) and by plotting these values as fold response with respect to control (CTR). Limit of Detection (LOD) was calculated as the TNFα concentration that corresponds to the blank plus three times the standard deviation. All measurements were performed in duplicate and repeated with different cell cartridges at least three times.

2.6. Selectivity of the biosensor

To evaluate the selectivity of the inflammation spheroid biosensor we tested different chemicals including pollutants and pesticides, i.e., isoproturon, aclonifen and naphthalene regulated by the European Union (Water Framework Directive 2000/60/EC) and World Health Organization. The maximum allowable concentration Environmental Quality Standards (MAC-EQS) admitted by Directive 2013/39/EU in inland surface waters were tested: 0.12 μg/L for aclonifen, 130 μg/L for naphthalene and 1.0 μg/L for isoproturon. Mixture solutions of different chemicals were analysed to assess additive or synergic effects of the compounds on the NFkB inflammation pathway. Four different mixtures were analysed: Mix 1 (isoproturon 1.0 μg/L + naphthalene 130 μg/L), Mix 2 (isoproturon 1.0 μg/L and aclonifen 0.12 μg/L), Mix 3 (aclonifen 0.12 μg/L and naphthalene 130 μg/L), Mix 4 (aclonifen 0.12 μg/L, naphthalene 130 μg/L and isoproturon 1.0 μg/L). To investigate the specific effects of reactive oxygen species (ROS) spheroid cartridges were treated with H_2O_2 solutions (concentration range from 0.5 mM to 10 mM in doubly distilled water).

Spheroid cartridges were treated in duplicate with 10 μL solutions of pure chemicals or mixtures 1–4. Cells transfected only with pNFkB_PpyRE-TS and induced with 10 ng/mL TNFα were also prepared as the inflammatory positive control; while doubly distilled water was used as the negative control. After 5 h incubation, a 50 μL volume of BrightGlo substrate was added to each well and BL images were acquired with the smartphone (4 s, ISO 800) and analysed as previously described with ImageJ.

2.7. Simulation of real samples

We investigated the suitability of the 3D spheroid biosensor to analyze samples with pro-inflammatory activity or general toxicity, thus being potentially harmful to human health. The chemical agent chosen for inflammation monitoring was PMA, a phorbol ester isolated from *Jatropa Curcas*, a plant widely used as biodiesel feedstock that contains pro-inflammatory phorbol esters (EFSA CONTAM Panel, 2015).

Spheroid cartridges were treated in duplicate with 10 μL PMA solutions ranging from 0.1 nM to 10 μM in 5% DMSO. Cells transfected only with pNFkB_PpyRE-TS and induced with 10 ng/mL TNFα were also prepared as the inflammatory positive control; while, DMSO, 1% final concentration, was used as the negative control. After 5 h incubation, a 50 μL volume of BrightGlo substrate was added to each well and BL images were acquired with the smartphone (4 s, ISO 800) and analysed as previously described with ImageJ. In order to obtain a robust biosensor and a reproducible assay for on-site applications, the analytical performances of spheroid cartridges were also evaluated after one week storage. Cell-cartridges with immobilized spheroids in L-15 Medium (Leibovitz) were maintained at room temperature (25 °C) for up to one week before assay execution. All measurements were repeated with 3 different cartridges.

3. Results and discussion

The possibility to use the smartphone camera to detect bio/chemiluminescent reactions has been previously reported (Roda et al., 2014b; Cevenini et al., 2016b; Kim et al., 2017). However, the full exploitation of a smartphone-integrated CMOS camera to simultaneously detect multiple colors emitted by genetically engineered cells in the same well has not been reported yet. In addition, the implementation of 3D cell cultures, i.e. spheroids, for smartphone-based biosensing has not been addressed.

The proposed biosensing platform for on-site analysis required adaptation to preserve the functionality of the cells while maintaining

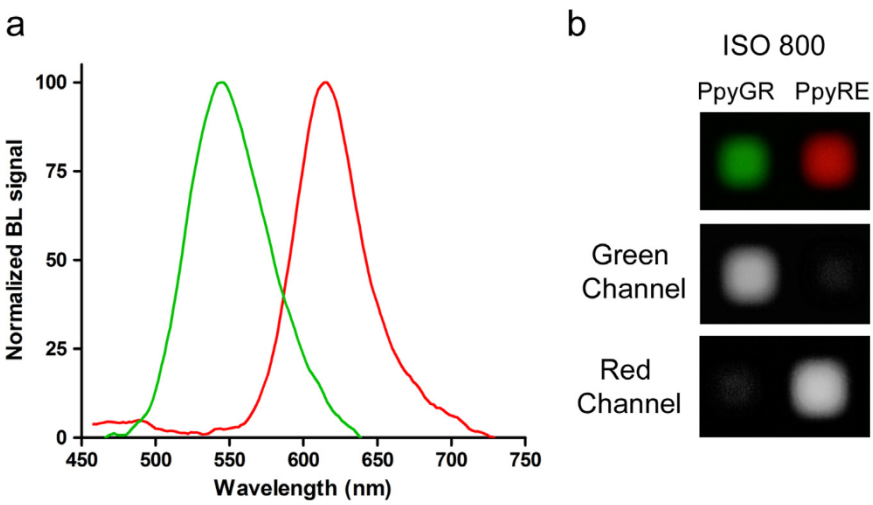

Fig. 3. (a) BL emission spectra of HEK293-spheroids expressing green (PpyGR-TS) and red-emitting (PpyRE-TS) thermostable luciferase mutants obtained with Varioskan Flash luminometer; (b) Color image of green and red-emitting luciferases in HEK293-spheroids acquired with the smartphone for 4 s at ISO 800 and same image split into green and red channels to evaluate the crosstalk between PpyGR-TS and PpyRE-TS emission.

adequate sensitivity. In fact, although spheroid-biosensors have been reported (Wittig et al., 2013), integration within a biosensor device has not been effectively demonstrated. Prompted by proof-of-principle biosensors and cell-based assays relying on 3D cell cultures (Cevenini et al., 2017; Dubiak-Szepietowska . et al., 2016), we developed a new 3D cell format in which spheroids are immobilized into a 3D cartridge that plugs into a smartphone. Here, we report a dual-color BL spheroid-biosensor platform, in which a red-emitting luciferase is induced by the presence of pro-inflammatory stimuli and a green-emitting reporter is constitutively expressed and used as a viability control. The presence of inflammatory compounds in the sample will increase the red BL signal and the independent viability green signal will allow us to correct the response for nonspecific effects or general toxicity activity. Thus, this dual sensor will distinguish between pro-inflammatory agents and chemicals having general cell toxicity.

3.1. Fabrication of 3D cell-culture cartridges and smartphone accessories

As shown in Fig. 2a, we developed a customized 3D-printed cartridge (40 × 40 mm) containing 16 square wells (5 mm wide and 5 mm deep). The cartridge was printed with black PLA over a resin film containing 500 μm microstructures with 400 μm depth. We could not opt for ABS as the printing material, although its feasibility for integrating bioluminescent cell biosensors was recently reported (Cevenini et al., 2016a, 2016b), because it requires a heating bed. Heat beds are commonly used in 3D printing to avoid warping and improve print quality; however, the temperatures used for ABS (100–110 °C) would destroy the cone-shaped microstructures (about 200 cones per cm^2). Therefore, we used black PLA, which does not require a heated bed and preserves the microstructures.

The cartridge surface was then treated with poly-HEMA to facilitate cell-cell rather than cell-plastic interactions, thus promoting cell aggregation into spheroids. Poly-HEMA hydrogels are polymers approved by federal agencies for the use in several biomedical and pharmaceutical applications. The non-toxicity and the biocompatibility of the poly-HEMA makes it suitable for most biotechnological applications. Moreover, thanks to the presence of polar groups and hydrophobic α-methyl groups, the polymer has excellent chemical properties in terms of mechanical strength stability and compatibility with water (Kim et al., 2015).

HEK293 were selected to provide endogenous expression of TNFα receptor, a potent mediator of inflammation, as they aggregate very quickly and form spheroids within a few hours (Fig. 2b, c). After an overnight incubation, HEK293 spheroids of 190 ± 20 μm were formed. The sphericity factor (ϕ) of 20 spheroids was calculated according to Eq. (1) obtaining an average value of 0.93 ± 0.02, which is consistent with that obtained in commercial 96-well micropatterned plates (Cevenini et al., 2017). This cartridge configuration provides 16 wells, each containing approximately 50 spheroids, thus providing a ready-to-use platform that can be snapped into the smartphone and imaged.

3.2. Bioluminescence characterization of red and green-emitting 3D spheroids with the smartphone

To fully exploit the possibilities offered by the color BI-CMOS camera of smartphones, we set up a dual-color biosensor based on the expression of two luciferases emitting at different wavelengths. The implementation of dual-color imaging represents a significant upgrade in smartphone-based devices (Wang et al., 2017); nevertheless, the implementation of low-light emitting probes, such as bioluminescent reporters, challenges the sensitivity of the smartphone integrated camera. Therefore we selected two highly stable mutant luciferases, PpyGR-TS and PpyRE-TS luciferases that showed advantageous properties, i.e., high emission intensity, glow-type kinetics (Branchini et al., 2007), and high pH stability, as the viability control and inflammation reporter, respectively. These thermostable human codon optimized luciferases (Fig. 3a), with emission maxima at 549 nm and 615 nm and corresponding bandwidths at half maxima of 70 nm and 50 nm, respectively, provide well separated emission spectra using the same D-luciferin substrate. These optimal spectral features enable the analysis of complex matrices. Thus, the assay is highly cost effective. In addition, the BL emission spectra of these luciferases nearly overlap the spectral transmittance of the green and red filters of the Bayer matrix in the smartphone CMOS sensor, allowing sensitive detection of BL signals.

In this work, we took advantage of the smartphone Nokia Lumia 1020, which is equipped with a camera with built-in ProCam application enabling manual selection of different parameters. In particular, the possibility to set the shutter speed up to 4 s and to use ISO values up to 4000, makes this smartphone suitable for low-light imaging applications. To optimize the acquisition of BL signals, we imaged HEK293 spheroids expressing the green- or red-emitting luciferase, using different exposure times and ISO values from 100 to 4000. Use of a low exposure time (i.e. 1 or 2 s) in combination with high ISO values, resulted in noisy images (data not shown). At ISO 800, about 95% of green luciferase emission is acquired in the green channel and only a 5% is detected in the red channel (and vice versa) (Fig. 3b). The crosstalk between channels increases with higher sensitivity settings and the signal to background ratio is not significantly improved (less than 8%). At ISO 1600, a significant interference was observed, with about 25% of PpyGR-TS emission detected in the red channel and 15% of PpyRE-TS acquired in the green channel. For this reason, for the

quantification of the spheroid-biosensor response, we acquired BL images for 4 s at ISO 800 to achieve the best sensitivity and lowest crosstalk between the two luciferases.

3.3. Optimization and analytical performance of smartphone-based dual-color inflammation biosensor

It is recognized that 3D cell cultures are stable for longer lifespans than 2D cell cultures and provide more suitable tools to develop cell biosensors with adequate responsiveness over time. For example, Bhise et al. reported that bioprinted hepatic spheroids remained functional during a 30 day culture period (Bhise et al., 2016). However, the reported liver-on-a-chip platform, used for toxicity assessment, required continuous perfusion and cannot be implemented into a low-cost platform. Moreover, another issue to be considered is related to the limited diffusional transport posed by the 3D structure of the spheroids. Multicellular aggregates are composed of proliferating cells, non-proliferating viable cells, and necrotic cells. The presence of multiple phenotypes mimics the in vivo tumor physiology and may represent an advantage in cancer research (Jeong et al., 2012). However, this could represent a caveat in biosensing with bioluminescent reporters due to the limited availability of the analytes and substrates for the chemical reaction, as well as oxygen, which is required for all luciferase-based reactions. In spheroids with a diameter of 150 μm, the majority of cells have sufficient oxygen for BL reactions, with a negligible necrotic core composed of only 2% of cells (Langan et al., 2016). Therefore, we decided to obtain spheroids in the range of 150–200 μm.

In order to obtain a stand-alone spheroid-based biosensing platform for on-site analysis, we integrated the spheroid-biosensors in a ready-to-use 3D printed cartridge. To this end, BL spheroid biosensors were immobilized with a medium solution containing 5% v/v gelatin from porcine skin type A. It has been reported that the inclusion of gelatin microparticles increases the stiffness of the spheroid microenvironment (Baraniak et al., 2012), enabling quick and easy interaction with the sample (and the availability of the chemical substrate for the BL reaction).

We aimed at obtaining color-coded visual information in which the green emission is associated with “safe”; while, the red corresponds to “harmful” samples. Since the green luciferase is constitutively expressed, the presence of compounds able to activate the intracellular inflammatory pathway will produce a yellowish to orange color proportional to induction levels and to general toxicity effects. Obtaining a color emission which covers a wide range of green to red hues, largely depends on the relative expression of the two luciferases. This can be tuned by adjusting the promoter strength and the ratio between the two reporter plasmids used for cell transfection. We first expressed the green luciferase under the strong CMV promoter (pCMV_PpyGR-TS). When incubating HEK293 co-transfected with pNFkB_PpyRE-TS and pCMV_PpyGR-TS with TNFα concentrations in the range 0.5–20 ng/mL, the signal of constitutive green-emitting luciferase was too high, overlapping the red channel. It was not possible to perform spectral resolution to quantitatively elaborate the corrected inflammatory response (data not shown). Therefore, to reduce the expression level of PpyGR-TS, the weaker Herpes simplex virus thymidine kinase promoter was selected (Qin et al., 2010). We then optimized the transfection protocols to achieve the optimum balance between red and green emission. Cells were transfected with a 1:1 and 1:3 ratio of pTK_PpyGR-TS and pNFkB_PpyRE-TS vectors. Using the same amount of reporter plasmids, the LOD for TNFα was 20 ng/mL, limiting the applicability of the assay. Therefore, a ratio of 1:3 control: reporter vector was selected, providing the full range of “traffic light” emissions. Fig. 4a shows a typical image obtained with the smartphone by incubating the spheroid-biosensor with increasing concentrations of TNFα. Spheroids expressing only PpyRE-TS induced with 20 ng/mL TNFα and spheroids incubated with vehicle only are also present in each cartridge as positive and negative inflammatory controls, respectively.

Multicolor cell-based assays performed with conventional instrumentation (i.e. luminometer) usually relies on the use of optical emission filters to acquire the BL signals from luciferases emitting at different wavelength and on a spectral unmixing algorithm for the separation of emitted light. Despite the spectral overlap between the two luciferases, the low crosstalk between channels (5%) allows the user to simply quantify the BL emission of PpyGR-TS and PpyRE-TS on green- and red-channel split images (Fig. 4b), respectively. The BL signal of both luciferases in the blue channel is negligible (less than 1%) and is excluded from calculations. The BL signal of green- and red-emitting luciferases were quantified on corresponding images, by selecting a square ROI around each well, and plotted as the mean ± SD of duplicate wells. A mirror was also placed under the cartridge to increase the acquisition of BL emission. Back-reflection towards the CMOS sensor through the transparent gelatin layer provided an increase of about 40% in the light collected.

The calibration curve for TNFα was obtained by calculating the corrected BL signal (PpyRE-TS/PpyGR-TS emission ratio) for each concentration and by plotting the corresponding fold response with respect to the control (CTR) (Fig. 4c). The ratiometric measurement provides a more robust analysis since aspecific effects on cell viability as well as small variations in spheroid number and dimension are corrected. In optimized conditions, i.e. a cartridge with 50 spheroids/well transfected at a 1:3 viability: inflammatory reporter vector ratio, 5 h incubation, and acquisition for 4 s (ISO 800), the smartphone-based biosensor provides a LOD of 0.15 ± 0.05 ng/mL and an EC50 of 1.0 ± 0.1 ng/mL TNFα. Indeed, reporter-gene assays were suitable for the high throughput quantification of residual drug activity and anti-drug neutralizing antibody response to TNFα antagonists in serum samples (Lallemand et al., 2011). Therefore, a potential application could be as point-of-care diagnostics for patients with inflammatory disease, such as Crohn's disease, treated with a TNFα antagonist.

3.4. Selectivity of the biosensor

To assess the selectivity of the biosensor we evaluated the inflammatory activity and toxicity of different toxic chemicals having dissimilar modes of action and classified as priority substances or pollutants by the European Union (EU) and the United States Environmental Protection Agency (EPA). We analysed the activity of these compounds at the Maximum Allowable Concentration for inland surface waters defined in the Environmental Quality Standards (MAC-EQS) of Directive 2013/39/EU. We selected isoproturon, an agricultural herbicide of low acute toxicity and medium toxicity after short- and long-term exposures, which has been detected in surface and ground water at concentrations below 0.1 μg/L (WHO, 2003). We also analysed aclonifen, a biocide causing oxidative damage via the formation of reactive oxygen species (ROS) (Almeida et al., 2017) and naphthalene, whose exposure has been associated with hemolytic anemia and damage to the liver, which has been classified as a possible human carcinogen by EPA (Höke and Zellerhoff, 1998). As expected, at the tested concentrations, i.e., 0.12 μg/L for aclonifen, 130 μg/L for naphthalene and 1.0 μg/L for isoproturon, these compounds did not produce any activation of the NF-κB pathway and did not show significant cell toxicity. Pollutants, and in particular pesticides, may occur at low concentrations in mixtures with other chemicals (Hernández et al., 2013). Therefore, from a toxicological perspective, it is of paramount importance to assess the overall activity of a sample (Busch et al., 2016). Since a potential application of the proposed biosensor is the evaluation of total toxicity of an environmental sample to rapidly identify potential threats to human and animal health, we also analysed mixtures of these compounds which could be present in inland surface waters, encompassing rivers, lakes, and artificial water bodies. Interestingly, the mixtures Mix 3 (aclonifen 0.12 μg/L and naphthalene 130 μg/L) and Mix 4 (aclonifen 0.12 μg/L, naphthalene 130 μg/L, and isoproturon 1 μg/L) presented significant toxic effects with a drop in

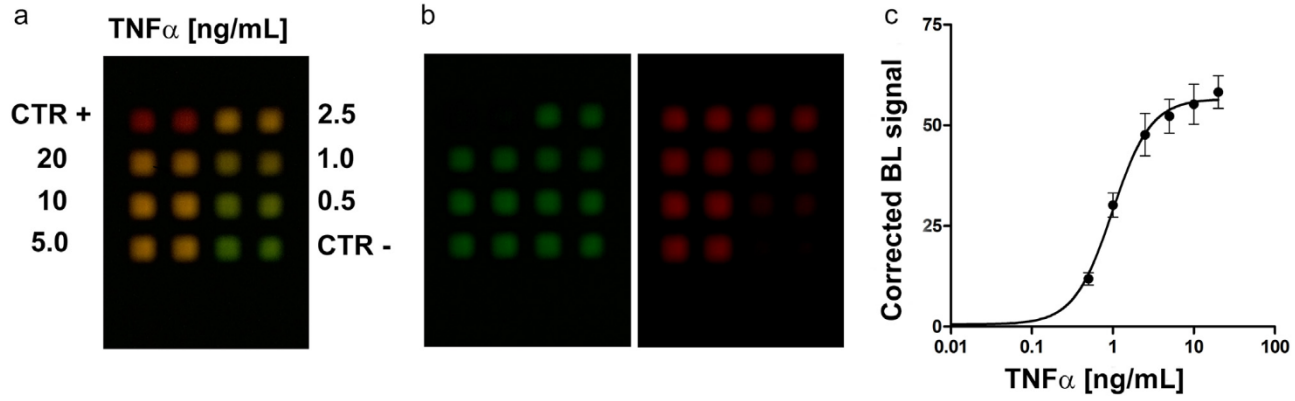

Fig. 4. (a) Image acquired with the smartphone obtained by incubating the spheroid-biosensor with increasing concentrations of TNFα; (b) Green- and red-channel images corresponding to the PpyGR-TS (viability signal) and PpyRE-TS (inflammatory response) emission; (c) corrected dose-response curve for TNFα.

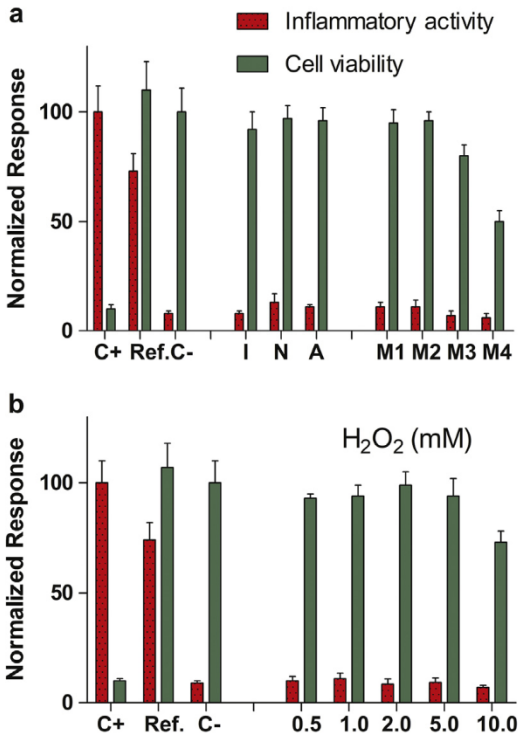

Fig. 5. (a) Results obtained by incubating the 3D cell biosensor with chemicals for 5 h at room temperature (25 °C) and imaged with the smartphone. Positive inflammatory control C+ : 10 ng/mL TNFα; Ref.: 2.5 ng/mL TNFα, Viability control Ctr-: doubly distilled water; I: isoproturon 1.0 μg/L; N: naphthalene 130 μg/L; A: aclonifen 0.12 μg/L; M1: mixture solution containing isoproturon 1.0 μg/L and naphthalene 130 mg/L; M2: mixture solution containing isoproturon 1 mg/L and aclonifen 0.12 mg/L; M3: mixture solution containing aclonifen 0.12 mg/L and naphthalene 130 mg/L; M4: mixture solution containing aclonifen 0.12 mg/L, naphthalene 130 mg/L and isoproturon 1 mg/L). (b) Results obtained with 5 h incubation at 25 °C of the 3D biosensor with different concentrations of H_2O_2 (concentration range 0.5–10 mM). Cell viability was normalized with respect to the green emission of control wells, while inflammatory activity was reported as the fold induction of the red-calibrator emission. Values are the mean ± standard deviations of three experiments performed in duplicate.

cell viability of 20 ± 5% and 51 ± 8%, respectively (Fig. 5a).

3.5. Simulation of real sample analysis

As proof of concept, the response of the dual-color biosensor was tested using spiked samples containing different concentration of PMA, a NF-kB activator that is used in pharmacology as a potent tumor promoter and for activating protein kinase C (Lee et al., 2002). PMA is extracted from the *Jatropha curcas* plant, which gained importance in recent years as it grows in different soil conditions and its seeds are a source of oil for biofuel production (EFSA CONTAM Panel, 2015). The by-product called Jatropha meal has a high nutritional value and may be used as a feed ingredient for the animal industry. However, due to the presence of phorbol esters, well-known toxicants having tumor promoting activity, detoxification treatments are necessary prior to its use in animal feed. PMA in fact induces malignant transformation of cells via the activation of c-Jun and c-Fos. The subsequent proinflammatory response to tumor promotion is then mediated through activation of NF-κB (Goel et al., 2007). A simple biosensing platform might be useful for the evaluation of treatment efficacy and to monitor the phorbol esters content in Jatropha derived products or possible contamination in the environment (e.g. water).

To create a user-friendly platform, each cartridge also provides a traffic light like response as a reference for a quick evaluation of the sample's activity. This was obtained by including i) spheroids transfected with reporter vector only and induced with 10 ng/mL TNFα, which provide a red emission (positive control, Ctr+), ii) spheroids transfected with both reporter and control vectors and induced with 2.5 ng/mL TNFα, which provide a yellow-orange emission, and iii) spheroids transfected with both reporter and control vectors and incubated with vehicle (DMSO 1%), resulting in green-emission only (negative control, Ctr-) (Fig. 6).

By testing the same concentration of PMA (10 nM) the response of the biosensor was reproducible with an intra-assay variability of 13% and an inter-assay variability of 17%, the latter obtained with different cartridges.

It is known that inflammatory pathways and cellular oxidative stress are interconnected and reactive oxygen intermediates (e.g., H_2O_2) act as NF-κB inducers (Legrand-Poels et al., 1995). Therefore, to better understand if PMA effects were due to pure NF-κB activation or mediated by cellular oxidative stress, we investigated the effect of H_2O_2 on the biosensor. As shown in Fig. 5b, only at a concentration of 10 mM was H_2O_2 able to decrease cell viability (27 ± 5%) within the 5 h of incubation. None of the tested H_2O_2 concentrations (range 0.5–10 mM) produced pro-inflammatory effects (Fig. 5b).

We evaluated the possibility to store cartridges at room temperature (25 °C) for one week. To this end we replaced DMEM with L15 medium, which is formulated for use in carbon dioxide free systems. In a previous work, ready-to-use cartridges with immobilized HEK293 cells showed a 40 ± 7% drop in bioluminescence after 48 h at 25 °C storage (Cevenini et al., 2016a). Such loss in viability caused a non-reliable response after 2 days storage of the cartridge. On the other hand, spheroids showed a much slower decrease in viability (20 ± 8% drop in bioluminescence after one week storage at room temperature),

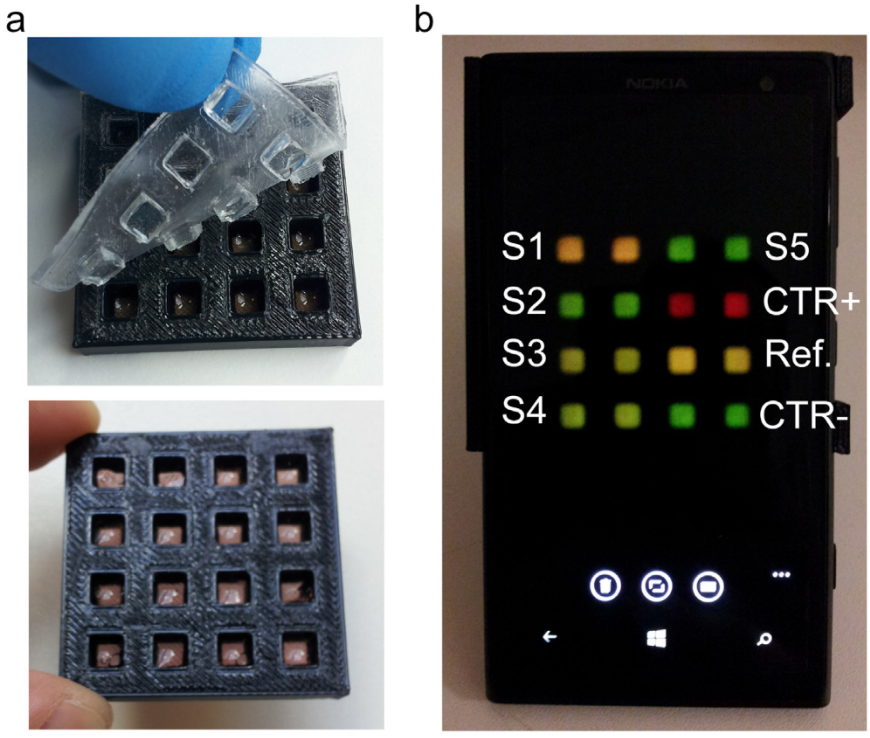

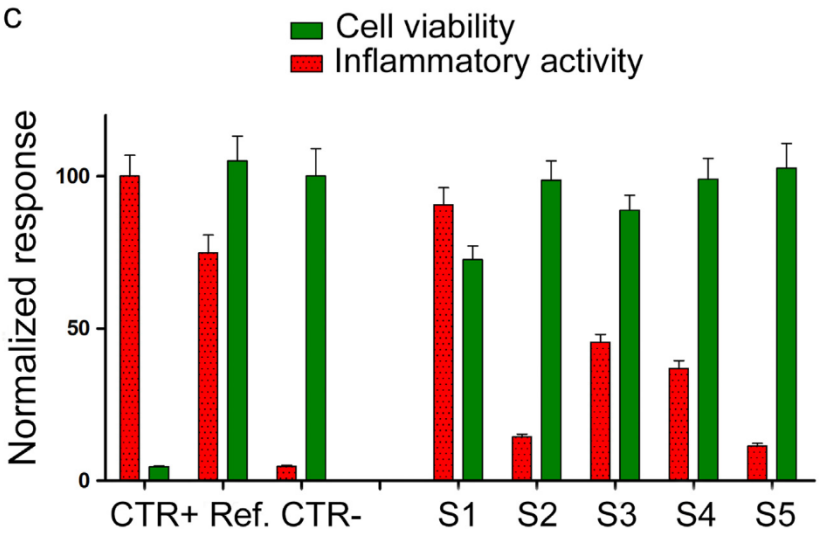

Fig. 6. (a) Picture of the 3D printed cartridge containing the immobilized spheroid-biosensor. Each cartridge can be used to analyze up to five samples in duplicate. It contains a positive control (Ctr+), a reference, and a negative control (Ctr-) resulting in a sort of "traffic light" response for direct comparison of the sample's activity; (b) BL image, obtained with the smartphone, of a cell cartridge incubated with different concentrations of PMA: S1 (10 μM PMA), S2 (1 nM PMA), S3 (1 μM PMA), S4 (50 nM PMA), S5 (0.1 nM PMA), Ctr+ (10 ng/mL TNFα), Ref. (2.5 ng/mL TNFα), Ctr- (1% DMSO); (c) Results obtained after image elaboration of the tested samples. Cell viability was normalized with respect to the green emission of control wells, while inflammatory activity was reported as the fold induction of the red-calibrator emission.

which, in conjunction with the use of internal correction, provided a correct evaluation of inflammatory activity of the samples even after seven days. For example sample S3 containing 1 μM PMA showed corrected inflammatory activities of 49% and 47% compared to Ctr + (10 ng/mL TNFα), at day 0 and after 7 days of storage, respectively (corresponding viabilities were 91 ± 8% and 75 ± 8%).

As expected, an higher variability between duplicates was reported (CV% = 20%) after one week storage, however, due to their higher stability, spheroids provided a significant improvement in the cells' shelf-life when compared to cells immobilized in conventional matrices. These pre-loaded cartridges could be shipped or transported with commercially available portable incubators directly to the site were the analysis is required. This greatly simplifies the transport and use of our biosensor in laboratories non equipped with cell-culture facilities (e.g., cell culture incubators with CO_2 controlled atmosphere) and benchtop instrumentation for bioluminescence detection.

4. Conclusion

We implemented a multicolor bioluminescent 3D cell biosensor in a smartphone-based platform. The biosensor consists of immobilized spheroids of human cell lines expressing red- and green light emitting luciferase under the regulation of the NFkB pathway and a constitutive promoter, respectively. The 3D cell biosensor enables the assessment of the actual toxicity and inflammatory effects of a sample, rather than identifying single constituents. Such a biosensor could be thus very helpful in those situations in which mixtures of compounds with unknown toxicities and different mode of action are present, such as the aquatic environment. From this perspective, the proposed biosensing platform would aim to become a useful tool for an initial screening of environmental samples or toxic substances on-site, thus identifying samples for a more accurate chemical analysis. However, it must be pointed out that 3D cell models still do not compete with the robustness of microbial biosensors based on bacterial or yeast cells and future work

will regard the development of new immobilization matrices to improve the shelf-life of 3D cell models. Moreover, spheroids obtained from different engineered cell lines could be obtained to enlarge the spectrum of target bioactivities, including liver toxicity, genotoxicity, and oxidative stress response.

Acknowledgments

This research was sponsored in part by the NATO Science for Peace and Security Programme under Grant No. 985042, by Italian Ministry of Education under grants PRIN 2015 (Prot. 2015TWP83Z) and PRIN2015 (Prot. 2015FFY97L), and LAV.

Conflict of interests

The authors declare no competing financial interest.

References

Almeida, A.C., Gomes, T., Langford, K., Thomas, K.V., Tollefsen, K.E., 2017. Aquat. Toxicol. 189, 50–59.
Arts, R., den Hartog, I., Zijlema, S.E., Thijssen, V., van der Beelen, S.H., Merkx, M., 2016. Anal. Chem. 88, 4525–4532.
Baraniak, P.R., Cooke, M.T., Saeed, R., Kinney, M.A., Fridley, K.M., McDevitt, T.C., 2012. J. Mech. Behav. Biomed. Mater. 1, 63–71.
Bazin, I., Seo, H.B., Suehs, C.M., Ramuz, M., De Waard, M., Gu, M.B., 2017. Environ. Sci. Pollut. Res. Int. 24, 33–41.
Bhise, N.S., Manoharan, V., Massa, S., Tamayol, A., Ghaderi, M., Miscuglio, M., Lang, Q., Shrike Zhang, Y., Shin, S.R., Calzone, G., Annabi, N., Shupe, T.D., Bishop, C.E., Atala, A., Dokmeci, M.R., Khademhosseini, A., 2016. Biofabrication 81, 014101.
Branchini, B.R., Ablamsky, D.M., Murtiashaw, M.H., Uzasci, L., Fraga, H., Southworth, T.L., 2007. Anal. Biochem. 361, 253–262.
Busch, W., Schmidt, S., Kühne, R., Schulze, T., Krauss, M., Altenburger, R., 2016. Environ. Toxicol. Chem. 35, 1887–1899.
Cevenini, L., Calabretta, M.M., Lopreside, A., Branchini, B.R., Southworth, T.L., Michelini, E., Roda, A., 2017. Photochem. Photobiol. 93, 531–535.
Cevenini, L., Calabretta, M.M., Lopreside, A., Tarantino, G., Tassoni, A., Ferri, M., Roda, A., Michelini, E., 2016a. Anal. Bioanal. Chem. 408, 8859–8868.
Cevenini, L., Calabretta, M.M., Tarantino, G., Michelini, E., Roda, A., 2016b. Sens. Actuators B: Chem. 225, 249–257.
Cevenini, L., Camarda, G., Michelini, E., Siciliano, G., Calabretta, M.M., Bona, R., Kumar, T.R., Cara, A., Branchini, B.R., Fidock, D.A., Roda, A., Alano, P., 2014. Anal. Chem. 86, 8814–8821.
Cevenini, L., Lopreside, A., Calabretta, M.M., D'Elia, M., Simoni, P., Michelini, E., Roda, A., 2018. Anal. Bioanal. Chem. 410, 1237–1246.
Choi, J., Lee, E.K., Choo, J., Yuh, J., Hong, J.W., 2015. Biotechnol. J. 10, 1682–1688.
Comina, G., Suska, A., Filippini, D., 2016. Biosens. Bioelectron. 77, 1153–1167.
Ding, Y., Hua, X., Chen, H., Liu, F., González-Sapien, G., Wang, M., 2018. Anal. Chem. 90, 2230–2237.
Directive 2000/60/EC of the European Parliament and of the Council of 23 October 2000 establishing a framework for Community action in the field of water policy. ⟨http://ec.europa.eu/environment/water/water-framework/index_en.html⟩.
Dubiak-Szepietowska, M., Karczmarczyk, A., Winckler, T., Feller, K.H., 2016. Toxicology 370, 60–69.
EFSA CONTAM Panel (EFSA Panel on Contaminants in the Food Chain), 2015. EFSA J. 13, 4321.
Elad, T., Lee, J.H., Gu, M.B., Belkin, S., 2010. Adv. Biochem. Eng. Biotechnol. 117, 85–108.
Goel, G., Makkar, H.P., Francis, G., Becker, K., 2007. Int J. Toxicol. 26, 279–288.
He, W., Yuan, S., Zhong, W.H., Siddikee, M.A., Dai, C.C., 2016. Appl. Microbiol. Biotechnol. 100, 1109–1119.
Hernández, A.F., Parrón, T., Tsatsakis, A.M., Requena, M., Alarcón, R., López-Guarnido, O., 2013. Toxicology 307, 136–145.
Höke, H., Zellerhoff, R., 1998. Toxicology 126, 1–7.
Inoue, J., Gohda, J., Akiyama, T., Semba, K., 2007. Cancer Sci. 98 (3), 268–274.
Jeong, S.H., Lee, D.W., Kim, S., Kim, J., Ku, B., 2012. Biosens. Bioelectron. 35, 128–133.
Kabessa, Y., Eyal, O., Bar-On, O., Korouma, V., Yagur-Kroll, S., Belkin, S., Agranat, A.J., 2016. Biosens. Bioelectron. 79, 784–788.
Kelm, J.M., Timmins, N.E., Brown, C.J., Fussenegger, M., Nielsen, L.K., 2003. Biotechnol. Bioeng. 83, 173–180.
Kim, H.J., Jeong, H., Lee, S.J., 2018. Anal. Bioanal. Chem. 410, 1191–1203.
Kim, H., Jung, Y., Doh, I.J., Lozano-Mahecha, R.A., Applegate, B., Bae, E., 2017. Sci. Rep. 7, 40203.
Kim, J.H., Lim, I.R., Joo, H.J., Choi, S.C., Choi, J.H., Cui, L.H., Iim, L., Hong, S.J., Lim, D.S., 2015. Biochem. Biophys. Res. Commun. 468, 372–379.
Kloss, D., Fischer, M., Rothermel, A., Simon, J.C., Robitzki, A.A., 2008. Lab Chip. 8, 879–884.
Lallemand, C., Kavrochorianou, N., Steenholdt, C., Bendtzen, K., Ainsworth, M.A., Meritet, J.F., Blanchard, B., Lebon, P., Taylor, P., Charles, P., Alzabin, S., Tovey, M.G., 2011. J. Immunol. Methods 373, 229–239.
Langan, L.M., Dodd, N.J., Owen, S.F., Purcell, W.M., Jackson, S.K., Jha, A.N., 2016. PLoS One 11, e0149492.
Lee, H.W., Ahn, D.H., Crawley, S.C., Li, J.D., Gum, J.R., Basbaum, C.B., Fan, N.Q., Szymkowski, D.E., Han, S.Y., Lee, B.H., Sleisenger, M.H., Kim, Y.S., 2002. J. Biol. Chem. 277 (32624-32624).
Legrand-Poels, S., Bours, V., Piret, B., Pflaum, M., Epe, B., Rentier, B., Piette, J., 1995. J. Biol. Chem. 270, 6925–6934.
Lundstrom, K., 2017. Expert Opin. Drug Discov. 12, 335–343.
Michelini, E., Roda, A., 2012. Anal. Bioanal. Chem. 402, 1785–1797.
Niwa, K., Ichino, Y., Kumata, S., Nakajima, Y., Hiraishi, Y., Kato, D., Viviani, V.R., Ohmiya, Y., 2010. Photochem. Photobiol. 86, 1046–1049.
Preechaburana, P., Suska, A., Filippini, D., 2014. Trends Biotechnol. 32, 351–355.
Qin, J.Y., Zhang, L., Clift, K.L., Hulur, I., Xiang, A.P., Ren, B.Z., Lahn, B.T., 2010. PLoS One 5 (5), e10611.
Raut, N., O'Connor, G., Pasini, P., Daunert, S., 2012. Anal. Bioanal. Chem. 402, 3147–3159.
Roda, A., Cevenini, L., Borg, S., Michelini, E., Calabretta, M.M., Schüler, D., 2013. Lab Chip. 13, 4881–4889.
Roda, A., Guardigli, M., Calabria, D., Calabretta, M.M., Cevenini, L., Michelini, E., 2014a. Analyst 139, 6494–6501.
Roda, A., Michelini, E., Cevenini, L., Calabria, D., Calabretta, M.M., Simoni, P., 2014b. Anal. Chem. 86, 7299–7304.
Roda, A., Michelini, E., Zangheri, M., Di Fusco, M., Calabria, D., Simoni, P., 2016a. TrAC 79, 317–325.
Roda, A., Mirasoli, M., Michelini, E., Di Fusco, M., Zangheri, M., Cevenini, L., Roda, B., Simoni, P., 2016b. Biosens. Bioelectron. 76, 164–179.
Roggo, C., van der Meer, J.R., 2017. Curr. Opin. Biotechnol. 45, 24–33.
Sicard, C., Glen, C., Aubie, B., Wallace, D., Jahanshahi-Anbuhi, S., Pennings, K., Daigger, G.T., Pelton, R., Brennan, J.D., Filipe, C.D., 2015. Water Res. 70, 360–369.
Thouand, G., 2018. Anal. Bioanal. Chem. 410, 1189–1190.
Turner, A.P., 2013. Chem. Soc. Rev. 42, 3184–3196.
Wang, Q.X., Xue, S.F., Chen, Z.H., Ma, S.H., Zhang, S., Shi, G., Zhang, M., 2017. Biosens. Bioelectron. 15, 388–393.
WHO, 2003. Isoproturon in drinking-water. Background document for preparation of WHO Guidelines for drinking-water quality. Geneva, World Health Organization (WHO/SDE/WSH/03.04/37).
Wittig, R., Richter, V., Wittig-Blaich, S., Weber, P., Strauss, W.S., Bruns, T., Dick, T.P., Schneckenburger, H.J., 2013. Biomol. Screen. 18, 736–743.
Zhang, D., Liu, Q., 2016. Biosens. Bioelectron. 75, 273–284.

7

Conclusion and Future Perspective

7 Conclusion and Future Perspectives

During this PhD work, whole-cell and transcriptional and translational cell-free biosensors for point-of-need rapid routine monitoring have been developed. These biosensors could be suitable for environmental monitoring and point-of-care applications. Compared to other analytical tools, these biosensors do not require sample treatment steps, sophisticated equipment or trained personnel. Indeed, thanks to the specificity of the biological recognition element, an analyte of interest, or a class of analytes, can be selectively detected in complex matrices (i.e. body fluids, wastewater). Moreover, whole-cell biosensors offer unique features as they are able to provide information about the bioavailable fraction and synergic effects, being able to detect also unknown compounds.

Thanks to synthetic biology and genetic engineering tools, several optical reporter proteins (colorimetric, fluorescent and bioluminescent) have been exploited in order to find the best candidate for our purpose. Optimizing different parameters and experimental conditions, including coding sequences, promoters and plasmids, the analytical performance of the biosensors, in terms of dynamic range, limit of detection and response time, have been improved providing fast and sensitive whole-cell biosensors. Taking advantage of bioluminescence spectral separation, multiplexing detection was achieved within the same cell, increasing the robustness of the developed biosensors for on-field applications.

Different chassis cells (bacteria, yeast and mammalian cell lines) have been exploited to improve analytical performance and predictivity of the biosensors. Bacterial cells provided easy and robust host for fast environmental monitoring; while yeast and 3D mammalian cell biosensors were used as they are more predictive for toxicant effect on human health.

Recent studies have pointed out that conventional laboratory 2D cell cultures often do not reflect the morphology and functionality of living organisms, limiting the predictive value. Therefore, 3D cell cultures of HEK293T cell have been selected for developing more predictive biosensor. 3D cell cultures have indeed the capability to generate the extracellular matrix and restore cell-to-cell communications, thus being the most suitable model to mimic in vivo physiology.

Different immobilization methods and 3D printing technology have been also investigated to integrate the newly developed biosensors into portable platforms. Several user-friendly devices, like smartphone and action cameras, have been exploited as light detectors for real setting applications.

As future perspective, in order to provide a more predictive and comprehensive information about sample toxic effects on humans and animal wildlife, a combination of the developed cell biosensors based on different cell types could be developed. To increase the multiplexing, different bioluminescent reporter proteins could be also implemented and combined into the same cartridge. Each colour could be associated with a biological effect, i.e., general toxicity, inflammation, or to a target analyte. To this end, numerous challenges will have to be faced, such as cross contamination issues, the use of a single buffer for all cell lines, bioluminescent signal acquisition and cells' shelf-life.

Recent development in genetically modified biosensors field have allowed biosensors to become one of the most promising tools for several analytical applications. Nevertheless, improvements are needed for biosafety issues, in particular for on-field applications by non-trained users. Thanks to synthetic biology tools several strategies have already been evaluated such as conditionally lethal mutations and self-killing pathway, but there is still a long way to go.

The development of ready to be used cartridge that can be stored for a long period of time is a further point that need to be solved for real-life applications of whole-cell biosensors.

Another important future perspective is the optimization of in vitro transcriptional and translational systems. Till now, the analytical performance of these systems is not yet comparable to that achieved with whole-cell biosensors, however this approach could solve problems related to safety issues connected with unintentional spreading of genetically modified organisms in the environment.

Compared to conventional cell-free systems, transcriptional and translational cell-free systems based on reporter gene technology offers the unique opportunity to monitor the integration of different metabolic cell pathway and converging stimuli of complex samples.

Bioluminescent proteins among others provide a suitable alternative to monitor several mechanisms at the same time by mean of multiplexed detection.

Acknowledgment

The present works have been performed in the Laboratory of Analytical and Bioanalytical Chemistry of Bologna University headed by Prof. Aldo Roda. I thank him and his co-workers, especially my supervisor Prof. Elisa Michelini, Dr. Maria Maddalena Calabretta, Dr. Luca Cevenini and PhD student Laura Montali.

Part of this work have been performed in the laboratory of Synthetic Biological Circuit Engineering Lab of Edinburgh University headed by Dr Baojun Wang. I thank him and his co-workers, especially Dr Xinyi Wan.